LECTURE NOTES IN COMPUTATIONAL SCIENCE AND ENGINEERING 81

Carmelo Clavero · José Luis Gracia
Francisco J. Lisbona Editors

BAIL 2010 - Boundary and Interior Layers, Computational and Asymptotic Methods

Springer

Lecture Notes
in Computational Science
and Engineering 81

Editors:

For further volumes:
http://www.springer.com/series/3527

Carmelo Clavero • José Luis Gracia
Francisco J. Lisbona
Editors

BAIL 2010 - Boundary and Interior Layers, Computational and Asymptotic Methods

Springer

Editors
Carmelo Clavero
José Luis Gracia
University of Zaragoza
Dept. of Applied Mathematics
Centro Politécnico Superior
María de Luna 3
50018 Zaragoza
Spain
clavero@unizar.es
jlgracia@unizar.es

Francisco J. Lisbona
University of Zaragoza
Dept. of Applied Mathematics
Facultad de Ciencias
Pedro Cerbuna 12
50009 Zaragoza
Spain
lisbona@unizar.es

ISSN 1439-7358
ISBN 978-3-642-19664-5 e-ISBN 978-3-642-19665-2
DOI 10.1007/978-3-642-19665-2
Springer Heidelberg Dordrecht London New York

Library of Congress Control Number: 2011928233

Mathematics Subject Classification (2010): 65L11, 65L12, 65L20, 65N06, 65N12

Cover design: deblik, Berlin

Printed on acid-free paper

Springer is part of Springer Science+Business Media (www.springer.com)

Preface

These proceedings contain selected papers associated with the lectures presented at BAIL 2010 (Boundary and Interior Layers – Computational and Asymptotic Methods). This conference was held from 5 to 9 July 2010 at the University of Zaragoza, Spain. The 64 participants came from many different countries, namely: Argentina, China, France, Germany, India, Ireland, Italy, Russia, South Korea, Spain, Sweden, the UK, and the USA. The BAIL series of conferences are the result of an initiative by Professor John Miller, who organized the first three in Dublin in 1980, 1982, and 1984. Subsequent conferences were then held in Novosibirsk (1986), Shanghai (1988), Copper Mountain, Colorado (1992), Beijing (1994), Perth (2002), Toulouse (2004), Göttingen (2006), and Limerick (2008). The next BAIL Conference will be in Pohang, South Korea, in 2012.

Totally 61 lectures were presented at the BAIL 2010, of which 5 were plenary lectures, 17 were given at the mini-symposia Finite Element Methods Using Layer-Adapted Grids and Robust Methods for Time-Dependent Singularly Perturbed Problems, and 39 were contributions on other subjects. The main objective of the BAIL conferences is to bring together researchers interested in boundary and interior layers. This includes mathematicians and engineers who work on their theoretical and numerical aspects, and also those researchers concerned with their application to a variety of areas such as fluid dynamics, semiconductors, control theory, chemical reactions, and porous media.

The lectures presented at the conference showed the diversity of investigations related to these topics. The proceedings provide a unique overview of research into various aspects of singularly perturbed problems and in particular the efficient resolution of boundary and interior layers using numerical methods. They also include examples of applications of this class of problems.

All papers in the proceedings were subjected to a standardized refereeing process. We would like to thank the authors for their cooperation in the publication of their work in this volume of LNCSE and also the anonymous referees for their work and dedication, without which it would have been impossible to produce this publication.

Finally, we wish to thank the sponsors of the conference: the Spanish Government's project MTM2009-07637-E, the Government of Aragón, the University of Zaragoza, and the Instituto Universitario de Matemáticas y Aplicaciones. Our

thanks also go to the members of the Scientific Committee, the organizers of the mini-symposia, all the attendees for their participation in the conference, and the research group Numerical Methods for Partial Differential and Integral Equations for its work in handling all organizational tasks.

January 2010

Carmelo Clavero
José Luis Gracia
Francisco Lisbona

Contents

Contributors

Rajai S. Alassar Department of Mathematics and Statistics, King Fahd University of Petroleum & Minerals, Box # 1620, Dhahran 31261, Saudi Arabia, alassar@kfupm.edu.sa

Markus Bause Department of Mechanical Engineering, Helmut Schmidt University, University of the Federal Armed Forces Hamburg, Holstenhofweg 85, 22043 Hamburg, Germany, bause@hsu-hh.de

J.M.L. Bernard CEA-DIF, DAM, 91297 Arpajon, France
and
LRC MESO, CMLA, ENS Cachan, 61 av. du Prés. Wilson, 94235 Cachan Cedex, France, jean-michel.bernard@cea.fr

Igor Boglaev Institute of Fundamental Sciences, Massey University, Palmerston North, New Zealand, I.Boglaev@massey.ac.nz

M. Braack Mathematisches Seminar, Christian-Albrechts-Universität zu Kiel, Ludewig-Meyn-Str. 4, 24098 Kiel, Germany, braack@math.uni-kiel.de

J. Casado-Díaz Departamento de Ecuaciones Diferenciales y Análisis Numérico, Universidad de Sevilla, c/Tarfia s/n, 41012 Sevilla, Spain, jcasadod@us.es

P. Cathalifaud Université de Toulouse, INPT, UPS, CNRS, IMFT, 31400 Toulouse, France, catalifo@imft.fr

Naresh M. Chadha School of Mathematics, Statistics, and Applied Mathematics, National University of Ireland, Galway, Ireland, Naresh.Chadha@NUIGalway.ie

C. Clavero Department of Applied Mathematics, University of Zaragoza, Zaragoza, Spain, clavero@unizar.es

Ramon Codina Universitat Politècnica de Catalunya, Jordi Girona 1-3, Edifici C1, 08034 Barcelona, Spain, ramon.codina@upc.edu

J. Cousteix DMAE, ONERA, ISAE, Toulouse, France, Jean.Cousteix@onecert.fr

Carlo de Falco Dipartimento di Matematica “F. Brioschi”, Politecnico di Milano, P.zza Leonardo da Vinci 32, 20133 Milano, Italy, carlo.defalco@polimi.it

M.H. Doweidar Area de Mecánica de Medios Continuos y Teoría de Estructuras, Departamento de Ingeniería Mecánica, Universidad de Zaragoza, C/María de Luna 7, 50018 Zaragoza, Spain, mohamed@unizar.es

Sebastian Franz Department of Mathematics and Statistics, University of Limerick, Limerick, Ireland, sebastian.franz@ul.ie

S. Fuentes LITEC (CSIC) – Universidad de Zaragoza, Area de Mecánica de Fluidos, C/María de Luna 3, 50018 Zaragoza, Spain, ghauke@unizar.es

M. Benítez García Departamento de Matemática Aplicada, Universidade de Santiago de Compostela, Campus Sur s/n, 15182 Santiago de Compostela, Spain, marta.benitez@udc.es

J.L. Gracia Department of Applied Mathematics, University of Zaragoza, Zaragoza, Spain, jlgracia@unizar.es

G. Hauke LITEC (CSIC) – Universidad de Zaragoza, Area de Mecánica de Fluidos, C/María de Luna 3, 50018 Zaragoza, Spain, ghauke@unizar.es

J. Horáček Institute of Thermomechanics, Academy of Sciences of the Czech Republic, Dolejškova 5, Praha 8, Czech Republic, jaromirh@it.cas.cz

R. Bruce Kellogg Department of Mathematics, University of South Carolina, Columbia, SC 29208, USA, rbmjk@windstream.net

Karel Kozel Faculty of Mechanical Engineering, Department of Technical Mathematics, Czech Technical University in Prague, Karlovo nám. 13, 121 35 Praha 2, Czech Republic, karel.kozel@fs.cvut.cz

Petr Louda Institute of Thermomechanics v.v.i., Czech Academy of Sciences, Dolejškova 5, 182 00 Praha 8, Czech Republic, louda@it.cas.cz

Johannes Löwe Institute for Numerical and Applied Mathematics, Georg-August University, Göttingen, 37083 Göttingen, Germany, loewe@math.uni-goettingen.de

Gert Lube Institute for Numerical and Applied Mathematics, Georg-August University Göttingen, 37083 Göttingen, Germany, lube@math.uni-goettingen.de

M. Luna-Laynez Departamento de Ecuaciones Diferenciales y Análisis Numérico, Universidad de Sevilla, c/Tarfia s/n, 41012 Sevilla, Spain, mllaynez@us.es

Niall Madden School of Mathematics, Statistics, and Applied Mathematics, National University of Ireland, Galway, Ireland, Niall.Madden@NUIGalway.ie

M. Gómez Mármol Departamento de Ecuaciones Diferenciales y Análisis Numérico, Universidad de Sevilla, C/Tarfia s/n, 41012 Sevilla, Spain, macarena@us.es

Gunar Matthies Institut für Mathematik, Universität Kassel, Fachbereich 10, Heinrich-Plett-Strase 40, 34132 Kassel, Germany, matthies@mathematik.uni-kassel.de

J. Mauss Université de Toulouse, INPT, UPS, CNRS, IMFT, 31400 Toulouse, France, mauss@cict.fr

Kajal Kumar Mondal Alipurduar College, Jalpaiguri, West Bengal, India, kkmondol@gmail.com

G. Narbona-Reina Departamento de Matemática Aplicada I, Universidad de Sevilla, Avda. Reina Mercedes 2, 41012 Sevilla, Spain, gnarbona@us.es

E. O'Riordan School of Mathematical Sciences, Dublin City University, Dublin, Ireland, eugene.oriordan@dcu.ie

Jaromír Příhoda Institute of Thermomechanics v.v.i., Czech Academy of Sciences, Dolejškova 5, 182 00 Praha 8, Czech Republic, prihoda@it.cas.cz

J. Quinn School of Mathematical Sciences, Dublin City University, Dublin, Ireland, jason.quinn25@mail.dcu.ie

T. Chacón Rebollo Departamento de Ecuaciones Diferenciales y Análisis Numérico, Universidad de Sevilla, C/Tarfia s/n, 41012 Sevilla, Spain, chacon@us.es

Lars Röhe Institute for Numerical and Applied Mathematics, Georg-August University Göttingen, 37083 Göttingen, Germany, roehe@math.uni-goettingen.de

Riccardo Sacco Dipartimento di Matematica "F. Brioschi", Politecnico di Milano, P.zza Leonardo da Vinci 32, 20133 Milano, Italy, riccardo.sacco@polimi.it

G.I. Shishkin Institute of Mathematics and Mechanics, Russian Academy of Sciences, Moscow, Russia, shishkin@imm.uran.ru

L.P. Shishkina Institute of Mathematics and Mechanics, Russian Academy of Sciences, Ekaterinburg, Russia, Lida@convex.ru

Martin Stynes Department of Mathematics, National University of Ireland, Cork, Ireland, m.stynes@ucc.ie

F.J. Suárez-Grau Departamento de Ecuaciones Diferenciales y Análisis Numérico, Universidad de Sevilla, c/Tarfia s/n, 41012 Sevilla, Spain, fjsgrau@us.es

P. Sváček Faculty of Mechanical Engineering, Department of Technical Mathematics, CTU in Prague, Karlovo nam. 13, Praha 2, Czech Republic, Petr.Svacek@fs.cvut.cz

B. Tews Mathematisches Seminar, Christian-Albrechts-Universität zu Kiel, Ludewig-Meyn-Str. 4, 24098 Kiel, Germany, tews@math.uni-kiel.de

Martin Viscor Department of Mathematics, University College Cork, Cork, Ireland, m.viscor@ucc.ie

M. Zagzoule Université de Toulouse, INPT, UPS, CNRS, IMFT, 31400 Toulouse, France, zagzoule@imft.fr

Modeling Acoustic Streaming On A Vibrating Particle

Rajai S. Alassar

Abstract In this study, we present the details of a Legendre series truncation method where the stream function and vorticity are expanded in terms of associated Legendre functions to calculate the secondary currents induced by a vibrating spherical particle. The time-dependent differential equations which result from the expansions are solved using a Crank-Nicolson numerical scheme.

1 Introduction

The phenomenon of secondary currents produced by the vibration of a particle in a fluid has been observed for a long time. A good review on the subject can be found in Kotas et al. [1], Lighthill [2], and Riley [3,4]. The importance of this phenomenon is currently gaining momentum due to the hypothesis of Yoda et al. [5]. Current models of hearing state that a fish directionalizes sound via direct stimulation of macular hair cells by acoustic particle velocity (Shellart and de Munck [6], Rogers et al. [7]). Yoda et al. [5] hypothesize, instead, that the fish ear is an "auditory retina," where macular hair cells are stimulated by acoustically-induced flow velocities (i.e. secondary currents). The densely packed hair cells visualize the flow patterns due to the acoustically induced flow in the complex three-dimensional geometry between the otolith and the macula, much like a tuft visualization. The complex geometry of fish otoliths may help to distinguish flow patterns for sound from different directions. By converting acoustic signals into spatial patterns sampled with extremely high spatial resolution by the macular hair cells, directionalizing sound becomes a pattern recognition problem, not unlike the visual patterns imaged by the retina.

In this paper, the secondary currents caused by the harmonic oscillation of an infinite body of fluid past a spherical particle are calculated by a semi analytical method. The stream function and vorticity are first expanded in terms of associated

R.S. Alassar
King Fahd University of Petroleum & Minerals, Department of Mathematics and Statistics, Box # 1620, Dhahran 31261, Saudi Arabia
e-mail: alassar@kfupm.edu.sa

C. Clavero et al. (eds.), *BAIL 2010 – Boundary and Interior Layers, Computational and Asymptotic Methods*, Lecture Notes in Computational Science and Engineering 81,
DOI 10.1007/978-3-642-19665-2_1,

Legendre functions and the resulting time-dependent differential equations are then solved using a Crank-Nicolson numerical scheme. Although no intention is made here to describe the mechanism of fish hearing, the study offers an initial numerical exploration into the relevance of the acoustically-induced flow to directionalization of sound and characterizing the steady streaming region (practically the region that would be sampled by the hair cells next to the sphere which is considered as a simplified geometry of the fish otolith). It is important to mention here that a study on the physics of steady streaming has been conducted by the present author, [8]. The present paper, however, is different in that it presents the mathematics behind the semi-analytical technique used. It shows how some interesting integrals of special functions developed by the author are incorporated and made use of in the context of steady streaming.

We consider a solid spherical particle of diameter $2a$ suspended in an unbounded oscillating incompressible stream, Fig. 1. The unsteady but uniform free-stream exhibits a sinusoidal oscillatory motion. The fluid motion is governed by the conservation principles of momentum and mass which can be expressed by the following equations:

$$\rho\left[\frac{\partial \mathbf{w}}{\partial t} + (\mathbf{w} \bullet \nabla)\mathbf{w}\right] = -\nabla p + \mathbf{F} + \mu\nabla^2\mathbf{w} \tag{1}$$

$$\nabla \bullet \mathbf{w} = 0 \tag{2}$$

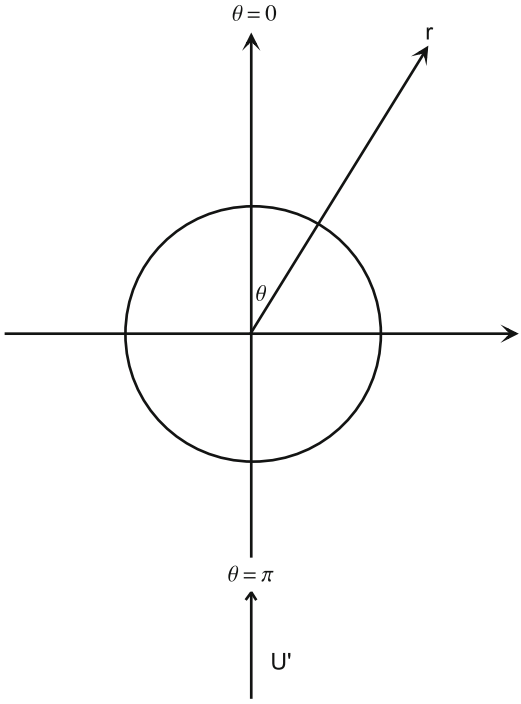

Fig. 1 Sphere in oscillating stream

where ρ is the fluid density, t is time, $\mathbf{w}$ is the velocity vector, p is the pressure in the fluid, $\mathbf{F}$ is the body force vector, and μ is the dynamic viscosity.

2 Method of Solution

First, we recast the equations governing the flow process (1–2) in spherical coordinates. The equations governing, in spherical coordinates, can be written in terms of the dimensionless vorticity (ζ) and the dimensionless stream function (ψ) as:

$$e^{3\xi}\sin\theta\,\zeta + \frac{\partial^2\psi}{\partial\xi^2} + \frac{\partial^2\psi}{\partial\theta^2} - \frac{\partial\psi}{\partial\xi} - \cot\theta\frac{\partial\psi}{\partial\theta} = 0 \tag{3}$$

$$e^{2\xi}\frac{\partial\zeta}{\partial t} + \frac{e^{-\xi}}{\sin\theta}\left[\frac{\partial\psi}{\partial\theta}\left(\frac{\partial\zeta}{\partial\xi} - \zeta\right) - \frac{\partial\psi}{\partial\xi}\left(\frac{\partial\zeta}{\partial\theta} - \cot\theta\,\zeta\right)\right] = \frac{2}{Re}\left[\frac{\partial^2\zeta}{\partial\xi^2} + \frac{\partial^2\zeta}{\partial\theta^2} + \frac{\partial\zeta}{\partial\xi} + \cot\theta\frac{\partial\zeta}{\partial\theta} - \frac{\zeta}{\sin^2\theta}\right] \tag{4}$$

where $Re = 2aU_o/\nu$ is the Reynolds number, U_o is the amplitude of the free-stream velocity, and ν is the coefficient of kinematic viscosity. The logarithmic transformation $\xi = \ln(r/a)$ is used, where r is the dimensional radial distance. The variables ψ, ζ, and $t*$(the star is dropped in 3–4) in the governing equations are defined in terms of the usual dimensional quantities ψ', ζ', and t as: $\psi = \psi'/U_o a^2$, $\zeta = \zeta' a/U_o$, and $t* = U_o\, t/a$.

The oscillations of the free-stream velocity are given in the form $U = U'/U_o = \cos(S\,t)$ where U' is the dimensional free-stream velocity, and $S = a\omega/U_o$ is the Strouhal number with ω being the frequency of oscillations.

The boundary conditions to be satisfied are the no slip and impermeability conditions on the surface of the sphere and the free-stream conditions away from it. These can be written as:

$$\psi = \frac{\partial\psi}{\partial\theta} = \frac{\partial\psi}{\partial\xi} = 0 \qquad at \quad \xi = 0 \tag{5}$$

$$\left.\begin{array}{l} \frac{\partial\psi}{\partial\xi} \to e^{2\xi}\sin^2\theta \quad \cos(S\,t) \quad , \; and \quad \frac{\partial\psi}{\partial\theta} \to e^{2\xi}\sin\theta\;\cos\theta\;\cos(S\,t) \\ or,\;\; \psi \to \frac{e^{2\xi}}{2}\sin^2\theta \quad \cos(S\,t) \\ \zeta \to 0 \qquad\qquad\qquad , \end{array}\right\} \; as\; \xi \to \infty \tag{6}$$

In order to solve the governing equations subject to the boundary conditions, we adopt a series truncation method based on expanding ψ and ζ using Associated Legendre polynomials, Alassar et al. [9], as:

$$\left\{\begin{array}{c}\psi\\ \zeta\end{array}\right\} = \left\{\begin{array}{c} \sum_{n=1}^{\infty} f_n(\xi,t) \int_z^1 P_n(\gamma)\,d\gamma \\ \sum_{n=1}^{\infty} g_n(\xi,t)\; P_n^1(z) \end{array}\right\} \tag{7}$$

where $P_n(z)$ *and* $P_n^1(z)$ are the Legendre and first associated Legendre polynomials of order n respectively, and $z = \cos\theta$. The integrals needed to undergo the transformation of the differential equations onto the modes of the series (7) can be obtained using an approach similar to that reported by Mavromatis and Alassar [10].

The Legendre function $P_n(x)$, as known to physicists, usually arises in studies of systems with three dimensional spherical symmetry. They satisfy the differential equation $(1-x^2)y'' - 2xy' + n(n+1)y = 0$, and the orthogonality relation $\int_{-1}^{1} P_m(x)P_n(x)\,dx = 0 \;\; for \;\; n \neq m$. The first associated Legendre function $P_n^1(x)$ is a special case of the more general associated Legendre functions (not necessarily polynomials) $P_n^m(x)$ which are obtained from derivatives of the Legendre polynomials according to $P_n^m(x) = (-1)^m(1-x^2)^{m/2}\frac{d^m P_n(x)}{dz^m}$. Notice that $P_n^m(x)$ reduce to $P_n(x)$ for $m = 0$.

Substituting from (7) into (3–4) and integrating over z from -1 to 1, the following expressions can be obtained by manipulation of the Legendre functions,

$$\frac{\partial^2 f_n}{\partial\xi^2} - (n+1/2)^2\, f_n = n(n+1)\, e^{5/2\xi}\, g_n \tag{8}$$

$$e^{2\xi}\frac{\partial g_n}{\partial t} = \frac{2}{Re}\left[\frac{\partial^2 g_n}{\partial\xi^2} + \frac{\partial g_n}{\partial\xi} - n(n+1)\, g_n\right] + S_n \tag{9}$$

where,

$$S_n = -e^{-\xi/2}\left[\sum_{i=1}^{\infty}\sum_{j=1}^{\infty}\alpha_{ij}^n\, f_i\left(\frac{\partial g_j}{\partial\xi} - g_j\right) + \sum_{i=1}^{\infty}\sum_{j=1}^{\infty}\beta_{ij}^n\, g_j\left(\frac{\partial f_i}{\partial\xi} + \frac{1}{2}f_i\right)\right] \tag{10}$$

$$\alpha_{ij}^n = -(2n+1)\sqrt{\frac{j(j+1)}{n(n+1)}} \quad \begin{pmatrix} n & i & j \\ -1 & 0 & 1 \end{pmatrix} \begin{pmatrix} n & i & j \\ 0 & 0 & 0 \end{pmatrix} \tag{11}$$

$$\beta_{ij}^n = (2n+1)\sqrt{\frac{j(j^2-1)(j+2)}{n(n+1)\,i\,(i+1)}} \quad \begin{pmatrix} n & i & j \\ -1 & -1 & 2 \end{pmatrix} \begin{pmatrix} n & i & j \\ 0 & 0 & 0 \end{pmatrix} \tag{12}$$

and $\begin{pmatrix} j_1 & j_2 & j_3 \\ m_1 & m_2 & m_3 \end{pmatrix}$ are the 3-j symbols.

The power of this technique is evident through the fact that the series expansions resulted in the elimination of the independent variable (θ). The governing equations are now written in the form of a set of differential equations with the dependent variables being the coefficients (f_n, g_n) of the series. The resulting equations represent two sets of differential equations, with every set containing infinite number of equations, as compared to the original two partial differential equations. However, we will solve only few of these equations and yet obtain a highly accurate solution.

In the process of obtaining (8–9), one encounters integrals such as $\int_{-1}^{1} P_n^k(z)\, P_m^k(z)\, dz$, $\int_{-1}^{1} P_n^1(z)\; P_i^1(z)\; P_j(z)\; dz$, $\int_{-1}^{1} P_n^1(z)\; P_i^1(z)\; P_j^2(z)\; dz$, and others. These integrals make it possible to eliminate the angular direction θ. They are of the general form:

$$\int_{-1}^{1} P_{j_1}^{m_1}(z)\; P_{j_2}^{m_2}(z)\; P_{j_3}^{m_3}(z)\; dz \tag{13}$$

These integrals are very essential and can be obtained from the following relation:

$$\begin{aligned}\int_{-1}^{1} P_{j_1}^{m_1}(z)\; P_{j_2}^{m_2}(z)\; P_{j_3}^{m_3}(z)\; dz = & \sqrt{\tfrac{(j_2+m_2)!(j_1+m_1)!}{(j_2-m_2)!(j_1-m_1)!}} \\ & \times \sum_n \left[(-1)^{m_1+m_2}(2n+1) \begin{pmatrix} j_1 & j_2 & n \\ 0 & 0 & 0 \end{pmatrix} \begin{pmatrix} j_1 & j_2 & n \\ m_1 & m_2 & -m_1-m_2 \end{pmatrix} \right. \\ & \left. \times \sqrt{\tfrac{(n-m_1-m_2)!}{(n+m_1+m_2)!}} \int_{-1}^{1} P_{j_3}^{m_3}(z)\, P_n^{m_2+m_1}(z)\, dz \right]\end{aligned} \tag{14}$$

where $|j_1 - j_2| \le n \le j_1 + j_2$, and

$$\begin{aligned}\int_{-1}^{1} P_{j_1}^{m_1}(z)\, P_{j_2}^{m_2}(z)\, dz = & \tfrac{(-1)^{m_2}\pi}{2^{2(|m_2-m_1|)+1}\,\Gamma(\frac{1}{2}+\frac{|m_2-m_1|}{2})\,\Gamma(\frac{3}{2}+\frac{|m_2-m_1|}{2})} \sqrt{\tfrac{(j_1+m_1)!(j_2+m_2)!}{(j_1-m_1)!(j_2-m_2)!}} \\ & \times \sum_k (-1)^{-m_1+m_2}(2k+1) \begin{pmatrix} j_1 & j_2 & k \\ 0 & 0 & 0 \end{pmatrix} \begin{pmatrix} j_1 & j_2 & k \\ -m_1 & m_2 & m_1-m_2 \end{pmatrix} \\ & \times (1+(-1)^{k+|m_2-m_1|}) \sqrt{\tfrac{(k+|m_2-m_1|)!}{(k-|m_2-m_1|)!}} \\ & \times {}_3F_2\left[\tfrac{|m_2-m_1|+k+1}{2}, \tfrac{|m_2-m_1|-k}{2}, \tfrac{|m_2-m_1|}{2}+1; |m_2-m_1|+1, \tfrac{3+|m_2-m_1|}{2}; 1 \right]\end{aligned} \tag{15}$$

where, $|j_1 - j_2| \le k \le j_1 + j_2$, Γ is the Gamma function, and ${}_3F_2$ is the generalized hypergeometric function. A detailed discussion on these integrals can be found in Mavromatis and Alassar [10] who showed that the hypergeometric function in (15) is always a finite series, and indeed is also Saalschutzian, i.e.

$$\begin{aligned}{}_3F_2\left[\tfrac{|m_2-m_1|+k+1}{2}, \tfrac{|m_2-m_1|-k}{2}, \tfrac{|m_2-m_1|}{2}+1; |m_2-m_1|+1, \tfrac{3+|m_2-m_1|}{2}; 1 \right] = \\ \tfrac{\Gamma(1/2)\Gamma(k/2)\Gamma(|m_2-m_1|+1)\Gamma(-k/2-1/2)}{\Gamma((|m_2-m_1|-k)/2+1/2)\,\Gamma|m_2-m_1|/2)\,\Gamma((|m_2-m_1|+k)/2+1)\,\Gamma(-|m_2-m_1|/2-1/2)}\end{aligned} \tag{16}$$

The 3-j symbols $\begin{pmatrix} j_1 & j_2 & j_3 \\ m_1 & m_2 & m_3 \end{pmatrix}$ are transformation coefficients that appear in the problem of adding angular momenta. They represent the probability amplitude that three angular momenta j_1, j_2, and j_3 with projections m_1, m_2, and m_3 are coupled to yield zero angular momentum. They are related to the famous Clebsch-Gordan

coefficients (C). These symbols, however, possess simpler symmetry properties. The relation between the 3-j symbols and the Clebsch-Gordan coefficients is given by:

$$\begin{pmatrix} j_1 & j_2 & j_3 \\ m_1 & m_2 & m_3 \end{pmatrix} = (-1)^{j_3+m_3+2j_1} \frac{1}{\sqrt{2j_3+1}} C^{j_3 m_3}_{j_1 -m_1 j_2 -m_2} \tag{17}$$

Many representations of the 3-j symbols are available. They may be represented by the square 3×3 array of the Regge R-symbol, by algebraic sums, or in terms of the generalized hypergeometric function of unit argument (${}_3F_2$). The following formula should give a flavor of the many representations available:

$$\begin{aligned} C^{c\gamma}_{a\alpha b\beta} &= \delta_{\gamma,\alpha+\beta} \frac{\Delta(abc)}{(a+b-c)!(-b+c+\alpha)!(-a+c-\beta)!} \left[\frac{(a+\alpha)!(b-\beta)!(c+\gamma)!(c-\gamma)!(2c+1)!}{(a-\alpha)!(b+\beta)!} \right]^{\frac{1}{2}} \\ &\times {}_3F_2 \left[\begin{matrix} -a-b+c, -a+\alpha, -b-\beta \\ -a+c-\beta+1, -b+c+\alpha+1 \end{matrix} \middle| 1 \right] \end{aligned} \tag{18}$$

where,

$$\Delta(abc) = \left[\frac{(a+b-c)!(a-b+c)!(-a+b+c)!}{(a+b+c+1)!} \right]^{\frac{1}{2}} \tag{19}$$

For detailed discussion, representations, properties, and tabulated values, the reader is referred to Varshalovich et al. [11, pp. 235–411]. The 3-j symbols can also be obtained through the famous software MATHEMATICA.

The boundary conditions (5–6) are transferred on to the modes of the series (7) by utilizing the same process by which the differential equations are treated with. The boundary conditions can now be written as:

$$f_n(0,t) = \frac{\partial f_n}{\partial \xi}(0,t) = 0 \tag{20}$$

$$f_n(\xi,t) \to e^{3/2\xi} \cos(St)\ \ \delta_{n1}\,, \quad \frac{\partial f_n(\xi,t)}{\partial \xi} \to \frac{3}{2}\, e^{3/2\xi} \cos(St)\ \ \delta_{n1}\ \ as \quad \xi \to \infty \tag{21}$$

$$g_n(\xi,t) \to 0 \qquad as \quad \xi \to \infty \tag{22}$$

where δ_{ij} is the Kronecker delta.

Finally, an integral condition based on (8) to be satisfied by the functions g_n can be obtained after making use of the boundary conditions (20–22) as:

$$\int_0^\infty e^{(2-n)\,\xi} g_n \, d\xi = \frac{3}{2} \cos(St)\, \delta_{n1} \tag{23}$$

The solutions of the functions ψ and ζ are advanced in time by first solving (9) using a Crank-Nicolson finite-difference scheme similar to that used by Dennis et al. [12].

Since the problem is solved numerically the conditions at ∞ are applied at $\xi = \xi_m$ where ξ_m defines the distance away from the sphere at which ζ has negligible value. Equation (9), when written in difference form using the Crank-Nicolson finite difference scheme and applied at every mesh point in the range from $\xi = 0\ to\ \xi = \xi_m$, will result in a set of algebraic equations that forms a tridiagonal matrix problem which is solved for each value of n between 1 and N iteratively. N designates the number of terms taken in the series defined in (7). The boundary conditions $g_n(0,t)$ which are needed to complete the integration procedure are obtained by writing the integral condition defined in (19) as a numerical quadrature formula which then relates the boundary value to values of the corresponding function at internal points of the computational domain. This gives the extra condition needed to determine the boundary values for g_n and thus the formulation of the solution of (9) is complete.

A straightforward finite-difference solution for (8) results in an unstable solution especially for large n. Therefore, the solution of these equations is obtained using a step-by-step integration scheme modified from that used by Badr et al. [13]. The method is based on splitting (8) into two first order differential equations one of which is integrated by a stable method in the direction of increasing ξ while the other is integrated in the backward direction from $\xi = \infty$ to $\xi = 0$. The method is well explained by Badr et al. [13] and can be easily modified to suit our problem and need not be discussed further.

The whole iterative numerical scheme can be summarized as follows:

At time t, the known solution at time $(t - \Delta t)$ is used as a starting solution. The tridiagonal system resulting from (9) with the most recently available information is solved to obtain the functions $g_n(\xi, t)$. Secondly, we apply the integral condition (19) to obtain a better approximation for $g_n(0,t)$. Then, (8) is solved using the stable step-by-step numerical procedure mentioned above to obtain $f_n(\xi, t)$. The procedure is then repeated until convergence is reached. The condition set for convergence is $\left|g_n^{m+1}(\xi) - g_n^m(\xi)\right| < 10^{-10}$ where m denotes the iteration number. Time is then incremented and the whole process is repeated.

Following the start of fluid motion, very small time steps were used since the time variation of vorticity is quite fast. As time increases, the time step was gradually increased. Smaller time steps were used for higher Strouhal numbers. The number of points in the ξ direction used is 201 with a space step of 0.025. This makes $\xi_m = 5$ which sets the outer boundary at a physical distance of approximately 148 times the radius of the sphere. This is necessary to ensure that the conditions at infinity are appropriately incorporated in the numerical solution. The effect of ξ_m on the flow field near the sphere was examined by comparing the results when using different values of ξ_m. The effect of the step size on the flow field near the sphere was also examined by comparing the results when using different values. No significant changes in the values of the drag or the surface vorticity were detected by reducing the step size further than the given value. As there is no intrinsic way to determine them, the total number of terms taken in the series was found by numerical experiments. The number of terms taken in the series starts with only 3 terms. One more term is added when the last term in the series exceeds 10^{-6}. The total number of terms is dependent on Reynolds and Strouhal numbers. More terms are needed for high Reynolds and low Strouhal numbers.

One last modification is taken here through defining a dimensionless time τ which is related to the previously defined dimensionless time t by

$$\tau = St/2\pi \tag{24}$$

Scaling time by the Strouhal number is appropriate in dealing with relatively high-frequency flows. Consequently, each cycle has a period of unity with 400 divisions and $\Delta\tau = 0.0025$.

The accuracy of the method of solution was verified by Alassar et al. [9] through comparisons with the forced and mixed convection cases available in the literature such as Wong et al. [14], Sayegh and Gauvin [15], Dennis and Walker [16], and others. The comparisons were satisfactory.

Figure 2 shows the secondary currents calculated by the present method for the cases Re $= 5, 50$, and 200 with S $= \pi/4$ and a photo from experiments by Kotas et al. [1].

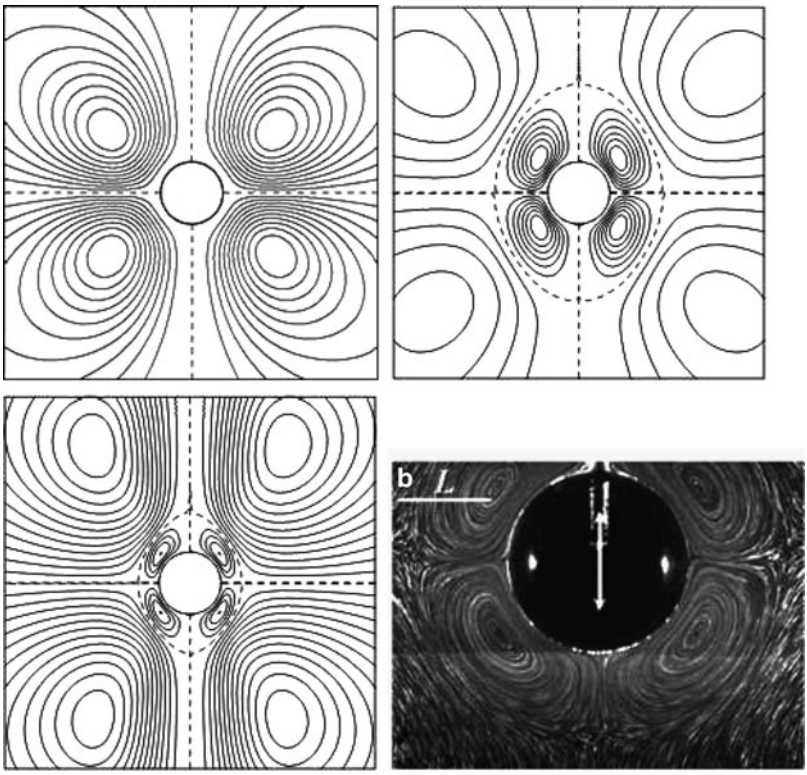

Fig. 2 Secondary currents for the cases Re $= 5, 50$, and 200 with S $= \pi/4200$, and a photo from experiments by Kotas et al. [1]

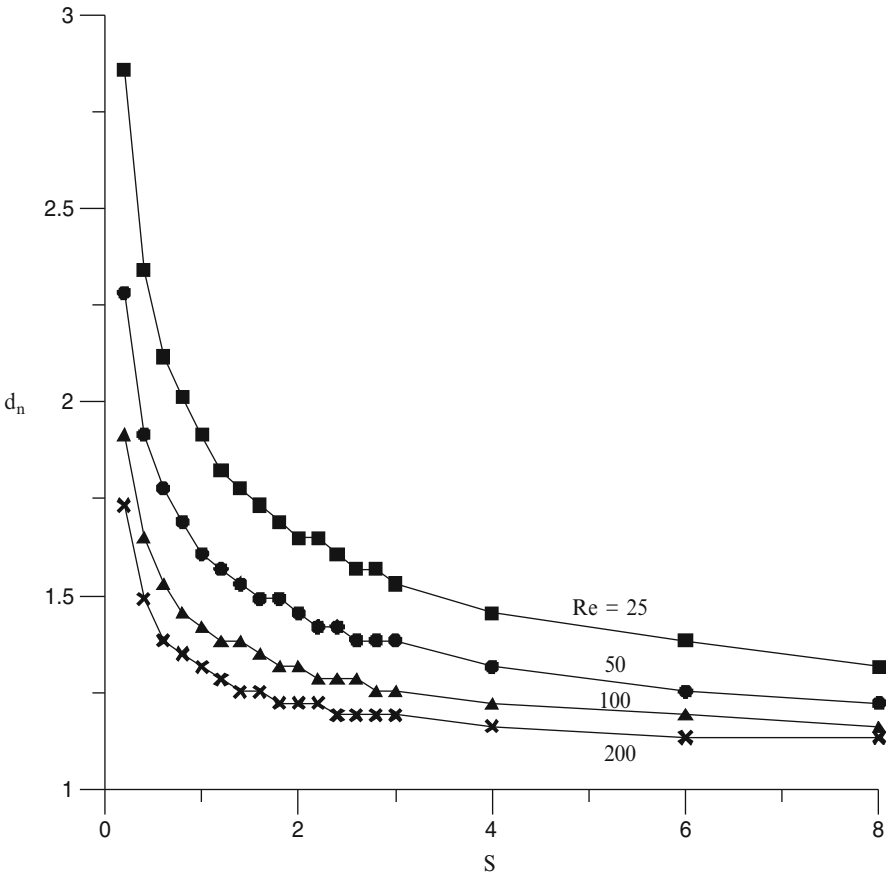

Fig. 3 Variation of d_n with S

An important characteristic length is the distance from the center of the sphere to the center of the near (inner) recirculation region d_n. Figure 3 shows the variation of d_n with Strouhal and Reynolds numbers. As S increases, the distance from the center of the sphere to the center of the inner rotating region (stagnation point) becomes smaller for all Re cases. Obviously, d_n is smaller for higher Reynolds numbers.

Acknowledgements I would like to express my sincere appreciation to King Fahd University of Petroleum & Minerals (KFUPM) for supporting this research.

References

1. C. W. Kotas, M. Yoda, and P. H. Rogers, Visualization of steady streaming near oscillating spheroids. EXP FLUIDS 42(1): 111–121 JAN (2007).
2. J. Lighthill, Acoustic streaming. J Sound Vib 61(3): 391–418, DOI 10.1016/0022-460X(78) 90388-7, (1978).

3. N. Riley, On a sphere oscillating in a viscous fluid. Quart. Journ. Mech. and Applied Math., vol. XIX, Pt. 4 (1966).
4. N. Riley, Steady streaming, Annu Rev Fluid Mech, 33:43, 65, DOI 10.1146/annurev.fluid. 33.1.43, (2001).
5. M. Yoda, P. H. Rogers and K. E. Baxter, "Is the fish ear an auditory retina? Steady streaming in the otolith-macula gap," *Bioacoustics* **12**, 131–134 (2002).
6. N.A.M. Shellart, and J.C. de Munck, "A model for directional ands distance hearing in swim-bladder bearing fish based on the displacement orbits of the hair cells", J. Acoust. Soc. Am. 82, 822–829 (1987).
7. P.H. Rogers, A.N. Popper, M.C. Hastings, and W.M. Saidel, "Processing of acoustic signals in the auditory system of bony fish", J. Acoust. Soc. Am. 83, 338–349 (1998).
8. R. S. Alassar, Acoustic streaming on spheres, International Journal of Nonlinear Mechanics, 43, pp. 892–897 (2008).
9. R. S. Alassar, H. M. Badr, and H. A. Mavromatis, Heat convection from a sphere placed in an oscillating free stream. Int. J. Heat Mass Transfer, Vol. 42, pp. 1289–1304 (1999).
10. H. A. Mavromatis, and R. S. Alassar, A generalized formula for the integral of three associated Legendre polynomials. Applied Mathematics Letters, vol. 12, pp. 101–105, (1999).
11. D. A. Varshalovich, A. N. Moskalev, and V. K. Khersonskii, Quantum theory of angular momentum. Singapore: World Scientific, (1988).
12. S. C. R. Dennis, J. D. A. Walker, and J. D. Hudson, Heat transfer from a sphere at low Reynolds numbers. J. Fluid Mech., vol. 60, part 2, pp. 273–283 (1973).
13. H. M. Badr, S. C. R. Dennis, and P. J. S. Young, Steady and unsteady flow past a rotating circular cylinder at low Reynolds numbers, Computers & Fluids, vol. 17, no. 4, pp. 579–609 (1989).
14. K-L. Wong, S-C. Lee, and C-K. Chen, Finite element solution of laminar combined convection from a sphere. Transactions of the ASME, Vol. 108, pp. 860–865 (1986).
15. N. N. Sayegh and W. H. Gauvin, Numerical analysis of variable property heat transfer to a single sphere in high temperature surroundings. AIChe Journal, Vol. 25, No. 3, pp. 522–534 (1979).
16. S. C. R. Dennis and M. S. Walker, Forced convection from heated spheres. Aeronautical Research Council no. 26, 105 (1964).

Performance of Stabilized Higher-Order Methods for Nonstationary Convection-Diffusion-Reaction Equations

Markus Bause

Abstract We study the performance properties of a class of stabilized higher-order finite element approximations of convection-diffusion-reaction models with nonlinear reaction mechanisms. Streamline upwind Petrov-Galerkin (SUPG) stabilization together with anisotropic shock-capturing as an additional stabilization in crosswind-direction is used. We show that these techniques reduce spurious oscillations in crosswind-direction and increase the accuracy of simulations.

1 Introduction

Time-dependent convection-diffusion-reaction equations

$$\partial_t u + \boldsymbol{b} \cdot \nabla u - \nabla \cdot (a \nabla u) + r(u) = f \tag{1}$$

are often studied in various technical and environmental applications. Here, $u = u(\boldsymbol{x}, t)$ denotes the unknown where $\boldsymbol{x} \in \Omega \subset \mathbb{R}^d$, with $d \geq 2$, and $t \in (0, T)$ for some $T > 0$. Further, $a \in L^\infty(0, T; W^{1,\infty}(\Omega))$ is the diffusion coefficient, $\boldsymbol{b} \in L^\infty(0, T; \boldsymbol{W}^{1,\infty}(\Omega))$ is the velocity field, $r \in C^1(\mathbb{R}_0^+)$ is the parametrization of the reaction rate and $f \in L^2(0, T; L^2(\Omega))$ is a prescribed right-hand side term. We suppose that $\nabla \cdot \boldsymbol{b}(\boldsymbol{x}, t) = 0$ and $a(x, t) \geq \alpha > 0$ almost everywhere. Throughout the paper we use standard notation.

The accurate numerical approximation of (1) is still a challenging task. In applications, the transport equation (1) is often convection- and/or reaction-dominated and characteristic solutions have sharp layers. In these cases standard finite element methods cannot be applied. Stabilized finite element approaches are required. For a review of these techniques we refer to the recent work of John and Schmeyer [3].

M. Bause
Helmut Schmidt University, University of the Federal Armed Forces Hamburg, Department of Mechanical Engineering, Holstenhofweg 85, 22043 Hamburg, Germany
e-mail: bause@hsu-hh.de

C. Clavero et al. (eds.), *BAIL 2010 – Boundary and Interior Layers, Computational and Asymptotic Methods*, Lecture Notes in Computational Science and Engineering 81,
DOI 10.1007/978-3-642-19665-2_2,

Stabilization methods are well-understood for linear steady convection-diffusion-reaction problems; cf., e.g., [3, 4]. However, there is still a considerable lack in the analysis, design and application of these methods for unsteady nonlinear problems which is addressed here. Rigorous analyses are rare for the unsteady and nonlinear case.

2 Discretization Scheme

Equipping (1) with initial and homogeneous Dirichlet boundary conditions and discretizing (1) in time by the θ-scheme, with $\theta \in (0, 1]$, leads to a sequence of stationary boundary value problems: *Find* $\{u^k\}_{k=1}^N$ *such that*

$$\alpha_k u^k + \theta \boldsymbol{b}(t_k) \cdot \nabla u^k - \theta \nabla \cdot (\boldsymbol{a}(t_k) \nabla u^k) + \theta r(u^k) = \tilde{f}^k \quad \text{in } \Omega\,, \tag{2}$$

with $\tilde{f}^k = \alpha_k u^{k-1} + \theta f(t_k) + (1-\theta) f(t_{k-1}) - (1-\theta)\boldsymbol{b}(t_{k-1}) \cdot \nabla u^{k-1} + (1-\theta)\nabla \cdot (\boldsymbol{a}(t_{k-1})\nabla u^{k-1}) - (1-\theta) r(\boldsymbol{u}^{k-1})$, $\alpha_k = 1/(t_k - t_{k-1})$ *and* $u^k = 0$ *on* $\partial\Omega$, $u^0 = u(t_0)$.

In the sequel, we suppose that the solution u of (1) is non-negative and bounded from above, i.e., $0 =: u_0 \leq u \leq u_1$ almost everywhere in $\Omega \times (0, T)$, which is admissible from the sake of physical realism, for instance, if u denotes the concentration of a chemical species. We make the assumption that

$$r \in C^1(\mathbb{R}_0^+)\,, \qquad r(0) = 0\,, \qquad r'(s) \geq r_0 \geq 0 \quad \text{for } s \geq 0\,,\ s \in \mathbb{R}\,. \tag{3}$$

To calculate approximations of $\{u^k\}_{k=1}^N$, a standard hp-version of the finite element method is assumed; cf. [1, 4, 7]. For a family of admissible and shape-regular triangulations $\mathcal{T}_h = \{T\}$ of the polyhedral domain $\Omega \subset \mathbb{R}^d$ let

$$V_h^{\boldsymbol{p}} = X_h^{\boldsymbol{p}} \cap H_0^1(\Omega) \quad \text{with} \quad X_h^{\boldsymbol{p}} = \{v \in C(\overline{\Omega}) \mid v_{|T} \circ F_T \in \mathcal{P}_{p_T}(\widehat{T})\ \forall T \in \mathcal{T}_h\}$$

denote the underlying finite element space of piecewise polynomials of local order p_T for all $T \in \mathcal{T}_h$. Here, $\widehat{T}$ is the (open) unit simplex or the (open) unit hypercube in $\mathbb{R}^d$ and $\mathcal{P}_n(\widehat{T})$, with $n \geq 1$, is the set of all polynomials of degree at most n on $\widehat{T}$. We assume that each $T \in \mathcal{T}_h$ is a smooth bijective image of $\widehat{T}$, i.e., $T = F_T(\widehat{T})$. The vector $\boldsymbol{p}$ is defined by $\boldsymbol{p} = \{p_T \mid T \in \mathcal{T}_h\}$. In our analysis the local inverse inequalities

$$\|\nabla w_h\|_{L^2(T)} \leq \mu_{\text{inv}}\, p_T^2 h_T^{-1} \|w\|_{L^2(T)} \quad \forall w_h \in X_h^{\boldsymbol{p}} \quad \text{on } T \in \mathcal{T}_h \tag{4}$$

are applied. Here, μ_{inv} depends on the shape-regularity parameter; cf. [7].

Skipping for brevity the indices in (2), the SUPG-stabilized approximation of (2) is: *Find* $u_h \in V_h^{\boldsymbol{p}}$ *such that*

$$A_s(u_h, v_h) = L_s(v_h) \tag{5}$$

for all $v_h \in V_h^p$, *where*

$$A_s(u,v) = A_{\rm lin}(u,v) + \theta\langle \widehat{r}(u), v\rangle + \sum_{T\in\mathcal{T}_h} \delta_T \langle \widehat{L}u, \boldsymbol{b}\cdot\nabla v\rangle_{L^2(T)}\,, \tag{6}$$

$$L_s(v) = \langle \tilde{f}, v\rangle + \sum_{T\in\mathcal{T}_h} \delta_T \langle \tilde{f}, \boldsymbol{b}\cdot\nabla v\rangle_{L^2(T)}\,, \tag{7}$$

$$A_{\rm lin}(u,v) = \alpha\langle u, v\rangle + \theta\langle \boldsymbol{b}\cdot\nabla u, v\rangle + \theta\langle a\nabla u, \nabla v\rangle\,, \tag{8}$$

$$\widehat{L}u = \widehat{L}_{\rm lin}u + \theta\widehat{r}(u)\,, \quad \widehat{L}_{\rm lin}u_{|T} = \alpha u + \theta\boldsymbol{b}\cdot\nabla u - \theta\nabla\cdot\Pi_T(a\nabla u)\,. \tag{9}$$

If in addition shock-capturing is applied, we get: *Find* $u_h \in V_h^p$ *such that*

$$A_s(u_h, v_h) + A_{\rm sc}(u_h; u_h, v_h) = L_s(v_h) \tag{10}$$

for all $v_h \in V_h^p$, *where*

$$A_{\rm sc}(w; u, v) := \sum_{T\in\mathcal{T}_h} \langle \tau_T(w)\boldsymbol{D}_{\rm sc}\nabla u, \nabla v\rangle\,. \tag{11}$$

Together, the last terms on the right-hand sides of (6) and (7), respectively, represent the SUPG-stabilization. The choice of the stabilization parameter δ_T is given in Remark 2 below. In (8) we changed $r(\cdot)$ to $\widehat{r}(\cdot)$ where $\widehat{r}(u) = r(u_0) + r'(u_0)(u-u_0)$ for $u \le u_0$, $\widehat{r}(u) = r(u)$ for $u_0 \le u \le u_1$ and $\widehat{r}(u) = r(u_1) + r'(u_1)(u-u_1)$ for $u \ge u_1$. This modification is necessary to prove an error estimates when r' grows with $|u|$. It is probably not necessary in practical computations but easy to incorporate if desired. It holds that

$$|\widehat{r}(u) - \widehat{r}(v)| \le L_r|u-v| \quad \forall u, v \in \mathbb{R}\,, \tag{12}$$

with some constant $L_r > 0$. In (9), the mapping $\Pi_T : \boldsymbol{L}^2(\Omega) \mapsto (\mathcal{P}_{p_T}(T))^d$ is the (elementwise) orthogonal projection onto $(\mathcal{P}_{p_T}(T))^d$. In (11), we use an anisotropic variant of shock-capturing (cf. [2]):

$$\boldsymbol{D}_{\rm sc} := \begin{cases} \boldsymbol{I} - \dfrac{\boldsymbol{b}\otimes\boldsymbol{b}}{|\boldsymbol{b}|^2}\,, & \boldsymbol{b} \neq \boldsymbol{0} \\ \boldsymbol{0}\,, & \boldsymbol{b} = \boldsymbol{0} \end{cases}\,, \quad \tau_T(w) := l_T(w)R_T^*(w) \equiv \frac{l_T(w)R_T(w)}{|w|_{H^1(T)} + \kappa}\,,$$

$$R_T(w) := \|\widehat{L}w - f\|_{L^2(T)}\,, \qquad l_T(w) := l_0 h_T \max\left\{0, \beta - \frac{2\|a\|_{L^\infty(T)}}{h_T R_T^*(w)}\right\}\,. \tag{13}$$

The non-negative limiter function $\tau_T(w)$ aims to restrict the effect of shock-capturing to subregions where the residual $\widehat{L}w - f$ is too large. The term $\frac{h_T R_T^*(w)}{2\|a\|_{L^\infty(T)}}$

can be seen as a pseudo mesh Peclet number. The choice of l_0, κ and β is given in Sect. 3. We note that $\tau_T(u_h)$ depends nonlinearly on u_h. Since $r(\cdot)$ is assumed to be nonlinear, the shock-capturing term (11) does not change the type of the discrete problem. This is in contrast to linear convection-diffusion-reaction models that become nonlinear by adding (11).

For the limiter function $\tau_T(\cdot)$ we suppose that

$$0 \leq \tau_T(w) \leq M_T(h_T) \quad \text{with} \lim_{h\to 0} M_T(h) = 0 \tag{14}$$

holds for $w \in V_h^p$ and all $T \in \mathcal{T}_h$. The shock-capturing approach discussed here is covered by the class of methods satisfying (14); cf. [5, Example 3.2].

The existence and stability of a discrete solution $u_h \in V_h^p$ of (10) is ensured. To show this, the following norm is introduced:

$$|||v||| := \left(\sum_{T\in\mathcal{T}_h} \left(\|\sqrt{a}\nabla v\|^2_{L^2(T)} + (\alpha + r_0)\|v\|^2_{L^2(T)} + \delta_T \|\boldsymbol{b}\cdot\nabla v\|^2_{L^2(T)} \right) \right)^{1/2} .$$

Moreover, the following auxiliary estimates are needed.

Lemma 1. *Suppose that assumption (3) and the condition*

$$0 \leq \delta_T \leq \frac{1}{4} \min\left\{ \frac{h_T^2}{p_T^4 \mu_{\text{inv}}^2 \|a\|_{L^\infty(\Omega)}}; \frac{1}{\alpha}; \frac{\alpha + r_0}{L_r^2} \right\} \tag{15}$$

are satisfied. Then, the semilinear form A_s in (6) satisfies

$$A_s(v_h, v_h) \geq \frac{1}{4} |||v_h|||^2 \quad \forall v_h \in V_h^p . \tag{16}$$

For $u \in H_0^1(\Omega)$ with $(\nabla\cdot(a\nabla u))_{|T} \in L^2(T)$ and $v_h \in V_h^p$ it holds that

$$\begin{aligned} &A_{\text{lin}}(u, v_h) + \sum_{T\in\mathcal{T}_h} \delta_T \langle \widehat{L}_{\text{lin}} u, \boldsymbol{b}\cdot\nabla v_h\rangle \leq Q_s(u)|||v_h||| , \\ &Q_s(u) := |||u||| + \left(\sum_{T\in\mathcal{T}_h} \min\left\{ \frac{1}{\delta_T}; \frac{\|\boldsymbol{b}\|_{L^\infty(T)}}{\alpha_T} \right\} \|u\|^2_{L^2(T)} \right. \cdot \\ &\qquad \left. + \sum_{T\in\mathcal{T}_h} \left(\delta_T \| -\nabla\cdot(\Pi_T(a\nabla u) + \alpha u\|^2_{L^2(T)} \right) \right)^{1/2} , \end{aligned} \tag{17}$$

where $\alpha_T := \inf_{x\in T} a(x)$.

The proof of Lemma 1 is given in [1, Lemma 2.1].

Theorem 1. *Let (3), (14) and (15) be satisfied. Suppose that the limiter function $\tau(w)$ is continuous with respect to w. Then, the SUPG scheme with shock-capturing stabilization (10) admits a solution $u_h \in V_h^p$ satisfying*

$$|||u_h|||^2 + \sum_{T\in\mathcal{T}_h} \left\| \sqrt{\tau_T(u_h)}\boldsymbol{D}_{\rm sc}^{1/2}\nabla u_h \right\|^2_{L^2(T)} \le C|||\tilde{f}|||_*^2 \tag{18}$$

with the dual norm $|||\tilde{f}|||_* := \sup_{v_h\in V_h^p\setminus\{0\}} L(v_h)/|||v_h|||$.

Proof. To prove Theorem 1 we use a variant of Brouwer's fixed point theorem; cf. [9, II Lemma 1.4]. For this, let V_h^p be equipped with the inner product $[u_h, v_h] = \langle\nabla u_h, \nabla v_h\rangle$. Let $P : V_h^p \mapsto V_h^p$ be defined by

$$[P(u_h), v_h] = \langle\nabla P(u_h), \nabla v_h\rangle = A_{\rm sc}(u_h; u_h, v_h) + A_s(u_h, v_h) - L_s(v_h)\,.$$

First, we note that

$$\begin{aligned}
&[P(u_h) - P(v_h), P(u_h) - P(v_h)] = \|\nabla(P(u_h) - P(v_h))\|^2_{L^2(\Omega)}\\
&= A_{\rm sc}(u_h; u_h - v_h, P(u_h) - P(v_h))\\
&\quad + \sum_{T\in\mathcal{T}_h} (\langle\tau_T(u_h) - \tau_T(v_h))\boldsymbol{D}_{\rm sc}\nabla v_h, \nabla(P(u_h) - P(v_h)))\rangle_T\\
&\quad + A_{\rm lin}(u_h - v_h, P(u_h) - P(v_h)) + \langle\widehat{r}(u_h) - \widehat{r}(v_h), P(u_h) - P(v_h)\rangle\\
&\qquad + \sum_{T\in\mathcal{T}_h} \delta_T\langle\widehat{L}_{\rm lin}(u_h - v_h), \boldsymbol{b}\cdot\nabla(P(u_h) - P(v_h)))\rangle_T\\
&\qquad + \sum_{T\in\mathcal{T}_h} \delta_T\langle\widehat{r}(u_h) - \widehat{r}(v_h), \boldsymbol{b}\cdot\nabla(P(u_h) - P(v_h)))\rangle_T\,.
\end{aligned}$$

Under the hypotheses of Theorem 1, using Lemma 1 and the Poincaré inequality we get from this identity that

$$\begin{aligned}
&[P(u_h) - P(v_h), P(u_h) - P(v_h)] = \|\nabla(P(u_h) - P(v_h))\|^2_{L^2(\Omega)}\\
&\le \max_{T\in\mathcal{T}_h}\{M_T(h_T)\}C_{\boldsymbol{D}_{\rm sc}}\|\nabla(u_h - v_h)\|^2_{L^2(\Omega)}\|\nabla(P(u_h) - P(v_h))\|_{L^2(\Omega)}\\
&\quad + C_{\boldsymbol{D}_{\rm sc}}\|v_h\|_{W^{1,\infty}(\Omega)}\|\tau(u_h) - \tau(v_h)\|_{L^2(\Omega)}\|\nabla(P(u_h) - P(v_h))\|_{L^2(\Omega)}\\
&\quad + (Q_s(u_h - v_h) + L_r|||u_h - v_h|||)|||P(u_h) - P(v_h)|||\\
&\quad + L_r\|u_h - v_h\|_{L^2(\Omega)}\|\nabla(P(u_h) - P(v_h))\|_{L^2(\Omega)}\,.
\end{aligned}$$

Recalling (14), using the Poincaré inequality and (4) we get that

$$\|\nabla(P(u_h) - P(v_h))\|_{L^2(\Omega)} \leq C(\|\tau(u_h) - \tau(v_h)\|_{L^2(\Omega)} + \|\nabla(u_h - v_h)\|_{L^2(\Omega)}),$$

which proves the continuity of P, since $\tau(\cdot)$ is assumed to be continuous.

Further, by Lemma 1 and the inequality of Cauchy-Young we get that

$$\begin{aligned}[P(v_h), v_h] &= A_{\mathrm{sc}}(v_h; v_h, v_h) + A_s(v_h, v_h) - L_s(v_h) \\ &\geq A_{\mathrm{sc}}(v_h; v_h, v_h) + \frac{1}{4}|||v_h|||^2 - |||f|||_*|||v_h||| \geq \frac{1}{8}|||v_h|||^2 - 2|||f|||_*^2 .\end{aligned} \tag{19}$$

From (19) we conclude that $[P(v_h), v_h] > 0$ for all $v_h \in V_h^p$ with $\|\nabla v_h\|_{L^2(\Omega)} > 4a_0^{-1/2}|||f|||_*$. Brouwer's fixed point theorem (cf. [9, II Lemma 1.4]) now yields the existence of at least one solution $u_h \in V_h^p$ of $P(u_h) = 0$ and, therefore, of (10). Estimate (18) follows from (19), using that $P(u_h) = 0$.

Remark 1. A (local) uniqueness result for the shock-capturing method is still open. The application of Banach's fixed point theorem would require Lipschitz continuity of the parameters $\tau_T(\cdot)$. But such condition is seemingly too restrictive in practice. Another possibility is to apply a uniqueness result for the Brouwer fixed point theorem which could be proved similarly as a corresponding result for the Schauder fixed point theorem; cf. [5] and the references therein. Unfortunately, the assumptions on $\tau_T(\cdot)$ are too severe.

Remark 2. In [1] the quasi-optimal error estimate

$$|||u - u_h|||^2 \leq C \sum_{T \in \mathcal{T}_h} \frac{h_T^{2(l_T-1)}}{p_T^{2(k_T-1)}} \|u\|^2_{H^{k_T}(T)}, \quad C > 0,$$

with $l_T = \min\{p_T + 1, k_T\}$ is proved for the SUPG-stabilized finite element approximation of (2) with and without additional shock-capturing stabilization. It is supposed that the parameter δ_T in (6), (7) is chosen of the order of magnitude $\delta_T \sim \min\left\{\frac{h_T}{p_T\|\boldsymbol{b}\|_{L^\infty(T)}}; \frac{h_T^2}{p_T^4\mu_{\mathrm{inv}}^2\|a\|_{L^\infty(\Omega)}}; \frac{1}{\alpha + r_0}; \frac{\alpha + r_0}{L_r^2}\right\}$. Thus, the additional diffusion term (11) does not perturb the asymptotic convergence behaviour. Our numerical studies will show that shock-capturing stabilization reduces at the same time spurious oscillations in crosswind direction.

3 Numerical Studies

Now we study the numerical performance properties of the schemes. We show that higher order finite element methods combined with SUPG and shock-capturing stabilization are able to resolve interior layers and lead to accurate approximations of solutions of problem (1). For the discretization in time we use the Crank-Nicholson

method corresponding to $\theta = 1/2$ in (2). All computations were done with the Toolbox ALBERTA [6] on triangular meshes.

Example 3.1. Our first numerical study is devoted to the quasi-stationary case. It is a stationary nonlinear variant of the second example in [3, Sect. 7]. We consider (2) for fixed k and $\theta = 1$ on $\Omega = (0,1)^2$ with $\alpha = 1.0$, $a = 10^{-6}$ and $\boldsymbol{b}(\boldsymbol{x}) = (2,3)^\top$. The reaction mechanism is governed by an Arrhenius law $r(u) = k_{Ar}\,\mathrm{e}^{\frac{b_{Ar}(u-1)}{1+a_{Ar}(u-1)}}$ with $k_{Ar} = 50$, $b_{Ar} = 10$ and $a_{Ar} = 0.8$. Studies for polynomial reaction rates are given in [1,8]. The source $\tilde{f}$ is chosen in such a way that $u(\boldsymbol{x}) = 16x_1(1-x_1)x_2(1-x_2)\cdot\left[0.5 + \pi^{-1}\arctan\left(2a^{-1/2}(0.25^2 - (x_1-0.5)^2 - (x_2-0.5)^2)\right)\right]$ is the exact solution. It is characterized by an interior layer of thickness $\mathcal{O}(\sqrt{a})$. We study solutions of (5) and (10). In (13), we put $l_0 = 0.2$, $\kappa = 10^{-4}$, $\beta = 0.7$.

In Table 1 we summarize the calculated errors for different P_p-elements for $p \in \{2,4\}$. Although the SUPG-scheme shows a slightly smaller error, we observe that the errors of the either schemes are of the same order of magnitude, as claimed in Remark 2. The larger errors of the shock-capturing approach are due to its additional artificial crosswind-diffusion that however reduces spurious oscillations. In Table 1 we do not observe the optimal uniform convergence rates since u depends on the diffusion parameter a. In such cases optimal convergence rates are observed for very small step sizes only.

To study the effects of additional crosswind-diffusion more precisely, cross-section plots of the solution at the outflow boundary without and with shock-capturing stabilization are presented in Fig. 1. Significant over- and undershoots of the SUPG-solution without shock-capturing in the neighborhood of the layer are

Table 1 Mesh size, number of degrees of freedom, errors in $|||\cdot|||$ and convergence rates for the SUPG-scheme without (SUPG) and with (SC-CD) shock-capturing/crosswind diffusion and h-refinement for Example 3.1

h	d.o.f.	$p=2, \|\|\|\cdot\|\|\|$				d.o.f.	$p=4, \|\|\|\cdot\|\|\|$			
		SUPG		SC-CD			SUPG		SC-CD	
8.839e-2	545	3.721e-2	–	3.726e-2	–	2113	2.444	–	2.453	–
4.419e-2	2113	2.456e-2	0.60	2.459e-2	0.60	8321	1.507	0.70	1.512	0.70
2.210e-2	8321	1.466e-2	0.74	1.468e-2	0.74	33025	6.475e-1	1.22	6.485e-1	1.22
1.105e-2	33025	6.469e-3	1.18	6.475e-3	1.18	131585	3.351e-1	0.95	3.350e-1	0.95
5.524e-3	131585	2.501e-3	1.37	2.504e-3	1.37	525313	1.346e-1	1.32	1.346e-1	1.32

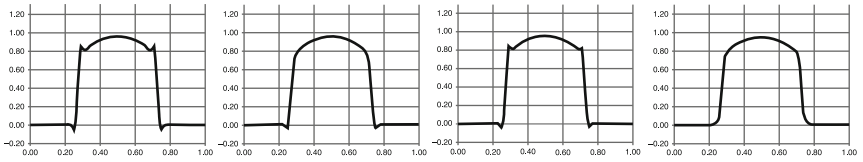

Fig. 1 Cross-section plot for the SUPG-scheme without shock-capturing/crosswind diffusion ($p = 1$, $p = 4$) and with shock-capturing/crosswind diffusion ($p = 1$, $p = 3$) for Example 3.1 with $h = 2.21\text{e-}2$; *from left to right*

observed. This also holds for higher order finite element methods. The unphysical oscillations are clearly damped by higher order finite element approximations along with SUPG and shock-capturing stabilization. No significant improvement is obtained by shock-capturing stabilization if linear finite element methods are applied. This was also observed in [3]. We note that the strong gradient of the SUPG solution in the layer is preserved by the shock-capturing technique. This underlines its proper construction.

Example 3.2. Now we study the performance properties of the schemes for the nonstationary counterpart of Example 3.1; cf. [3, Sec. 7]. We consider (1) on $\Omega = (0,1)^2$. We put $a = 10^{-6}$, $\boldsymbol{b}(\boldsymbol{x}) = (2,3)^\top$ and $r(u) = u^2$. The given solution with corresponding right-hand side f is $u(\boldsymbol{x},t) = 16\sin(\pi t)x_1(1-x_1)x_2(1-x_2)\cdot\left[0.5 + \pi^{-1}\arctan\left(2a^{-\frac{1}{2}}(0.25^2 - (x_1 - 0.5)^2 - (x_2 - 0.5)^2)\right)\right]$. Now the hump changes its height in time. We use the time step size $\Delta t = 10^{-3}$. The final time is $T = 1.0$. The finite element mesh size is $h = 5.52\text{e-}3$. In Table 2 we present $\|e_h\|_{L^\infty(L^2)} := \|e_h\|_{L^\infty(0,T;L^2(\Omega))}$, $e_h := u - u_h$, and var(t) $:= \max_{(x,y)\in\Omega} u_h(x_1,x_2,t) - \min_{(x,y)\in\Omega} u_h(x_1,x_2,t)$, where the maximum and minimum were computed in the degrees of freedom of the mesh cells. The numbers $\|e_h\|_{L^\infty(L^2)}$ give some indication of the accuracy of the methods whereas var(t) measures the size of the spurious oscillations. Here we use the variation of the discrete solution at $t = 0.5$ (maximal height of the hump). The value for u is var(0.5) $= 0.997453575$. In Fig. 2 we further visualize the computed profiles of the solution for $t = 0.5$.

Similarly to the stationary case, a positive impact on the accuracy is obtained by using higher order finite element methods together with SUPG and shock-capturing stabilization. Oscillations close to the layer are completely eliminated. The profiles of the numerical solutions show oscillations behind the hump in the direction of convection. They are damped by higher order approaches. If fourth order finite elements are used, they vanish almost completely. In [3], all schemes show significant oscillations behind the hump.

Table 2 Results with SUPG and shock-capturing stabilization for Example 3.2

p	$\|e_h\|_{L^\infty(L^2)}$	var(0.5)	p	$\|e_h\|_{L^\infty(L^2)}$	var(0.5)
1	2.8090e-2	1.2088	3	6.3204e-3	1.0319
2	1.3973e-2	1.1019	4	4.5312e-3	1.0203

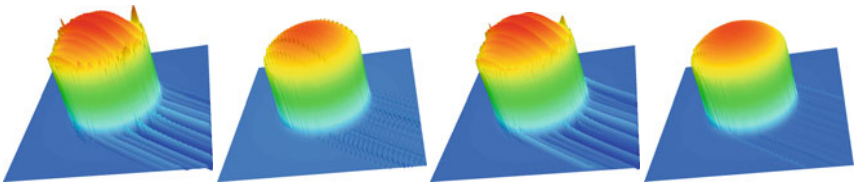

Fig. 2 Profile of the computed solution at $t = 0.5$ without ($p = 1$, $p = 4$) and with shock-capturing stabilization ($p = 1$, $p = 4$) for Example 3.2 with $h = 5.52\text{e-}3$; *from left to right*

References

1. M. Bause, *Stabilized higher-order finite element approximation of nonstationary and nonlinear convection-diffusion-reaction equations*, to appear (2010), 1–32.
2. R. Codina, O. Soto, *Finite element implementation of two-equation and algebraic stress turbulence models for steady incompressible flows*, Int. J. Numer. Methods. Fluids, **90** (1999), 309–343.
3. V. John, E. Schmeyer, *Finite element methods for time-dependent convection-diffusion-reaction equations with small diffusion*, Comput. Methods Appl. Mech. Engrg., **198** (2008), 475–494.
4. G. Lube, G. Rapin, *Residual-based stabilized higher order FEM for advection-dominated problems*, Comput. Methods Appl. Mech. Engrg., **195** (2006), 4124–4138.
5. T. Knopp, G. Lube, G. Rapin, *Stabilized finite element methods with shock capturing for advection-diffusion problems*, Comput. Methods Appl. Mech. Engrg., **191** (2002), 2997–3013.
6. A. Schmidt, K. G. Siebert, *Design of Adaptive Finite Element Software*, Springer, Berlin, 2005.
7. C. Schwab, *p- and hp-Finite Element Methods*, Clarendon Press, Oxford, 1998.
8. K. Schwegler, *Stabilized finite element methods for non-stationary non-linear convection-diffusion-reaction models*, Diploma Thesis, University of Erlangen-Nuremberg, Erlangen, 2010.
9. R. Temam, *Navier–Stokes Equations*, North-Holland, Amsterdam, 1984.

Numerical Approximation of Convection-Diffusion Problems Through the PSI Method and Characteristics Method

M. Benítez García, T. Chacón Rebollo, M. Gómez Mármol, and G. Narbona-Reina

Abstract In this work we present some numerical methods for solving evolutive convection-diffusion problems. In order to obtain a physically admissible solution we search for monotone and accurate methods that are also non-linear due to the Godunov's theorem. We will center in Fluctuation Splitting methods, [8], in particular in PSI scheme, and characteristic type methods, where a new Lagrangian method is proposed. Finally, a numerical test is presented to assess the performance of the numerical methods described in the present work.

Keywords Convection-diffusion equation · Characteristics method · Fluctuation splitting schemes · Galerkin discretization

1 Introduction

In this work we consider the following evolutive convection-diffusion problem:

$$\begin{cases} \dfrac{\partial \phi}{\partial t} + \mathbf{v} \cdot \operatorname{grad} \phi - \nu \Delta \phi = f & \text{in } \Omega \times (0,T), \\ \phi = 0 & \text{on } \Gamma \times (0,T), \\ \phi(x,0) = \phi^0(x) & \text{in } \Omega, \end{cases} \tag{1}$$

M.B. García
Departamento de Matemática Aplicada, Universidade de Santiago de Compostela, Campus Sur s/n 15182 Santiago de Compostela
e-mail: marta.benitez@udc.es

T.C. Rebollo and M.G. Mármol
Departamento de Ecuaciones Diferenciales y Análisis Numérico, Universidad de Sevilla, C/Tarfia s/n, 41012 Sevilla
e-mail: chacon@us.es, macarena@us.es

G. Narbona-Reina (✉)
Departamento de Matemática Aplicada I, Universidad de Sevilla, Avda. Reina Mercedes 2, 41012 Sevilla
e-mail: gnarbona@us.es

C. Clavero et al. (eds.), *BAIL 2010 – Boundary and Interior Layers, Computational and Asymptotic Methods*, Lecture Notes in Computational Science and Engineering 81,
DOI 10.1007/978-3-642-19665-2_3,

where Ω is a bounded domain of $\mathbb{R}^d$, $d \geq 2$, with boundary Γ and $T > 0$. Also, $\mathbf{v} : \Omega \times (0,T) \longrightarrow \mathbb{R}^d$ is the convection vector field, $f : \Omega \times (0,T) \longrightarrow \mathbb{R}$ is the source term, $\phi^0 : \Omega \longrightarrow \mathbb{R}$ is the initial data and $\nu > 0$ is the diffusion coefficient. For simplicity we assume the transporting fluid to satisfy the no-slip condition so equivalently, we consider that the velocity field vanishes on the boundary.

Linear convection-diffusion equations model a variety of important problems from different fields of engineering and applied sciences. In many cases the diffusive term is much smaller than the convective one, giving rise to the so-called convection dominated problems. For convection-diffusion problems with dominant convection, methods of characteristics and the Fluctuation Splitting (FS) methods, for convective term discretization, are extensively used (see [6, 8, 11]).

Characteristics methods are based on time discretization of the material time derivative. For space discretization, they has been combined with finite differences [9], finite elements [4, 5, 10, 11], spectral finite elements [1], discontinuous finite elements [2], and so on. When combined with finite elements they are also called Lagrange-Galerkin methods. In particular, when the characteristic methods are formulated in Lagrangian coordinates (respectively, Eulerian coordinates) they are called Lagrangian methods (respectively, semi-Lagrangian methods). In the present work we will consider the combination of Lagrangian and semi-Lagrangian methods with a spatial discretization by using finite elements spaces.

One of the most successful nonlinear Fluctuation Splitting schemes is the PSI method, introduced in [8]. The PSI method is specifically designed to be exact for linear solutions of the pure transport equation. It is monotone and is particularly accurate in zones of strong gradients or discontinuities of the solution. In the present case, to approximate the equation in (1) we discretize the convection operator by the PSI scheme, the time derivative by a Crank-Nicolson scheme and the diffusion operator by the standard Galerkin method, using linear finite elements. In order to perform the theoretical analysis, the PSI method is formulated as a nonlinear finite element Petrov-Galerkin (see [6]), so the usual techniques are used to develop the existence, convergence and error estimates theory.

After the present section we introduce the PSI method applied to problem (1). In Sect. 3 a second order full Lagrangian characteristic method is proposed. Finally, to test the proposed methods, a numerical example is presented in Sect. 4 which has a solution developing a steep layer and a velocity field which is not divergence-free.

2 The PSI Method

The PSI method is one of the most advantageous FS schemes. Their main design idea is to split the element convective residual $R^T = \int_T \mathbf{v} \cdot \operatorname{grad} \phi$ between the nodes of the element that are downstream according to the velocity $\mathbf{v}$. This distribution is made through coefficients β_i^T such that $\beta_i^T R^T$ is the residual contribution of the element T to the node x_i. For consistency these coefficients must satisfy: $0 \leq \beta_i^T \leq 1$ and $\sum_i \beta_i^T = 1$. The way in which these constants are defined is

what distinguishes the different FS schemes. For the particular PSI method these coefficients are determined in order to exactly solve the stationary pure transport equation.

We assume Ω to be a polygonal or polyhedral domain and consider a triangulation $\mathcal{T}_h$ of Ω by triangles in 2D and tetrahedra in 3D. We define the finite-dimensional space of piecewise affine finite elements built on $\mathcal{T}_h$:

$$V_h^1 = \left\{\varphi_h \in C^0(\overline{\Omega}) :\ \varphi_{h|_T} \in P_1(T),\ \forall T \in \mathcal{T}_h,\ v_h = 0 \text{ on } \Gamma\right\}.$$

We use the PSI method just to discretize the convective part. For this aim the test functions corresponding to this term are taken from a new space of piecewise constant functions W_h directly related to the flux distribution coefficients β_i^T. We introduce an interpolation operator Π_{ϕ_h} from V_h^1 onto the space W_h, in particular we have $\Pi_{\phi_h}\varphi_h = \sum_i \varphi_h(x_i)\beta_i^T(\phi_h)$ (see [6] for more details). Notice that it depends on the unknown ϕ_h due to the non-linear nature of the PSI method.

We introduce the number of time steps, N, the time step $\Delta t = T/N$, and the mesh-points, $t_n = n\Delta t$ for $n = 0, 1/2, 1, \ldots, N$. Next, we define the form $a_h^n : V_h^1 \times V_h^1 \longrightarrow \mathbb{R}$ for $0 \le n \le N$ as

$$a_h^n(\phi_h, \psi_h) = \int_\Omega (\overline{\mathbf{v}}^n \cdot \operatorname{grad}\phi_h)\Pi_{\phi_h}\psi_h + \nu \int_\Omega \operatorname{grad}\phi_h \cdot \operatorname{grad}\psi_h \tag{2}$$

being $\overline{\mathbf{v}}_{|_T} = \dfrac{1}{|T|}\displaystyle\int_T \mathbf{v}\, dx$, $\forall T \in \mathcal{T}_h$. Here, the time discretization scheme we are going to consider is a Crank-Nicholson-like scheme. It arises from approximating the time derivative at $t = t_{n+\frac{1}{2}}$, for $0 \le n \le N-1$, by a centered formula and using a second order interpolation formula involving values at $t = t_n$ and $t = t_{n+1}$ to approximate the rest of the terms at the same time $t = t_{n+\frac{1}{2}}$.

Thus, we have the following discrete variational approximation of (1)

$$\begin{cases} \text{Given } \phi_{\Delta t,h}^0 \in V_h^1,\ \text{find } \widehat{\phi_{\Delta t,h}} = \{\phi_{\Delta t,h}^n\}_{n=1}^N \in \left[V_h^1\right]^N \text{ such that} \\ \displaystyle\int_\Omega \frac{\phi_{\Delta t,h}^{n+1} - \phi_{\Delta t,h}^n}{\Delta t}\psi_h\, dx + \frac{1}{2}\left(a_h^{n+1}(\phi_{\Delta t,h}^{n+1}, \psi_h) + a_h^n(\phi_{\Delta t,h}^n, \psi_h)\right) \\ = \dfrac{1}{2}\displaystyle\int_\Omega \left(f^{n+1} + f^n\right)\psi_h\, dx,\ \forall \psi_h \in V_h^1,\ \text{for } n = 0, \ldots, N-1. \end{cases} \tag{3}$$

In practice, to eliminate the nonlinearity of convective term we use the following approximation

$$\int_\Omega (\overline{\mathbf{v}}^{n+1} \cdot \operatorname{grad}\phi_{\Delta t,h}^{n+1})\Pi_{\phi_{\Delta t,h}^{n+1}}\psi_h \simeq \int_\Omega (\overline{\mathbf{v}}^{n+1} \cdot \operatorname{grad}\phi_{\Delta t,h}^{n+1})\Pi_{\phi_{\Delta t,h}^{n}}\psi_h.$$

Notice that due to the use of the PSI method to discretize the convective term, the approximate problem (3) is written under a Petrov-Galerkin formulation. Is just this

writing what allows us to develop the theoretical analysis of the discrete problem by using the tools of functional analysis adapted to this kind of formulation.

In [6] the PSI method combined with piecewise linear finite elements is presented and analyzed for steady convection-diffusion equations. The authors perform a convergence, error and maximum principle analysis. In particular, it is proved that the scheme is first-order accurate in H^1 norm and well-balanced up to second order for convection-dominated flows.

3 Characteristics Method

In this section we consider a second order characteristics scheme combined with quadratic finite elements for discretization of (1). We denote by X_e the motion corresponding to the velocity $\mathbf{v}$ and P its reference map, and define the material description Ψ_m of a spatial field Ψ by

$$\Psi_m(p,t) = \Psi(X_e(p,t),t). \tag{4}$$

We recall that, according to the standard formalism of continuum mechanics, $x = X(p,t)$ is the position at time t of the material point p, while the reference map $P(x,t)$ yields the material point located at position x at time t. We assume that $X_e(p,0) = p$, $\forall p \in \overline{\Omega}$. We are going to write the problem (1) in Lagrangian coordinates p. For this, we introduce the change of variable $x = X_e(p,t)$ and use the chain rule, obtaining (see [3])

$$\begin{cases} \dot{\phi}_m \det F - \nu \operatorname{Div}\left[F^{-1}F^{-T}\nabla\phi_m \det F\right] = f_m \det F & \text{in } \Omega\times(0,T), \\ \phi_m = 0 & \text{on } \Gamma\times(0,T), \\ \phi_m(p,0) = \phi^0(p) & \text{in } \Omega, \end{cases} \tag{5}$$

being $F(\cdot,t)$ the Jacobian matrix of the deformation $X_e(\cdot,t)$. The time discretization scheme we are going to consider is a Crank-Nicholson-like scheme. It arises from approximating the material time derivative at $t = t_{n+\frac{1}{2}}$, for $0 \le n \le N-1$, by a centered formula and using a second order interpolation formula involving values at $t = t_n$ and $t = t_{n+1}$ to approximate the rest of the terms at the same time $t = t_{n+\frac{1}{2}}$.

Regarding the space discretization we use the piecewise quadratic finite elements space. We consider the finite-dimensional spaces of piecewise quadratic finite elements built on $\mathcal{T}_h$:

$$V_h^2 = \left\{\varphi_h \in C^0(\overline{\Omega}) :\ \varphi_{h|_T} \in P_2(T),\ \forall T \in \mathcal{T}_h,\ \varphi_h = 0 \text{ on } \Gamma\right\}.$$

Thus, we have the following discrete variational approximation of (5)

$$\begin{cases} \text{Given } \phi^0_{m,\Delta t,h} \in V_h^2, \text{ find } \widehat{\phi_{m,\Delta t,h}} = \{\phi^n_{m,\Delta t,h}\}_{n=1}^N \in \left[V_h^2\right]^N \text{ such that} \\ \dfrac{1}{2}\displaystyle\int_\Omega \left(\det F^{n+1} + \det F^n\right) \dfrac{\phi^{n+1}_{m,\Delta t,h} - \phi^n_{m,\Delta t,h}}{\Delta t}\psi_h \\ + \dfrac{\nu}{4}\displaystyle\int_\Omega ([F^{-1}F^{-T}\det F]^{n+1} + [F^{-1}F^{-T}\det F]^n) \\ \qquad (\nabla\phi^{n+1}_{m,\Delta t,h} + \nabla\phi^n_{m,\Delta t,h})\cdot\nabla\psi_h \\ = \displaystyle\int_\Omega \dfrac{\det F^{n+1} f^{n+1}_m + \det F^n f^n_m}{2}\psi_h, \ \forall\psi_h \in V_h^2, \text{ for } n = 0,\dots,N-1. \end{cases} \tag{6}$$

Since usually the characteristic curves cannot be exactly computed, in practice, we replace in (6) the exact characteristic curves and gradient tensors by accurate enough approximations. More precisely, we use a second order Runge–Kutta approximation of X_e. Moreover, in order to obtain an approximate solution of ϕ^n in Eulerian coordinates, we are going to calculate the spatial description of material field $\phi^n_{m,\Delta t,h}$. More precisely, we calculate $\widehat{\phi_{\Delta t,h}} \sim \widehat{\phi}$ as follows

$$\phi^n_{\Delta t,h}(x) := \phi^n_{m,\Delta t,h}(P^n_{RK}(x)) \quad \forall x \in \overline{\Omega},\ 0 \le n \le N, \tag{7}$$

being P^n_{RK} the second order Runge–Kutta approximation of P^n.

Thus, we shall denote this Lagrangian method by $(\mathcal{LG})_2$. Furthermore, we shall denote by $(\mathcal{SLG})_2^1$ the semi-Lagrangian scheme analogous to $(\mathcal{LG})_2$, but re-initializing the transformation to the identity at the beginning of each time step (see [3] for more details).

In [3] the Lagrange Galerkin method (6) with a second order Runge–Kutta approximation of X_e is analyzed for a more general problem. A $l^\infty(L^2)$ stability inequality is stated and $l^\infty(L^2)$ error estimates of order $O(\Delta t^2) + O(h^2)$ are obtained; these estimates are uniform in the hyperbolic limit. More precisely, for Δt small enough, the following estimate is obtained:

$$\left|\left|\widehat{\phi_m - \phi_{m,\Delta t,h}}\right|\right|_{l^\infty(L^2(\Omega))} + \sqrt{\nu}\left|\left|\widehat{\mathcal{S}[\nabla\phi_m - \nabla\phi_{m,\Delta t,h}]}\right|\right|_{l^2(\mathbf{L}^2(\Omega))} \le J_1(\Delta t^2 + h^2), \tag{8}$$

where $\widehat{\mathcal{S}[\psi]} := \{\psi^{n+1} + \psi^n\}_{n=0}^{N-1}$ for a sequence $\widehat{\psi} = \{\psi\}_{n=0}^N$. Here, J_1 is bounded in the hyperbolic limit. In particular, this result is also valid when $\nu = 0$. Furthermore, stability and error estimates of order $O(\Delta t^2) + O(h^2)$ are proved in the $l^\infty(H^1)$-norm. More precisely, the following estimate is obtained:

$$\left|\left|\widehat{\mathcal{R}_{\Delta t}[\phi_m - \phi_{m,\Delta t,h}]}\right|\right|_{l^2(L^2(\Omega))} + \sqrt{\nu}\left|\left|\widehat{\nabla\phi_m - \nabla\phi_{m,\Delta t,h}}\right|\right|_{l^\infty(\mathbf{L}^2(\Omega))} \le J_2(\Delta t^2 + h^2), \tag{9}$$

where $\widehat{\mathcal{R}_{\Delta t}[\psi]} := \left\{ \dfrac{\psi^{n+1} - \psi^n}{\Delta t} \right\}_{n=0}^{N-1}$ for a sequence $\widehat{\psi} = \{\psi\}_{n=0}^{N}$. Here, J_2 does not depend on ν. From these estimates and by using appropriate changes of variable, analogous estimates in Eulerian coordinates are deduced.

4 Numerical Results

We consider the following example to compare the numerical results obtained with semi-Lagrangian, (full) Lagrangian methods and the PSI method.

The spatial domain is $\Omega = (0,1) \times (0,1)$, $T = 1$, and $\mathbf{v} = \nabla\psi$, $\nu = \sigma_1$, $f = 0$, being $\psi = (1-cos(2\pi x_1))(1-cos(2\pi x_2))$ and $\sigma_1 = 0.001$. The initial data varies between $\phi^0(0,0) = 0$ and $\phi^0(1,1) = 1$ according to the following expression:

$$\phi^0(x_1, x_2) = \begin{cases} 0 & \text{if } \xi < 0, \\ \frac{1}{2}(1 - cos(\pi\xi)) & \text{if } 0 \le \xi \le 1, \\ 1 & \text{if } 1 < \xi, \end{cases} \tag{10}$$

where $\xi = x_1 + x_2 - 1/2$. We impose Dirichlet boundary conditions given by the initial data. In Fig. 1 we plot the velocity field and the initial data. This example has been solved in [7] with a semi-Lagrangian method combined with a discontinuous Galerkin discretization, and also with a standard Galerkin scheme. The Gibbs phenomena is observed for both methods. The oscillations produced by the standard Galerkin scheme are observed even far from the transition layer.

Here we solve this problem with the Lagrangian method $(\mathcal{LG})_2$, the semi-Lagrangian scheme $(\mathcal{SLG})_2^1$ and with the PSI scheme given by (3).

In Figs. 2, 3 and 4 we represent the numerical solution contours at final time $T = 1$ and the section $x_1 \longrightarrow \phi_{\Delta t,h}^N(x_1, 1/2)$, computed by using the $(\mathcal{SLG})_2^1$, $(\mathcal{LG})_2$ and PSI methods, respectively. The semi-Lagrangian method presents

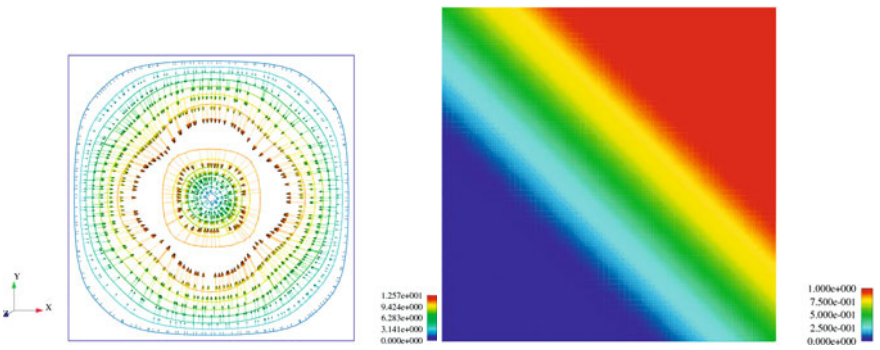

Fig. 1 Velocity field (*left*) and initial date (*right*)

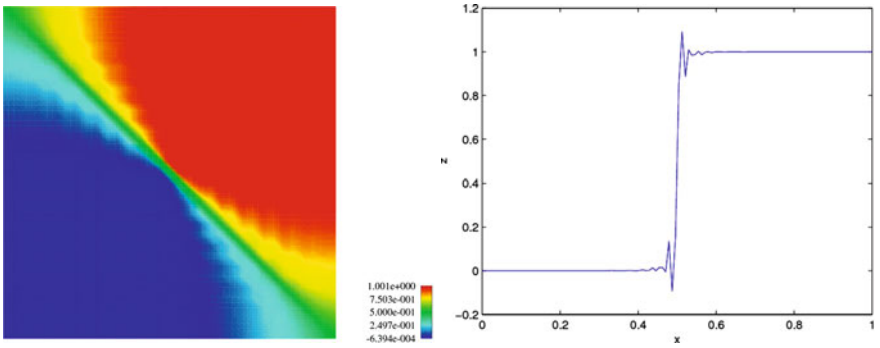

Fig. 2 Numerical solution contours at $T = 1$ (*left*) and the section $x_1 \longrightarrow \phi^N_{\Delta t,h}(x_1, 1/2)$ (*right*) for the $(\mathcal{SLG})^1_2$ scheme, $h = 1/16$, $\Delta t = 1/60$

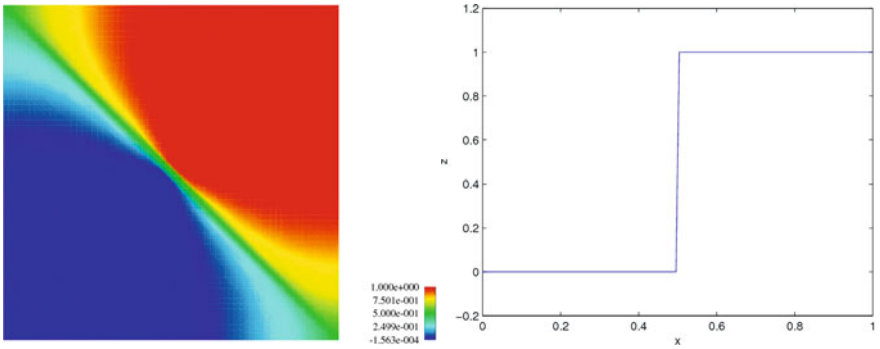

Fig. 3 Numerical solution contours at $T = 1$ (*left*) and the section $x_1 \longrightarrow \phi^N_{\Delta t,h}(x_1, 1/2)$ (*right*) for the $(\mathcal{LG})_2$ scheme, $h = 1/16$, $\Delta t = 1/60$

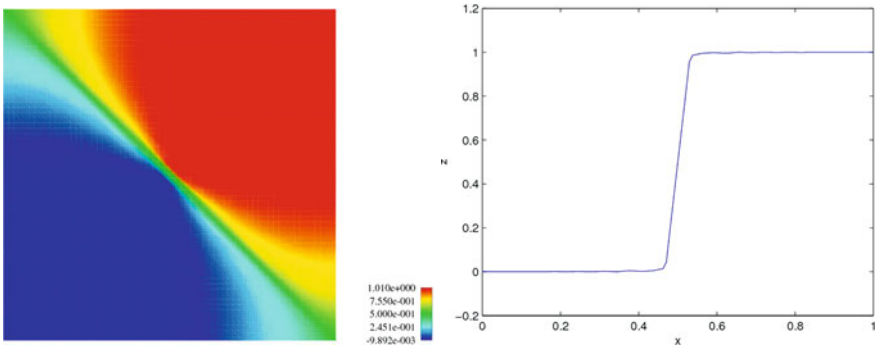

Fig. 4 Numerical solution contours at $T = 1$ (*left*) and the section $x_1 \longrightarrow \phi^N_{\Delta t,h}(x_1, 1/2)$ (*right*) for the $(\mathcal{PSI})$ scheme, $h = 1/32$, $\Delta t = 1/60$

oscillations near the transition layer, so Gibbs phenomena is observed, while the Lagrangian method and the PSI scheme are accurate even in the steep layer around the diagonal. These features can be observed on the plots of the sections.

So we can conclude that for obtaining a physically acceptable solution, both $(\mathcal{LG})_2$ and PSI can be used. In order to compare them, we can say that although $(\mathcal{LG})_2$ is less diffusive than PSI, it is also computationally more expensive (see [3]).

Acknowledgements The research of T. Chacón Rebollo, M. Gómez Mármol y M. Benítez García to carry on this work was partially supported by the "Proyecto de Excelencia de la Junta de Andalucía P07-FQM-02538".

References

1. Baker, M.D., Suli, E., Ware, A.F.: Stability and convergence of the spectral Lagrange-Galerkin method for mixed periodic/non-periodic convection-dominated diffusion problems. IMA J. Numer. Anal., **19**, 637–663 (1999)
2. Baranger, J., Machmoum A.: A "natural" norm for the method of characteristics using discontinuous finite elements: 2D and 3D case. Math. Model. Numer. Anal., **33**, 1223–1240 (1999)
3. Benítez, M.: Métodos numéricos para problemas de convección difusión. Aplicación a la convección natural. MA Thesis, Universidade Santiago de Compostela, http://dl.dropbox.com/u/14459353/tesis_benitez.pdf, (2009)
4. Bercovier, M., Pironneau, O., Sastri V.: Finite elements and characteristics for some parabolic-hyperbolic problems. Appl. Math. Modelling, **7**, 89–96 (1983)
5. Bermúdez, A., Durany, J.: Numerical solution of steady-state flow through a porous dam. Comput. Methods Appl. Mech. Engrg., **68**, 55–65 (1988)
6. Chacón, T., Gómez, M., Narbona, G.: Numerical analysis of the PSI solution of advection-diffusion problems through a Petrov-Galerkin formulation. Math. Models Meth. Appl. Sci., **17**, 1905–1936 (2007)
7. Chrysafinos, K.,Walkington, N. J.: Lagrangian and moving mesh methods for the convection diffusion equation. M2AN Math. Model. Numer. Anal., **42**, 25–55 (2008)
8. Deconinck, H., Struijs, R., Bourgeois, P., Roe, P.L.: Compact advection schemes on unstructed meshes. Comput. Fluid Dynamics: VKI Lecture Series (1993)
9. Douglas, J., Russell, T.F.: Numerical methods for convection-dominated diffusion problems based on combining the method of characteristics with finite element or finite difference procedures. SIAM J. Numer. Anal., **19**, 871–885 (1982)
10. Morton, K.W., Priestley, A., Süli, E.: Stability of the Lagrange-Galerkin Method with non-exac integration. M2AN Math. Model. Numer. Anal., **22**, 625–653 (1998)
11. Pironneau, O.: On the Transport-Diffusion Algorithm and Its Applications to the Navier-Stokes Equations. Numer. Math., **38**, 309–332 (1982)

On Novel Properties of Multimode Boundary Conditions in Electromagnetism and Their Consequences

J.M.L. Bernard

1 Introduction

In electromagnetism, a surface composed of a homogeneous planar substrate on a perfectly reflecting plane can be modelled by boundary layer method as a plane which satisfies surface boundary conditions with high order normal derivatives of the field (Fig. 1):

$$\prod_{j=1}^{N} \left(\frac{\partial}{\partial z} - ikg_j\right) u_{tot}|_{z=0} = 0 \tag{1}$$

where u is some components of the fields.

It can be shown that, in case of a metamaterial substrate having both a permittivity and a permeability with negative real parts, the roots of the characteristic equation have exceptional positions in the complex plane, which implies particular properties of the field for point source (dipole) illumination. The roots $g_i = \sin\theta_i$ for left-handed multilayer metamaterials with ϵ and μ of negative real parts can be in the domain $\mathrm{Re}\, g < 0$ with $\mathrm{Re}(ik\cos\theta_i) < 0$, which implies we go through the branch-cut of the solution as we come from the common case where ϵ and μ are with positive real parts. Thus, new general expressions are necessary (Fig. 2).

When $\theta_i \in \Omega_g^{\varphi}$, we notice for example the presence of some particular waves with a $e^{ikR\sin(\theta_i+\varphi)}$ term in the expression of the field that we don't encounter for ϵ and μ positive (for common material only leaky waves with $e^{ikR\sin(\theta_i-\varphi)}$ for large R are present). New exact closed form expressions of the field derived in [1], which permit to exhibit these properties, are now presented.

J.M.L. Bernard
CEA-DIF, DAM, 91297 Arpajon, France
and
LRC MESO, CMLA, ENS Cachan, 61 av. du Prés. Wilson, 94235, France
e-mail: jean-michel.bernard@cea.fr

C. Clavero et al. (eds.), *BAIL 2010 – Boundary and Interior Layers, Computational and Asymptotic Methods*, Lecture Notes in Computational Science and Engineering 81,
DOI 10.1007/978-3-642-19665-2_4,

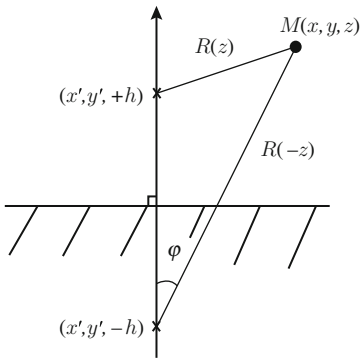

Fig. 1 geometry for the radiation at M of a point source at $z = h$

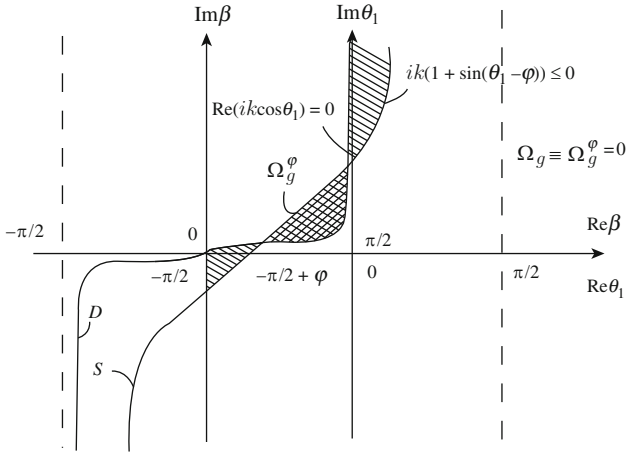

Fig. 2 definition of branch-cut $Re(ik\cos\theta_i)$

2 Formulation of the Problem

The problem can be reduced for a large class of multimode boundary conditions. Following R.F. Harrington [2] in 1961 (see also Jones [3] in 1964), we can write the electric field E and the magnetic field H satisfying the Maxwell equations, with two scalar potentials $\mathcal{E}$ and $\mathcal{H}$, following

$$\begin{aligned} E &= -ik\,\mathrm{rot}(\mathcal{H}\hat{z}) + (\mathrm{grad}(\mathrm{div}(.)) + k^2)(\mathcal{E}\hat{z}) \\ \sqrt{\frac{\mu_0}{\epsilon_0}}H &= ik\,\mathrm{rot}(\mathcal{E}\hat{z}) + (\mathrm{grad}(\mathrm{div}(.)) + k^2)(\mathcal{H}\hat{z}) \end{aligned} \tag{2}$$

where $(\Delta + k^2)\mathcal{E} = 0$ and $(\Delta + k^2)\mathcal{H} = 0$ outside the sources, with $k = \omega\sqrt{\mu_0\epsilon_0}$, the constants ϵ_0 and μ_0 being respectively the permittivity and the permeability of the medium above the plane.

Thereafter, we denote $(\mathcal{E}_{inc}, \mathcal{H}_{inc})$ and $(\mathcal{E}_s, \mathcal{H}_s)$ the potentials corresponding to the incident field and the scattered field, and write $(E, \sqrt{\frac{\mu_0}{\epsilon_0}} H)(z) = \mathcal{L}(\widehat{z}\mathcal{E}, \widehat{z}\mathcal{H})(z)$. We then consider the class of multimode boundary conditions on an isotropic plane,

$$\prod_{j=1}^{N} (\frac{\partial}{\partial z} - ikg_j^e) E_{z,tot}|_{z=0} = 0, \prod_{j=1}^{P} (\frac{\partial}{\partial z} - ikg_j^h) H_{z,tot}|_{z=0} = 0, \tag{3}$$

which corresponds to the reflection coefficients for the principal polarizations TM (components of electric field E in the plane of incidence) and TE (components of magnetic field H in the plane of incidence), given by,

$$R_{TM}(\varphi) = \prod_{j=1}^{N} \frac{\cos\varphi - g_j^e}{\cos\varphi + g_j^e}, R_{TE}(\varphi) = \prod_{j=1}^{P} \frac{\cos\varphi - g_j^h}{\cos\varphi + g_j^h}, \tag{4}$$

where φ is the angle of observation with the normal $\widehat{z}$. This class of problem corresponds to the reflection by a substrate with different layers composed of isotropic media, or more generally, of uniaxial anisotropic media with principal axis along z. From the symmetry at normal incidence, we notice that the condition

$$R_{TE}(0) = -R_{TM}(0) \text{ i.e. } \prod_{j=1}^{N} \frac{1 - g_j^e}{1 + g_j^e} = -\prod_{j=1}^{P} \frac{1 - g_j^h}{1 + g_j^h}, \tag{5}$$

is satisfied, which implies, for monomode conditions ($N = P = 1$), that $g_1^{(e,h)} = 1/g_1^{(h,e)}$.

Following the boundary conditions on the field, we can then choose to search the two scalar potentials $\mathcal{E}_s$ and $\mathcal{H}_s$, satisfying the Helmholtz equation as $z > 0$, regular and vanishing as $z \to \infty$ when $|\arg(ik)| < \pi/2$, which satisfy

$$\begin{aligned} \prod_{i=1}^{N} (\frac{\partial}{\partial z} - ikg_j^e) \mathcal{E}_s(z) &= \prod_{j=1}^{N} (\frac{\partial}{\partial z} + ikg_j^e) \mathcal{E}_{inc}(-z) \\ \prod_{j=1}^{P} (\frac{\partial}{\partial z} - ikg_j^h) \mathcal{H}_s(z) &= \prod_{j=1}^{P} (\frac{\partial}{\partial z} + ikg_j^h) \mathcal{H}_{inc}(-z) \end{aligned} \tag{6}$$

A compact expression of $\mathcal{E}_{inc}$ and $\mathcal{H}_{inc}$, first necessary, is presented.

3 An Expression of Potentials $(\mathcal{E}_s, \mathcal{H}_s)$ for Arbitrary Source

3.1 The Determination of $(\mathcal{E}_{inc}, \mathcal{H}_{inc})$

Let us consider the incident field (E, H) at r of coordinates (x, y, z), radiated by arbitrary bounded sources J and M [3],

$$E = \mathrm{rot}(G * M) + \frac{i}{\omega\epsilon_0}(\mathrm{grad}(\mathrm{div}(.)) + k^2)(G * J)$$
$$\sqrt{\frac{\mu_0}{\epsilon_0}}H = -\sqrt{\frac{\mu_0}{\epsilon_0}}\mathrm{rot}(G * J) + \frac{i}{k}(\mathrm{grad}(\mathrm{div}(.)) + k^2)(G * M) \qquad (7)$$

where $G = -\frac{e^{-ik\sqrt{\rho^2+z^2}}}{4\pi\sqrt{\rho^2+z^2}}$ with $\rho = \sqrt{x^2+y^2}$, and $*$ is the convolution product. and we search the scalar potentials $\mathcal{E}_{inc}$ and $\mathcal{H}_{inc}$, satisfying the Helmholtz equation as $\pm z > 0$ and vanishing at infinity when $|\arg(ik)| < \pi/2$ as $\pm z \to \infty$.

After some particular calculation given in [1], we derive an original expression of $(\mathcal{E}_{inc},\mathcal{H}_{inc})$.

Proposition 1. *A definite expression of the potentials $\mathcal{E}_{inc}$ and $\mathcal{H}_{inc}$ in the region $\pm z > 0$, for the field radiated by arbitrary bounded sources J and M in the domain $\mp z > 0$, $|\arg(ik)| \le \pi/2$ is given by*

$$(\mathcal{E}_{inc}, \mathcal{H}_{inc}) = \frac{\widehat{z}}{8\pi k^2}(\sqrt{\frac{\mu_0}{\epsilon_0}}(grad(div(J)) + k^2 J, ik\ rot(J)) +$$
$$+ (-ik\ rot(M), grad(div(M)) + k^2 M)) * \mathcal{W}, \qquad (8)$$

where

$$\mathcal{W}(r) = (e^{ik|z|}E_1(ik(|r|+|z|)) + e^{-ik|z|}(E_1(ik(|r|-|z|)) + 2\ln\rho)) \qquad (9)$$

with $|r| = \sqrt{\rho^2+z^2}$, $\rho = \sqrt{x^2+y^2}$ at $r(x,y,z)$, E_1 being the exponetial integral [4].

3.2 Expression of the Potentials $(\mathcal{E}_s, \mathcal{H}_s)$ for a Multimode Plane

We have obtained an expression for the potentials $(\mathcal{E}_{inc}, \mathcal{H}_{inc})$ attached to the radiation of arbitrary sources, and we can now present the scalar potentials $\mathcal{E}_s$ and $\mathcal{H}_s$ given in [1]

Proposition 2. *The potentials $\mathcal{E}_s(r)$ and $\mathcal{H}_s(r)$ at $r(x,y,z)$, for arbitrary bounded sources J and M above the multimode plane, $|\arg(ik)| \le \pi/2$, verify as $z \ge 0$,*

$$\mathcal{E}_s(z) = \mathcal{E}_{inc}(-z) + ((\frac{\widehat{z}}{\omega\epsilon_0}\frac{grad(div(J)) + k^2 J}{8\pi k} + \frac{\widehat{z}}{k}\frac{(-ik\ rot(M))}{8\pi k}) *$$
$$* \sum_{\epsilon=-1,1}\sum_{j=1}^{N}\frac{a_j^e}{(g_j^e - \epsilon)}(\mathcal{V}_\epsilon + \epsilon\mathcal{K}_{g_j^e}))(-z)$$

$$= \mathcal{E}_{inc}(-z) + ((\frac{\widehat{z}}{\omega\epsilon_0}\frac{grad(div(J)) + k^2 J}{8\pi k} + \frac{\widehat{z}}{k}\frac{(-ik\ rot(M))}{8\pi k}) *$$
$$* \sum_{\epsilon=-1,1}((\prod_{j=1}^{N}\frac{\epsilon + g_j^e}{\epsilon - g_j^e} - 1)\mathcal{V}_\epsilon + \sum_{j=1}^{N}\frac{\epsilon a_j^e \mathcal{K}_{g_j^e}}{(g_j^e - \epsilon)}))(-z) \tag{10}$$

and

$$\mathcal{H}_s(z) = \mathcal{H}_{inc}(-z) + ((\frac{\widehat{z}}{\omega\epsilon_0}\frac{(ik\ rot(J))}{8\pi k} + \frac{\widehat{z}}{k}\frac{(grad(div(M)) + k^2 M)}{8\pi k})*$$
$$* \sum_{\epsilon=-1,1}\sum_{j=1}^{P}\frac{a_j^h}{(g_j^h - \epsilon)}(\mathcal{V}_\epsilon + \epsilon\mathcal{K}_{g_j^h}))(-z)$$
$$= -\mathcal{H}_{inc}(-z) + ((\frac{\widehat{z}}{\omega\epsilon_0}\frac{(ik\ rot(J))}{8\pi k} + \frac{\widehat{z}}{k}\frac{(grad(div(M)) + k^2 M)}{8\pi k})*$$
$$* \sum_{\epsilon=-1,1}((\prod_{j=1}^{P}\frac{\epsilon + g_j^h}{\epsilon - g_j^h} + 1)\mathcal{V}_\epsilon + \sum_{j=1}^{P}\frac{\epsilon a_j^h \mathcal{K}_{g_j^h}}{(g_j^h - \epsilon)}))(-z) \tag{11}$$

where $\mathcal{V}_\epsilon$, $\mathcal{K}_g$ *and the* $a_j^{e,h}$ *satisfy*

$$\mathcal{V}_\epsilon(z) = e^{-\epsilon ikz}(E_1(ik(|r| - \epsilon z)) + (1 - \epsilon)\ln\rho),\ \mathcal{K}_g(z) = e^{-ikgz}\mathcal{J}_g(z)$$
$$\prod_{j=1}^{N,P}\frac{\cos\beta - g_j^{e,h}}{\cos\beta + g_j^{e,h}} = 1 + \sum_{j=1}^{N,P}a_j^{e,h}\frac{1}{\cos\beta + g_j^{e,h}}\ ,\ \frac{a_j^{e,h}}{2g_j^{e,h}} = -\prod_{i\neq j}^{N,P}\frac{g_j^{e,h} + g_i^{e,h}}{g_j^{e,h} - g_i^{e,h}}$$
$$with\ \prod_{j=1}^{N}\frac{\epsilon + g_j^e}{\epsilon - g_j^e} = -\prod_{j=1}^{P}\frac{\epsilon + g_j^h}{\epsilon - g_j^h} \tag{12}$$

This is a very compact form for arbitrary J and M (sources above the plane), where the special functions to calculate are only $\mathcal{J}_{g_j^{e,h}}$ and $\partial_\rho\mathcal{J}_{g_j^{e,h}}$ in complex plane.

4 A Correct Definition of the Expression of $\mathcal{J}_g$ for Arbitrary g in Complex Plane, and Numerical Results

Proposition 3. *A correct definition of* $\mathcal{J}_g$ *for arbitrary* $g = \sin\theta_1$ *derived in [1] is given by*

$$\mathcal{J}_g(\rho, -z) = -\int_{-ib}^{\infty} e^{-a\cosh t}dt = i\int_{b}^{i\infty} e^{-a\cos\alpha}d\alpha \tag{13}$$

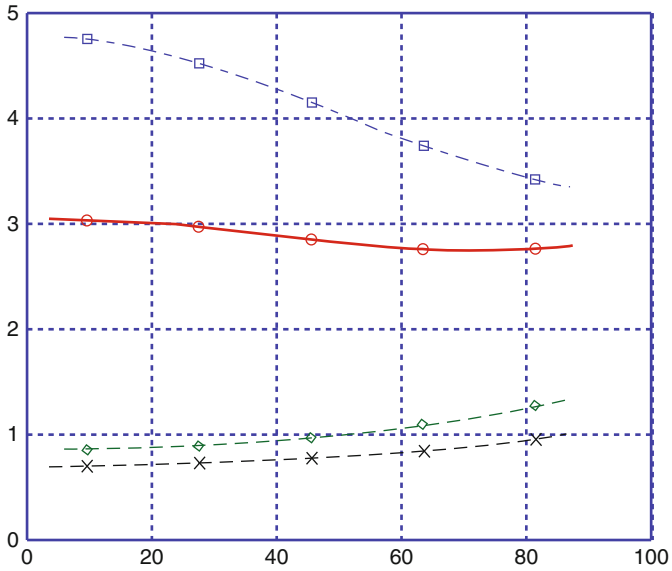

Fig. 3 Diagram of $\mathcal{I}_g = e^{ikgz}\mathcal{J}_g(\rho = R\sin\varphi, -z = -R\cos\varphi)$ for $kR = 1$

where $a = \epsilon ikR(-z)\sin\varphi\cos\theta_1$, $\epsilon = sign(Re(ik\cos\theta_1))$ *(*$Re(a) = 0$ *being considered as a limit case),* b *satisfies*

$$e^{\mp ib} = c_\pm = \frac{ikR(-z)}{a}(1 \pm \sin\theta_1)(1 \pm \cos\varphi), \tag{14}$$

and $\rho = R(-z)\sin\varphi, z = R(-z)\cos\varphi$. *Different novel expansions, taking account of the cut in complex plane are given in [1].*

We then give the absolute value of $\mathcal{J}$ as φ varies for $kR = 1$ (Fig. 3) and $kR = 3$ (Fig. 4), for different choices of g with $\mathrm{Re}g = -.3$ and $\mathrm{Im}g$ varying from $-.5$ to $+.5$., as we go through the cut. We notice the particular change of behaviour when we go through the branch cut of $\mathcal{J}_g$, $\mathrm{Re}(ik\cos\theta_i) = 0$ with $g = \sin\theta_i$, in the region $\mathrm{Re}g < 0$.

5 Conclusion

The high order impedance boundary conditions on metamaterials with negative permittivity ϵ and permeability μ imply exceptional new behaviour as we go through the branch cut in the expression of the field. New exact closed form expressions of the scattered potentials for arbitrary bounded sources J and M above

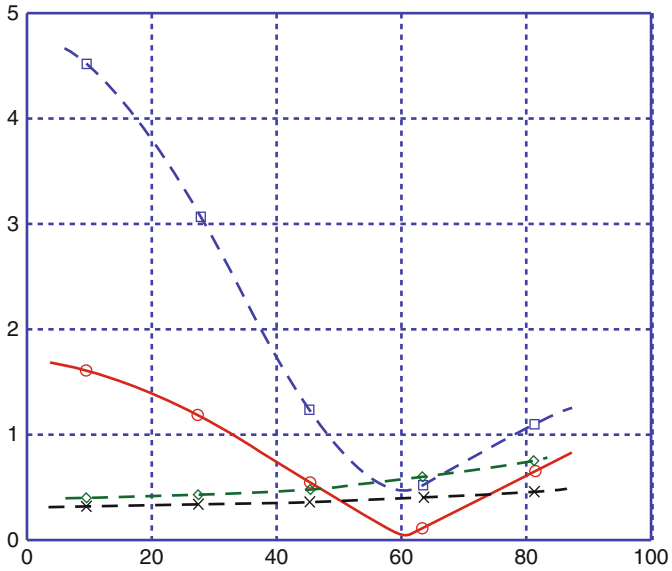

Fig. 4 Diagram of $\mathcal{I}_g = e^{ikgz}\mathcal{J}_g(\rho = R\sin\varphi, -z = -R\cos\varphi)$ for $kR = 3$, where *dashed line with diamond* an impedance mode $g = -0.3 - 0.5i$ (below the cut), *dashed line with cross* an impedance mode $g = -0.3 - 0.1i$ (below the cut), *dashed line with square* an impedance mode $g = -0.3 + 0.1i$ (above the cut), *dashed line with circle* an impedance mode $g = -0.3 + 0.5i$ (above the cut)

the imperfectly conducting plane are presented. Numerical results show the rapid change of behaviour as we cross the branch-cut of the solution.

References

1. J.M.L. Bernard, 'On the expression of the field scattered by a multimode plane', The Quarterly Journal of Mechanics and Applied Mathematics, pp. 237–266, 63, 3, 2010
2. R.F. Harrington, 'Time-harmonic electromagnetic field', Mc Graw-Hill Book, 1961.
3. D.S. Jones, 'The theory of electromagnetism', Pergamon Press, 1964.
4. M. Abramowitz, I. Stegun, 'Handbook of mathematical functions', Dover, Inc., 1972.

Uniform Quadratic Convergence of Monotone Iterates for Semilinear Singularly Perturbed Elliptic Problems

Igor Boglaev

1 Introduction

In this paper we give a numerical treatment for a semilinear singularly perturbed elliptic problem. Let ω be a bounded connected domain in $\mathbb{R}^{\kappa}$, $\kappa \geq 1$, with a boundary $\partial\omega$. Consider the elliptic problem

$$-\mu^2 \sum_{\nu=1}^{\kappa} \frac{\partial^2 U}{\partial x_{\nu}^2} + f(x,U) = 0, \quad x \in \omega, \quad U(x) = g(x), \quad x \in \partial\omega, \qquad (1)$$

where μ is a small positive parameter, the functions f and g are smooth in their respective domains, and f satisfies the constraint

$$f_u \geq c_* = \text{const} > 0, \quad (x,U) \in \overline{\omega} \times (-\infty, \infty). \qquad (2)$$

For $\mu \ll 1$, the problem is singularly perturbed and characterized by boundary layers (regions with rapid change of solutions) near the boundary $\partial\omega$.

In the study of numerical methods for nonlinear singularly perturbed problems, the two major points to be developed are: (a) constructing robust difference schemes (this means that unlike classical schemes, the error does not increase to infinity, but rather remains bounded, as the small parameter approaches zero); (b) obtaining reliable and efficient computing algorithms for solving nonlinear discrete problems. For solving these nonlinear discrete systems, the iterative approach presented in this paper is based on the method of upper and lower solutions and associated monotone iterates. By using upper and lower solutions as two initial iterations, one can construct two monotone sequences which converge monotonically from above and below, respectively, to a solution of the problem. Since the initial iteration in the monotone iterative method is either an upper or lower solution, which can

I. Boglaev
Institute of Fundamental Sciences, Massey University, Palmerston North, New Zealand
e-mail: I.Boglaev@massey.ac.nz

C. Clavero et al. (eds.), *BAIL 2010 – Boundary and Interior Layers, Computational and Asymptotic Methods*, Lecture Notes in Computational Science and Engineering 81,
DOI 10.1007/978-3-642-19665-2_5,

be constructed directly from the difference equation without any knowledge of the exact solution, this method simplifies the search for the initial iteration as is often required in Newton's method.

In [2], we investigate uniform convergence properties of the monotone iterative method from [1] applied to solving the semilinear problem (1). This monotone method possesses linear convergence rate. In this paper, we extend the accelerated monotone iterative method from [4] to the case when an ordered pair of upper and lower solutions is calculated inside the accelerated monotone iterative method, and investigate uniform convergence properties of the modified accelerated monotone iterative method.

The structure of the paper as follows. In Sect. 2, we introduce a nonlinear difference scheme for the numerical solution of (1). The monotone iterative method is presented in Sect. 3. Section 4 deals with quadratic convergence of the monotone iterates. An analysis of uniform convergence of the monotone iterates to the solution of the nonlinear difference scheme is given in Sect. 5. In Sect. 6, we investigate uniform convergence of the monotone iterates method to the exact solution of (1). The final Sect. 7 presents results of numerical experiments where iteration counts are compared with the monotone iterative method from [2], which converges with linear rate.

2 A Nonlinear Difference Scheme

On $\overline{\omega}$, we introduce a computational mesh $\overline{\omega}^h$, and for a mesh function $u(p)$, $p \in \overline{\omega}^h$, consider the nonlinear difference scheme in the canonical form [5]

$$\mathcal{L}u(p) + f(p,u) = 0, \quad p \in \omega^h, \quad u(p) = g(p), \quad p \in \partial\omega^h, \tag{3}$$

$$\mathcal{L}u(p) = d(p)u(p) - \sum_{p' \in \sigma'(p)} e(p,p')u(p'),$$

where $\sigma'(p) = \sigma(p) \setminus \{p\}$, $\sigma(p)$ is a stencil of the scheme at an interior mesh point $p \in \omega^h$ and $\partial\omega^h$ is the boundary of $\overline{\omega}^h$. We make the following assumptions on the coefficients of the difference operator $\mathcal{L}$:

$$d(p) > 0, \quad e(p,p') > 0, \quad d(p) - \sum_{p' \in \sigma'(p)} e(p,p') \geq 0, \quad p \in \omega^h. \tag{4}$$

We introduce the linear version of problem (3)

$$(\mathcal{L} + c)w(p) = f_0(p), \quad p \in \omega^h, \tag{5}$$

$$w(p) = g(p), \quad p \in \partial\omega^h, \quad c(p) \geq 0, \quad p \in \overline{\omega}^h.$$

We now formulate the maximum principle for the difference operator $\mathcal{L} + c$ and give an estimate of the solution to (5).

Lemma 1. *Let the coefficients of the difference operator $\mathcal{L}$ from (5) satisfy (4) and the mesh $\overline{\omega}^h$ be connected.*

(i) If a mesh function $w(p)$ satisfies the conditions

$$(\mathcal{L} + c)w(p) \geq 0 \ (\leq 0), \quad p \in \omega^h, \quad w(p) \geq 0 \ (\leq 0), \quad p \in \partial\omega^h,$$

then $w(p) \geq 0 \ (\leq 0)$, $p \in \overline{\omega}^h$.

(ii) If $c(p) \geq c_*$, then the following estimate of the solution to (5) holds true

$$\|w\|_{\overline{\omega}^h} \leq \max\left[\|g\|_{\partial\omega^h}, \|f_0/c\|_{\omega^h}\right], \tag{6}$$

where $\|g\|_{\partial\omega^h} \equiv \max_{p\in\partial\omega^h} |g(p)|$, $\|f_0\|_{\omega^h} \equiv \max_{p\in\omega^h} |f_0(p)|$.

The proof of the lemma can be found in [5].

3 Monotone Iterative Method

We say that $u_1(p)$ is an upper solution if it satisfies

$$\mathcal{L}u_1(p) + f(p, u_1) \geq 0, \quad p \in \omega^h, \quad u_1(p) \geq g(p), \quad p \in \partial\omega^h.$$

Similarly, $u_{-1}(p)$ is a lower solution if it satisfies the reversed inequalities.

Initial upper and lower solutions $u_\alpha^{(0)}(p)$ ($\alpha = 1$ and $\alpha = -1$ correspond to, respectively, the upper and lower cases) are calculated by solving the linear problems

$$(\mathcal{L} + c_*)z_\alpha^{(0)}(p) = \alpha|\mathcal{R}(p, s)|, \quad p \in \omega^h, \quad z_\alpha^{(0)}(p) = 0, \quad p \in \partial\omega^h, \tag{7}$$

$$\mathcal{R}(p, s) \equiv \mathcal{L}s(p) + f(p, s), \quad u_\alpha^{(0)}(p) = s(p) + z_\alpha^{(0)}, \quad p \in \overline{\omega}^h,$$

where $s(p)$ is defined on $\overline{\omega}^h$ and satisfies the boundary condition $s(p) = g(p)$ on $\partial\omega^h$. For $n \geq 1$, we calculate upper and lower solutions by using the recurrence formulae

$$(\mathcal{L} + c^{(n-1)}(p))z_\alpha^{(n)}(p) = -\mathcal{R}(p, u_\alpha^{(n-1)}), \quad p \in \omega^h, \tag{8}$$

$$z_\alpha^{(n)}(p) = 0, \quad p \in \partial\omega^h, \quad \mathcal{R}(p, u_\alpha^{(n-1)}) \equiv \mathcal{L}u_\alpha^{(n-1)}(p) + f(p, u_\alpha^{(n-1)}),$$

$$u_\alpha^{(n)}(p) = u_\alpha^{(n-1)}(p) + z_\alpha^{(n)}(p), \quad p \in \overline{\omega}^h,$$

The mesh function $c^{(n-1)}$ is given by

$$c^{(n-1)}(p) = \max_u\{f_u(p, u), u_{-1}^{(n-1)}(p) \leq u \leq u_1^{(n-1)}(p)\}, \quad p \in \overline{\omega}^h. \tag{9}$$

where below in Theorem 1, we prove that $u_{-1}^{(n-1)}(p) \leq u_1^{(n-1)}(p)$, $p \in \overline{\omega}^h$.

The following theorem gives the monotone property of the iterative method (7)–(9).

Theorem 1. *Let assumptions (2) and (4) hold true and the computational mesh $\overline{\omega}^h$ be connected. Then the sequences $\{u_\alpha^{(n)}\}$, $\alpha = 1, -1$, generated by (7)–(9), converge monotonically to a unique solution u^* of (3):*

$$u_{-1}^{(n)}(p) \le u_{-1}^{(n+1)}(p) \le u^*(p) \le u_1^{(n+1)}(p) \le u_1^{(n)}(p), \quad p \in \overline{\omega}^h, \quad n \ge 0. \tag{10}$$

Proof. We show that $u_1^{(0)}$ defined by (7) is an upper solution. From the maximum principle in Lemma 1, it follows that $z_1^{(0)} \ge 0$ on $\overline{\omega}^h$. From (7), by the mean-value theorem, we have

$$\mathcal{L}(s(p) + z_1^{(0)}(p)) + f(p, s + z_1^{(0)}) = \mathcal{R}(p,s) + |\mathcal{R}(p,s)| + (f_u(p, e^{(0)}) - c_*) z_1^{(0)},$$

where $s(p) \le e^{(0)}(p) \le s(p) + z_1^{(0)}(p)$. From (2) and $z_1^{(0)} \ge 0$, we conclude that $u_1^{(0)}$ is an upper solution. Similarly, we can prove that $u_{-1}^{(0)}$ is a lower solution. Thus, $u_1^{(0)}$ and $u_{-1}^{(0)}$ are upper and lower solutions which satisfy (10) for $n = 0$.

We prove that

$$u_{-1}^{(1)}(p) \le u_1^{(1)}(p), \quad p \in \overline{\omega}^h. \tag{11}$$

By (8) for $n = 1$,

$$(\mathcal{L} + c^{(0)}) u_\alpha^{(1)}(p) = c^{(0)} u_\alpha^{(0)}(p) - f(p, u_\alpha^{(0)}), \ p \in \omega^h, \quad u_\alpha^{(1)}(p) = g(p), \ p \in \partial\omega^h,$$

Letting $w^{(n)} = u_1^{(n)} - u_{-1}^{(n)}$, from here, by the mean-value theorem, we have

$$(\mathcal{L} + c^{(0)}) w^{(1)}(p) = (c^{(0)} - f_u^{(0)}(p)) w^{(0)}(p), \ p \in \omega^h, \quad w^{(1)}(p) = 0, \ p \in \partial\omega^h,$$

where $f_u^{(0)}(p) = f_u(p, v^{(0)}(p))$, $u_{-1}^{(0)}(p) \le v^{(0)}(p) \le u_1^{(0)}(p)$. Taking into account that $w^{(0)}(p) \ge 0$, from here and (9) with $n = 0$, we conclude that

$$(\mathcal{L} + c^{(0)}(p)) w^{(1)}(p) \ge 0, \quad p \in \omega^h, \quad w^{(1)}(p) = 0, \quad p \in \partial\omega^h.$$

From (2) and (9), by the maximum principle in Lemma 1, we prove (11).

From (8) and $u_1^{(0)}$ is an upper solution, we have

$$(\mathcal{L} + c^{(0)}(p)) z_1^{(1)}(p) \le 0, \quad p \in \omega^h, \quad z_1^{(1)}(p) = 0, \quad p \in \partial\omega^h.$$

By Lemma 1, it follows that $z_1^{(1)}(p) \le 0$, $p \in \overline{\omega}^h$. Similarly, we can prove that $z_{-1}^{(1)}(p) \ge 0$, $p \in \underline{\omega}^h$. From here and (11), it follows that

$$u_{-1}^{(0)}(p) \le u_{-1}^{(1)} \le u_1^{(1)}(p) \le u_1^{(0)}(p), \quad p \in \overline{\omega}^h.$$

Thus, we prove (10) for $n = 1$.

Using the mean-value theorem and the equation for $z_1^{(1)}$, we represent $\mathcal{R}(p, u_1^{(1)})$ in the form

$$\mathcal{R}(p, u_1^{(1)}) = -(c^{(0)}(p) - f_u^{(1)}(p))z_1^{(1)}(p), \quad p \in \omega^h,$$

where $f_u^{(1)}(p) = f_u(p, e^{(1)})$, $u_1^{(1)}(p) \le e^{(1)}(p) \le u_1^{(0)}$. Since the mesh function $z_1^{(1)}$ is nonpositive on ω^h and taking into account (9), we conclude that $\mathcal{R}(p, u_1^{(1)}) \ge 0$, $p \in \omega^h$. Similarly, we can prove that $\mathcal{R}(p, u_{-1}^{(1)}) \le 0$, $p \in \omega^h$. From here and (11), it follows that $u_1^{(1)}$ and $u_{-1}^{(1)}$ are upper and lower solutions.

By induction on n, we can prove that $u_1^{(n)}$ and $u_{-1}^{(n)}$ are upper and lower solutions, and the monotone property in (10) holds.

For each $p \in \overline{\omega}^h$, one can conclude from (10) that the monotonically decreasing sequence $\{u_1^{(n)}\}$ is bounded below by any lower solution $u_{-1}^{(n)}$, $n \ge 0$. It follows from (8) that $\lim z_1^{(n)}(p) = 0$, $p \in \overline{\omega}^h$ as $n \to \infty$, therefore, the sequence converges to u_1. With a similar argument, we prove that the monotonically decreasing sequence $\{u_{-1}^{(n)}\}$ converges to u_{-1}. Now by linearity of the operator $\mathcal{L}$ and the continuity of f, we conclude that u_1 and u_{-1} are solutions to (3). By the maximum principle in Lemma 1, under assumption (2) the nonlinear difference (3) has a unique solution u^*, hence, $u_1 = u_{-1} = u^*$.

4 Quadratic Convergent Rate of Monotone Sequences

Introduce the notation

$$c_1 \equiv \min_{p \in \overline{\omega}^h} [\min_u \{ f_u(p, u), u_{-1}^{(0)}(p) \le u \le u_1^{(0)}(p) \}] \ge c_*, \tag{12}$$

$$c_2 \equiv \max_{p \in \overline{\omega}^h} [\max_u \{ |f_{uu}(p, u)|, u_{-1}^{(0)}(p) \le u \le u_1^{(0)}(p) \}], \tag{13}$$

where initial upper and lower solutions $u_1^{(0)}(p)$ and $u_{-1}^{(0)}(p)$, respectively, are calculated in (7).

The following theorem gives the quadratic convergence of the monotone method (7)–(9).

Theorem 2. *Let the assumptions in Theorem 1 be satisfied. Then the following estimate holds:*

$$\|u_1^{(n)} - u_{-1}^{(n)}\|_{\overline{\omega}^h} \le \frac{c_2}{c_1} \|u_1^{(n-1)} - u_{-1}^{(n-1)}\|_{\overline{\omega}^h}^2, \tag{14}$$

where $\|u\|_{\overline{\omega}^h} \equiv \max_{p \in \overline{\omega}^h} |u(p)|$.

Proof. From (8), by the mean-value theorem, we conclude that

$$(\mathcal{L} + c^{(n-1)})w^{(n)}(p) = [c^{(n-1)} - f_u(p, v^{(n-1)})]w^{(n-1)}(p), \quad p \in \omega^h, \tag{15}$$

$$u_1^{(n)}(p) = u_{-1}^{(n)}(p), \quad p \in \partial\omega^h.$$

where $w^{(n)} \equiv u_1^{(n)} - u_{-1}^{(n)}$ and $u_{-1}^{(n-1)}(p) \le v^{(n-1)}(p) \le u_1^{(n-1)}(p)$. From (9), it follows that

$$c^{(n-1)}(p) = f_u(p, r^{(n-1)}), \quad u_{-1}^{(n-1)}(p) \le r^{(n-1)}(p) \le u_1^{(n-1)}(p). \tag{16}$$

Thus, we represent the right hand side of the difference equation from (15) in the form $[f_u(p, r^{(n-1)}) - f_u(p, v^{(n-1)})]w^{(n-1)}(p)$. Applying again the mean-value theorem, we get

$$f_u(p, r^{(n-1)}) - f_u(p, v^{(n-1)}) = f_{uu}(p, t^{(n-1)})(r^{(n-1)}(p) - v^{(n-1)}(p)),$$

where $t^{(n-1)}(p)$ lies between $r^{(n-1)}(p)$ and $v^{(n-1)}(p)$. Taking into account that $|r^{(n-1)}(p) - v^{(n-1)}(p)| \le w^{(n-1)}(p)$, $c^{(n)}(p) \ge c_1$ and (13), by (6) applied to problem (15), we prove (14).

5 Uniform Convergence to the Solution of (3)

In this section, we investigate uniform convergence of the monotone method (7)–(9) to the solution of (3). Without loss of generality, we suppose that the boundary condition in (3) is zero, that is, $g(p) = 0$, $p \in \partial\omega^h$. This assumption can always be obtained via a change of variables. Choosing $s(p) = 0$, $p \in \overline{\omega}^h$ in (7), we get the linear problems for $u_\alpha^{(0)}$, $\alpha = 1, -1$,

$$(\mathcal{L} + c_*)u_\alpha^{(0)}(p) = \alpha|f(p, 0)|, \quad p \in \omega^h, \quad u_\alpha^{(0)}(p) = 0, \quad p \in \partial\omega^h. \tag{17}$$

Theorem 3. *Let the assumptions in Theorem 1 be satisfied. Then the monotone iterative method (8), (9), (17) converges μ-uniformly to the unique solution of the nonlinear difference scheme (3).*

Proof. We introduce the notation $q_n = \|u_1^{(n)} - u_{-1}^{(n)}\|_{\overline{\omega}^h}$, $\nu_n = c_3 q_n$ and $c_3 = c_2/c_1$, where c_1 and c_2 from (12) and (13), respectively. Multiplying (14) by c_3, we have $\nu_{n+1} \le \nu_n^2, n \ge 0$. Since $\{u_1^{(n)}\}$ and $\{u_{-1}^{(n)}\}$ converge to the solution u^* of (3), then for some n_* the inequality $\nu_* \equiv \nu_{n_*} < 1$ holds. By induction, we show that

$$\nu_n \le \nu_*^{2^{n-n_*}}, \quad n \ge n_*. \tag{18}$$

It is true for $n = n_*$. Assuming that it holds for $n = l$, we have

$$v_{l+1} \le v_l^2 \le (v_*^{2^{l-n_*}})^2 = v_*^{2^{l+1-n_*}},$$

and prove (18). From (14) and (18), we conclude

$$q_n \le \frac{1}{c_3}(c_3 q_{n_*})^{2^{n-n_*}}, \quad n \ge n_*, \quad c_3 q_{n_*} < 1. \tag{19}$$

From (17), by (6), we get the estimate $\|u_\alpha^{(0)}\|_{\overline{\omega}^h} \le \|f(p,0)\|_{\overline{\omega}^h}/c_*$. It means that $u_\alpha^{(0)}$, $\alpha = 1, -1$, are μ-uniformly bounded. From here, (12) and (13), it follows that c_1 and c_2 are independent of μ. From here and (14), we conclude that q_n is μ-uniformly bounded for all $n \ge 0$. Now taking into account that q_{n_*} in (19) is μ-uniformly bounded, from (19) it follows that the sequence $\{q_n\}$ converges μ-uniformly to 0. Representing q_n in the form $q_n = \|u_1^{(n)} - u^* + u^* - u_{-1}^{(n)}\|_{\overline{\omega}^h}$ and taking into account (10), we conclude the inequalities

$$\|u_1^{(n)} - u^*\|_{\overline{\omega}^h} \le q_n, \quad \|u_{-1}^{(n)} - u^*\|_{\overline{\omega}^h} \le q_n.$$

From here and uniform convergence of $\{q_n\}$, it follows that the sequences $\{u_\alpha^{(n)}\}$, $\alpha = 1, -1$, converge μ-uniformly to the solution u^* of the nonlinear difference scheme (3).

6 Uniform Convergence to the Solution of (1)

In this section we assume that ω is the two dimensional rectangular domain

$$\omega = \omega^x \times \omega^y = \{0 < x < 1\} \times \{0 < y < 1\}. \tag{20}$$

On $\overline{\omega}$ we introduce the piecewise uniform mesh $\overline{\omega}^h = \overline{\omega}^{hx} \times \overline{\omega}^{hy}$ of Shishkin-type [3]. The boundary layer thicknesses σ_x and σ_y are chosen as

$$\sigma_x = \min\left\{0.25, (1/\sqrt{c_*})\mu \ln N_x\right\}, \quad \sigma_y = \min\left\{0.25, (1/\sqrt{c_*})\mu \ln N_y\right\},$$

and mesh spacings $h_{x\mu}$, h_x, $h_{y\mu}$ and h_y are defined by

$$h_{x\mu} = \frac{4\sigma_x}{N_x}, \quad h_x = \frac{2(1-2\sigma_x)}{N_x}, \quad h_{y\mu} = \frac{4\sigma_y}{N_y}, \quad h_y = \frac{2(1-2\sigma_y)}{N_y},$$

where N_x and N_y are number of mesh points in x- and y-directions, respectively. The mesh $\overline{\omega}^{hx}$ is constructed thus: in each of the subintervals $[0, \sigma_x]$ and $[1-\sigma_x, 1]$ the fine mesh spacing is $h_{x\mu}$ while in the interval $[\sigma_x, 1-\sigma_x]$ the coarse mesh

spacing is h_x. The mesh $\overline{\omega}^{hy}$ is defined similarly. For approximation of the differential operator, we use the classical difference operator which satisfies the assumptions from (4). The difference scheme (3) based on the classical difference operator and the piecewise uniform mesh converges μ-uniformly to the solution of (1):

$$\|U-u\|_{\overline{\omega}^h} \le CN^{-2}\ln^2 N, \quad N=\min\left\{N_x,N_y\right\},$$

where constant C is independent of μ and N (see [3] for details). From here and Theorem 3, we conclude the following theorem.

Theorem 4. *The monotone iterative method (8), (9), (17), based on the classic difference approximation and the piecewise uniform mesh, converges μ-uniformly to the unique solution of (1).*

7 Numerical Experiments

In this section, we compare convergence properties of the monotone iterative method (8), (9), (17) and monotone iterative method from [2]. The monotone iterative method from [2] is constructed in the assumption that $c_* \le f_u \le c^*$, $c^* = \text{const} > 0$. This method utilizes c^* in (8) instead of $c^{(n-1)}(p)$.

The test problem is the two dimensional elliptic problem (1) on the rectangular domain (20) with $f(x,y,U)=(U-3)/(4-U)$ and $g(x,y)=0$. The initial upper and lower solutions are

$$u_1^{(0)}(p)=3, \quad p\in\omega^h, \quad u_1^{(0)}(p)=0, \quad p\in\partial\omega, \quad u_{-1}^{(0)}(p)=0, \quad p\in\overline{\omega}^h.$$

Using these initial upper and lower solutions and $f_u=1/(4-u)^2$, we get

$$c_*=1/16, \quad c^*=\max_{p\in\overline{\omega}^h}[\max_u\{f_u(p,u), u_{-1}^{(0)}(p)\le u\le u_1^{(0)}(p)\}]=1,$$

where initial upper and lower solutions $u_1^{(0)}(p)$ and $u_{-1}^{(0)}(p)$, respectively, are calculated in (7). Thus, in the monotone iterative method from [2], $c^*=1$ is in use. Since $f_{uu}=2/(4-u)^3\ge 0$ in $u_{-1}^{(0)}\le u\le u_1^{(0)}$, from here, (9) and (16), we conclude that $c^{(n)}(p)=f_u(p,u_1^{(n)})$. It means that only the sequence of upper solutions is required for this test problem.

We choose the stopping test in the form

$$\|u_1^{(n+1)}-u_1^{(n)}\|_{\overline{\omega}^h}\le\delta,$$

where $\delta=10^{-5}$. In Table 1, for various values of μ and N ($N=N_x=N_y$), we present convergence iteration counts $\Delta;\nabla$, where Δ for the monotone iterative method (8), (9), (17) and ∇ for the monotone iterative method from [2]. From the

Table 1 Convergence iteration counts for different values of μ and N

$\mu \backslash N$	32	64	128	256	512
10^{-1}	5;15	5;15	5;15	5;15	5;15
10^{-2}	5;15	5;15	5;15	4;15	4;15
$\leq 10^{-3}$	5;15	5;15	4;15	4;15	4;15

Table 2 Convergence iteration counts for different values of μ and δ

$\mu \backslash \delta$	10^{-3}	10^{-4}	10^{-5}	10^{-6}
10^{-1}	4;9	5;12	5;15	6;18
10^{-2}	4;9	5;12	5;15	6;18
$\leq 10^{-3}$	4;9	5;12	5;15	6;17

Table 3 The maximum error for different values of μ and N

$\mu \backslash N$	32	64	128	256
10^{-1}	1.051×10^{-1}	2.392×10^{-2}	0.938×10^{-2}	1.054×10^{-3}
10^{-2}	1.259×10^{-1}	4.279×10^{-2}	1.237×10^{-2}	3.376×10^{-3}
$\leq 10^{-3}$	1.467×10^{-1}	6.346×10^{-2}	1.843×10^{-2}	5.128×10^{-3}

numerical data, it follows that for all values of μ and N, the monotone iterative method (8), (9), (17) converges faster than the corresponding monotone iterative method from [2]. For N fixed and $\mu \leq 10^{-3}$, the convergence iteration counts are uniform with respect to μ. These numerical experiments confirm our theoretical results on uniform convergence of the monotone iterative method (8), (9), (17).

In Table 2, for various values of the small parameter μ, the tolerance δ in the stopping test and $N = 64$, we present convergence iteration counts for the monotone iterative method (8), (9), (17) and for the monotone iterative method from [2]. In [2], we proved that the monotone iterative method under investigation converges with the linear rate $\|u_1^{(n+1)} - u_1^{(n)}\|_{\overline{\omega}^h} \leq C\rho^n$, $\rho = c_*/c^*$, where constant C is independent of μ and N. From here, it follows that $n_2/n_1 \approx \log \delta_2 / \log \delta_1$, where n_1 and n_2 are convergence iteration counts for δ_1 and δ_2, respectively. The numerical experiments from Table 2 confirm this theoretical result. From (19), under the assumptions $n_* = 0$ ($\nu_0 < 1$) and $c_3 = \mathcal{O}(1)$, we conclude that $n_2/n_1 \approx \log(\log|\delta_2|)/\log(\log|\delta_1|)$ for the monotone iterative method (8), (9), (17). The numerical experiments from Table 2 confirm the theoretical observation that ratio n_2/n_1 ($\delta_2 < \delta_1$) increases slightly as δ_2/δ_1 decreases.

By u^N, we denote the numerical solution computed by the monotone iterative method (8), (9), (17) and take u^{1024} as the reference solution. In Table 3, for various values of μ and N, we present the maximum error $\|u^N - u^{1024}\|_{\overline{\omega}^h}$. The numerical results show that for $\mu \leq 10^{-3}$, the maximum error is independent of μ and decreases with N.

References

1. Boglaev, I.: On monotone iterative methods for a nonlinear singularly perturbed reaction-diffusion problem. J. Comput. Appl. Math., **162**, 445–466 (2004)
2. Boglaev, I.: Uniform convergence of monotone iterative methods for semilinear singularly perturbed problems of elliptic and parabolic types. Electron. Trans. Numer. Anal., **20**, 86–103 (2005)
3. Miller, J.J.H., O'Riordan, E., Shishkin, G.I.: Fitted Numerical Methods for Singular Perturbation Problems. World Scientific, Singapore (1996)
4. Pao, C.V.: Accelerated monotone iterations for numerical solutions of nonlinear elliptic boundary value problems. Computers Math. Applic., **46**, 1535–1544 (2003)
5. Samarskii, A.: The Theory of Difference Schemes. Marcel Dekker, New York Basel (2001)

Finite Element Discretizations of Optimal Control Flow Problems with Boundary Layers

M. Braack and B. Tews

Abstract We study the effect of different stabilized finite element methods to distributed control problems governed by singular perturbed Oseen equations. On the one hand, the residual based stabilized finite element method SUPG/PSPG leads to different optimality systems depending on the discretization approach: first discretize the state equation and then formulate the corresponding optimality system or derive first the optimality system on the continuous level and then discretize it. On the other hand, for symmetric stabilization as for instance the local projection stabilization (LPS) both approaches lead to the same symmetric optimality system. In particular, we address the question whether a possible commutation error in optimal control problems with boundary layers discretized by stabilized finite element methods may affect the accuracy significantly or not.

1 Optimal Control Problem of the Oseen System

Let $\Omega \subset \mathbb{R}^d, d \in \{2, 3\}$ be a bounded polyhedral domain with Lipschitz boundary $\partial\Omega$. The velocity v belongs to the vector Sobolev space $H_0^1(\Omega)^d$ and the pressure p to the space $L_0^2(\Omega)$ which stands for the L^2-integrable functions over Ω with vanishing mean. By u we denote the vector of velocities and pressure, $u = (v, p)$. Hence, u is sought in the Hilbert space $X := [H_0^1(\Omega)]^d \times L_0^2(\Omega)$. Furthermore, let $Q \subset L^2(\Omega)^d$ a subspace and $q \in Q$ a control function. In order to express the variational formulation of the state equation we introduce the bilinear forms

$$a(u, \varphi) := (\nabla \cdot v, \xi) + (\sigma v, \phi) + ((b \cdot \nabla)v, \phi) + (\mu \nabla v, \nabla \phi) - (p, \nabla \cdot \phi)$$
$$b(q, \phi) := (q, \phi),$$

M. Braack (✉) and B. Tews
Mathematisches Seminar, Christian-Albrechts-Universität zu Kiel, Ludewig-Meyn-Str. 4, D-24098 Kiel, Germany
e-mail: braack@math.uni-kiel.de, tews@math.uni-kiel.de

C. Clavero et al. (eds.), *BAIL 2010 – Boundary and Interior Layers, Computational and Asymptotic Methods*, Lecture Notes in Computational Science and Engineering 81,
DOI 10.1007/978-3-642-19665-2_6,

where $\mu, \sigma > 0$ and b a divergence free vector field, $\nabla \cdot b = 0$. The optimal control problem consists in determining $q \in Q$ such that a functional J becomes minimal:

$$J(u,q) := \frac{1}{2}\|v - v_d\|_0^2 + \frac{\alpha}{2}\|q\|_0^2 \quad \rightarrow \quad \min.$$

Here, v_d is a target velocity field, and $\alpha > 0$ is a given positive constant. The state constraint for $u = (v, p) \in X$ in weak formulation reads:

$$a(u,\varphi) + b(q,\phi) = \langle f, \phi \rangle \quad \forall \varphi = (\phi, \xi) \in X. \tag{1}$$

To derive necessary and, due to convexity, also sufficient first order optimality conditions we define the Lagrange functional $\mathscr{L} : X \times Q \times X \rightarrow \mathbb{R}$ with multiplier $z \in X$,

$$\mathscr{L}(u,q,z) := J(u,q) - a(u,z) - b(q,z) + \langle f, z \rangle.$$

To minimize this unconstraint functional we built the Frechet-derivatives with respect to the variables. The derivative with respect to the Lagrange multiplier leads to the state equation (1). The derivative with respect to the state leads to the *adjoint equation*,

$$\partial_u \mathscr{L}(u,q,z)(\psi) \equiv 0 \quad \Rightarrow \quad a(\psi, z) = (v - v_d, \psi) \quad \forall \psi \in X. \tag{2}$$

The derivative with respect to the control leads to the *gradient equation*.

$$\partial_q \mathscr{L}(u,q,z)(\lambda) \equiv 0 \quad \Rightarrow \quad \alpha(q,\lambda) = b(\lambda, z) \quad \forall \lambda \in Q. \tag{3}$$

For every control $q \in Q$ and every right hand side $f \in L^2(\Omega)^d$ the equation (1) possess a weak solution. Therefore, we can define a continuous linear solution operator $S : Q \rightarrow X$, by $u = Sq$. Furthermore, we introduce the reduced cost functional $j : Q \rightarrow \mathbb{R}$ by

$$j(q) := J(q, Sq).$$

Lemma 1. *Let $z \in X$ be the solution of the dual equation (2). It holds*

$$j'(q)(\delta q) = -b(\delta q, z) + \alpha(q, \delta q) \quad \forall q, \delta q \in Q. \tag{4}$$

Proof. For $u = Sq$ and arbitrary $z \in X$ it holds $j(q) = J(u,q) = \mathscr{L}(u,q,z)$, and therefore we obtain for the derivative

$$j'(q)(\delta q) = \partial_q \mathscr{L}(u,q,z)(\delta q) + \partial_u \mathscr{L}(u,q,z)(S\delta q) \qquad \forall z \in X. \tag{5}$$

The assertion follows with (2). □

2 Discretization of the Optimality System

In order to discretize the optimality system (1)–(3) we make use of conforming equal order finite elements. Given a family of shape-regular, admissible decompositions $\mathscr{T}_h$ of Ω into d-dimensional quadrilaterals ($d = 2$) or hexahedrals ($d = 3$), let h_K be the diameter of a cell $K \in \mathscr{T}_h$. Assume that for each $K \in \mathscr{T}_h$, there exists a bilinear mapping $F_K : \hat{K} \to K$ which maps the reference element $\hat{K}$ onto K. Set $Q_h^r := \{\varphi \in L^2(\Omega) : \varphi \circ F_K \in Q_r, K \in \mathscr{T}_h\}$ with the space Q_r of all polynomials on the reference $\hat{K}$ with maximal degree $r \geq 1$ in each coordinate direction. The discrete state, dual and control spaces are given by:

$$X_h := X \cap [Q_h^r \cap C(\overline{\Omega})]^{d+1}, Z_h := X \cap [Q_h^l \cap C(\overline{\Omega})]^{d+1},$$
$$Q_h := Q \cap [Q_h^m \cap C(\overline{\Omega})]^d,$$

with $r, l \geq 1$ and $m \geq 0$. For equal order interpolation the discrete inf-sup condition is not fulfilled. Furthermore, in the convection dominated case there may occur unphysical oscillations. Hence, we need to add a stabilization term s_h^p to the Galerkin formulation. The choice of this term and its effect to the discrete optimality system will be shown later on. The discrete state equation reads: Find $u_h \in X_h$ such that

$$a(u_h, \varphi) + b(q_h, \phi) + s_h(u_h, q_h)(\varphi) = \langle f_h, \phi \rangle \quad \forall \varphi = (\phi, \xi) \in X_h. \tag{6}$$

The right-hand side may changed to f_h which also may involve stabilization terms. If the discrete state equation (6) is uniquely solvable, we can define the discrete solution operator $S_h : Q \to X_h$ analogously to the continuous case by $u_h = S_h q$. The coercivity of j follows directly by definition of the functional j_h:

Lemma 2. *If (6) has a unique solution, then the second derivative of the discrete reduced cost functional j_h is coercive: $j_h''(\delta q, \delta q) = \alpha \|\delta q\|_0^2 + \|S_h \delta q\|_0^2$.*

Many stabilization methods for the Oseen problem have the property to be additive in the sense that it holds

$$s_h(u_h, q_h)(\varphi) = s_h(u_h, 0)(\varphi) + s_h(0, q_h)(\varphi). \tag{7}$$

In the following we give two examples of such stabilizations leading to unique solutions of (6) . It is useful to introduce the discrete bilinear forms

$$a_h(u, \varphi) := a(u, \varphi) + s_h(u, 0)(\varphi),$$
$$b_h(q, \varphi) := b(q, \phi) + s_h(0, q)(\varphi).$$

The optimality system for the *discretize-optimize* strategy becomes:

$$u_h \in X_h: \ a_h(u_h,\varphi) + b_h(q_h,\varphi) = \langle f_h,\varphi\rangle \qquad \forall \varphi \in X_h, \tag{8}$$
$$z_h \in X_h: \ a_h(\psi,z_h) - (v_h,\psi) = -(v_d,\psi) \qquad \forall \psi \in X_h \tag{9}$$
$$q_h \in Q_h: \ b_h(\lambda,z_h) - \alpha(q,\lambda) = 0 \qquad \forall \lambda \in Q_h. \tag{10}$$

The optimality system for the *optimize-discretize* strategy becomes:

$$u_h \in X_h: \ a_h(u_h,\varphi) + b_h(q_h,\varphi) = \langle f_h,\varphi\rangle \quad \forall \varphi \in X_h, \tag{11}$$
$$z_h \in X_h: \ a(\psi,z_h) + s_h^*(z_h, v_d - v_h)(\psi) - (v_h,\psi) = -(v_d,\psi) \qquad \forall \psi \in X_h, \tag{12}$$
$$q_h \in Q_h: \ b(\lambda,z_h) - \alpha(q,\lambda) = 0 \quad \forall \lambda \in Q_h \tag{13}$$

with a stabilization term s_h^* appropriate for the (strong formulation of the) adjoint equation (2). Note that the discrete primal equations (8) and (11) are identical independent of the type of stabilization scheme.

SUPG/PSPG-stabilization: The classical combination of pressure stabilized Petrov-Galerkin (PSPG) [5] and streamline upwind Petrov-Galerkin (SUPG) [7] which allows the splitting (7) read

$$\begin{aligned} s_h^{sd}(u_h,q_h)(\varphi) &:= \sum_{K\in\mathscr{T}_h} \delta_K(-\mu\Delta v_h + (b\cdot\nabla)v_h + \sigma v_h + \nabla p_h + q_h, (b\cdot\nabla)\phi + \nabla\xi)_K \\ &\quad + \sum_{K\in\mathscr{T}_h} \gamma_K(\nabla\cdot v_h, \nabla\cdot\phi)_K, \\ \langle f_h,\varphi\rangle &:= \langle f,\phi\rangle + \sum_{K\in\mathscr{T}_h} \delta_K(f,(b\cdot\nabla)\phi + \nabla\xi)_K. \end{aligned}$$

The parameters δ_K and γ_K are cell-wise constants and usually chosen as

$$\delta_K = \delta_0 \tfrac{1}{2} \min\left\{ \tfrac{1}{\sigma}, \tfrac{h_K^2}{\mu}, \tfrac{h_K}{\|b\|_{0,\infty;K}} \right\}, \quad \gamma_K = \gamma_0 h_K. \tag{14}$$

Related to this stabilization method is the following norm:

$$|||u|||_{sd}^2 := \mu|v|_1^2 + \sigma\|v\|_0^2 + \rho\|p\|_0^2 + \sum_{K\in\mathscr{T}_h} \delta_K\|(b\cdot\nabla)v + \nabla p\|_{0;K}^2 + \gamma_K\|\nabla\cdot v\|_{0;K}^2,$$

with a sufficiently small parameter $\rho > 0$. For the choice (14) the discrete bilinear form is inf-sup stable, i.e.

$$\exists \beta > 0, \text{s.t.} \qquad \inf_{u_h\in X_h} \sup_{\varphi\in X_h} \frac{a_h(u_h,\varphi)}{|||u_h|||_{sd}\ |||\varphi|||_{sd}} \geq \beta, \tag{15}$$

and therefore the discrete state equation (6) admits an unique solution $u_h \in X_h$.

The SUPG method was investigated in [6] for optimal control with scalar convection-diffusion-reaction problems.

Local projection stabilization: The main idea of local projection stabilization (LPS) is to include fine grid fluctuations of the pressure and of the velocity gradient in the stabilization term. For simplicity, we restrict here to the so called *two-level* version of LPS [1,3] in contrast to the *one-level* method [8]. Let $\mathscr{T}_{2h}$ be the coarser mesh obtained by a "global coarsening" of $\mathscr{T}_h$. The finer mesh $\mathscr{T}_h$ contains 2^d times more elements than $\mathscr{T}_{2h}$. The elements of $\mathscr{T}_{2h}$ will be denoted by "patches". Let

$$\pi_h : L^2(\Omega) \to Q_{2h}^{r-1},$$

be the L^2-projection operator on discontinuous finite elements characterized by the property for $v \in L^2(\Omega)$:

$$(v - \pi_h v, \phi) = 0 \quad \forall \phi \in Q_{2h}^{r-1}.$$

Important is the fact that this projection acts locally on patches of elements, so that the numerical effort for computing this projection is very low. The operator giving the space fluctuations is denoted by

$$\varkappa_h := i - \pi_h,$$

with the identity mapping i. We use the same notations π_h, $\varkappa_h$ for the mappings of vector-valued functions, for instance, $\pi_h : L^2(\Omega)^d \to [Q_{2h}^{r-1}]^d$.

The discrete primal equation of the optimal control problem with local projection is as in (6) with a stabilization term independent of the control q:

$$s_h^{lps}(u,0)(\varphi) := ((b\cdot\nabla)v, \delta\varkappa_h[(b\cdot\nabla)\phi)] + (\nabla p, \delta\varkappa_h\nabla\xi) + (\nabla\cdot v, \gamma\varkappa_h(\nabla\cdot\xi)),$$
$$s_h^{lps}(0,q)(\varphi) := 0.$$

The parameters δ and γ are patch-wise constant and depend (similar to PSPG and SUPG) on the local Peclet number. Associated to this method is the semi-norm

$$|||u|||_{lps}^2 := \mu|v|_1^2 + \sigma\|v\|_0^2 + s_h^{lps}(u,u).$$

3 A-Priori Error Analysis

For an a priori analysis for LPS we refer to [2] where symmetric stabilization methods for optimal control problems with the Oseen system are analyzed. The local projection stabilization is a particular technique which fits into that framework so that no difference in optimize-stabilize or stabilize-optimize occur, because the resulting systems are completely identical. Moreover the following result was shown:

Theorem 1. *Let $(u,z,q) \in X \times X \times Q$ be the solution of the continuous optimization problem (1)–(3) and $(u_h, z_h, q_h) \in X_h$ the solutions of the discrete optimization problem (8)–(10) with LPS stabilization and $m = r = l$. Under the assumption $\mu < \|b\|_{K,\infty} h_K$, and the regularity $u, z \in H^{r+1}(\Omega)^{d+1}$ and $q \in H^{r+1}(\Omega)^d$ it holds*

$$\|q - q_h\|_0^2 + |\!|\!| u - u_h |\!|\!|_{lps}^2 \lesssim \sum_{K \in \mathcal{T}_h} h_K^{2r+1} (\|u\|_{r+1}^2 + \|z\|_{r+1}^2 + \|q\|_{r+1}^2).$$

Here, we use the symbol $\lesssim$ which means $\leq$ up to a h-independent constant. Note that this semi-norm does not include the L^2-norm of p. However, an a priori estimate of $\|p - p_h\|$ with optimal order can be easily achieved as shown in [3]. For a proof of the two following a priori estimates with SUPG/PSPG, see [4]:

Theorem 2. *For the discretize-optimize strategy with SUPG/PSPG, $\mu < \|b\|_{K,\infty} h_K$, it holds the estimate*

$$\begin{aligned}\|q - q_h\|_0^2 \lesssim \sum_{K \in \mathcal{T}_h} \Big\{ & h_K^{2(m+1)} \|q\|_{m+1;K}^2 + h_K^{2r+1} \|p\|_{r+1;K}^2 + h_K^{2l+1} \|z^p\|_{l+1;K}^2 \\ & + h_K^{2r+1} \|v\|_{r+1;K}^2 + h_K^{2l+1} \|z^v\|_{l+1;K}^2 + \delta_K \|(b \cdot \nabla) z^v + \nabla z^p\|_{0;K} \Big\}.\end{aligned}$$

Now, we first build up the optimality system on the continuous level and then discretize each equation separately. That means that we can choose an adequate stabilization term for the dual equation, which we denote by s_h^z. This term contains the full residual of the dual equation and therefore depends on z and u. The optimality system for the *optimize-discretize-* strategy is (11)–(13) with

$$\begin{aligned}s_h^z(z_h, v_d - v_h)(\varphi) = \sum_{K \in \mathcal{T}_h} & \gamma_K (\nabla \cdot z_h^v, \nabla \cdot \phi) + \delta_K \, (-\mu \Delta z_h^v - (b \cdot \nabla) z_h^v \\ & + \sigma z_h^v + \nabla z_h^p + v_d - v_h, -b \cdot \nabla \phi + \nabla \xi).\end{aligned}$$

Theorem 3. *With the parameter choice of (14), $\mu < \|b\|_{K,\infty} h_K$, we obtain for the* optimize-discretize *strategy with SUPG/PSPG the estimate*

$$\|q - q_h\|_0^2 \lesssim \sum_{K \in \mathcal{T}_h} \Big\{ h_K^{2(m+1)} \|q\|_{m+1;K}^2 + \alpha h_K^{2r+1} \|u\|_{r+1;K}^2 + \alpha h_K^{2l+1} \|z\|_{l+1;K}^2 \Big\}.$$

4 Numerical Experiment

In order to validate the analytical results presented so far, we consider a model problem with analytical solution. The domain is $\Omega = (0,1)^2$ with the boundaries Γ_i, $1 \leq i \leq 4$, numbered counterclockwise. The boundary conditions are

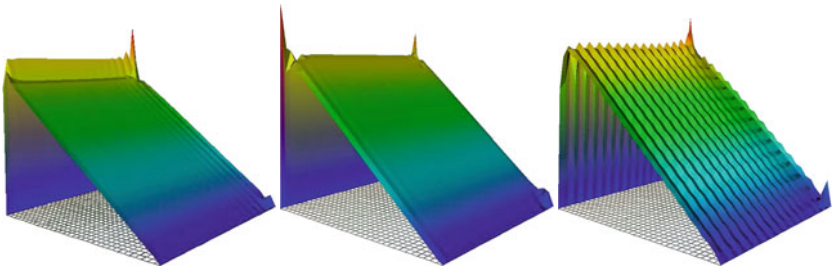

Fig. 1 Adjoint solutions with SUPG/PSPG: Q1 *discretize-optimize* (*left*), Q2 *optimize-discretize* (*middle*) and Q2 *discretize-optimize* (*right*)

$$v_1 = 0; \quad \mu(\nabla v_2, n) - p n_2 = 0 \quad \text{on } \Gamma_1 \cup \Gamma_3,$$
$$v_2 = 0; \quad \mu(\nabla v_1, n) - p n_1 = 0 \quad \text{on } \Gamma_2 \cup \Gamma_4.$$

The exact primal state $u = (v, p)$ and adjoint state $z = (z^v, z^p)$ are

$$u(x, y) = (g(y), g(x), 0), \quad z(x, y) = (g(1 - y), g(1 - x), 0),$$

with the viscosity-depending function $g(x) := x - \frac{1-e^{x/\mu}}{1-e^{1/\mu}}$. The viscosity is set to $\mu = 0.0075$ in order to enforce a sharp boundary layer. The constants in the stabilization parameters are always chosen as $\gamma_0 = \delta_0 = 0.2$.

The obtained adjoint solution z_h with SUPG/PSPG is shown in Fig. 1 in the combination *optimize-discretize* and *discretize-optimize* with Q2 and with Q1 elements, as well. The Q2 solution with *discretize-optimize* exhibit strong oscillations. We expect that this has a significant influence on the control q_h.

The obtained errors in the primal solution, in the adjoint solution, in the control and in the target functional are listed in Table 1 for SUPG/PSPG. For Q1 elements no substantial difference between *optimize-discretize* and *discretize-optimize* is observable. In the L^2-norm all quantities show a convergence rate of about $3/2$. However, the situation is different for Q2 and SUPG/PSPG. Here, the *optimize-discretize* strategy shows a convergence order in L^2 in all quantities of about $5/2$, whereas with *discretize-optimize* $\|z - z_h\|_0$ and $\|q - q_h\|$ converge with an order of less than $3/2$. Obviously, the non-optimal stabilization of the adjoint state and the hereby created non-physical oscillations leads to a decline of accuracy in the control. Hence, an higher order residual based stabilization scheme should not be used in the combination *discretize-optimize*.

The obtained results for LPS (where *discretize-optimize* and *optimize-discretize* are identical) are given in Table 2. With Q1 elements the convergence order in L^2 is between $3/2$ and 2. The error in the target functional $j(q) - j(q_h)$ is better than 2 on finer meshes. With Q2 elements the convergence order in L^2 reaches order 3 on the finest mesh and in the functional the convergence order is even beyond 4. Comparing the error $j(q) - j(q_h)$ for SUPG/PSPG in the DO setting and for LPS, the error is better by more than 3 magnitudes on the same mesh (the finest one) and the same finite element (bi-quadratics) when a symmetric stabilization is chosen. We think that this is a remarkable result.

Table 1 Errors and convergence orders obtained with SUPG/PSPG

$h =$	$\|u-u_h\|$				$\|z-z_h\|$				$\|q-q_h\|$		$j(q)-j(q_h)$	
2^{-l}	$\|\cdot\|_0$	Order	$\|\|\|\cdot\|\|\|_{sd}$	Order	$\|\cdot\|_0$	Order	$\|\|\|\cdot\|\|\|_{sd}$	Order	$\|\cdot\|_0$	Order	Value	Order
SUPG/PSPG Q1 *optimize-discretize*												
3	2.65e−1		9.58e−1		2.68e−1		9.76e−1		1.89e−1		2.91e−2	
4	1.50e−1	0.82	7.77e−1	0.30	1.50e−1	0.83	7.77e−1	0.33	1.06e−1	0.83	2.06e−2	0.50
5	6.62e−2	1.18	7.44e−1	0.06	6.62e−2	1.18	7.43e−1	0.06	4.68e−2	1.18	1.03e−2	1.00
6	2.42e−2	1.45	5.30e−1	0.49	2.42e−2	1.45	5.29e−1	0.49	1.71e−2	1.45	4.24e−3	1.28
7	8.15e−3	1.57	2.96e−1	0.84	8.15e−3	1.57	2.96e−1	0.84	5.76e−3	1.57	1.59e−3	1.42
SUPG/PSPG Q1 *discretize-optimize*												
3	2.67e−1		9.55e−1		2.70e−1		9.70e−1		1.52e−1		4.33e−2	
4	1.50e−1	0.83	7.77e−1	0.30	1.51e−1	0.84	7.78e−1	0.32	7.85e−2	0.95	2.53e−2	0.78
5	6.61e−2	1.19	7.44e−1	0.06	6.65e−2	1.19	7.44e−1	0.06	2.86e−2	1.46	1.17e−2	1.12
6	2.42e−2	1.45	5.30e−1	0.49	2.43e−2	1.45	5.30e−1	0.49	6.62e−3	2.11	4.58e−3	1.35
7	8.11e−3	1.58	2.96e−1	0.84	8.16e−3	1.57	2.96e−1	0.84	1.52e−3	2.12	1.65e−3	1.47
SUPG/PSPG Q2 *optimize-discretize*												
3	1.91e−1		7.52e−1		1.89e−1		7.47e−1		1.34e−1		6.59e−2	
4	9.86e−2	0.96	9.67e−1	−0.36	9.77e−2	0.95	9.66e−1	−0.37	6.91e−1	0.95	3.22e−2	1.03
5	4.05e−2	1.29	6.27e−1	0.63	4.00e−2	1.29	6.26e−1	0.63	2.83e−2	1.29	1.17e−2	1.26
6	1.06e−2	1.93	2.32e−1	1.44	1.03e−2	1.95	2.31e−1	1.44	7.32e−3	1.95	2.62e−3	2.16
7	1.69e−3	2.65	5.68e−2	2.03	1.55e−3	2.74	5.68e−2	2.03	1.09e−3	2.75	2.54e−4	3.37
SUPG/PSPG Q2 *discretize-optimize*												
3	1.89e−1		7.50e−1		2.20e−1		1.68e+0		9.01e−2		8.05e−2	
4	9.74e−2	0.95	9.66e−1	−0.37	1.29e−1	0.77	1.62e+0	0.05	4.49e−2	1.01	3.83e−2	1.07
5	4.01e−2	1.28	6.26e−1	0.63	7.54e−2	0.78	1.52e+0	0.09	2.59e−2	0.80	1.35e−2	1.50
6	1.05e−2	1.93	2.32e−1	1.44	3.76e−2	1.00	1.20e+0	0.34	1.31e−2	0.98	3.00e−3	2.17
7	1.66e−3	2.66	5.58e−2	2.03	1.48e−2	1.35	7.86e−1	0.62	5.27e−3	1.32	3.18e−4	3.24

Table 2 Errors and convergence orders obtained with LPS

2^{-l}	$\|u-u_h\|$		$\|z-z_h\|$		$\|q-q_h\|$		$j(q)-j(q_h)$	
	$\|\cdot\|_0$	Order	$\|\cdot\|_0$	Order	$\|\cdot\|_0$	Order	Value	Order
LPS Q1								
3	2.70e−1		2.77e−1		1.96e−1		4.80e−3	
4	1.58e−1	0.77	1.60e−1	0.79	1.13e−1	0.79	3.03e−3	0.66
5	7.20e−2	1.14	7.25e−2	1.15	5.12e−2	1.15	1.06e−3	1.52
6	2.48e−2	1.54	2.48e−2	1.54	1.76e−2	1.54	1.62e−4	2.71
7	6.46e−3	1.94	6.48e−3	1.94	4.58e−3	1.94	1.60e−5	3.35
LPS Q2								
3	2.00e−1		2.04e−1		1.44e−1		1.80e−3	
4	9.24e−2	1.12	9.31e−2	1.13	1.44e−1	1.13	1.13e−3	0.67
5	3.08e−2	1.59	3.09e−2	1.59	2.18e−2	1.59	1.35e−4	3.06
6	6.28e−3	2.29	6.29e−3	2.30	4.44e−3	2.30	6.72e−6	4.33
7	7.80e−4	3.01	7.81e−4	3.01	5.53e−4	3.01	2.28e−7	4.88

References

1. Becker, R., Braack, M.: A two-level stabilization scheme for the Navier-Stokes equations. In: e.a. M. Feistauer (ed.) Numerical Mathematics and Advanced Applications, ENUMATH 2003, pp. 123–130. Springer (2004)
2. Braack, M.: Optimal control in fluid mechanics by finite elements with symmetric stabilization. SIAM J. Control Optimization **48**(2), 672–687 (2009)
3. Braack, M., Burman, E.: Local projection stabilization for the Oseen problem and its interpretation as a variational multiscale method. SIAM J. Numer. Anal. **43**(6), 2544–2566 (2006)
4. Braack, M., Tews, B.: Linear-quadratic optimal control for the Oseen equations with stabilized finite elements. Tech. rep., University of Kiel, submitted paper (2010)
5. Brooks, A., Hughes, T.: Streamline upwind Petrov-Galerkin formulation for convection dominated flows with particular emphasis on the incompressible Navier-Stokes equations. Comput. Methods Appl. Mech. Engrg. **32**, 199–259 (1982)
6. Heinkenschloss, M., Leykekhman, D.: Local error estimates for SUPG solutions of advection-dominated elliptic linear-quadratic optimal control problems. SIAM J. Numer. Anal. **47**(6), 4607–4638 (2010)
7. Johnson, C., Saranen, J.: Streamline diffusion methods for the incompressible Euler and Navier-Stokes equations. Math. Comput. **47**, 1–18 (1986)
8. Matthies, G., Skrzypacz, P., Tobiska, L.: A unified convergence analysis for local projection stabilisations applied ro the Oseen problem. M2AN **41**(4), 713–742 (2007)

Asymptotic Behavior of a Viscous Fluid Near a Rough Boundary

J. Casado-Díaz, M. Luna-Laynez, and F.J. Suárez-Grau

Abstract The purpose of this paper is to study the asymptotic behavior of a viscous fluid satisfying Navier's condition on a slightly rough boundary. We consider the case of a fluid contained in a domain that has height 1 and the case of a fluid contained in a domain of small height ε. In both cases we show that three different behaviors are possible.

1 Introduction

For a viscous fluid in a three-dimensional domain with a rough boundary, it is known that if the normal velocity vanishes on the boundary (slip condition), then the fluid behaves as if the whole velocity vector vanishes on the boundary (adherence condition). This gives a mathematical explanation of why it is usual for a viscous fluid to impose the adherence condition. The above assertion was proved in [3] for a boundary described by the equation (see Fig. 1 below)

$$x_3 = -\varepsilon\Psi\left(\frac{x_1}{\varepsilon}, \frac{x_2}{\varepsilon}\right) \quad \forall (x_1, x_2) \in \omega, \tag{1}$$

with $\varepsilon > 0$ devoted to converge to zero, ω a Lipschitz bounded open set of $\mathbb{R}^2$ and Ψ a smooth periodic function such that

$$\text{Span}(\{\nabla\Psi(z') : z' \in \mathbb{R}^2\}) = \mathbb{R}^2. \tag{2}$$

An extension to non-periodic boundaries was obtained in [1].

Our aim in Sect. 2 is to generalize the result given in [3] to the case of weak rugosities of small period ε and amplitude δ_ε described by (see Fig. 2 below)

J. Casado-Díaz, M. Luna-Laynez, and F.J. Suárez-Grau (✉)
Dpto. de Ecuaciones Diferenciales y Análisis Numérico, Universidad de Sevilla, c/Tarfia s/n, 41012 Sevilla, Spain
e-mail: jcasadod@us.es, mllaynez@us.es, fjsgrau@us.es

C. Clavero et al. (eds.), *BAIL 2010 – Boundary and Interior Layers, Computational and Asymptotic Methods*, Lecture Notes in Computational Science and Engineering 81,
DOI 10.1007/978-3-642-19665-2_7,

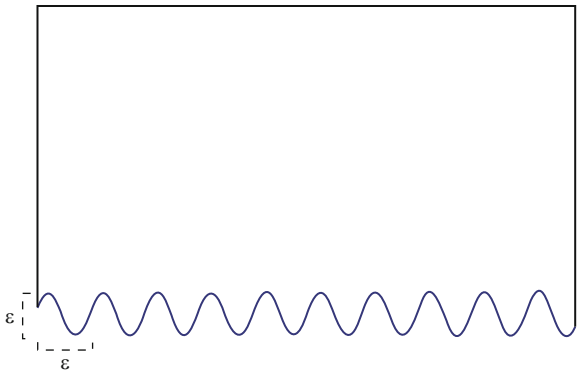

Fig. 1 Rough boundary in 2D described by (1).

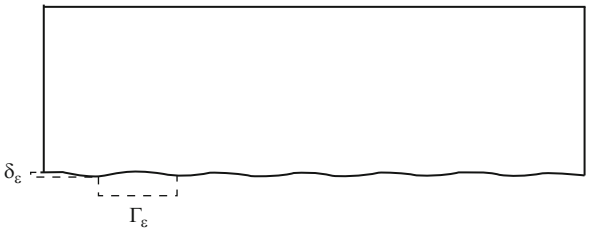

Fig. 2 Rough boundary in 2D described by (3)

$$\Gamma_\varepsilon = \left\{x = (x_1, x_2, x_3) \in \omega \times \mathbb{R} : \ x_3 = -\delta_\varepsilon \Psi\left(\frac{x_1}{\varepsilon}, \frac{x_2}{\varepsilon}\right)\right\}, \tag{3}$$

where $\omega \subset \mathbb{R}^2$ is a Lipschitz bounded open set, Ψ in $W^{2,\infty}_{loc}(\mathbb{R}^2)$ is a periodic function of period $Z' = (-1/2, 1/2)^2$ and $\delta_\varepsilon > 0$ satisfies $\lim\limits_{\varepsilon \to \mathbf{0}} \dfrac{\delta_\varepsilon}{\varepsilon} = 0$. Taking the oscillating domain Ω_ε by

$$\Omega_\varepsilon = \left\{x = (x_1, x_2, x_3) \in \omega \times \mathbb{R} : -\delta_\varepsilon \Psi\left(\frac{x_1}{\varepsilon}, \frac{x_2}{\varepsilon}\right) < x_3 < 1\right\}, \tag{4}$$

we show that if the limit of $\delta_\varepsilon/\varepsilon^{\frac{3}{2}}$ tends to infinity and (2) holds, the slip and the adherence boundary conditions are still asymptotically equivalent. However, this result does not hold if the limit λ of $\delta_\varepsilon/\varepsilon^{\frac{3}{2}}$ belongs to $(0, +\infty)$. In this case we do not have the adherence condition in the limit but the rugosity is large enough to enlarge the friction coefficient in the limit. When $\delta_\varepsilon/\varepsilon^{\frac{3}{2}}$ converges to zero, we prove that the rugosity is so small that it has no effect on the limit problem. For a related result we refer to [2, 4, 5].

In Sect. 3 we will generalize the results obtained in Sect. 2 to a thin domain of small height ε. Taking ω and Ψ as above, our aim is to study the behavior of the

fluid near the rough periodic boundary of period r_ε and amplitude δ_ε defined by

$$\Gamma_\varepsilon^{thin} = \left\{ x = (x_1, x_2, x_3) \in \omega \times \mathbb{R} : \; x_3 = -\delta_\varepsilon \Psi \left(\frac{x_1}{r_\varepsilon}, \frac{x_2}{r_\varepsilon} \right) \right\}, \tag{5}$$

with $r_\varepsilon,\ \delta_\varepsilon > 0$ satisfying $\lim\limits_{\varepsilon \to 0} \dfrac{r_\varepsilon}{\varepsilon} = 0,\ \lim\limits_{\varepsilon \to 0} \dfrac{\delta_\varepsilon}{r_\varepsilon} = 0$. Defining $\Omega_\varepsilon^{thin}$ by

$$\Omega_\varepsilon^{thin} = \left\{ x = (x_1, x_2, x_3) \in \omega \times \mathbb{R} : \; -\delta_\varepsilon \Psi \left(\frac{x_1}{r_\varepsilon}, \frac{x_2}{r_\varepsilon} \right) < x_3 < \varepsilon \right\}, \tag{6}$$

we show analogous results to those presented in Sect. 2, but in this case the behavior of the fluid near Γ^{thin} depends on the limit of a $\dfrac{\delta_\varepsilon}{r_\varepsilon} \sqrt{\dfrac{\varepsilon}{r_\varepsilon}}$. That is, the behavior only depend on the small height of the domain, and not only on the parameters describing the rough boundary. When ε goes to 1 we recover the previous case.

2 Asymptotic Behavior of a Viscous Fluid in a Rough Domain

From now on, the points x of $\mathbb{R}^3$ are supposed to be decomposed as $x = (x', x_3)$ with $x' \in \mathbb{R}^2$, $x_3 \in \mathbb{R}$. We also use the notation x' to denote a generic vector of $\mathbb{R}^2$.

Given a bounded connected Lipschitz open set $\omega \subset \mathbb{R}^2$ and $\Psi \in W^{2,\infty}_{loc}(\mathbb{R}^2)$, periodic of period $Z' = (-1/2, 1/2)^2$, we define the domain Ω_ε by (4) and its rough boundary Γ_ε by (3). Then, for $f \in L^2(\omega \times (-1, 1))^3$, we consider the Navier-Stokes system in Ω_ε,

$$\begin{cases} -\mu \Delta u_\varepsilon + \nabla p_\varepsilon + (u_\varepsilon \cdot \nabla) u_\varepsilon = f \ \text{ in } \Omega_\varepsilon, \qquad \operatorname{div} u_\varepsilon = 0 \ \text{ in } \Omega_\varepsilon, \\ u_\varepsilon = 0 \ \text{ on } \partial\Omega_\varepsilon \setminus \Gamma_\varepsilon, \\ u_\varepsilon \cdot \nu = 0 \ \text{ on } \Gamma_\varepsilon, \qquad \dfrac{\partial u_\varepsilon}{\partial \nu} \ \text{ parallel to } \nu \ \text{ on } \Gamma_\varepsilon. \end{cases} \tag{7}$$

Here, $\mu > 0$ corresponds to the viscosity of the fluid and ν denotes the unitary outside normal vector to Ω_ε on Γ_ε. It is well known that (7) has at least a solution $(u_\varepsilon, p_\varepsilon) \in H^1(\Omega_\varepsilon)^3 \times L^2_0(\Omega_\varepsilon)$ ($L^2_0(\Omega_\varepsilon)$ denotes the space of functions in $L^2(\Omega_\varepsilon)$ whose integral in Ω_ε is zero). Moreover, we can show the following estimates

$$\|u_\varepsilon\|_{H^1(\Omega_\varepsilon)^3} + \|p_\varepsilon\|_{L^2(\Omega_\varepsilon)} \leq C, \quad \forall \varepsilon > 0. \tag{8}$$

Our problem is to describe the asymptotic behavior of the sequences u_ε and p_ε when ε tends to zero. This is given by the following theorem which is the main result of this section.

Theorem 2.1 *We assume that* $(u_\varepsilon, p_\varepsilon)$ *is a solution of (7). Then, there exists* $(u, p) \in H^1(\Omega)^3 \times L^2_0(\Omega)$*, such that, up to a subsequence,*

$$u_\varepsilon \rightharpoonup u \ \text{ in } H^1(\Omega)^3, \qquad p_\varepsilon \rightharpoonup p \ \text{ in } L^2(\Omega), \qquad \text{where } \Omega = \omega \times (0,1). \tag{9}$$

The pair (u, p) *satisfies the Navier-Stokes system*

$$-\mu\Delta u + \nabla p + (u\cdot\nabla)u = f \ \text{ in } \Omega, \qquad \text{div } u = 0 \text{ in } \Omega, \tag{10}$$

the adherence condition $u = 0$ *on* $\partial\Omega \setminus \Gamma$ *and the vertical component of the limit velocity satisfies* $u_3 = 0$ *on* Γ*, where* $\Gamma = \omega \times \{0\}$*. Moreover, denoting (this limit exists at least for a subsequence)*

$$\lambda = \lim_{\varepsilon\to 0} \frac{\delta_\varepsilon}{\varepsilon^{\frac{3}{2}}} \in [0, +\infty], \tag{11}$$

the tangential component of the limit velocity, u'*, also satisfies the following boundary condition on* Γ

i) If $\lambda = 0$*, then*

$$\partial_3 u' = 0 \ \text{ on } \Gamma. \tag{12}$$

ii) If $\lambda \in (0, +\infty)$*, then defining* $(\widehat{\phi}^i, \widehat{q}^{\,i})$*,* $i = 1, 2$ *as a solution of*

$$\begin{cases} -\mu\Delta_z\widehat{\phi}^i + \nabla_z\widehat{q}^i = 0 \ \text{ in } \mathbb{R}^2 \times (0,+\infty), \\ \text{div}_z\,\widehat{\phi}^i = 0 \ \text{ in } \mathbb{R}^2 \times (0,+\infty), \\ \widehat{\phi}^i_3(z',0) + \partial_{z_i}\Psi(z') = 0, \ \partial_{z_3}(\widehat{\phi}^i)'(z',0) = 0, \\ \widehat{\phi}^i(.,z_3),\ \widehat{q}^{\,i}(.,z_3) \text{ periodic of period } Z', \\ D_z\widehat{\phi}^i \in L^2(Z'\times(0,+\infty))^{3\times 3},\ \widehat{q}^{\,i} \in L^2(Z'\times(0,+\infty)), \end{cases} \tag{13}$$

and $R \in \mathbb{R}^{2\times 2}$ *by* $R_{ij} = \mu \displaystyle\int_{Z'\times(0,+\infty)} D_z\widehat{\phi}^i : D_z\widehat{\phi}^j \, dz, \quad \forall\, i, j \in \{1,2\}$ (14)

we have

$$-\mu\partial_3 u' + \lambda^2 R u' = 0 \ \text{ on } \Gamma. \tag{15}$$

iii) If $\lambda = +\infty$*, then defining*

$$W = Span(\{(\nabla\Psi(z'), 0) : z' \in Z'\}), \tag{16}$$

we have

$$u' \in W^\perp \ \text{ on } \Gamma, \quad \partial_3 u' \in W. \tag{17}$$

Remark 2.2 *For* $\lambda = 0$*, the rugosity of* Γ_ε *is very slight and the solution* $(u_\varepsilon, p_\varepsilon)$ *of (7) behaves as if* Γ_ε *coincides with the plane boundary* Γ*. For* $0 < \lambda < +\infty$ *(critical size), the boundary condition satisfied by the limit* u *of* u_ε *on the tangent*

space to Γ *contains the new term* $\lambda^2 Ru'$. *The effect of the rugosity of the wall* Γ_ε *is not worthless in this case. Finally, for* $\lambda = +\infty$ *the rugosity is so strong that the limit* u *of* u_ε *does not only satisfies the condition* $u_3 = 0$ *on* Γ, *but it is also such that its tangent velocity on* Γ, u', *is in* $W^\perp$, *for every* $z' \in Z'$. *In particular, if the linear space spanned by* W *has dimension 2 (this holds if and only if* Ψ *is not constant in any straight line of* $\mathbb{R}^2$, *see [3–5]), we get that* u *satisfies the adherence condition* $u = 0$ *on* Γ, *i.e. although we have imposed a slip condition on* Γ_ε, *the rugosity forces* u *to satisfy a no-slip (adherence) condition on* Γ. *This result extends to the case where*

$$\lim_{\varepsilon\to 0} \frac{\delta_\varepsilon}{\varepsilon} = 0, \qquad \lim_{\varepsilon\to 0} \frac{\delta_\varepsilon}{\varepsilon^{\frac{3}{2}}} = +\infty,$$

the results obtained in [3] for $\delta_\varepsilon = \varepsilon$ *(see also [2] for the nonperiodic case).*

The limit equation (15) corresponding to the critical size $\lambda \in (0, +\infty)$ *can be considered as the general one. In fact, if* λ *is tending to zero or* $+\infty$ *in (15) we get (12) and (17) respectively.*

Remark 2.3 *In the cases* $\lambda = 0$ *or* $+\infty$, *we can prove that the convergences in (9) are strong. In fact, assuming* ω *smooth enough (for example* C^2*), we can show that we have*

$$\int_{\Omega_\varepsilon} |u_\varepsilon - u|^2 dx \to 0, \quad \int_{\Omega_\varepsilon} |D(u_\varepsilon - u)|^2 dx \to 0, \quad \int_{\Omega_\varepsilon} |p_\varepsilon - p|^2 dx \to 0.$$

In the critical case $\lambda \in (0, +\infty)$, *defining* $\bar{u}_\varepsilon$ *and* $\bar{p}_\varepsilon$ *by*

$$\bar{u}_\varepsilon(x) = u(x) - \lambda\sqrt{\varepsilon}\left(u_1(x', 0)\widehat{\phi}^1(\frac{x}{\varepsilon}) + u_2(x', 0)\widehat{\phi}^2(\frac{x}{\varepsilon})\right),$$

$$\bar{p}_\varepsilon(x) = p(x) - \frac{\lambda}{\sqrt{\varepsilon}}\left(u_1(x', 0)\widehat{q}^1(\frac{x}{\varepsilon}) + u_2(x', 0)\widehat{q}^2(\frac{x}{\varepsilon})\right),$$

then the above assertion still holds by replacing u *and* p *by* $\bar{u}_\varepsilon$ *and* $\bar{p}_\varepsilon$, *respectively.*

3 Asymptotic Behavior of a Viscous Fluid in a Rough Thin Domain

In this section we will generalize the results given in Sect. 2 to the thin domain $\Omega_\varepsilon^{thin}$ given by (6) with a rough boundary $\Gamma_\varepsilon^{thin}$ described by (5). Then, for $f = (f', f_3) \in L^2(\omega)^3$ we consider the Navier-Stokes system

$$\begin{cases} -\mu\Delta u_\varepsilon + \nabla p_\varepsilon + (u_\varepsilon \cdot \nabla)u_\varepsilon = f \ \text{ in } \Omega_\varepsilon^{thin}, \qquad \operatorname{div} u_\varepsilon = 0 \ \text{ in } \Omega_\varepsilon^{thin}, \\ u_\varepsilon = 0 \ \text{ on } \partial\Omega_\varepsilon^{thin} \setminus \Gamma_\varepsilon^{thin}, \\ u_\varepsilon \cdot \nu = 0 \ \text{ on } \Gamma_\varepsilon^{thin}, \qquad \dfrac{\partial u_\varepsilon}{\partial \nu} \ \text{ parallel to } \nu \ \text{ on } \Gamma_\varepsilon^{thin}. \end{cases} \tag{18}$$

This system has at least a solution $(u_\varepsilon, p_\varepsilon) \in H^1(\Omega_\varepsilon)^3 \times L^2_0(\Omega_\varepsilon)$. Moreover it satisfies

$$\int_{\Omega_\varepsilon^{thin}} |u_\varepsilon|^2 dx \le C\varepsilon^4, \quad \int_{\Omega_\varepsilon^{thin}} |Du_\varepsilon|^2 dx \le C\varepsilon^2, \quad \int_{\Omega_\varepsilon^{thin}} |p_\varepsilon|^2 dx \le C. \tag{19}$$

As in the previous section, our aim is to study the asymptotic behavior of u_ε and p_ε when ε tends to zero. For this purpose, as usual, we use a dilatation in the variable x_3 in order to have the functions defined in an open set of fixed height. Namely, we define $\tilde{u}_\varepsilon \in H^1(\Omega)^3$, $\tilde{p}_\varepsilon \in L^2_0(\Omega)$ by

$$\tilde{u}_\varepsilon(y) = u_\varepsilon(y', \varepsilon y_3), \quad \tilde{p}_\varepsilon(y) = p_\varepsilon(y', \varepsilon y_3), \quad \text{a.e. } y \in \Omega = \omega \times (0,1). \tag{20}$$

Then, our problem is to describe the asymptotic behavior of these sequences $\tilde{u}_\varepsilon$, $\tilde{p}_\varepsilon$. This is given by the following theorem.

Theorem 3.1 *Let $(u_\varepsilon, p_\varepsilon) \in H^1(\Omega_\varepsilon)^3 \times L^2_0(\Omega_\varepsilon)$ be a solution of (18) and let $\tilde{u}_\varepsilon$, $\tilde{p}_\varepsilon$ be defined by (20). Then, there exist $v \in H^1(0,1; L^2(\omega))^2$, $w \in H^2(0,1; H^{-1}(\omega))$ and $p \in L^2_0(\Omega)$, where p does not depend on y_3, such that, up to a subsequence,*

$$\begin{gathered} \frac{\tilde{u}_\varepsilon}{\varepsilon} \rightharpoonup 0 \text{ in } H^1(\Omega)^3, \quad \frac{\tilde{u}_\varepsilon}{\varepsilon^2} \rightharpoonup (v,0) \text{ in } H^1(0,1; L^2(\omega))^3, \\ \frac{\tilde{u}_{\varepsilon,3}}{\varepsilon^3} \rightharpoonup w \text{ in } H^2(0,1; H^{-1}(\omega)), \end{gathered} \tag{21}$$

$$\tilde{p}_\varepsilon \rightharpoonup p \text{ in } L^2(\Omega), \quad \frac{\partial_{y_3} \tilde{p}_\varepsilon}{\varepsilon} \rightharpoonup f_3 \text{ in } H^{-1}(\Omega). \tag{22}$$

According to the value of λ^{thin} defined by

$$\lambda^{thin} = \lim_{\varepsilon \to 0} \frac{\delta_\varepsilon}{r_\varepsilon} \sqrt{\frac{\varepsilon}{r_\varepsilon}} \in [0, +\infty], \tag{23}$$

the functions v, w and p are given by

(i) If $\lambda^{thin} = +\infty$, then denoting by $P_{W^\perp}$ the orthogonal projection from $\mathbb{R}^2$ to the orthogonal of the space W defined by (16), we have that v is given by

$$v(y) = \frac{(y_3 - 1)}{2\mu} \left(y_3 I + P_{W^\perp} \right) \left(\nabla_{y'} p(y') - f'(y') \right), \quad \text{a.e. } y \in \Omega,$$

where p satisfies

$$\begin{cases} -div_{y'} \left(\left(\frac{1}{3} I + P_{W^\perp} \right) (\nabla_{y'} p - f') \right) = 0 \text{ in } \omega, \\ \left(\frac{1}{3} I + P_{W^\perp} \right) (\nabla_{y'} p - f') \cdot \nu = 0 \text{ on } \partial\omega. \end{cases}$$

Moreover, the distribution w is given by

$$w(y) = -\int_0^{y_3} div_{y'} v(y', s) ds, \quad in\ \Omega. \tag{24}$$

(ii) If $\lambda \in (0, +\infty)$*, then defining* $(\widehat{\phi}^i, \widehat{q}^i)$*,* $i = 1, 2$*, as solutions of the Stokes systems (13) and the matrix R by (14), we have*

$$v(y) = \frac{(y_3 - 1)}{2\mu} \left(y_3 I + \left(I + \frac{\lambda^2}{\mu} R \right)^{-1} \right) \left(\nabla_{y'} p(y') - f'(y') \right), \ a.e.\ y \in \Omega,$$

where p satisfies

$$\begin{cases} -\mathrm{div}_{y'} \left(\left(\frac{1}{3} I + \left(I + \frac{\lambda^2}{\mu} R \right)^{-1} \right) (\nabla_{y'} p - f') \right) = 0 \ \ in\ \omega, \\ \left(\frac{1}{3} I + \left(I + \frac{\lambda^2}{\mu} R \right)^{-1} \right) (\nabla_{y'} p - f') \cdot \nu = 0 \ \ on\ \partial\omega. \end{cases}$$

Moreover, the distribution w is given by (24).

(iii) If $\lambda = 0$*, then* $v(y) = \dfrac{(y_3^2 - 1)}{2\mu} (\nabla_{y'} p(y') - f'(y')), \quad a.e.\ y \in \Omega,$

where p satisfies $-\Delta_{y'} p = -div_{y'} f'$ *in* ω, $\dfrac{\partial p}{\partial \nu} = f' \cdot \nu$ *on* $\partial\omega$.

Moreover, the distribution w is zero.

Remark 3.2 *The role of the parameter* λ^{thin} *in Theorem 3.1 is similar to the one of* λ *in Theorem 2.1. Indeed, we remember that for* $\varepsilon = 1$ *both parameters agree (note that the parameter* ε *in Theorem 2.1 is now called* r_ε*).*

Remark 3.3 *In the cases* $\lambda^{thin} = 0$ *or* $+\infty$*, we can prove that the convergences in (21)–(22) are strong. In fact, assuming* ω *smooth enough, we prove that defining* $\bar{u}_\varepsilon$*,* $\bar{p}_\varepsilon$ *by*

$$\bar{u}_\varepsilon(x) = \left(\varepsilon^2 v(x', \frac{x_3}{\varepsilon}), 0 \right), \quad \bar{p}_\varepsilon(x) = p(x') \ \ a.e.\ x \in \Omega_\varepsilon^{thin},$$

we have

$$\frac{1}{\varepsilon^4} \int_{\Omega_\varepsilon} |u_\varepsilon - \bar{u}_\varepsilon|^2 dx \to 0, \quad \frac{1}{\varepsilon^2} \int_{\Omega_\varepsilon} |D(u_\varepsilon - \bar{u}_\varepsilon)|^2 dx \to 0, \quad \int_{\Omega_\varepsilon} |p_\varepsilon - \bar{p}_\varepsilon|^2 dx \to 0.$$

In the critical case $\lambda^{thin} \in (0, +\infty)$*, the above assertion still holds replacing* $\bar{u}_\varepsilon$ *by*

$$\bar{u}_\varepsilon(x) = \left(\varepsilon^2 v(x', \frac{x_3}{\varepsilon}), 0 \right) - \lambda \varepsilon \sqrt{\varepsilon r_\varepsilon} \left(v_1(x', 0) \widehat{\phi}^1(\frac{x}{r_\varepsilon}) + v_2(x', 0) \widehat{\phi}^2(\frac{x}{r_\varepsilon}) \right).$$

Acknowledgements This work has been partially supported by the projects MTM2008-00306/MTM of the “Ministerio de Ciencia e Innovación" and FQM309 of the “Junta de Andalucía".

References

1. Bucur, D., Feireisl, E., Nečsová, N.: Boundary behavior of viscous fluids: Influence of wall roughness and friction-driven boundary conditions. Archiv. Rational Mech. Anal., **197**, 117–138 (2010).
2. Bucur, D., Feireisl, E., Nečasová, S., Wolf, J.: On the asymptotic limit of the Navier−Stokes system on domains with rough boundaries. J. Differential Equations, **244**, 2890–2908 (2008).
3. Casado-Díaz, J., Fernández-Cara, E., Simon, J.: Why viscous fluids adhere to rugose walls: A mathematical explanation. J. Differential Equations, **189**, 526–537 (2003).
4. Casado-Díaz, J., Luna-Laynez, M., Suárez-Grau, F.J.: Asymptotic behavior of a viscous fluid with slip boundary conditions on a slightly rough wall. Math. Mod. Meth. Appl. Sci., **20**, 121–156 (2010).
5. Casado-Díaz, J., Luna-Laynez, M., Suárez-Grau, F.J.: A viscous fluid in a thin domain satisfying the slip condition on a slightly rough boundary. C. R. Mathematique, doi:10.1016/j.crma.2010.07.023 (2010).

High Reynolds Channel Flows: Upstream Interaction of Various Wall Deformations

P. Cathalifaud, M. Zagzoule, J. Cousteix, and J. Mauss

1 Introduction

The upstream non linear interaction at high Reynolds number in a channel with local or global wall distortion is considered. Three methods are used to study the anticipated fluid response to the distal disturbance:

- A new asymptotic approach called Successive Complementary Expansion Method (SCEM) leading to a uniformly valid reduced model termed GIBL for Global Interactive Boundary Layer [1, 3].
- An eigenmode analysis.
- Full Navier–Stokes simulation.

The three approaches confirm the Smith [2] result: the length of the non linear upstream influence of an *accident* at $x = x_0$ at the walls, Δ, is $O(R_e^{1/7})$, where R_e is the Reynolds number. The only hypothesis on the wall *accident* is that it is significant enough to perturb the Poiseuille flow, so that the Poiseuille flow is no more a good approximation in the boundary layer.

Then by assuming an exponential variation in x of the perturbed flow, in order to obtain the Poiseuille flow as $x \to -\infty$ (i.e. far upstream the wall deformations), we perform an eigenmode analysis, which shows that the first mode is related to asymmetric wall deformations. Finally, comparison with full Navier–Stokes simulation shows that the GIBL model is well founded.

P. Cathalifaud (✉), M. Zagzoule, and J. Mauss
Université de Toulouse; INPT, UPS; CNRS; IMFT; F-31400 Toulouse, France
e-mail: catalifo@imft.fr, zagzoule@imft.fr, mauss@cict.fr

J. Cousteix
DMAE, ONERA, ISAE; Toulouse, France
e-mail: Jean.Cousteix@onecert.fr

C. Clavero et al. (eds.), *BAIL 2010 – Boundary and Interior Layers, Computational and Asymptotic Methods*, Lecture Notes in Computational Science and Engineering 81,
DOI 10.1007/978-3-642-19665-2_8,

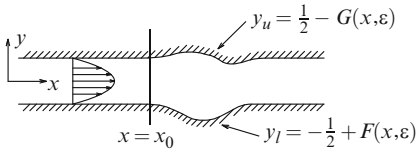

Fig. 1 (i) case: Local wall perturbation; location of the accident at $x = x_0$

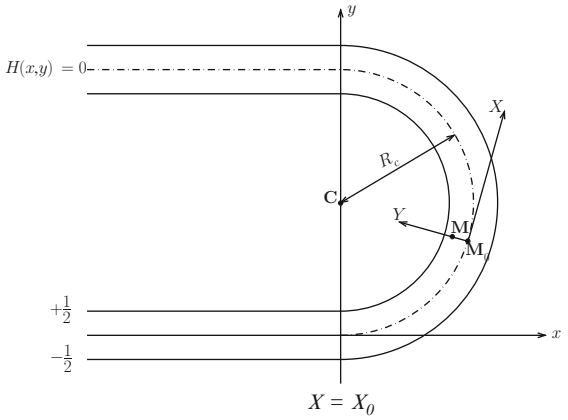

Fig. 2 (ii) case: Global wall curvature; location of the accident at $X = X_0$

2 Geometrical Configuration

Two kinds of geometrical configuration have been considered for the *accident*: (i) a local wall perturbation as in Fig. 1, or (ii) a global wall curvature as in Fig. 2.

In the test case (i), the walls are deformed in a domain $x_0 \leq x \leq x_0 + L$ such as:

$$F = \frac{h_l}{2}\left(1 + \cos\frac{2\pi(x - x_0)}{L}\right); G = -\frac{h_u}{2}\left(1 + \cos\frac{2\pi(x - x_0)}{L}\right). \quad (1)$$

where h_u and h_l are small parameters.

In the test case (ii), we use a generalized system of coordinates, where X and Y are distances along and perpendicular to the line $H = 0$. We call it the median line if the upper (or inner) and lower (or external) walls are respectively given by $Y = \pm\frac{1}{2}$.

For a point M with general coordinates X and Y, we can write $\overrightarrow{OM} = \overrightarrow{OM_0} + Y\,\mathbf{n}$, where $\mathbf{n}$ is the unit normal vector. Then, $\mathrm{d}\overrightarrow{M} = \mathrm{d}X\,(1 + KY)\,\boldsymbol{\tau} + \mathrm{d}Y\,\mathbf{n}$, where $\boldsymbol{\tau}$ is the unit vector tangent at M_0 to the median line in such a way that $(\boldsymbol{\tau}, \mathbf{n})$ is direct; $K(X)$ is the algebraic curvature of this line. Thus, $K < 0$ in the case of Fig. 2. The curvature K and its variation in X are small. We thus describe the channel variable curvature for $X > 0$ by $K = \delta k(X)$, where δ is a small positive

parameter. Let U and V denote the velocity components parallel and perpendicular to the line $H = 0$, then, as $\mathbf{V} = U\boldsymbol{\tau} + V\mathbf{n}$, the full equations of motion written in generalized coordinates are given in [4]. These equations must be solved with boundary conditions: $U = V = 0$ for $Y = \pm\frac{1}{2}$.

3 Fully Established Flow in a Curved Channel

For a channel of constant curvature δ, the fully established flow U_0 is solution of

$$(1 + \delta Y)\frac{\mathrm{d}^2 U_0}{\mathrm{d}Y^2} + \delta\frac{\mathrm{d}U_0}{\mathrm{d}Y} - \frac{\delta^2}{1 + K_0 Y}U_0 = -GR_e \tag{2}$$

where $G = -\dfrac{\partial P}{\partial X}$ is constant, and with $U_0 = 0$ for $Y = \pm\dfrac{1}{2}$. Notice that for $\delta = 0$ we retrieve the equation for the Poiseuille flow: $\dfrac{\mathrm{d}^2 U_0}{\mathrm{d}Y^2} = -2$. For more details see Zagzoule et al.[4].

The exact solution is given by:

$$U_0(Y) = \frac{1}{64}GR_e\frac{f(\delta, Y)}{(\delta^2(1 + \delta Y))} \tag{3}$$

where

$$\begin{aligned} f(\delta, Y) = {} & \left[\delta^3(1 - 4Y^2) + 8\delta^2 Y(2Y - 1) + 4\delta(-4Y^2 + 8Y - 3)\right. \\ & \left. +16(1 - 2Y)\right]\ln\left(\frac{2 - \delta}{2\delta}\right) + \\ & \left[-\delta^3(1 - 4Y^2) + 8\delta^2 Y(2Y + 1) + 4\delta(4Y^2 + 8Y + 3)\right. \\ & \left. +16(1 + 2Y)\right]\ln\left(\frac{2 + \delta}{2\delta}\right) - \\ & 32\left(2\delta Y + \delta^2 Y^2 + 1\right)\ln\left(\frac{1 + \delta Y}{\delta}\right) \end{aligned}$$

As shown in Fig. 3, the corresponding exact solution $U_0(Y)$ bends towards the internal wall of the bend. Notice that, for a small constant curvature δ and for a flow rate of $1/6$, an approximate solution $\mathrm{O}(\delta)$ is $U_0(Y) = \left(\dfrac{1}{4} - Y^2\right)\left(1 - \dfrac{2\delta}{3}Y\right)$, which implies that the skin friction $C_f\dfrac{R_e}{2} = 1 \mp \dfrac{\delta}{3}$. If $\delta = 0$ (straight channel) then $U_0(Y) = u_0(Y) = \frac{1}{4} - Y^2$.

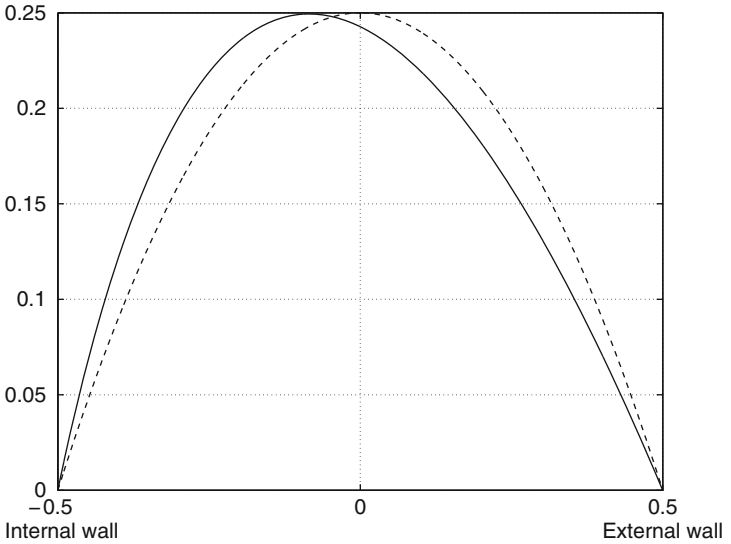

Fig. 3 Velocity profile $U_0(Y)$: Poiseuille flow $u_0(Y)$ (*dashed line*); curved flow for $\delta = 1$ (*solid line*)

4 Global Interactive Boundary Layer (GIBL) Model

According to the SCEM, a Uniformaly Valid Approximation (UVA) for the velocity and pressure fields (U, V, P) is obtained by complementing the core approximation $(U_1 = u_0 + \delta u_1, V_1 = \delta v_1, P_1 = p_0 + \delta p_1)$ by the correcting terms (U_{BL}, V_{BL}, P_{BL}) such as:

$$\begin{aligned} U &= u_0(Y) + \delta\,[u_1(X, Y, \delta) + U_{BL}(X, \eta, \delta)] \\ V &= \delta\,[v_1(X, Y, \delta) + \varepsilon V_{BL}(X, \eta, \delta)] \\ P &= p_0(X) + \delta\,[p_1(X, Y, \delta, \varepsilon) + \Delta(\varepsilon) P_{BL}(X, \eta, \delta, \varepsilon)] \end{aligned} \tag{4}$$

where $u_0(Y) = \dfrac{1}{4} - Y^2$ and $p_0(X) = -\dfrac{2X}{R_e}$ correspond to the Poiseuille flow in a 2D straight channel, and $\eta = \dfrac{\frac{1}{2} \pm Y}{\varepsilon}$ is the boundary layer variable, with ε the boundary layer thickness. Necessarily $\lim\limits_{\eta\to\infty} U_{BL} = 0$, $\lim\limits_{\eta\to\infty} V_{BL} = 0$ and $\lim\limits_{\eta\to\infty} P_{BL} = 0$ to retrieve in the core flow the core approximation (U_1, V_1, P_1). By analysing the various orders of magnitude, it can be shown that the gauge function $\Delta(\varepsilon) = \mathrm{O}(\varepsilon^3)$ (see Zagzoule et al.[4] for more details).

Thus, we obtain Uniformaly Valid Approximation (UVA) equations:

$$\frac{\partial U}{\partial X} + \frac{\partial V}{\partial Y} = 0$$
$$U\frac{\partial U}{\partial X} + V\frac{\partial U}{\partial Y} = -\frac{\partial P_1}{\partial X} + \frac{1}{R_e}\frac{\partial}{\partial Y}\left[(1+KY)\frac{\partial U}{\partial Y}\right]$$

with the following boundary conditions, $U = V = 0$, for $Y = \pm\frac{1}{2}$. The core equations being:

$$u_0\frac{\partial V_1}{\partial X} - Ku_0^2 = -\frac{\partial P_1}{\partial Y}$$
$$-u_0\frac{\partial V_1}{\partial Y} + V_1\frac{du_0}{dY} = -\frac{\partial(P_1 - p_0)}{\partial X}$$

A simplified model for the pressure gives

$$\frac{\partial P_1}{\partial X} = \frac{\mathrm{d}p_0}{\mathrm{d}X} + \delta\left(A''' + k'\right)\int_{Y_c}^{Y} u_0^2(Y')\,\mathrm{d}Y' \quad + \delta B'(X),$$

where $A(X)$ and $B(X)$ are 2 unknown functions to determine. At the median line, i.e. for $Y = Y_c$, since the UVA V should match the core approximation V_1, we impose the coupling condition $V = V_1 = -A'(X)u_0$.

For more details about GIBL, see the companion paper Zagzoule et al.[5].

5 Upstream Interaction

5.1 Upstream Length

In a straight channel, upstream of the wall *accident*, for $x < 0$, the GIBL and core equations become:

$$U\frac{\partial U}{\partial x} + V\frac{\partial U}{\partial y} = -\frac{\partial P_1}{\partial x} + \frac{1}{Re}\frac{\partial^2 U}{\partial y^2} \tag{5}$$
$$\frac{\partial U}{\partial x} + \frac{\partial V}{\partial y} = 0 \tag{6}$$
$$-u_0\frac{\partial V_1}{\partial y} + V_1\frac{\mathrm{d}u_0}{\mathrm{d}y} = -\frac{\partial(P_1 - P_0)}{\partial x} \tag{7}$$
$$u_0\frac{\partial V_1}{\partial x} = -\frac{\partial(P_1 - P_0)}{\partial y} \tag{8}$$

We now consider perturbations of the following form: $U = u_0 + \varepsilon u$, $V = \varepsilon v$ and $P_1 = P_0 + \lambda p_1$.

If the critical unknown streamwise length scale is Δ, then, with $\overline{x} = \dfrac{x}{\Delta}$ and thus $\overline{V} = \Delta V$, we obtain from (5), (6), (7), (8) the following perturbation equations:

$$\frac{\partial u}{\partial \overline{x}} + \frac{\partial \overline{v}}{\partial y} = 0 \tag{9}$$

$$u_0 \frac{\partial u}{\partial \overline{x}} + \overline{v} \frac{\mathrm{d}u_0}{\mathrm{d}y} + \varepsilon \left(u \frac{\partial u}{\partial \overline{x}} + \overline{v} \frac{\partial u}{\partial y} \right) = -\frac{\lambda}{\varepsilon} \frac{\partial p_1}{\partial \overline{x}} + \frac{\Delta}{Re} \frac{\partial^2 u}{\partial y^2} \tag{10}$$

$$-u_0 \frac{\partial \overline{v_1}}{\partial y} + \overline{v_1} \frac{\mathrm{d}u_0}{\mathrm{d}y} = -\frac{\lambda}{\varepsilon} \frac{\partial p_1}{\partial \overline{x}} \tag{11}$$

$$u_0 \frac{\partial \overline{v_1}}{\partial \overline{x}} = -\frac{\lambda \Delta^2}{\varepsilon} \frac{\partial p_1}{\partial y} \tag{12}$$

If ε is the boundary layer thickness, the first significant perturbation is such as $u_0 = \mathrm{O}(\varepsilon)$, $\overline{v} = \mathrm{O}(\varepsilon)$ in the boundary layers, which implies from (10) that ε, $\dfrac{\lambda}{\varepsilon}$ and $\dfrac{\Delta}{\varepsilon^2 R_e}$ are of same order. An upstream interaction takes place if we have a generation of a significant transverse pressure gradient in the core flow, which implies from (12) that $\dfrac{\lambda \Delta^2}{\varepsilon} = \mathrm{O}(1)$. Thus, we easily obtain (as did Smith [2] by regular asymptotic expansions) the following crucial orders:

$$\Delta = \mathrm{O}(R_e^{1/7}), \quad \varepsilon = \mathrm{O}(R_e^{-2/7}) \quad \text{and} \quad \lambda = \mathrm{O}(R_e^{-4/7}). \tag{13}$$

5.2 Eigenmode Analysis

For $x < 0$, the linearized UVA system of equations may be written as :

$$\begin{cases} u_0 \dfrac{\partial u}{\partial x} + u_0' v = -\dfrac{\partial p_1}{\partial x} + \dfrac{1}{Re} \dfrac{\partial^2 u}{\partial y^2} \\ \dfrac{\partial u}{\partial x} + \dfrac{\partial v}{\partial y} = 0 \\ u_0 \dfrac{\partial v_1}{\partial x} = -\dfrac{\partial p_1}{\partial y} \end{cases} \tag{14}$$

By replacing v_1 by v in the transverse core momentum equation, and by assuming the following form for u, v and p_1 :

$$u(x, y) = \hat{u}(y) \mathrm{e}^{\theta x}, \quad v(x, y) = \hat{v}(y) \mathrm{e}^{\theta x}, \quad p_1(x, y) = \hat{p}_1(y) \mathrm{e}^{\theta x} \tag{15}$$

we obtain the following compact formulation for the perturbation equations:

$$\theta \begin{pmatrix} u_0 & 0 & 1 \\ 1 & 0 & 0 \\ 0 & u_0 & 0 \end{pmatrix} \hat{q} = \begin{pmatrix} \frac{D^2}{Re} & -u_0' & 0 \\ 0 & -D^1 & 0 \\ 0 & 0 & -D^1 \end{pmatrix} \hat{q} \tag{16}$$

where $\hat{q} = \begin{pmatrix} \hat{u} \\ \hat{v} \\ \hat{p}_1 \end{pmatrix}$, $D^1 = \dfrac{\partial}{\partial y}$ and $D^2 = \dfrac{\partial^2}{\partial y^2}$.

In the case of a wall distortion which produces streamwise growing perturbations starting from $x = 0$, assuming an exponential x-variation, $e^{\theta x}$, for the perturbed flow means that we'll consider the $\theta > 0$ cases, and it thus allows to recover the Poiseuille flow as $x \to -\infty$, i.e. far upstream the wall distortion.

We just have now to find the eigenvalues and eigenfunctions of the matrix $B^{-1}A$, where :

$$A = \begin{pmatrix} \frac{D^2}{Re} & -u_0' & 0 \\ 0 & -D^1 & 0 \\ 0 & 0 & -D^1 \end{pmatrix} \text{ and } B = \begin{pmatrix} u_0 & 0 & 1 \\ 1 & 0 & 0 \\ 0 & u_0 & 0 \end{pmatrix} \tag{17}$$

The smallest positive eigenvalue, θ_1, of $B^{-1}A$, will give us the longest upstream influence length of the perturbation, i.e. Δ.

For $R_e = 1,000$, the first positive eigenvalue found is $\theta_1 \simeq 2.0441$. The Fig. 4a represents the eigenfunctions of this mode. Notice the asymmetrical form of the $\hat{u}$ and $\hat{p}_1$ profiles, which is related to an asymmetric wall disturbance (see [3]). As shown in Fig. 4b, by computing this first positive eigenvalue for different Reynolds

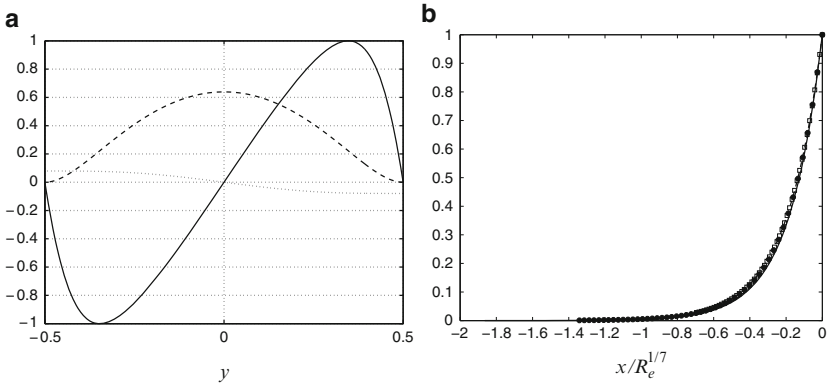

Fig. 4 (**a**) Profiles of the first mode eigenfunctions $\hat{u}$ (*straight line*), $\hat{v}$ (*dashed line*) and $\hat{p}_1$ (*dotted line*) for $Re = 1,000$; (**b**) $e^{\theta_1 x}$ evolution for $Re = 10^3$ (*solid line*), 10^4 (*black circle*), 10^5 (*dashed line*), 10^6 (*white square*)

number ranging from 10^3 to 10^6, and by rescaling x such as $\overline{x} = \dfrac{x}{R_e^{1/7}}$, all the curves collapse with $e^{\theta_1 \overline{x}}$ being negligible for $\overline{x} < 1$. We can thus deduce that the upstream influence $\Delta = O(R_e^{1/7})$ as in the analysis of the Sect. 5.1.

6 Results

Both the order analysis of Sect. 5.1 and the eigenmode analysis of Sect. 5.2 show that $\Delta = O(R_e^{1/7})$. We now compute the flow field using the GIBL model described in Sect. 4 for different accident types at $x = 0$.

First, we have considered a straight channel connected at $x = 0$ to a curved channel of constant curvature. The Fig. 5a and b represent the median curved length evolution of $V(X, \eta_c)$ normalized by $V(0, \eta_c)$ for, respectively, a fixed $\delta = 0.2$ at different Reynolds numbers, and a fixed $R_e = 1,000$ at different wall curvature. These two results show that $V(X, \eta_c)$ becomes negligible for $x < R_e^{1/7}$ confirming that $\Delta = O(R_e^{1/7})$.

Then, we have considered an asymmetrically perturbed straight channel at $x = 0$ with $L = 4H$ and $h_u = h_l = 0.3$. The Fig. 6 represents the streamwise evolution of the normalized $V(x, \eta_c)$, where we recover as previously $\Delta = O(R_e^{1/7})$. Finally, we have compared the Navier–Stokes, GIBL and eigenmode analysis results. In Fig. 7, we have plotted the u, v and p_1 profiles in the (ii) case $R_e = 1,000$ and $\delta = 0.2$, obtained using Navier–Stokes and GIBL. We have also plotted on the same figure the first eigenmode obtained for $R_e = 1,000$. All the results are very similar.

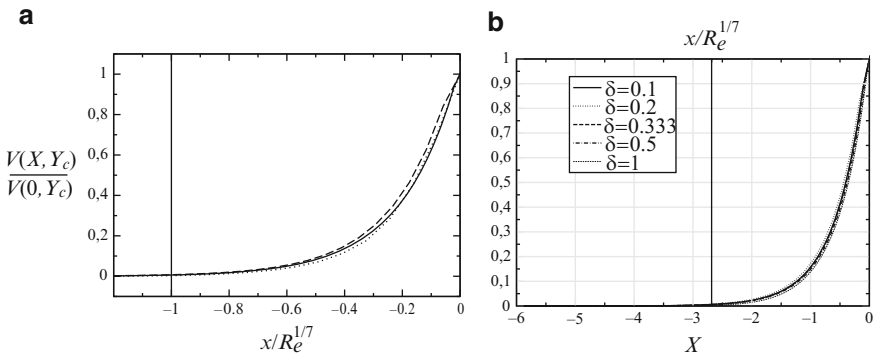

Fig. 5 (ii) case: straight channel connected at $x = 0$ to a curved channel of constant curvature; (**a**) $\delta = 0.2$, R_e from 100 to 10,000; (**b**) $R_e = 1,000$, δ from 0.1 to 1

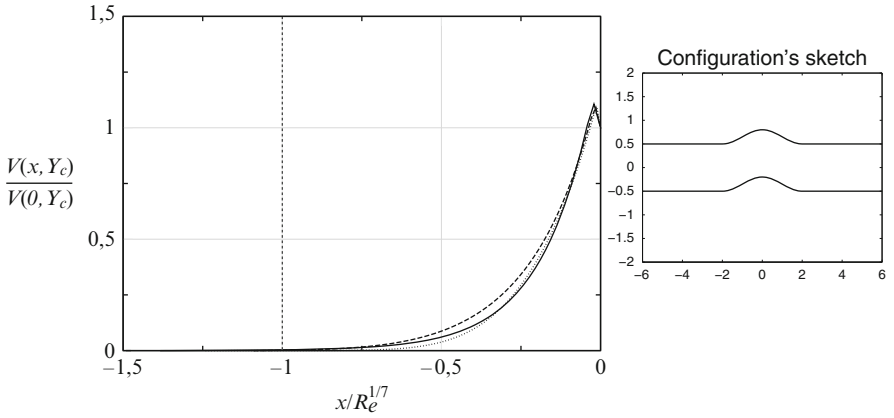

Fig. 6 (i) case: straight channel perturbed at $x = 0$ with $L = 4H$, $h_u = h_l = 0.3$; x-evolution of the adimensionnalized $V(x, \eta_c)$ for different values of R_e (from 100 to 10, 000)

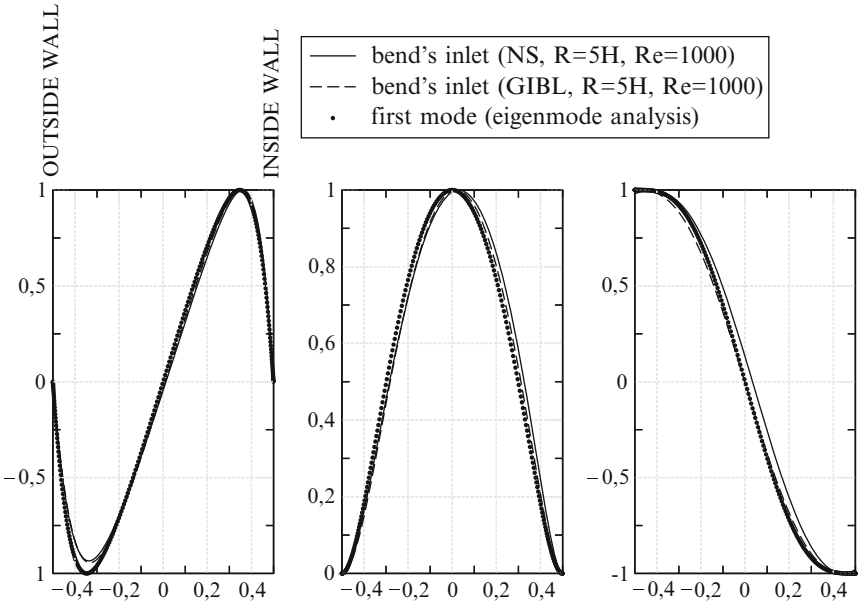

Fig. 7 NS, GIBL, first eigenmode comparison; $R_e = 1,000$, $\delta = 0.2$; *left*: u profile; *middle*: v profile; *right*: p_1 profile

References

1. J. COUSTEIX AND J. MAUSS, *Asymptotic Analysis and Boundary Layers*. Scientific Computation, vol. XVIII, Springer, Berlin, Heidelberg, 2007.
2. F.T. SMITH, Upstream interactions in channel flows. *Journal of Fluid Mechanics* **79** (4), 631–655, (1977).

3. P. CATHALIFAUD, J. MAUSS AND J. COUSTEIX, Non linear aspects of high Reynolds number channel flows. *European Journal of Mechanics B/Fluids* **29** (4), 295–304 (2010).
4. M. ZAGZOULE, P. CATHALIFAUD, J. MAUSS AND J. COUSTEIX, Uniformaly Valid Approximation Flow analysis in Curved Channels. *Submitted to Physics of Fluids* (2010).
5. M. ZAGZOULE, P. CATHALIFAUD, J. MAUSS AND J. COUSTEIX, High Reynolds Channel Flows: Variable curvature. *Lecture Notes in Computational Science and Engineering* (2010).

Uniformly Convergent Finite Difference Schemes for Singularly Perturbed 1D Parabolic Reaction–Diffusion Problems

C. Clavero and J.L. Gracia

Abstract In this paper we present a numerical method to approximate the solution of 1D parabolic singularly perturbed problems of reaction-diffusion type. The method combines the Crank-Nicolson scheme and the central finite difference scheme defined on nonuniform special meshes. We give a new proof of the asymptotic behavior of the semidiscrete problems resulting after the time discretization. Numerical results show in practice almost second order of uniform convergence of the discrete method.

1 Introduction

We consider the 1D parabolic reaction-diffusion singularly perturbed problem

$$\begin{cases} u_t + \mathcal{L}_{x,\varepsilon} u = f(x,t), & (x,t) \in Q = \Omega \times (0,T] \equiv (0,1) \times (0,T], \\ u(x,0) = 0, & x \in \overline{\Omega}, \\ u(0,t) = u(1,t) = 0, & t \in (0,T], \end{cases} \tag{1}$$

where the spatial differential operator is given by $\mathcal{L}_{x,\varepsilon} u \equiv -\varepsilon u_{xx} + \beta u$. We assume that $0 < \varepsilon \leq 1$ and it can be sufficiently small, β is a positive constant and sufficient regularity and compatibility conditions hold in order that the exact solution $u \in \mathcal{C}^{(6,3)}(\overline{Q})$. The solution of (1) has a parabolic boundary layer of width $\mathcal{O}(\sqrt{\varepsilon})$ at $x = 0,\ x = 1$ (see [6]) and it can be decomposed as $u = v + w$, where the regular component is the solution of the problem $v_t + \mathcal{L}_{x,\varepsilon} v = f$, in Q, $v(x,0) = 0$, in Ω, and the boundary conditions are given by the reduced problem $z_t + \beta z = f(x,t)$, $z(x,0) = 0$. The singular component is the solution of the problem

C. Clavero (✉) and J.L. Gracia
Department of Applied Mathematics. University of Zaragoza, Spain
e-mail: clavero@unizar.es, jlgracia@unizar.es

C. Clavero et al. (eds.), *BAIL 2010 – Boundary and Interior Layers, Computational and Asymptotic Methods*, Lecture Notes in Computational Science and Engineering 81,
DOI 10.1007/978-3-642-19665-2_9,

$$\begin{cases} w(x,0) = 0, \text{ in } \Omega, \\ w_t + \mathcal{L}_{x,\varepsilon} w = 0, \text{ in } Q, \\ w(0,t) = u(0,t) - v(0,t),\ w(1,t) = u(1,t) - v(1,t). \end{cases} \tag{2}$$

Moreover, for $0 \leq k \leq 3$ and $0 \leq m \leq 4$ it holds (see [2])

$$\left\| \frac{\partial^k v}{\partial t^k} \right\|_{\infty,\overline{Q}} \leq C, \quad \left\| \frac{\partial^m v}{\partial x^m} \right\|_{\infty,\overline{Q}} \leq C(1 + \varepsilon^{(2-m)/2}), \tag{3}$$

$$\left| \frac{\partial^k w}{\partial t^k}(x,t) \right| \leq C B_\varepsilon(x), \quad \left| \frac{\partial^m w}{\partial x^m}(x,t) \right| \leq C \varepsilon^{-m/2} B_\varepsilon(x), \tag{4}$$

where $\|\cdot\|_{\infty,\overline{Q}}$ denotes the L_∞ norm on $\overline{Q}$ and $B_\varepsilon(x) = e^{-\sqrt{\beta/\varepsilon}x} + e^{-\sqrt{\beta/\varepsilon}(1-x)}$, and for the cross–derivatives it holds

$$\left\| \frac{\partial^3 v}{\partial x^2 \partial t} \right\|_{\infty,\overline{Q}} \leq C, \quad \left| \frac{\partial^3 w}{\partial x^2 \partial t}(x,t) \right| \leq C \varepsilon^{-1} B_\varepsilon(x). \tag{5}$$

In [1] it was defined a first order method to approximate problem (1) and here we are interested in a higher order uniformly convergent method. The analysis of the uniform convergence of the scheme follows the technique given in [1]. Henceforth, C denotes a generic positive constant independent of the diffusion parameter ε and also of the discretization parameters N and τ.

2 The Time Semidiscretization

In $[0,T]$ we consider a uniform mesh $\overline{\omega}^M = \{t_k = k\tau,\ 0 \leq k \leq M, \tau = T/M\}$. To discretize in time we use the Crank–Nicolson method defined by

$$\begin{cases} u^0(x) = 0,\ x \in \bar{\Omega}, \\ \begin{cases} (I + (\tau/2)\mathcal{L}_{x,\varepsilon}) u^n(x) = (\tau/2)(f(x,t_n) + f(x,t_{n-1})) + (I - (\tau/2)\mathcal{L}_{x,\varepsilon}) u^{n-1}(x), \\ u^n(0) = u^n(1) = 0, \quad 1 \leq n \leq M, \end{cases} \end{cases} \tag{6}$$

To prove the uniform convergence of this method we consider the problems

$$\begin{cases} (I + (\tau/2)\mathcal{L}_{x,\varepsilon}) \widehat{u}^n(x) = (\tau/2)(f(x,t_n) + f(x,t_{n-1})) + (I - (\tau/2)\mathcal{L}_{x,\varepsilon}) u(x,t_{n-1}), \\ \widehat{u}^n(0) = \widehat{u}^n(1) = 0, \quad 1 \leq n \leq M. \end{cases} \tag{7}$$

Theorem 1. *The global error associated to the method (6) satisfies* $\|u(x,t_n) - u^n(x)\|_{\infty,\overline{\Omega}} \leq C\tau^2$, $1 \leq n \leq M$, *where* $\|\cdot\|_{\infty,\overline{\Omega}}$ *denotes the* L_∞ *norm on* $\overline{\Omega}$.

Proof. First, from [2] we know that the local error satisfies $\|u(x,t_n) - \widehat{u}^n(x)\|_{\infty,\overline{\Omega}} \leq C\tau^3, 1 \leq n \leq M$. In the case of the classical heat equation $u_t - u_{xx} = 0$, the

resolvent set of the sectorial operator $\mathcal{L}_0 := -u_{xx}$ satisfies $\|(\lambda I + \mathcal{L}_0)^{-1}\|_{\infty,\overline{\Omega}} \leq C/|\lambda|$ (see for example [5]). If we consider the problem (1), it easily follows the parameter uniform estimate

$$\|(\lambda I + \varepsilon\mathcal{L}_0 + \beta I)^{-1}\|_{\infty,\overline{\Omega}} = \|(\lambda+\beta)^{-1}\left(I + \frac{\varepsilon}{\lambda+\beta}\mathcal{L}_0\right)^{-1}\|_{\infty,\overline{\Omega}} \leq \frac{C}{|\lambda+\beta|}, \tag{8}$$

proving the stability in the maximum norm of the Crank-Nicolson method. The result follows from the stability of the method. For β constant we have the full prove of the stability from (8). For the variable case $b := b(x,t) \geq \beta > 0$, we do not know a full prove of the stability following the idea given in the previous proof based on the resolvent of the differential operator even for classical problems (without a perturbation parameter). Nevertheless we think that same result can be obtained for the variable case.

Below, to analyze the error of the spatial discretization we will need to know the asymptotic behavior of the solution of problem (6). Then, we consider the decomposition $u^n = v^n + w^n$, where for $1 \leq n \leq M$, the regular component is the solution of the problem

$$\begin{cases} v^0(x) = 0, \ x \in \overline{\Omega}, \\ \{(I+(\tau/2)\mathcal{L}_{x,\varepsilon})v^n(x) = (\tau/2)(f(x,t_n)+f(x,t_{n-1}))+(I-(\tau/2)\mathcal{L}_{x,\varepsilon})v^{n-1}(x), \end{cases} \tag{9}$$

where the values at the boundaries $x = 0$ and $x = 1$ are given by

$$\begin{cases} (I + (\tau/2)\beta)v^n(x) = (\tau/2)(f(x,t_n) + f(x,t_{n-1})) + (I - (\tau/2)\beta)v^{n-1}(x), \\ v^0 = 0, \end{cases}$$

and the singular component is the solution of the problem

$$\begin{cases} w^0(x) = 0, \ x \in \Omega, \\ \begin{cases} (I + (\tau/2)\mathcal{L}_{x,\varepsilon})w^n(x) = (I - (\tau/2)\mathcal{L}_{x,\varepsilon})w^{n-1}(x), \\ w^n(0) = u^n(0) - v^n(0), \quad w^n(1) = u^n(1) - v^n(1). \end{cases} \end{cases} \tag{10}$$

Lemma 1. *The regular component solution of (9) satisfies*

$$|v_{xx}(x,t_n) - v^n_{xx}(x)| \leq C\tau, \ \left\|\frac{d^k v^n}{dx^k}\right\|_{\infty,\overline{\Omega}} \leq C(1+\varepsilon^{1-k/2}), \ 0 \leq k \leq 4. \tag{11}$$

The singular component solution of (10) satisfies

$$|w_{xx}(x,t_n) - w^n_{xx}(x)| \leq C\tau\varepsilon^{-1}B_\varepsilon(x), \ \left|\frac{d^k w^n}{dx^k}(x)\right| \leq C\varepsilon^{-k/2}B_\varepsilon(x), \ 0 \leq k \leq 4. \tag{12}$$

Proof. We only show the proof for the regular component; for the singular component it is similar. The proof proceeds by induction. For $n = 1$ the proof follows similar ideas to these ones in [2] for a coupled reaction-diffusion system. Note that now $v^1 = \hat{v}^1$, where $\hat{v}^1$ is the solution of the first step of the auxiliary problem (7). We assume that the bounds are valid for $0 \leq n-1 < M$ and we analyze the next time level n. Using that $\|\mathcal{L}_{x,\varepsilon} v^{n-1}(x)\|_{\infty,\overline{\Omega}} \leq C$, the hypothesis of induction and applying the maximum principle to (9) at the nth time level, it follows that $\|v^n(x)\|_{\infty,\overline{\Omega}} \leq C$. In addition, from the special choice of the boundary conditions $v^n(0)$ and $v^n(1)$, we have that $v^n_{xx}(0) = v^n_{xx}(1) = 0$, and using that $\|v^{n-1}_{xx}(x)\|_{\infty,\overline{\Omega}} \leq C$, and $\|\varepsilon v^{n-1}_{xxxx}(x)\|_{\infty,\overline{\Omega}} \leq C$, following to Madden and Stynes [3] we can deduce $\|v^n_x(x)\|_{\infty,\overline{\Omega}} \leq C$, $\|v^n_{xx}(x)\|_{\infty,\overline{\Omega}} \leq C$. Differentiating twice equation (9), we have that $(v_{xx}(x,t_n) - v^n_{xx})$ is solution of the problem

$$\begin{cases} \left(I + (\tau/2)\mathcal{L}_{x,\varepsilon}\right)(v_{xx}(x,t_n) - v^n_{xx}(x)) = g_1(x,t_n,t_{n-1}), \\ v_{xx}(0,t_n) - v^n_{xx}(0) = 0, \quad v_{xx}(1,t_n) - v^n_{xx}(1) = 0. \end{cases} \tag{13}$$

Using that $\|v_x(x,t)\|_{\infty,\overline{Q}} \leq C$, $\|v_{xx}(x,t)\|_{\infty,\overline{Q}} \leq C$, $\|v_{xxt}(x,t)\|_{\infty,\overline{Q}} \leq C$, $\|v^{n-1}_{xx}(x)\|_{\infty,\overline{\Omega}} \leq C$, $\|\varepsilon v^{n-1}_{xxxx}(x)\|_{\infty,\overline{\Omega}} \leq C$, and the hypothesis of induction, it follows that $\|g_1(x,t_n,t_{n-1})\|_{\infty,\overline{\Omega}} \leq C\tau$. Then, applying the maximum principle to (13), easily we can deduce that $\|v_{xx}(x,t_n) - v^n_{xx}(x)\|_{\infty,\overline{\Omega}} \leq C\tau$, and therefore $\|v^n_{xx}(x) - v^{n-1}_{xx}(x)\|_{\infty,\overline{\Omega}} \leq C\tau$ follows.

For higher order derivatives, differentiating twice (9), we have

$$|\mathcal{L}_{x,\varepsilon} v^n_{xx}(x)| = |f_{xx}(x,t_n) + f_{xx}(x,t_{n-1}) + (2/\tau)(v^{n-1}_{xx} - v^n_{xx}) - \mathcal{L}_{x,\varepsilon} v^{n-1}_{xx}| \leq C,$$

and therefore $\|v^n_{xxxx}(x)\|_{\infty,\overline{\Omega}} \leq C\varepsilon^{-1}$. From the bounds for the second and fourth derivatives, we can obtain $\|v^n_{xxx}(x)\|_{\infty,\overline{\Omega}} \leq C\varepsilon^{-1/2}$.

3 The Fully Discrete Scheme

To discretize in space we consider a nonuniform mesh $\overline{\Omega}^N = \{0 = x_0 < \ldots < x_N = 1\}$ condensing the grid points in the boundary layers. We consider two different special nonuniform meshes:

The Shishkin mesh [4]. It is a piecewise uniform mesh, depending on two transition points which are defined by means of the transition parameter

$$\sigma = \min\left\{1/4, \sigma_0\sqrt{\varepsilon}\ln N\right\}, \tag{14}$$

where σ_0 is a constant to be fixed later. A uniform mesh is placed in $[0,\sigma]$, $[\sigma, 1-\sigma]$, and $[1-\sigma, 1]$, such that $x_0 = 0$, $x_{N/4} = \sigma$, $x_{3N/4} = 1-\sigma$ and $x_N = 1$. Therefore,

the mesh points are given by $x_i = 4i\sigma/N$, for $i = 0, 1, \ldots, N/4$, $x_i = \sigma + 2(i - N/4)(1 - 2\sigma)/N$, for $i = N/4 + 1, \ldots, 3N/4$ and $x_i = 1 - \sigma + 4(i - 3N/4)\sigma/N$, for $i = 3N/4 + 1, \ldots, N$.

The Vulanovic mesh [7]. This mesh is a generalized Shishkin mesh constructed by using a suitable generating function $\aleph$, which also depends on two transition points. To simplify, we use the same parameter σ given in (14). The grid points are defined by $x_j = \aleph(j/N)$, $j = 0, 1, \ldots, N/2$, with $\aleph \in C^2[0, 1/2]$ and

$$\aleph(z) = \begin{cases} 4\sigma/N, & z \in [0, 1/4], \\ p(z - 1/4)^3 + 4\sigma(z - 1/4) + \sigma, & z \in [1/4, 1/2]. \end{cases}$$

The coefficient p is such that $\aleph(1/2) = 1/2$ and the mesh is symmetric with respect to the point $x = 1/2$. Note that in $[0, \sigma]$ and $[1 - \sigma, 1]$ the mesh points are the same than in the Shishkin mesh. Otherwise, in $[\sigma, 1 - \sigma]$ it is nonuniform but the step sizes satisfy $|h_{i+1} - h_i| \leq CN^{-2}$, $i = N/4, \ldots, 3N/4$, where $h_i = x_i - x_{i-1}$, $i = 1, \cdots, n$.

From now on we assume that any of the two meshes is nonuniform. Otherwise a classical analysis of the convergence can be performed deducing second order convergence in time and space. On these meshes we approximate problem (6) by using the classical central difference scheme

$$\begin{cases} U_i^0 = 0, \quad 0 \leq i \leq N, \\ \begin{cases} (I + (\tau/2)L^N)U_i^n = (\tau/2)(f(x_i, t_n) + f(x_i, t_{n-1})) + (I - (\tau/2)L^N)U_i^{n-1}, \\ \qquad\qquad\qquad\qquad\qquad\qquad\qquad\qquad 0 \leq i \leq N, \end{cases} \\ U_0^n = U_N^n = 0, \quad 1 \leq n \leq M, \end{cases} \tag{15}$$

with $L^N Z_i := -\varepsilon\delta^2 Z_i + \beta Z_i$, and

$$\delta^2 Z_i = (2/(h_i + h_{i+1}))\left((Z_{i+1} - Z_i)/h_{i+1} - (Z_i - Z_{i-1})/h_i\right).$$

The convergence of this method is analyzed at each time level by using an inductive argument. In that proof we will need some properties of the transition operator $(I + (\tau/2)L^N)^{-1}(I - (\tau/2)L^N)$.

Lemma 2. *Assume that $\Lambda_h = [-a_i \; c_i \; - b_i]$ is a tridiagonal matrix with $a_i, c_i, b_i > 0$ and*

$$\left\| (I + (\tau/2)\Lambda_h)^{-1} \right\|_\infty \leq 1/(1 + \beta\tau/2),$$

and here the norm is the matrix maximum norm. Then, the eigenvalues λ_i of the matrix $(I + (\tau/2)\Lambda_h)^{-1}(I - (\tau/2)\Lambda_h)$ are real and they satisfy

$$-1 < \lambda_i \leq \frac{1 - \beta\tau/2}{1 + \beta\tau/2} < 1.$$

and therefore its spectral radius is bounded by 1.

Proof. Note that if λ_i are the eigenvalues of matrix $(I+(\tau/2)\Lambda_h)^{-1}(I-(\tau/2)\Lambda_h)$, then the eigenvalues of matrix $(I+(\tau/2)\Lambda_h)^{-1}$ are $(\lambda_i+1)/2$, and using that $\rho(A)\leq\|A\|$, for any matrix norm, then we easily deduce that

$$|(\lambda_i+1)/2|\leq 1/(1+\beta\tau/2). \tag{16}$$

Noting that Λ_h is a tridiagonal matrix, irreducible, with positive diagonal entries and negative off diagonal entries, then it is possible to prove that its eigenvalues are real, simple and positive. Using these properties in (16) the result trivially follows.

Remark 1. Note that the operator L^N belongs to the class of operators given in Lemma 2 using the M-criterium with $e=(1,\ldots,1)^t$. Although this condition on the spectral radius ensures the boundedness of the computed solution it does not guarantee convergence unless it holds

$$\left\|[(I+(\tau/2)L^N)^{-1}(I-(\tau/2)L^N)]^k\right\|_\infty < C, \quad \forall k. \tag{17}$$

The proof of this result is an open question but in the section devoted to the numerical experiments we will show some numerical evidences corroborating that this property is true.

To obtain bounds for the error of the spatial discretization, similarly to the solution of the continuous and semidiscrete problems, the solution $U=V+W$ of (15) is decomposed in a regular and singular part given by

$$\begin{cases} V_i^0=0, \quad 0\leq i\leq N, \\ \begin{cases} (I+(\tau/2)L^N)V_i^n=(\tau/2)(f(x_i,t_n)+f(x_i,t_{n-1}))+(I-(\tau/2)L^N)V_i^{n-1}, \\ \qquad\qquad\qquad\qquad\qquad\qquad\qquad\qquad 0\leq i\leq N, \end{cases} \\ V_0^n=v^n(0), \quad V_N^n=v^n(1), \quad 1\leq n\leq M, \end{cases} \tag{18}$$

$$\begin{cases} W_i^0=0, \quad 0\leq i\leq N, \\ (I+(\tau/2)L^N)W_i^n=(I-(\tau/2)L^N)W_i^{n-1},\ 0\leq i\leq N,\ 1\leq n\leq M, \\ W_0^n=w^n(0), \quad W_N^n=w^n(1). \end{cases} \tag{19}$$

Theorem 2. *Assume that bounds (17) hold and that the constant σ_0 used to define the Shishkin and Vulanovic meshes satisfies $\sigma_0\geq 2/\sqrt{\beta}$. Then, if the method (15) is constructed on the Shishkin the error satisfies*

$$\|U_i^n-u^n(x_i)\|_{\infty,\overline{\Omega}^N}\leq C(N^{-1}\varepsilon+(N^{-1}\ln N)^2), \tag{20}$$

and on the Vulanovic meshes the error satisfies

$$\|U_i^n-u^n(x_i)\|_{\infty,\overline{\Omega}^N}\leq C(N^{-1}\ln N)^2, \tag{21}$$

where $\|\cdot\|_{\infty,\overline{\Omega}^N}$ denotes the discrete maximum norm on $\overline{\Omega}^N$.

Proof. Taking Taylor expansions for the truncation error $(I + (\tau/2)L^N)(V_i^n - v^n(x_i))$ and using the bounds (11) on the derivatives of the regular component, we can obtain

$$\left|(I + (\tau/2)L^N_{x,\varepsilon})(V_i^n - v^n(x_i))\right| \le C\tau N^{-1}(N^{-1} + \varepsilon) + \left|(I - (\tau/2)L^N_{x,\varepsilon})(V_i^{n-1} - v^{n-1}(x_i))\right|,$$

on the Shishkin mesh, and

$$\left|(I + (\tau/2)L^N_{x,\varepsilon})(V_i^n - v^n(x_i))\right| \le C\tau N^{-2} + \left|(I - (\tau/2)L^N_{x,\varepsilon})(V_i^{n-1} - v^{n-1}(x_i))\right|,$$

on the Vulanovic mesh. Assuming that all the powers of the transition parameter $(I + \frac{\tau}{2}L^N)^{-1}(I - \frac{\tau}{2}L^N)$ are parameter uniform bounded (17), using an inductive argument and the discrete maximum principle, we can prove

$$\|V_i^n - v^n(x_i)\|_{\infty,\overline{\Omega}^N} \le CN^{-1}(N^{-1} + \varepsilon), \quad \|V_i^n - v^n(x_i)\|_{\infty,\overline{\Omega}^N} \le CN^{-2},$$

on the Shishkin and Vulanovic meshes respectively.

For the singular component, using a standard argument we obtain bounds in $[\sigma, 1-\sigma]$ proving that $\|W_i^n - w^n(x_i)\|_{\infty,\overline{\Omega}^N} \le CN^{-2}$, $x_i \in [\sigma, 1-\sigma]$. Second, on the set $(0,\sigma) \cup (1-\sigma, 1)$, Taylor expansions are taken for the truncation error. From Lemma 1 and using again the hypothesis (17), for both the Shishkin and Vulanovic meshes we can prove

$$\left|(I + (\tau/2)L^N_{x,\varepsilon})(W_i^n - w^n(x_i))\right| \le C(N^{-1}\ln N)^2, \quad x_i \in (0,\sigma) \cup (1-\sigma, 1).$$

Using the discrete maximum principle on the intervals $[0,\sigma]$ and $[1-\sigma, 1]$ we deduce $\|(W_i^n - w^n(x_i))\|_{\infty,\overline{\Omega}^N} \le C(N^{-1}\ln N)^2$, $x_i \in (0,\sigma) \cup (1-\sigma, 1)$. Then, the result follows from the triangular inequality.

From Theorems 1 and 2 directly follows the main result of this paper.

Theorem 3. *Let U be the numerical solution of (15) and u be the solution of (1). We assume that bounds (17) hold and that the constant σ_0 used to define the Shishkin and Vulanovic meshes satisfies $\sigma_0 \ge 2/\sqrt{\beta}$. Then, on the Shishkin mesh the error satisfies*

$$\|U_i^n - u(x_i, t_n)\|_{\infty,\overline{\Omega}^N} \le C(N^{-1}\varepsilon + (N^{-1}\ln N)^2 + \tau^2), \tag{22}$$

and on the Vulanovic mesh the error satisfies

$$\|U_i^n - u(x_i, t_n)\|_{\infty,\overline{\Omega}^N} \leq C((N^{-1}\ln N)^2 + \tau^2). \tag{23}$$

4 Numerical Experiments

We consider the test problem

$$u_t - \varepsilon u_{xx} + ((1+x^2)/2)u = e^t - 1 + \sin(\pi x),\ (x,t) \in (0,1)\times(0,1], \tag{24}$$

with homogeneous initial and boundary conditions. Using a variant of the double mesh principle, we estimate the numerical errors by

$$D_{j,n}^{\varepsilon,N,\tau} = |U_{j,n}^{\varepsilon,N,\tau} - U_{j,n}^{\varepsilon,2N,\frac{\tau}{2}}|.$$

The uniform errors and the uniform orders of convergence are approximated by

$$D^{N,\tau} = \max_{\varepsilon}\max_{j,n} D_{j,n}^{\varepsilon,N,\tau},\ q_{uni} = \log\left(D^{N,\tau}/D^{2N,\tau/2}\right)/\log 2.$$

Although we only have theoretically almost second order convergence for Shishkin meshes when ε is sufficiently small, in practice same results have been obtained for Shishkin and Vulanovic meshes. Table 1 displays the uniform errors and the uniform orders of convergence, for the set of the values $\varepsilon \in \{2^0, 2^{-2}, \ldots, 2^{-30}\}$, taking $\sigma_0 = 2$ to define the mesh. From these results we observe almost second order convergence in agreement with Theorem 3.

To corroborate Lemma 2, the spectral radius for the transition operator associated with problem (14) is given in Table 2. In this table the value of the upper bound $R(\beta,\tau) = (1-\beta\tau/2)/(1+\beta\tau/2)$ also appears, and we observe that for fixed values of N and τ the spectral radius stabilizes and it is very close to the theoretical upper bound $R(\beta,\tau)$. For large ε we see that there is a discrepancy with the upper bound although it is less than 1 as it was theoretically proved.

Table 3 displays the matrix maximum norm for the transition operator for some values of ε, N and τ, observing that the infinity norm is less than 1.

Table 1 Maximum uniform errors and orders of uniform convergence

ε	N = 32 $\tau = 0.2$	N = 64 $\tau = 0.2/2$	N = 128 $\tau = 0.2/2^2$	N = 256 $\tau = 0.2/2^3$	N = 512 $\tau = 0.2/2^4$	N = 1024 $\tau = 0.2/2^5$
$D^{N,\tau}$	0.117E-1	0.494E-2	0.166E-2	0.578E-3	0.192E-3	0.595E-4
q_{uni}	1.247	1.569	1.527	1.590	1.690	

Table 2 Spectral radius and $R(\beta, \tau)$

ε	N = 16 $\tau = 0.2$	N = 32 $\tau = 0.2/2$	N = 64 $\tau = 0.2/2^2$	N = 128 $\tau = 0.2/2^3$	N = 256 $\tau = 0.2/2^4$
2^0	0.98048	0.99026	0.99513	0.99756	0.99878
2^{-6}	0.85554	0.92501	0.96178	0.98070	0.99030
2^{-12}	0.89877	0.94808	0.97369	0.98676	0.99336
2^{-18}	0.90369	0.95080	0.97511	0.98747	0.99372
2^{-24}	0.90463	0.95111	0.97528	0.98756	0.99376
2^{-30}	0.90474	0.95120	0.97529	0.98757	0.99377
$R(\beta, \tau)$	0.90476	0.95122	0.97531	0.98758	0.99377

Table 3 Maximum norm for the transition operator

	N = 16 $\tau = 0.2$	N = 32 $\tau = 0.2/2$	N = 64 $\tau = 0.2/2^2$	N = 128 $\tau = 0.2/2^3$	N = 256 $\tau = 0.2/2^4$
$\varepsilon = 10^{-4}$	0.9044794	0.9511403	0.9752864	0.9875717	0.9937679
$\varepsilon = 10^{-6}$	0.9047589	0.9512181	0.9753083	0.9875775	0.9937694
$\varepsilon = 10^{-8}$	0.9047617	0.9512194	0.9753086	0.9875776	0.9937694

Acknowledgements This research was partially supported by the projects MTM 2009-07637-E, MEC/FEDER MTM 2010-16917 and the Diputación General de Aragón.

References

1. C. Clavero, J.L. Gracia, On the uniform convergence of a finite difference scheme for time dependent singularly perturbed reaction-diffusion problems, Appl. Math. and Comp. **216** (2010) 1478–1488.
2. C. Clavero, J.L. Gracia, F.J. Lisbona, Second order uniform approximations for the solution of time dependent singularly perturbed reaction–diffusion systems, Int. J. Numer. Anal. Mod. **7** (2010) 428–443.
3. N. Madden, M. Stynes, A uniformly convergent numerical method for a coupled system of two singularly perturbed linear reaction-diffusion problems, *IMA J. Numer. Anal.* **23** (2003) 627–644.
4. J.J.H. Miller, E. O'Riordan, G.I. Shishkin, Fitted numerical methods for singular perturbation problems, World-Scientific, Singapore, 1996.
5. C. Palencia, A stability result for sectorial operators in Banach spaces, SIAM J. Numer. Anal. **30** (1993) 1373–1384.
6. H.-G. Roos, M. Stynes, L. Tobiska, Robust numerical methods for singularly perturbed differential equations, Springer Series in Computational Mathematics **24**, Springer-Verlag, Berlin, 2008.
7. R. Vulanovic, A high order scheme for quasilinear boundary value problems with two small parameters, Computing **67** (1986) 287–303.

Finite Element Approximation of the Convection-Diffusion Equation: Subgrid-Scale Spaces, Local Instabilities and Anisotropic Space-Time Discretizations

Ramon Codina

Abstract The objective of this paper is to give an overview of the finite element approximation of the convection-diffusion equation that we have been developing in our group during the last years, together with some recent methods. We discuss three main aspects, namely, the global stabilization in the convective dominated regime, the treatment of the local instabilities that still remain close to layers when a stabilized formulation is used and the way to deal with transient problems.

The starting point of our formulation is the variational multiscale framework. The main idea is to split the unknown into a finite element component and a remainder that is assumed that the finite element mesh cannot resolve. A closed form expression is then proposed for this remainder, referred to as subgrid-scale. When inserted into the equation for the finite element component, a method with enhanced stability properties is obtained. In our approach, we take the space for the subgrid-scales orthogonal to the finite element space.

Once global instabilities have been overcome, there are still local oscillations near layers due to the lack of monotonicity of the method. Shock capturing techniques are often employed to deal with them. Here, our point of view is that this lack of monotonicity is inherent to the integral as duality pairing intrinsic to the variational formulation of the problem. We claim that if appropriate weighting functions are introduced when computing the integral, giving a reduced weight to layers, the numerical behavior of the method is greatly improved.

The final point we treat is the time integration in time-dependent problems. Most stabilized finite element method require a link between the time step size of classical finite difference schemes in time and the mesh size employed for the spatial discretization. We show that this can be avoided by considering the subgrid-scales as time dependent, and discretizing them in time as well. That allows us to perform a complete numerical analysis which is not restricted by any condition on the time step size, thus permitting anisotropic space-time discretizations.

R. Codina
Universitat Politècnica de Catalunya, Jordi Girona 1-3, Edifici C1, 08034 Barcelona, Spain
e-mail: ramon.codina@upc.edu

C. Clavero et al. (eds.), *BAIL 2010 – Boundary and Interior Layers, Computational and Asymptotic Methods*, Lecture Notes in Computational Science and Engineering 81,
DOI 10.1007/978-3-642-19665-2_10,

1 Two-Scale Approximation of the Convection-Diffusion-Reaction Equation

The objective of this section is to summarize the basic stabilized finite element method we use to solve the convection-diffusion-reaction equation (CDRE) in the case in which diffusion is small, that is to say, convective effects are dominant. It is not our intention here neither to describe the details of the problem, which are well known, not to give a fair acknowledgment of the key contributions to design the final method that can be found in the literature. This is why, apart from our own work, only reference to the landmark paper [11] is made. References to other contributions can be consulted in those cited along this work.

Let us start with the problem we are interested in. For the purposes of this section it is enough to consider the stationary CRDE with homogeneous Dirichlet boundary conditions. The problem consists of finding u such that

$$\begin{aligned} \mathcal{L}u := -k\Delta u + \boldsymbol{a}\cdot\nabla u + su = f \qquad & \text{in } \Omega \\ u = 0 \qquad & \text{on } \partial\Omega \end{aligned}$$

where $k > 0$ is the diffusion coefficient, $s \geq 0$ the reaction coefficient, $\boldsymbol{a} \in \mathbb{R}^d$ is the advection coefficient and f a given datum. The problem is posed in the domain $\Omega \subset \mathbb{R}^d$ $(d = 2, 3)$. Constant coefficients will be assumed throughout, for the sake of conciseness.

The variational form of the problem can be written as follows: find $u \in V = H_0^1(\Omega)$ such that

$$B(u, v) = \langle f, v\rangle \quad \forall v \in V \tag{1}$$

where:

$$B(u, v) = k(\nabla u, \nabla v) + (\boldsymbol{a}\cdot\nabla u, v) + s(u, v)$$

As usual, $(\cdot,\cdot)$ denotes the L^2 inner product and $\langle\cdot,\cdot\rangle$ the integral of the product of two functions, including the duality pairing.

The conforming Galerkin finite element approximation of the problem is standard. If $V_h \subset V$ is a finite element space to approximate V, it consists of finding $u_h \in V_h$ such that

$$B(u_h, v_h) = \langle f, v_h\rangle \quad \forall v_h \in V_h$$

Again for simplicity, we will consider that the finite element partition associated to V_h is uniform, h being the size of the element domains.

It is well known that this formulation lacks stability when k is small. To justify the method we propose, it is interesting to start trying to elucidate which is the stability it has with some more detail than what is usual. If we take $v_h = u_h$ it is

readily seen that

$$B(u_h, u_h) = k\|\nabla u_h\|^2 + s\|u_h\|^2 \tag{2}$$

The question is, what control, if any, can be obtained over the convective term? That is to say, is it possible to have a bound for $\|\boldsymbol{a}\cdot\nabla u_h\|$? To answer this fundamental question, we may obtain an improved stability estimate for the Galerkin method in the form of an inf-sup condition. If we take the test function as $v_{h,0} = \tau P_h(\boldsymbol{a}\cdot\nabla u_h)$, with the parameter τ to be defined and P_h being the L^2 projection onto V_h, we obtain:

$$\begin{aligned} B(u_h, v_{h,0}) \gtrsim\ & \tau\|P_h(\boldsymbol{a}\cdot\nabla u_h)\|^2 \\ & - k\|\nabla u_h\|\frac{C_{\text{inv}}}{h}\tau\|P_h(\boldsymbol{a}\cdot\nabla u_h)\| \\ & - s\|u_h\|\tau\|P_h(\boldsymbol{a}\cdot\nabla u_h)\| \end{aligned}$$

where $\gtrsim$ stands for $\geq$ up to positive constants and C_{inv} is the constant in standard inverse inequalities. If the parameter τ is chosen such that $\tau \leq \min\left\{\frac{h^2}{C_{\text{inv}}^2 k}, \frac{1}{s}\right\}$ then

$$B(u_h, v_{h,0}) \gtrsim \tau\|P_h(\boldsymbol{a}\cdot\nabla u_h)\|^2 - k\|\nabla u_h\|^2 - s\|u_h\|^2$$

The last two terms can be controled, according to (2). It is then easily seen that $B(u_h, v_h) \gtrsim k\|\nabla u_h\|^2 + s\|u_h\|^2 + \tau\|P_h(\boldsymbol{a}\cdot\nabla u_h)\|^2$, with $v_h = u_h + \beta v_{h,0}$ (β sufficiently small), and that $k\|\nabla v_{h,0}\|^2 + s\|v_{h,0}\|^2 + \tau\|P_h(\boldsymbol{a}\cdot\nabla v_{h,0})\|^2 \lesssim \tau\|P_h(\boldsymbol{a}\cdot\nabla u_h)\|^2$, from where an inf-sup condition follows. Therefore, we may conclude that *only control over* $\tau\|P_h^{\perp}(\boldsymbol{a}\cdot\nabla u_h)\|^2$ *is missing*, with $P_h^{\perp} = I - P_h$, the projection orthogonal to the finite element space. This control is, *at least*, what any stabilized method must provide.

Let us describe now the formulation we propose. It is based on the splitting of the unknown u in a component u_h which can be resolved by the finite element space, and a remainder, that will be called subgrid scale (SGS). An approximation for the SGS is required to define a particular numerical formulation. The framework we use in based on [11]. Let $V = V_h \oplus \tilde{V}$, where $\tilde{V}$ is the space for the SGS. Then, problem (1) unfolds into two variational equations: we have to seek $u_h \in V_h$ and $\tilde{u} \in \tilde{V}$ such that

$$\begin{aligned} B(u_h, v_h) + B(\tilde{u}, v_h) &= \langle f, v_h\rangle \quad \forall v_h \in V_h \\ B(u_h, \tilde{v}) + B(\tilde{u}, \tilde{v}) &= \langle f, \tilde{v}\rangle \quad \forall \tilde{v} \in \tilde{V} \end{aligned}$$

Suppose for a moment that $\tilde{V}$ is made of smooth functions (which are anyhow dense in the complement of V_h). Then we may write

$$B(u_h, v_h) + \langle \tilde{u}, \mathcal{L}^* v_h\rangle = \langle f, v_h\rangle \quad \forall v_h \in V_h \tag{3}$$

$$\langle \mathcal{L}u_h, \tilde{v}\rangle + \langle \mathcal{L}\tilde{u}, \tilde{v}\rangle = \langle f, \tilde{v}\rangle \quad \forall \tilde{v} \in \tilde{V} \tag{4}$$

where second derivatives applied to finite element functions have to be understood in the sense of distributions. The problem now can be stated as: *how do we model $\tilde{u}$?*. At this point is where approximations are required and different methods may be devised according to the approximation chosen.

The first approximation we shall use is that

$$\langle \mathcal{L}v_h, \tilde{v} \rangle \approx \sum_K (\mathcal{L}v_h, \tilde{v})_K \equiv (\mathcal{L}v_h, \tilde{v})_h \tag{5}$$

This essentially means that jumps of derivatives of finite elements functions across edges of the mesh are neglected. We shall stick to this assumption, although it can be relaxed, as explained in [9].

The second approximation, which is definitely the most crucial, is

$$\langle \mathcal{L}\tilde{u}, \tilde{v} \rangle \approx \tau^{-1}(\tilde{u}, \tilde{v}) \quad \text{where} \quad \tau^{-1} = c_1 \frac{k}{h^2} + c_2 \frac{|\boldsymbol{a}|}{h} + c_3 s \tag{6}$$

where c_1, c_2 and c_3 are numerical parameters. There are many ways to arrive at this expression, which we shall not describe. For an overview, see [5].

Equation (6) can be understood as a *lumping* of the equation for the SGS. This lumping is needed *to make this equation directly solvable*, without the need to introduce additional degrees of freedom into the problem. Both (5) and (6) can be justified from an approximate Fourier analysis requiring $\tau^{-1} \approx \|\mathcal{L}\|$ [7]. Having introduced them, the final problem to be solved is

$$B(u_h, v_h) + (\tilde{u}, \mathcal{L}^* v_h)_h = \langle f, v_h \rangle \quad \forall v_h \in V_h \tag{7}$$

$$(\mathcal{L}u_h, \tilde{v})_h + \tau^{-1}(\tilde{u}, \tilde{v}) = \langle f, \tilde{v} \rangle \quad \forall \tilde{v} \in \tilde{V} \tag{8}$$

which has to be compared with (3)–(4).

At this point we may already check which is the stability of the two scales introduced, namely, u_h and $\tilde{u}$. Using standard inverse inequalities, we have that

$$\begin{aligned}
&B(u_h, u_h) + (\tilde{u}, \mathcal{L}^* u_h)_h + (\mathcal{L}u_h, \tilde{u})_h + \tau^{-1}(\tilde{u}, \tilde{u}) \\
&\quad = k\|\nabla u_h\|^2 + s\|u_h\|^2 + 2(\tilde{u}, -k\Delta u_h + s u_h)_h + \tau^{-1}\|\tilde{u}\|^2 \\
&\quad \gtrsim k\|\nabla u_h\|^2 + s\|u_h\|^2 - 2\left(\tau \frac{k}{h^2} C_{\text{inv}}^2\right) k\|\nabla u_h\|^2 \\
&\qquad - 2(\tau s)s\|u_h\|^2 - \frac{\tau^{-1}}{2}\|\tilde{u}\|^2 + \tau^{-1}\|\tilde{u}\|^2 \\
&\quad \gtrsim k\|\nabla u_h\|^2 + s\|u_h\|^2 + \tau^{-1}\|\tilde{u}\|^2
\end{aligned}$$

where the last step holds for an adequate choice of the constants in (6). We observe that we have the same control on the finite element component as for the Galerkin method *plus additional L^2 control on the SGS*.

The SGS is so far undefined. To choose the subspace $\tilde{V}$ we consider non-conforming approximations, and thus $\tilde{V}$ might not be a subspace of $H_0^1(\Omega)$ (see [9]). If $\tilde{P}$ is the L^2 projection to $\tilde{V}$, we have from (8) that

$$\tilde{u} = \tau \tilde{P}(f - \mathcal{L}u_h)$$

There are two obvious options:

- Choice I:

  $$\tilde{V} \subset \mathcal{L}V_h + \text{span}\{f\} \iff \tilde{u} = \tau(f - \mathcal{L}u_h)$$

  In this case, $\tilde{P}$ is the identity when applied to the finite element residual $f - \mathcal{L}u_h$. This option is the most common in the literature. It yields to stable formulations, as we shall see. From the conceptual point of view, the danger it has is that the assumption $V_h \cap \tilde{V} = \{0\}$, crucial to derive the method, may not hold.
- Choice II:

  $$\tilde{V} = V_h^{\perp} \iff \tilde{u} = \tau P_h^{\perp}(f - \mathcal{L}u_h)$$

  This option was proposed in [6, 7]. In fact, it can be shown that if the SGS are further approximated as

  $$\tilde{u} \approx -\tau P_h^{\perp}(\boldsymbol{a} \cdot \nabla u_h) \tag{9}$$

  the method keeps the order of accuracy. Some care is needed though in the treatment of boundary effects.

Once the two choices have been described, let us write down the final finite element problem to be solved and obtain a simple stability estimate. For choice I the final problem is

$$B(u_h, v_h) + \tau(\mathcal{L}u_h, -\mathcal{L}^* v_h)_h = \langle f, v_h \rangle + \tau(f, -\mathcal{L}^* v_h)_h$$

It is immediately checked that

$$B(u_h, u_h) + \tau(\mathcal{L}u_h, -\mathcal{L}^* u_h)_h \gtrsim k\|\nabla u_h\|^2 + s\|u_h\|^2 + \tau\|\boldsymbol{a} \cdot \nabla u_h\|^2$$

Therefore, this method provides control *over the whole convective term*.

For choice II the finite element problem is

$$B(u_h, v_h) + \tau(P_h^{\perp}(\boldsymbol{a} \cdot \nabla u_h), P_h^{\perp}(\boldsymbol{a} \cdot \nabla v_h))_h = \langle f, v_h \rangle$$

and now we have that

$$\begin{aligned} B(u_h, u_h) + \tau(P_h^{\perp}(\boldsymbol{a} \cdot \nabla u_h), P_h^{\perp}(\boldsymbol{a} \cdot \nabla u_h))_h \\ \gtrsim k\|\nabla u_h\|^2 + s\|u_h\|^2 + \tau\|P_h^{\perp}(\boldsymbol{a} \cdot \nabla u_h)\|^2 \end{aligned}$$

Thus, this simple stability estimate shows that the method provides control *only in the component of the convective term orthogonal to the finite element space*. However, *the term* $\tau \| P_h^{\perp}(\boldsymbol{a} \cdot \nabla u_h)\|^2$ *is precisely what the Galerkin method lacks*. It is not difficult to foresee that one can in fact obtain optimal stability with choice II.

The results of the numerical analysis of the formulations arising both from choice I and from choice II is summarized next. Let:

$$
\begin{aligned}
&|\!|\!| v |\!|\!|^2 := k\|\nabla v\|^2 + s\|v\|^2 + \tau\|\boldsymbol{a}\cdot\nabla v\|^2 \\
&E(h)^2 := \left(\frac{k}{h^2} + \frac{|\boldsymbol{a}|}{h} + s\right) h^{2(p+1)}|u|_{p+1}^2 \approx \tau^{-1} h^{2(p+1)}|u|_{p+1}^2
\end{aligned}
$$

where $|u|_{p+1}$ is the H^{p+1} seminorm of the exact solution u. If B_{stab} is the bilinear form of *any of the two* stabilized methods introduced, it holds

$$
\begin{aligned}
&\inf_{u_h \in V_h} \sup_{v_h \in V_h} \frac{B_{\text{stab}}(u_h, v_h)}{|\!|\!| u_h |\!|\!| \, |\!|\!| v_h |\!|\!|} \geq C > 0 \quad \text{Stability} \\
&|\!|\!| u - u_h |\!|\!| \lesssim E(h) \qquad\qquad\qquad\qquad \text{Optimal convergence}
\end{aligned}
$$

From these results, there are some remarks to be made:

- The stability and convergence estimates presented are optimal.
- These estimates remain meaningful for all values of the physical parameters, which is the main goal of stabilized finite element methods.
- There is no need to refer to "$h^{p+1/2}$" estimates.

2 Avoiding Local Instabilities

The methods proposed in the previous section yield stability and convergence *in global* norms. However, local oscillations may still remain in regions where the solution exhibits sharp layers. Even though these oscillations might be considered acceptable in linear problems, in nonlinear situations they may lead to a global failure of iterative schemes. Therefore, eliminating them in linear problems is a required step to extend the formulation to nonlinear equations. Methods aiming to avoid these local oscillations are often termed "shock capturing" or "discontinuity capturing" (DC) techniques.

To start, let us describe the guidelines to design DC methods as presented in [4] and references therein. Suppose that $s = 0$ and let

$$
\boldsymbol{a}_{\|} = \frac{\boldsymbol{a}\cdot\nabla u_h}{|\nabla u_h|} \quad \text{if} \quad |\nabla u_h| \neq 0, \quad \boldsymbol{a}_{\|} = \boldsymbol{0} \quad \text{otherwise}
$$

The following observations are crucial:

- For regular P_1 elements, the discrete maximum principle (DMP) holds if an artificial diffusion k_{art} is added, k_{art} being of the form

$$k_{\text{art}} = \frac{1}{2}\alpha h|\boldsymbol{a}_{\|}|, \quad \alpha \geq C - \frac{1}{\text{Pe}_{\|}}, \quad \text{Pe}_{\|} = \frac{|\boldsymbol{a}_{\|}|h}{2k} \tag{10}$$

  where C is a constant that depends on the shape of the elements.
- If the DMP holds, L^∞ stability can be proved.
- If a numerical scheme is *linear* then it is at most first order accurate in L^∞ (a reformulation of Godunov's theorem).

In view of these facts, DC methods may be designed trying to satisfy the DMP, at least in some simple situations, and need to be *nonlinear*.

The first family of DC methods proposed is that in which an artificial diffusion depending on the finite element residual is added to the basic stabilized formulation. The essential idea of these *residual based DC methods* is to design the artificial diffusion in a way similar to (10) but computing k_{art} with

$$\frac{|R(u_h)|}{|\nabla u_h|} \quad \text{instead of} \quad |\boldsymbol{a}_{\|}| = \frac{|\boldsymbol{a}\cdot\nabla u_h|}{|\nabla u_h|}$$

where $R(u_h) = f - \mathcal{L}u_h = f - (-k\Delta u_h + \boldsymbol{a}\cdot\nabla u_h + su_h)$ ($s \geq 0$ may be considered now). The resulting method is consistent, in the sense that if it is applied to the exact solution u the residual is zero.

The semilinear form of the problem is

$$B_{\text{dc}}(u_h, v_h) = B_{\text{stab}}(u_h, v_h) + \sum_K (k_{\text{dc}}\nabla u_h, \nabla v_h)_K \tag{11}$$

with

$$k_{\text{dc}} = \frac{1}{2}\alpha h\frac{|R(u_h)|}{|\nabla u_h|} \tag{12}$$

Several DC methods of this type can be found in the literature (see references in [4]).

A refinement of this approach was proposed in [4]. The idea is that the diffusion introduced by the basic stabilization method can be shown to satisfy the requirements posed by the DMP (in some model cases), but it is only introduced along the streamlines. Therefore, k_{art} needs to be added only in the crosswind direction. This is accomplished by adding a diffusive term with the diffusion tensor

$$\boldsymbol{k}_{\text{dc}} = \frac{1}{2}\alpha h\frac{|R(u_h)|}{|\nabla u_h|}\left(\boldsymbol{I} - \frac{1}{|\boldsymbol{a}|^2}\boldsymbol{a}\otimes\boldsymbol{a}\right)$$

to the basic stabilized finite element method, $\boldsymbol{I}$ being the second order identity tensor.

Following the guidelines to design DC methods discussed above, a different possibility to make the method consistent while introducing additional diffusion is to make it proportional to the projection of the gradient orthogonal to the finite element space. Thus, if k_{art} is the diffusion to be added, in order to make it active only in regions of sharp gradients *which cannot be resolved by the finite element mesh*, it can be multiplied by

$$\frac{|P_h^{\perp}(\nabla u_h)|}{|\nabla u_h|} \tag{13}$$

The semilinear form of the resulting problem is again (11), but now with k_{dc} given by

$$k_{\text{dc}} = \frac{1}{2}\alpha(|\boldsymbol{a}|h + sh^2)\frac{|P_h^{\perp}(\nabla u_h)|}{|\nabla u_h|}$$

instead of (12). Note that, apart from the factor (13), the artificial diffusion in this method is taken as $\frac{1}{2}\alpha(|\boldsymbol{a}|h + sh^2)$, independent of the finite element solution. As in the residual based DC methods, this diffusion can be introduced only in the cross-wind direction. Even though we have not published before this proposal, we have used it routinely in applications requiring a resolution of sharp gradients without local oscillations.

To conclude this section, let us describe another approach in which we have been working even if it has not been published before. The idea is as follows. Consider the problem $\mathcal{L}u = f$. The discrete problem can be formally written as a "projection" of this equation onto the finite element space, using the integral as "inner product". If P_h is this projection, it is well known that it is non-monotone, in the sense that if φ is discontinuous, $P_h(\varphi)$ is oscillating. Therefore, if local oscillations have to be avoided, a natural option seems to be to modify the projection. If, moreover, these oscillations appear in regions of sharp gradients, it seems reasonable *to introduce a weighting function ρ in the integral to lighten the weight of sharp layers*. This intuitive idea has many possible realizations. A possibility that we have successfully checked consists of replacing

$$\langle \mathcal{L}u_h, v_h\rangle = \langle f, v_h\rangle \quad \text{by} \quad \langle \mathcal{L}u_h, \rho v_h\rangle = \langle f, \rho v_h\rangle$$

where $\rho \to \rho_0 \ll 1$ as $|\nabla u_h| \to \infty$. An example of weight that we have tested is $\rho = \rho_0 + (1-\rho_0)\exp(-|\nabla u_h|/G)$, where G is a reference gradient. It is obvious that the method can be considered of Petrov-Galerkin type, with test function ρv_h.

This approach has the following properties:

- The diffusion term is non-symmetric.
- The partition-of-unity property is lost.
- The numerical performance that we have observed in several examples is excellent.

3 Time Dependent Problems

Let us move our attention now to time dependent problems. The statement of the initial and boundary problem we are interested in is:

$$\begin{aligned} \partial_t u + \mathcal{L}u &= f \quad \text{in } \Omega, t > 0 \\ u &= 0 \quad \text{on } \partial\Omega, t > 0 \\ u &= u^0 \quad \text{in } \Omega, t = 0 \end{aligned}$$

Our approach consists in extending the scale splitting introduced in Sect. 1 to this problem. The time dependent counterpart of (3)–(4) is

$$\begin{aligned} (\partial_t u_h + \partial_t \tilde{u}, v_h) + B(u_h, v_h) + \langle \tilde{u}, \mathcal{L}^* v_h \rangle &= \langle f, v_h \rangle \quad \forall v_h \in V_h \\ (\partial_t u_h + \partial_t \tilde{u}, \tilde{v}) + \langle \mathcal{L}u_h, \tilde{v} \rangle + \langle \mathcal{L}\tilde{u}, \tilde{v} \rangle &= \langle f, \tilde{v} \rangle \quad \forall \tilde{v} \in \tilde{V} \end{aligned}$$

The approximations used to arrive at (7)-(8) now lead to

$$\begin{aligned} (\partial_t u_h + \partial_t \tilde{u}, v_h) + B(u_h, v_h) + (\tilde{u}, \mathcal{L}^* v_h)_h &= \langle f, v_h \rangle \quad \forall v_h \in V_h \\ (\partial_t u_h + \partial_t \tilde{u}, \tilde{v}) + (\mathcal{L}u_h, \tilde{v})_h + \tau^{-1}(\tilde{u}, \tilde{v}) &= \langle f, \tilde{v} \rangle \quad \forall \tilde{v} \in \tilde{V} \end{aligned}$$

If the space of SGS is chosen as orthogonal to the finite element space and approximation (9) is used, the problem to be solved becomes

$$(\partial_t u_h, v_h) + B(u_h, v_h) - (\tilde{u}, \boldsymbol{a} \cdot \nabla v_h) = \langle f, v_h \rangle \quad \forall v_h \in V_h \tag{14}$$

$$(\partial_t \tilde{u}, \tilde{v}) + (\boldsymbol{a} \cdot \nabla u_h, \tilde{v}) + \tau^{-1}(\tilde{u}, \tilde{v}) = 0 \quad \forall \tilde{v} \in V_h^{\perp} \tag{15}$$

The important point is that the SGS have been considered time dependent [7, 10]. Their evolution equation can be written as

$$\partial_t \tilde{u} + \tau^{-1} \tilde{u} = -P_h^{\perp}(\boldsymbol{a} \cdot \nabla u_h)$$

If the time derivative of the SGS is neglected, they can be inserted into (14) to obtain a closed problem for the finite element component alone. The full analysis of the resulting formulation can be found in [1, 8].

It is interesting to analyze the dissipative structure of problem (14)-(15). This was done in [12] in the more complex case of the Navier–Stokes equations. Here we will apply the results of the cited reference to the CDRE.

If, for each fixed t, we take $v_h = u_h$ and $\tilde{v} = \tilde{u}$ in (14)-(15) it is readily checked that

$$\frac{\mathrm{d}}{\mathrm{d}t}\|u_h\|^2 + \mathcal{D}_h + \mathcal{T} = \mathcal{P}_h \tag{16}$$

$$\frac{\mathrm{d}}{\mathrm{d}t}\|\tilde{u}\|^2 + \tilde{\mathcal{D}} - \mathcal{T} = \tilde{\mathcal{P}} \tag{17}$$

with

$$\begin{aligned}
\mathcal{D}_h &= k\|\nabla u_h\|^2 + s\|u_h\|^2 && \text{Dissipation of the finite element scale}\\
\tilde{\mathcal{D}} &= \tau^{-1}\|\tilde{u}\|^2 && \text{Dissipation of the SGS}\\
\mathcal{T} &= (\tilde{u}, \mathcal{L}^* u_h)_h = -(\tilde{u}, \boldsymbol{a}\cdot\nabla v_h) && \text{Energy transfer between scales}
\end{aligned}$$

These definitions have been introduced thinking of the L^2 norm of the unknown as an energy. In this case, $\mathcal{P}_h$ and $\tilde{\mathcal{P}}$ can be considered the external power applied to the finite element scale and the SGS, respectively. From (16)-(17), with the definition of the different terms introduced above, we may draw an important conclusion. It is observed that the "energy balance" for the finite element component is the same as for the Galerkin method plus the addition of $\mathcal{T}$, which on average can be shown to be positive. In turn, this additional dissipation is precisely injected with a negative sign in the energy balance equation for the SGS. Therefore, the global energy is conserved, but there is an energy transfer from the "large" scales to the "small" scales. This is the correct dissipative structure for dissipative systems. In particular, it is crucial for the correct modelling of turbulence.

Let us present some stability and convergence results for (14)-(15). If T is the final time of analysis, let us start with stability estimates for $T < \infty$. Suppose that $s = 0$ for simplicity. Taking $v_h = u_h$, $\tilde{v} = \tilde{u}$ and integrating on $[0, t']$, $t' \leq T$ in (14)-(15) we obtain

$$\begin{aligned}
&\|u_h(t')\|^2 + \|\tilde{u}(t')\|^2 + \int_0^{t'} k\|\nabla u_h\|^2 \mathrm{d}t + \int_0^{t'} \tau^{-1}\|\tilde{u}\|^2 \mathrm{d}t\\
&\leq \int_0^{t'} \frac{1}{k}\|f\|_{-1}^2 \mathrm{d}t + \|u^0\|^2
\end{aligned}$$

from where

$$\begin{aligned}
&\|u_h\| \in L^\infty(0,T), \quad k^{1/2}\|\nabla u_h\| \in L^2(0,T)\\
&\|\tilde{u}\| \in L^\infty(0,T), \quad \tau^{-1/2}\|\tilde{u}\| \in L^2(0,T)
\end{aligned}$$

These results indicate that the stability of (14)-(15) is the same as for the Galerkin method *plus additional stability on the SGS*.

Let us move now to the long term behavior, that is to say $T = \infty$. The results to be presented are proved in [3] for the incompressible Navier–Stokes equations. Taking $v_h = u_h$, $\tilde{v} = \tilde{u}$ and using the classical Gronwall lemma it is found that

$$\|u_h\| \in L^\infty(0,\infty), \quad \|\tilde{u}\| \in L^\infty(0,\infty)$$

and also

$$\lim_{t\to\infty} \sup\left(\|u_h\| + \|\tilde{u}\|\right) \leq C\frac{|\Omega|^{2/d}}{k}\|f\|_{L^\infty(0,\infty;L^2(\Omega))}$$

from where we conclude that there is a $L^2(\Omega) \oplus L^2(\Omega)$-absorbing set in $V_h \oplus \tilde{V}$, not only in V_h, as for the Galerkin method.

We may also obtain stronger stability estimates using additional regularity assumptions. Using the uniform Gronwall lemma it is found that

$$k^{1/2}\|\nabla u_h\| \in L^\infty(0,\infty), \quad \tau^{-1/2}\|\tilde{u}\| \in L^\infty(0,\infty)$$

and

$$\lim_{t\to\infty} \sup \left(k\|\nabla u_h\|^2 + \tau^{-1}\|\tilde{u}\|^2\right) \leq C\left(a_1 + \frac{a_2}{\tilde{t}}\right)\exp(a_3)$$

for certain constants a_1, a_2 and a_3 that behave as k^{-4}. For the Navier–Stokes equations, this leads to the existence of an attractor (see [3]).

Finally, let us present a simple convergence result. Suppose that the time interval is discretized using a uniform partition of size δt. Let us denote with a superscript n the approximation to u and $t^n = n\delta t$. If the backward Euler scheme is used for the time integration, there holds

$$\|u(t^N) - u_h^N\|^2 + \sum_{n=1}^{N} \delta t k \|\nabla u^n - \nabla u_h^n\|^2 + \sum_{n=1}^{N} \delta t \tau \|\boldsymbol{a}\cdot\nabla u^n - \boldsymbol{a}\cdot\nabla u_h^n\|^2 \leq I_h + I_{\delta t}$$

where $I_{\delta t}$ and I_h are optimal interpolation errors in space and time (for a proof for the Stokes problem, see [2]).

From the stability and convergence properties described, and also from the design of the formulation itself, the following properties are particularly relevant:

- No relationship between δt and h is required. *Anisotropic space-time discretizations* are possible.
- No instabilities for small δt can appear.
- τ is independent of δt. "Consistent" behavior is obtained for $t \to \infty$ (the steady state solution does not depend on δt).

These properties do not hold for the most popular stabilized finite element methods for transient problems that can be found in the literature.

4 Conclusions

In this work we have summarized the formulation we have developed during the last years to approximate flow problems and, in particular, the CDRE. The most salient aspect we would like to stress is that in the splitting of the unknown into finite

element scales and SGS, the latter have their own "personality" and, in particular, their own variational equation.

We favor the choice of taking the SGS *orthogonal* to the finite element space. This leads to several advantages, in particular for transient problems. In this case, *dynamic* SGS solve inconsistencies encountered in several stabilized formulations (order of space and time discretization, link between h and δt, steady-state dependence on δt, etc.) In general, stability properties of the continuous problem are inherited by the finite element solution *plus the SGS*. Extension to anisotropic meshes is possible, the approach relying on appropriate definitions of τ and, obviously, anisotropic interpolation estimates. In applications, such estimates are usually not feasible. Methods with intrinsic stability are mandatory.

We have also discussed discontinuity capturing techniques, which are required if local instabilities need to be avoided. This is important in nonlinear problems in which sharp layers may be developed. Classical residual based DC methods have been reviewed, and two new ideas have been proposed.

References

1. S. Badia and R. Codina. Analysis of a stabilized finite element approximation of the transient convection-diffusion equation using an ALE framework. *SIAM Journal on Numerical Analysis*, 44:2159–2197, 2006.
2. S. Badia and R. Codina. On a multiscale approach to the transient Stokes problem. Transient subscales and anisotropic space-time discretization. *Applied Mathematics and Computation*, 207:415–433, 2009.
3. S. Badia, R. Codina, and J.V. Gutiérrez-Santacreu. Long term stability estimates and existence of global attractors in a finite element approximation of the Navier-Stokes equations with numerical sub-grid scale modeling. *SIAM Journal on Numerical Analysis*, 48:1013–1037, 2010.
4. R. Codina. A discontinuity-capturing crosswind-dissipation for the finite element solution of the convection-diffusion equation. *Computer Methods in Applied Mechanics and Engineering*, 110:325–342, 1993.
5. R. Codina. Comparison of some finite element methods for solving the diffusion-convection-reaction equation. *Computer Methods in Applied Mechanics and Engineering*, 156:185–210, 1998.
6. R. Codina. Stabilization of incompressibility and convection through orthogonal sub-scales in finite element methods. *Computer Methods in Applied Mechanics and Engineering*, 190:1579–1599, 2000.
7. R. Codina. Stabilized finite element approximation of transient incompressible flows using orthogonal subscales. *Computer Methods in Applied Mechanics and Engineering*, 191:4295–4321, 2002.
8. R. Codina and J. Blasco. Analysis of a stabilized finite element approximation of the transient convection-diffusion-reaction equation using orthogonal subscales. *Computing and Visualization in Science*, 4:167–174, 2002.
9. R. Codina, J. Principe, and J. Baiges. Subscales on the element boundaries in the variational two-scale finite element method. *Computer Methods in Applied Mechanics and Engineering*, 198:838–852, 2009.
10. R. Codina, J. Principe, O. Guasch, and S. Badia. Time dependent subscales in the stabilized finite element approximation of incompressible flow problems. *Computer Methods in Applied Mechanics and Engineering*, 196:2413–2430, 2007.

11. T.J.R. Hughes. Multiscale phenomena: Green's function, the Dirichlet-to-Neumann formulation, subgrid scale models, bubbles and the origins of stabilized formulations. *Computer Methods in Applied Mechanics and Engineering*, 127:387–401, 1995.
12. J. Principe, R. Codina, and F. Henke. The dissipative structure of variational multiscale methods for incompressible flows. *Computer Methods in Applied Mechanics and Engineering*, 199:791–801, 2010.

A Two-Weight Scheme for a Time-Dependent Advection-Diffusion Problem

Naresh M. Chadha and Niall Madden

Abstract We consider a family of two-weight finite difference schemes for a time-dependent advection-diffusion problem. For a given uniform grid-spacing in time and space, and for a fixed value of advection and diffusion parameters, we demonstrate how to optimally choose these weights by means of the notion of an equivalent differential equation. We also provide a geometric interpretation of the weights. We present numerical results that demonstrate that the approach is superior to other commonly used methods that also fit into the framework of a two-weight scheme.

1 Introduction

We consider the numerical solution of a one-dimensional advection-diffusion problem

$$\frac{\partial \Phi}{\partial t} + L\Phi = 0, \quad L := a\frac{\partial \Phi}{\partial x} - \varepsilon \frac{\partial^2 \Phi}{\partial x^2} \quad \text{for } (x,t) \in (0,l) \times (0,T], \tag{1a}$$

subject to the boundary and initial conditions

$$\Phi(0,t) = g_0(t), \quad \Phi(l,t) = g_l(t), \qquad t \in [0,T], \tag{1b}$$

$$\Phi(x,0) = f(x), \qquad x \in [0,l], \tag{1c}$$

were f, g_0 and g_l are known functions and are sufficiently smooth. It is assumed that ε and a, quantifying advection and diffusion processes respectively, are positive constants.

N.M. Chadha and N. Madden (✉)
School of Mathematics, Statistics, and Applied Mathematics, National University of Ireland, Galway, Ireland
e-mail: Naresh.Chadha@NUIGalway.ie, Niall.Madden@NUIGalway.ie

C. Clavero et al. (eds.), *BAIL 2010 – Boundary and Interior Layers, Computational and Asymptotic Methods*, Lecture Notes in Computational Science and Engineering 81,
DOI 10.1007/978-3-642-19665-2_11,

Models for the advection and diffusion of pollutants introduced into a fluid flow usually lead to problems of the form of (1) and its higher dimensional analogues. Many popular computer models for the two- and three-dimensional cases employ alternating direction implicit (ADI) techniques, where the problem is solved in only one coordinate direction over a fraction of a time-step. See, for example, the two-dimensional finite difference model DIVAST [3]. It solves a variant of the Navier–Stokes equations for calculating velocity fields, and then the time-dependent advection-diffusion equation for the solute transport problem, using a space-staggered uniform grid. Consequently, one is restricted to solving the solute transport problem on a uniform mesh. This leads naturally to the following question: *how can one design a finite difference scheme which offers a sufficiently accurate solution to (1) on a uniform grid, and which can be easily extended to higher dimensional problems?*

We propose to answer this question in the framework of a two-weight scheme, the general form of which is two-weight scheme is presented in Sect. 2. This general form is analyzed in Sect. 3 to derive certain useful bounds which enable us to get an insight into the specific roles of the weights involved in the scheme, as well as determining conditions for stability. Furthermore, we demonstrate that there is a subtle interplay between these two weights which allows to devise a numerical method which offers better accuracy in comparison to other conventional methods.

In Sect. 4 we employ the notion of an *equivalent differential equation* [8], and obtain *optimal* values of the weights that eliminate first two leading terms in the truncation error. Furthermore, the optimal values of the weights are combined with results of Sect. 3 to determine a range of values of the discretization parameters, Δx and Δt, that produce a von Neumann stable solution, as well as satisfying necessary conditions to be non-oscillatory. In Sect. 5, we give numerical results that compare the proposed method with several well-known techniques that may be considered as special cases of the general two-weight scheme.

2 A General Two-Weight Scheme

We construct a uniform finite difference, a tensor-product mesh $\{x_j, t^n\}$ on $[0, l] \times [0, T]$, where the grid points are defined as $(j\Delta x, n\Delta t)$, $j = 1, \ldots N, n = 0, \ldots, M$; Δt and Δx are the time and space step lengths, respectively. We denote by u_j^n the value of a mesh function $\{u\}$ at a particular point.

Define the standard discrete difference operators:

$$D^0 u_j = \frac{u_{j+1} - u_{j-1}}{2\Delta x}, \quad D^- u_j = \frac{u_j - u_{j-1}}{\Delta x},$$

$$\delta_{xx} u_j = \frac{u_{j+1} - 2u_j + u_{j-1}}{\Delta x^2}, \quad \text{and} \quad \delta_t u_j^n = \frac{u_j^{n+1} - u_j^n}{\Delta t}.$$

We can now define a spatial finite difference operator, weighted with the parameter ϕ that balances between the standard second-order central difference operator, which may be unstable for small ε, and 2-point upwinding operator that is stable, but only first-order accurate:

$$L_\phi^N u_j := \big(-\varepsilon\delta_{xx} + a\delta_x\big)u_j, \quad \text{where } \delta_x := \phi D^- + (1-\phi)D^0.$$

We then introduce the parameter θ that weights the scheme between being implicit and explicit in nature, giving our general method for (1) as

$$\delta_t \Phi_j^n + L_\phi^N \left(\theta\Phi_j^{n+1} + (1-\theta)\Phi_j^n\right) = 0, \tag{2}$$

for $j = 1, \ldots, N-1$ and $n = 1, \ldots, M$.

Several studies, such as [2], consider schemes that involve a weighted spatial discretization. For example, fixing $\theta = 0$, certain values of ϕ lead to some of the schemes considered in [2]. Moreover, for different combinations of θ and ϕ in (2), one obtains various standard difference-schemes used for linear advection-diffusion problems. For example,

- $\theta = 0$ and $\phi = 0$ correspond to forward Euler with central differencing.
- $\theta = 0$ and $\phi = a\Delta t/\Delta x$ give the standard Lax-Wendroff scheme.
- $\theta = 1$ and $\phi = 0$ give the backward Euler method with central differencing.
- $\theta = 1/2$ gives Crank-Nicolson type methods.

3 Analysis of the Scheme

In this section, we shall analyze the general scheme and derive some useful bounds for the weights involved in the scheme using various standard concepts, e.g., method of lines, and stability analysis. These bounds shall be used in Sect. 4. Furthermore, the geometric interpretation of these bounds enables us to get an insight into their specific roles in the scheme.

First, note that the scheme (2) can be rewritten as

$$A_1\Phi_{j-1}^{n+1} + B_1\Phi_j^{n+1} + C_1\Phi_{j+1}^{n+1} = A_2\Phi_{j-1}^n + B_2\Phi_j^n + C_2\Phi_{j+1}^n, \tag{3}$$

$$\text{where,} \quad A_1 = -\frac{\theta}{2}(c+\psi), \qquad B_1 = 1+\theta\psi, \qquad C_1 = \frac{\theta}{2}(c-\psi),$$

$$A_2 = \frac{1-\theta}{2}(c+\psi), \quad B_2 = 1-(1-\theta)\psi, \quad C_2 = \frac{1-\theta}{2}(-c+\psi),$$

where $s := \varepsilon\Delta t/(\Delta x)^2$, $c := a\Delta t/\Delta x$, $\psi := 2s + \phi c$. The scheme is consistent as $A_1 + B_1 + C_1 = A_2 + B_2 + C_2$. Next, we derive bounds for the weights in Sects. 3.1, 3.2, 3.3 using a notion of monotonicity, some standard concepts from method of lines, and stability analysis, respectively.

3.1 Using a Notion of Monotonicity

We rewrite the scheme (2) in a semi-discretized form as follows

$$\frac{d\Phi_j}{dt} = \sum_i \alpha_i(\Phi_{i+j} - \Phi_i),$$
$$\alpha_{-1} = \frac{a(1+\phi)}{2\Delta x} + \frac{\varepsilon}{\Delta x^2}; \quad \alpha_1 = -\frac{a(1-\phi)}{2\Delta x} + \frac{\varepsilon}{\Delta x^2}.$$

A necessary (but not itself sufficient) condition for the monotonicity of the scheme in this form is $\alpha_i \geq 0$, for all $i \neq 0$. This yields

$$\phi \geq 1 - 2s/c. \tag{4}$$

Remark 1. One may obtain the bound (4) using eigenvalue analysis. Consider the linear system that is solved at each time-step in the form (3). The eigenvalues of the matrix are given by $\lambda_j = B_1 + 2\sqrt{A_1 C_1}\cos(j\pi/(M-1))$, for $j = 1, 2, \ldots, M-1$. For solution to be spatially non-oscillatory, real eigenvalues are required (see [4]). This gives $A_1 C_1 \geq 0 \implies (1/4)\theta^2(c^2 - \psi^2) \leq 0$, which leads to (4).

3.2 Using the Method of Lines

As stated in Sect. 1, we assume that a and ε are constant. So, on an unbounded domain, one may apply Fourier analysis. We rewrite the difference scheme (2) as the following system of ordinary differential equations:

$$\frac{d\Phi_j}{dt} = -L_\phi^N \Phi_j, \qquad L_\phi^N \equiv -\varepsilon\delta_{xx} + a\delta_x. \tag{5}$$

We denote the Fourier transform of the operator L_ϕ^N by $\hat{L}_\phi^N(\beta) = e^{-\mathrm{i}j\beta} L_\phi^N e^{\mathrm{i}j\beta}$. A sufficient condition for von Neumann stability is

$$S_L \subseteq S, \quad S_L = \{-\Delta t \hat{L}_\phi^N(\beta) \in \mathbb{C} \ \forall\ \beta\},$$

where S is the stability domain of the time discretization method being used; for further details, see [9]. For the system (5), we have

$$\Delta t \hat{L}_\phi^N(\beta) = p(\beta) + \mathrm{i}q(\beta),$$
$$p(\beta) = 2(2s + \phi c)\sin^2(\beta/2), \quad q(\beta) = c\sin\beta.$$

It can easily be verified that the region S_L is fully contained in an ellipse given by

$$\left(\frac{v}{\psi}+1\right)^2+\left(\frac{w}{c}\right)^2=1;\quad \psi=2s+\phi c. \tag{6}$$

Furthermore, we have used the standard *theta-method* for the time integration, for which the stability-region is given by

$$S\equiv\left|\frac{1+z(1-\theta)}{1-z\theta}\right|\leq 1,\quad z=x+\mathrm{i}y, \tag{7}$$

which is equivalent to $(1-2\theta)(x^2+y^2)+2x\leq 0$. This implies that in a case $1-2\theta\neq 0$, S is a region inside a circle (including the boundary) defined as

$$(x+r)^2+y^2=r^2,\quad r=\frac{1}{1-2\theta}. \tag{8}$$

Since for von Neumann stability it is sufficient to prove $S_L\subseteq S$, from (6) and (8) we have

$$r\geq\max\{\psi,c,c^2/\psi\}. \tag{9}$$

Geometrically, the weight ϕ controls the length of horizontal axis of the ellipse (6), while the location of the center and the length of the radius of the circle (8) is controlled by θ. Moreover, in the case where ε is small, and $\phi=0$ (which corresponds to pure central differencing), this may lead to a situation where the boundary of the ellipse (6) would lie outside the circle (8), resulting in an oscillatory computed solution. On the other hand, $\phi=1$ (which corresponds to pure upwinding) may unnecessarily stretch the horizontal axis of the ellipse (6), causing damping in the computed solution. Thus, an optimal value of ϕ should be between 0 and 1, and should be positive, ensuring that ψ is positive. This implies that the ellipse (6) which is a cover of the eigenvalues associated with spatial discretization, should also be entirely in the left half-plane.

In general, it is desirable to have a time integration method whose stability region contains the entire left half-plane. Then one may take any time step for (5), provided that all the eigenvalues have negative real parts, as is often the case in practice [5, Sect. 8.3]. In our case, the region of stability given by (7) will be in left half-plane if and only if $1-2\theta\geq 0$. This suggests that

$$\theta\leq 1/2. \tag{10}$$

3.3 Using Stability Analysis

Following the standard von Neumann analysis, the amplification factor G can be found by substituting $\Phi_j^n=G^n e^{ij\beta}, \beta=\xi\Delta x$ in (3), and it is given as

$$G=\frac{A_2e^{-i\beta}+B_2+C_2e^{i\beta}}{A_1e^{-i\beta}+B_1+C_1e^{i\beta}}.$$

It can easily be checked that the requirement for stability, namely $|G| \leq 1$ for all β, leads to the following bounds:

$$(1-2\theta)c^2 - \psi \leq 0, \quad \text{and} \quad \psi\big((1-2\theta)\psi - 1\big) \leq 0. \tag{11}$$

Given (4), we have $\psi > 0$, and so the inequalities in (11) are automatically satisfied if $\theta \geq 1/2$. Thus *any scheme is unconditionally stable for* $\theta \geq 1/2$. For $\theta < 1/2$, the method is stable providing that

$$(1-2\theta)c^2 \leq \psi \leq (1-2\theta)^{-1}. \tag{12}$$

This can be rewritten more usefully as a sharp bound on Δt ensuring the stability of the method:

$$\Delta t \leq \frac{1}{1-2\theta} \min\left[\frac{2\varepsilon}{a^2} + \phi\frac{\Delta x}{a}, \left(\frac{2\varepsilon}{\Delta x^2} + \frac{\phi a}{\Delta x}\right)^{-1}\right].$$

For example, if $\theta = 0$ and $\phi = 0$ (forward Euler with central differencing), then one should take $\Delta t \leq \min(2\varepsilon/a^2, \Delta x^2/\varepsilon)$.

Note that it can easily be verified that (12) and (9) are the same conditions, but derived using two different approaches.

4 Optimal Values of the Parameters

In this section we obtain optimal values of the parameters using a notion of *equivalent differential equation* and the standard truncation error analysis.

Using the modified equation approach descried by Warming and Hyett [8], we can obtain *the modified partial differential equation* equivalent to the scheme (2), written as:

$$\frac{\partial \Phi}{\partial t} + a\frac{\partial \Phi}{\partial x} - \varepsilon\frac{\partial^2 \Phi}{\partial x^2} + \sum_{q=2}^{\infty} \frac{a\Delta x^{q-1}}{q!}\kappa_q(c,s)\frac{\partial^q \Phi}{\partial x^q} = 0.$$

This difference scheme is first-order accurate if $\kappa_2 \neq 0$, and is pth-order accurate if $\kappa_q = 0, q = 2, \ldots, p$, and $\kappa_{p+1} \neq 0$. The first two leading terms in the truncation error are associated with numerical dissipation and dispersion, respectively [4, Sect. 9.2]. Thus, by setting these two terms equal to zero, one may obtain a higher order scheme. In the process, an optimal value of each of the parameters, θ and ϕ can also be obtained. The desired coefficients are:

$$\kappa_2 = \phi - c(1-2\theta), \qquad \kappa_3 = 1 - 6s - c^2 + 6s\theta + 3\theta\psi + 3c^2\theta,$$

giving optimal value of the parameters:

$$\phi = c(1-2\theta), \qquad \theta = \frac{3(c^2+2s) \pm \sqrt{3(2c^2+c^4+12s^2)}}{6c^2}. \tag{13}$$

This expression leads to two possible values for θ and ϕ. In view of (10) and (4), we take the smaller of the two values for θ in (13), thus giving the optimal values of the parameters:

$$\phi_{\text{opt}} = c(1-2\theta), \qquad \theta_{\text{opt}} = \frac{3(c^2+2s) - \sqrt{3(2c^2+c^4+12s^2)}}{6c^2}. \tag{14}$$

For $\theta \neq 0$ the scheme (3) is implicit in nature, and at each step one must solve a linear system of equations. It can be easily verified that the matrix on the left-hand side of (3), is diagonally dominant providing that

$$|2(1+\theta\psi)| \geq |-\theta(c+\psi)| + |\theta(c-\psi)|.$$

This will be the case for the optimal value of the weights θ_{opt} and ϕ_{opt} given in (14), ensuring that the system is easily solved (Fig. 1).

Remark 2. The bound (4) may be combined with (14) to obtain another useful relation in terms of c and s, given as

$$c^4 - c^2 + 12s^2 \geq 0. \tag{15}$$

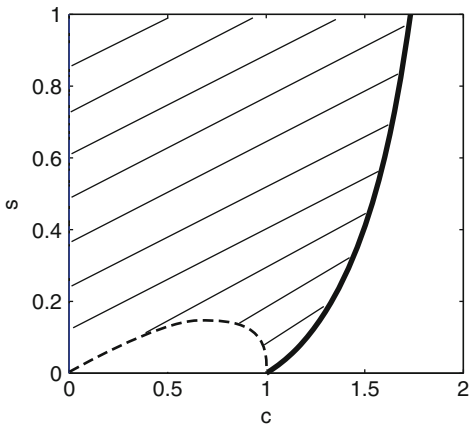

Fig. 1 The regions of stability and no-oscillations in c-s plane. The boundaries of the stability region (16), and no-oscillation region (15) are shown by *solid line*, and $\{- - -\}$, respectively. Any combination of $(\Delta x, \Delta t, \varepsilon, a)$ that falls into the shaded region would produce a von Neumann stable solution satisfying necessary conditions to be non-oscillatory

Moreover, by combining (12) and (14), we have

$$c^4 - c^2 + 12s^2 \leq 2s\sqrt{3(2c^2 + c^4 + 12s^2)}. \tag{16}$$

5 Numerical Experiments

To compare various representative methods within the framework of two-weight scheme for the model advection-diffusion problem (1), we consider a model predicting the transport of a Gaussian pulse with unit amplitude centered at $x = a$, given by

$$\Phi(x, 0) = \exp\left(\frac{-(x-a)^2}{4\varepsilon}\right), \quad 0 \leq x \leq 2.$$

This problem is widely used for comparison of different numerical schemes for the advection-diffusion problem; see, e.g., [1,6]. The exact solution to this problem is

$$\Phi(x, t) = \frac{1}{\sqrt{1+t}} \exp\left(\frac{-(x-(1+t)a)^2}{4\varepsilon(1+t)}\right), \quad 0 \leq x \leq 2, \quad t \geq 0.$$

The boundary conditions are taken from the exact solution.

In Table 1 we present a comparison between some commonly used methods and the scheme (14) for various values of N where we have taken the problem data as $a = .25$, $\varepsilon = 10^{-2}$ and $\Delta t = 2\Delta x$. The errors presented are the maximum point-wise errors at time $T = 2$.

We observe that, for all cases, the scheme (14) is superior to all of the others. Since we have taken $\Delta t = 2\Delta x$ there is nothing to ensure that the explicit schemes are stable, and indeed they fail entirely for some values of N.

To verify that there is nothing particularly advantageous for the scheme (14) in taking these parameters, we repeat the experiments for $\varepsilon = 10^{-4}$ and give the results in Table 2. Again we see that the method (14) yields a more accurate solution than the other schemes. In all cases, the methods are less accurate for $\varepsilon = 10^{-4}$ compared to $\varepsilon = 10^{-2}$; this is hardly surprising since a uniform mesh is used in all cases.

Table 1 Comparison of various schemes for test problem with $\varepsilon = 10^{-2}$

N	Forward Euler Central Diff	Explicit Lax-Wendroff	Implicit Upwinding	Crank-Nicolson Central Diff	Optimal scheme (14)
64	2.45e + 01	3.78e + 04	8.95e−02	5.38e−03	4.48e−04
128	1.77e + 33	8.11e + 35	4.99e−02	1.33e−03	1.24e−04
256	1.65e + 116	4.92e + 118	2.65e−02	3.33e−04	3.17e−05
512	—	—	1.37e−02	8.32e−05	7.96e−06
1024	—	—	6.97e−03	2.08e−05	1.99e−06

Table 2 Comparison of various schemes for test problem with $\varepsilon = 10^{-4}$

N	Forward Euler Central Diff	Explicit Lax-Wendroff	Implicit Upwinding	Crank-Nicolson Central Diff	Optimal scheme (14)
64	5.12e + 00	3.29e−01	4.83e−01	3.77e−01	2.12e−01
128	4.97e + 01	2.41e−01	4.50e−01	2.92e−01	9.92e−02
256	3.98e + 02	1.29e−01	4.02e−01	2.17e−01	2.31e−02
512	5.02e + 01	3.07e−02	3.39e−01	7.92e−02	3.07e−03
1024	6.56e−01	2.35e−03	2.66e−01	2.00e−02	2.54e−04

6 Conclusions

We have presented a two-weight scheme for a time dependent advection-diffusion problem. An optimal value of the weights involved have been obtained and their roles in the scheme have been geometrically interpreted. The supporting numerical results suggest that the method is promising.

There are several restrictions to note. Firstly, we have assumed that the coefficient of advection, a, is constant. We are in the process of relaxing this restriction for a more general case where $a = a(t)$. This only requires new values of ϕ and θ at each time step.

We also note that many studies of problems of the form (1) consider so-called *parameter robust methods*, (e.g., [7]), that perform well for arbitrarily small values of ε. However, due to the nature of our intended work related to enhancing certain existing hydrodynamics and solute transport models, we are restricted to using uniform meshes (and a range of values of ε that occur in applied problems). We do not claim that the method presented here is parameter robust. However, in the future we aim to extend the approach to allow for piecewise uniform meshes by employing domain decomposition techniques.

Finally, we note that the analysis presented here can be extended to higher dimensional analogous problems via standard ADI approaches; this is work in progress.

Acknowledgements This material is based upon works supported by the Science Foundation Ireland under Grant No. 08/RFP/CMS1205.

References

1. M.M. Cecchi and M.A. Pirozzi. High order finite difference numerical methods for time-dependent convection-dominated problems. *Appl. Numer. Math.*, 55(3):334–356, 2005.
2. M. Dehghan. Weighted finite difference techniques for the one-dimensional advection-diffusion equation. *Appl. Math. Comp.*, 147(2):307–319, 2004.
3. R.A. Falconer, B. Lin, Y. Wu, and E. Harris. *DIVAST User Manual*. Environmental Water Management Research Centre, Cardiff University, UK., 1998.
4. C.A.J. Fletcher. *Computational Techniques for Fluid Dynamics. Vol. I: Fundamental and General Techniques*. Springer Series in Computational Physics. Springer-Verlag, Berlin, 1991.

5. R.J. LeVeque. *Finite difference methods for ordinary and partial differential equations. Steady-state and time-dependent problems.* Philadelphia, PA: Society for Industrial and Applied Mathematics (SIAM). xv, 341 p., 2007.
6. A. Mohebbi and M. Dehghan. High-order compact solution of the one-dimensional heat and advection-diffusion equations. *Appl. Math. Model*, 34(10):3071–3084, 2010.
7. H-G. Roos, M. Stynes, and L. Tobiska. *Robust Numerical Methods for Singularly Perturbed Differential Equations*, volume 24 of *Springer Series in Computational Mathematics*. Springer-Verlag, Berlin, 2nd edition, 2008.
8. R.F. Warming and B.J. Hyett. The modified equation approach to the stability and accuracy analysis of finite-difference methods. *J. Comput. Phys.*, 14(2):159–179, 1974.
9. P. Wesseling. von Neumann stability conditions for the convection-diffusion equation. *IMA J. Numer. Anal.*, 16(4):583–598, 1996.

Error Estimates for a Mixed Hybridized Finite Volume Method for 2nd Order Elliptic Problems

Carlo de Falco and Riccardo Sacco

Abstract In this article, we carry out the convergence analysis of the dual–mixed hybridized finite volume scheme proposed in (Marco Brera et al., Comput. Methods Appl. Mech. Eng., in press, 2010) for the numerical approximation of transport problems in symmetrizable form. Using the results of (Micheletti et al., SIAM J. Sci. Comput., 23-1:245–270, 2001; Brezzi et al., Discretization of semiconductor device problems (i), Elsevier North-Holland, Amsterdam, 2005) optimal error estimates are obtained for the scalar unknown and the flux in the appropriate graph norm, while using the techniques and analysis of (Arnold and Brezzi, Math. Modeling Numer. Anal., 19-1:7–32, 1985; Brezzi and Fortin, Mixed and Hybrid Finite Element Methods, Springer, New York, 1991) the superconvergence of the hybrid variable and of its post-processed (nonconforming) reconstruction are proved. Numerical experiments are included to support the theoretical conclusions.

1 Introduction

In this article, we consider the elliptic model problem in *mixed form*:

$$\begin{cases} \mathrm{div}\boldsymbol{\sigma} = f & \text{in } \Omega \\ a^{-1}\boldsymbol{\sigma} + \nabla u = \mathbf{0} & \text{in } \Omega \\ u = 0 & \text{on } \Gamma, \end{cases} \tag{1}$$

where $\Omega \subset \mathbb{R}^2$ is a convex polygonal domain, while a is a piecewise smooth function over Ω such that $a(\boldsymbol{x}) \geq a_0 > 0$ almost everywhere (a.e.) in Ω and $f \in L^2(\Omega)$ is a given function. Using the terminology of Continuum Mechanics, the scalar

C. de Falco (✉) and R. Sacco
Dipartimento di Matematica "F. Brioschi", Politecnico di Milano,
P.zza Leonardo da Vinci 32, 20133 Milano, Italy
e-mail: carlo.defalco@polimi.it, riccardo.sacco@polimi.it

C. Clavero et al. (eds.), *BAIL 2010 – Boundary and Interior Layers, Computational and Asymptotic Methods*, Lecture Notes in Computational Science and Engineering 81,
DOI 10.1007/978-3-642-19665-2_12,

variable u is referred to as *displacement* while the vector-valued variable $\boldsymbol{\sigma}$ is the *flux* (or the *stress*). In [3], a dual–mixed Hybridized (DMH) finite element method with numerical integration of the local flux mass matrix has been proposed for the discretization of (1) in the case where such system represents the model for transport phenomena in symmetrizable form. The use of numerical integration allows to implement the DMH formulation as a genuine finite volume (FV) scheme for the approximation u_h of u that is a piecewise constant function over Ω. The resulting DMH-FV method enjoys the usual properties of dual-mixed approximations (interelement normal flux conservation and local self-equilibrium), and satisfies the discrete maximum principle (DMP) under the sole requirement that the finite element grid is of Delaunay type, with a considerable reduction of the computational effort compared to standard DMH formulations. In this article, we carry the error analysis of the DMH-FV method showing that it enjoys the same theoretical convergence properties as the corresponding DMH formulation. Precisely, after describing the DMH-FV scheme in Sects. 2, 3 and 4, we prove in Sect. 5 optimal error estimates for the scalar unknown and the flux in the appropriate graph norm, and the superconvergence of the hybrid variable and of its post-processed (nonconforming) reconstruction. The theoretical conclusions of Sect. 5 are then numerically validated in Sect. 6, where the model problem (1) is solved in the case of transport phenomena in symmetrized form.

2 Geometric Discretization

In view of the numerical discretization of (1), we consider a regular family of given partitions $\{\mathcal{T}_h\}$ of the domain Ω into open triangles K satisfying the usual admissibility condition (see [10], Sect. 3.1 and Def. 3.4.1). For a given $\mathcal{T}_h$, we denote by $|K|$ and h_K the area and the diameter of K, respectively, and we set $h = \max_{\mathcal{T}_h} h_K$. Let $\boldsymbol{x} = (x, y)^T$ be the position vector in Ω; then, for each $K \in \mathcal{T}_h$, we denote by $\boldsymbol{x}_q$, $q = 1, 2, 3$, the three vertices of K ordered according to a counterclockwise orientation, by $\boldsymbol{e}_q$ the edge of ∂K which is opposite to $\boldsymbol{x}_q$, by θ_q^K the angle opposite to $\boldsymbol{e}_q$ and by C_K the circumcenter of K. We denote by $|\boldsymbol{e}_q|$ the length of $\boldsymbol{e}_q$ and by $\boldsymbol{n}_q$ the outward unit normal vector along $\boldsymbol{e}_q$. Moreover, we define s_q^K as the signed distance between C_K and the midpoint M_q of $\boldsymbol{e}_q$. If $\theta_q^K < \pi/2$ then $s_q^K > 0$, while if K is obtuse in θ_q^K then $s_q^K < 0$, and C_K falls outside K. Notice also that if $\theta_q^K = \pi/2$ then $s_q^K = 0$, and C_K coincides with M_q. We denote by $\mathcal{E}_h$ the set of edges of $\mathcal{T}_h$, and by $\mathcal{E}_{h,int}$ those belonging to the interior of Ω. For each $e \in \mathcal{E}_{h,int}$, we indicate by K_e^1 and K_e^2 the pair of elements of $\mathcal{T}_h$ such that $e = \partial K_e^1 \cap \partial K_e^2$. Finally, we let $s_e = s_e^{K_e^1} + s_e^{K_e^2}$ denote the signed distance between $C_{K_e^1}$ and $C_{K_e^2}$. If $\theta_e^{K_e^1} + \theta_e^{K_e^2} < \pi$ for all $e \in \mathcal{E}_{h,int}$, then $s_e > 0$, and $\mathcal{T}_h$ is called a *Delaunay triangulation* [7]. The Delaunay condition prevents the occurrence of pairs of *obtuse* neighbouring elements in $\mathcal{T}_h$, still allowing the possibility of having single obtuse triangles in the computational grid (see [8] for algorithmic details). We assume from

now on that $\mathcal{T}_h$ is a Delaunay triangulation, and we refer to [3] for the case where $\mathcal{T}_h$ is a *degenerate Delaunay triangulation* (i.e., $s_e = 0$ for some $e \in \mathcal{E}_{h,int}$).

3 Finite Element Spaces

For $k \geq 0$ and a given set $\mathcal{S}$, we denote by $\mathbb{P}_k(\mathcal{S})$ the space of polynomials of degree $\leq k$ defined over $\mathcal{S}$. We also denote by $\mathbb{RT}_0(K) := (\mathbb{P}_0(K))^2 \oplus \mathbb{P}_0(K)\,\boldsymbol{x}$ the Raviart–Thomas (RT) finite element space of lowest degree [11], and by $\mathcal{P}_0$ the L^2-projection over constant functions. Then, we introduce the following finite element spaces:

$$\begin{aligned}
\mathbf{V}_h &:= \{\boldsymbol{v} \in (L^2(\Omega))^2 \,|\, \boldsymbol{v}|_K \in \mathbb{RT}_0(K)\ \forall K \in \mathcal{T}_h\} \\
W_h &:= \{w \in L^2(\Omega) \,|\, w|_K \in \mathbb{P}_0(K)\ \forall K \in \mathcal{T}_h\} \\
M_h &:= \{m \in L^2(\mathcal{E}_h) \,|\, m|_{\partial K} \in \mathcal{R}_0(\partial K) \forall K \in \mathcal{T}_h, \\
&\qquad m^{K_e^1}|_e = m^{K_e^2}|_e\ \forall e \in \mathcal{E}_{h,int},\ m|_e = 0, \forall e \in \Gamma\} \\
\Lambda_h &:= \{v_h \in L^2(\Omega) \,|\, v_h \in \mathbb{P}_1(K)\ \forall K \in \mathcal{T}_h, \\
&\qquad v_h(M_e^{K_e^1}) = v_h(M_e^{K_e^2})\ \forall e \in \mathcal{E}_{h,int},\ v_h(M_e) = 0\ \forall e \in \Gamma\},
\end{aligned} \tag{2}$$

where $\mathcal{R}_0(\partial K) := \{v \in L^2(\partial K) |\ v|_e \in \mathbb{P}_0(e)\ \forall e \in \partial K\}$, and $m^{K_e^1}$, $m^{K_e^2}$ are the restrictions of the generic function $m \in M_h$ on K_e^1 and K_e^2, respectively. Functions belonging to $\mathbf{V}_h$ and W_h are completely discontinuous over $\mathcal{T}_h$, while functions in M_h are single-valued on $\mathcal{E}_h$. Functions in Λ_h are discontinuous and piecewise linear over $\mathcal{T}_h$, with continuity only at the midpoint of each edge $e \in \mathcal{E}_{h,int}$.

4 The DMH-FV Method

The DMH-FV Galerkin approximation of problem (1) consists of finding $(\boldsymbol{\sigma}_h, u_h, \lambda_h) \in (\mathbf{V}_h \times W_h \times M_h)$ such that:

$$\begin{cases}
(A\,\boldsymbol{\sigma}_h, \boldsymbol{\tau}_h)_{\mathcal{T}_h,h} - (u_h, \mathrm{div}\boldsymbol{\tau}_h)_{\mathcal{T}_h} + \langle \lambda_h, \boldsymbol{\tau}_h \cdot \boldsymbol{n}\rangle_{\mathcal{E}_h} = 0 & \forall \boldsymbol{\tau}_h \in \mathbf{V}_h \\
(\mathrm{div}\boldsymbol{\sigma}_h\, q_h)_{\mathcal{T}_h} = (f, q_h)_{\mathcal{T}_h} & \forall q_h \in W_h \\
\langle \boldsymbol{\sigma}_h \cdot \boldsymbol{n}, \mu_h\rangle_{\mathcal{E}_h} = 0 & \forall \mu_h \in M_h,
\end{cases} \tag{3}$$

where $A := a^{-1}$ and where we denote by $(\cdot,\cdot)_{\mathcal{T}_h}$, $(\cdot,\cdot)_{\mathcal{T}_h,h}$ and $\langle\cdot,\cdot\rangle_{\mathcal{E}_h}$ the elementwise L^2 inner product over $\mathcal{T}_h$, its approximation using a numerical integration formula over each element $K \in \mathcal{T}_h$ yet unspecified, and the edgewise L^2 inner product over $\mathcal{E}_h$, respectively. The equations in (3) have the following interpretation: $(3)_1$ expresses the approximate local constitutive law; $(3)_2$ expresses the approximate

local self-equilibrium; $(3)_3$ expresses the approximate continuity of $\boldsymbol{\sigma} \cdot \boldsymbol{n}$ across each interelement edge. To construct the DMH-FV discretization, we assume, only for ease of presentation, that $\mathcal{T}_h$ is *strictly acute*, i.e., $\theta_q^K < \pi/2$ for each $K \in \mathcal{T}_h$ and $q = 1, 2, 3$. This implies that $s_q^K > 0$ $q = 1, 2, 3$ for each $K \in \mathcal{T}_h$. For each $K \in \mathcal{T}_h$, we denote by $\{\boldsymbol{\tau}_j\}_{j=1}^3$ the basis for $\mathbb{RT}_0(K)$ and set

$$\boldsymbol{\sigma}_h^K(\boldsymbol{x}) = \sum_{j=1}^{3} \Phi_j^K \boldsymbol{\tau}_j(\boldsymbol{x}) \qquad \boldsymbol{x} \in K, \tag{4}$$

where the degree of freedom Φ_j^K is the flux of $\boldsymbol{\sigma}_h^K$ across edge $\boldsymbol{e}_j$, $j = 1, 2, 3$. Then, we consider the following quadrature formula

$$(A\,\boldsymbol{\tau}_j, \boldsymbol{\tau}_i)_K \simeq (A\,\boldsymbol{\tau}_j, \boldsymbol{\tau}_i)_{K,h} := \frac{1}{2}\overline{A}_i^K \cot(\theta_i^K)\delta_{ij} = \overline{A}_i^K \frac{s_i^K}{|\boldsymbol{e}_i|}\delta_{ij} \quad i, j = 1, 2, 3, \tag{5}$$

where $\overline{A}_i^K := \int_{C_K}^{M_i} A^K(\zeta)\mathrm{d}\zeta/|s_i^K|$.

Proposition 1. *Assume that $a|_K \in W^{1,\infty}(K)$ for each $K \in \mathcal{T}_h$. Then, there exists a positive constant C_K depending only on the regularity of $\mathcal{T}_h$ such that $\forall\, \boldsymbol{p}, \boldsymbol{q} \in \mathbb{RT}_0(K)$ we have*

$$\left|(A\,\boldsymbol{p}, \boldsymbol{q})_K - (A\,\boldsymbol{p}, \boldsymbol{q})_{K,h}\right| \leq C_K \|A\|_{W^{1,\infty}(K)} h_K \|\boldsymbol{p}\|_{L^2(K)} \|\boldsymbol{q}\|_{L^2(K)}. \tag{6}$$

Proof. We first need to check that (6) holds in the case $A = 1$. This follows by inspection on the analysis of [2] and noting that the supremum in (12) of [2] can be taken on the larger set $(L^2(K))^2 \supset H(\mathrm{div}; K)$. Then, the estimate (6) easily follows by proceeding as in [5] pp. 375–376.

Remark 1. The quantities $\|\boldsymbol{p}\|_{L^2(K)}$ and $\|\boldsymbol{q}\|_{L^2(K)}$ can obviously be bounded by $\|\boldsymbol{p}\|_{H(\mathrm{div};K)}$ and $\|\boldsymbol{q}\|_{H(\mathrm{div};K)}$, respectively. This allows to recover the analogous estimates of the quadrature error associated with the approximation (5) proved in [5, 9].

Using (5) into $(3)_1$, we obtain the following system of linear algebraic equations for the degrees of freedom $\{\Phi^K\}_{K\in\mathcal{T}_h}$, $\{u^K\}_{K\in\mathcal{T}_h}$ and $\{\lambda_i\}_{e_i\in\mathcal{E}_{h,int}}$ associated with the DMH-FV method:

$$\begin{cases} \overline{A}_i^K \Phi_i^K \dfrac{s_i^K}{|\boldsymbol{e}_i|} - u^K + \lambda_i^K = 0 & \forall K \in \mathcal{T}_h \qquad i = 1, 2, 3 \\ \displaystyle\sum_{i=1}^{3} \Phi_i^K = f^K |K| & \forall K \in \mathcal{T}_h \\ \Phi_e^{K_e^1} + \Phi_e^{K_e^2} = 0 & \forall e \in \mathcal{E}_{h,int}, \end{cases} \tag{7}$$

where $f^K := \mathcal{P}_0 f|_K$ for each $K \in \mathcal{T}_h$. Eliminating from $(7)_1$ and $(7)_3$ the variables Φ_i^K and λ_i^K in favor of u^K, and using the fact that λ_h is single–valued on $\mathcal{E}_h$, we get the following finite volume set of equations

$$\begin{cases} -\sum_{i=1}^{3} \mathcal{H}_{e_i}(a) \dfrac{u^{K_i} - u^K}{s_i} |e_i| = f^K |K| & \forall K \in \mathcal{T}_h \\ u^{K_i} = 0 & \forall e_i \in \Gamma, \end{cases} \tag{8}$$

where, for each edge $e \in \mathcal{E}_h$, the positive quantity $\mathcal{H}_e(a)$ is the *harmonic average* of a across the edge e defined as

$$\mathcal{H}_e(a) := \left(\frac{\int_{s_e} a^{-1}(\zeta)\, d\zeta}{s_e} \right)^{-1} = \frac{s_e}{\overline{A}_e^{K_e^1} s_e^{K_e^1} + \overline{A}_e^{K_e^2} s_e^{K_e^2}}. \tag{9}$$

Proposition 2. *System* (8) *has a unique solution. Moreover, the DMH-FV satisfies the DMP.*

Proof. The set of linear algebraic equations (8) is a special instance of equations (5.7) of [9]. Therefore, Lemma 5.2 of [9] applies to conclude that the stiffness matrix associated with the DMH-FV method is a Stieltjes M-matrix [13]. This latter property immediately implies that the DMH-FV scheme satisfies the DMP by application of Theorem 3.1, p.202 of [12].

Once system (8) is solved for the piecewise constant values of u_h over $\mathcal{T}_h$, the degrees of freedom for λ_h can be easily computed by post-processing as

$$\lambda_e = \frac{(\overline{A}_e^{K_e^1} s_e^{K_e^1})^{-1} u^{K_e^1} + (\overline{A}_i^{K_e^2} s_e^{K_e^2})^{-1} u^{K_e^2}}{(\overline{A}_e^{K_e^1} s_e^{K_e^1})^{-1} + (\overline{A}_e^{K_e^2} s_e^{K_e^2})^{-1}} \qquad \forall e \in \mathcal{E}_{h,int}, \tag{10}$$

while $\lambda_e = 0$ for each $e \in \Gamma$. Then, $\boldsymbol{\sigma}_h$ can be computed over each element $K \in \mathcal{T}_h$ by using $(7)_1$ and (4).

Remark 2. Propositions 1 and 2 and the post-processing formula (10) still hold under the more general condition that $\mathcal{T}_h$ is a Delaunay triangulation. We refer to [3] for the details of the construction of the DMH-FV scheme under such assumption.

5 Error Estimates

In this section, we assume that the problem coefficients (and, as a consequence, the solution pair $(u, \boldsymbol{\sigma})$ of (1)) have at each step the required regularity required by the context. We also assume that exact integration is used to evaluate the right-hand side of $(3)_2$ in order to avoid dealing with the associated quadrature error. Moreover, we denote by C a positive constant, not depending on h and possibly depending on the

mesh regularity constant and on the regularity of the coefficients, whose value is not necessarily the same at each occurrence.

5.1 Internal Variables

Theorem 1. *There exists a positive constant C such that*

$$\|u - u_h\|_{L^2(\Omega)} + \|\boldsymbol{\sigma} - \boldsymbol{\sigma}_h\|_{H(\mathrm{div};\Omega)} \leq C h \left(\|u\|_{H^2(\Omega)} + \|f\|_{H^1(\Omega)}\right). \tag{11}$$

Proof. The estimate (11) is an immediate consequence of (7.16) of [9] in the case $\sigma = 0$.

Let us denote by $P_h u$ the L^2-projection of u over W_h. Then, the next superconvergence result is an immediate consequence of Theorem 1 and of the analysis at p. 186 of [4].

Theorem 2. *There exists a positive constant C such that*

$$\|P_h u - u_h\|_{L^2(\Omega)} \leq C h^2 \left(\|u\|_{H^2(\Omega)} + \|f\|_{H^1(\Omega)}\right). \tag{12}$$

This latter result indicates that the piecewise constant values of u_h are a very good approximation of the mean value of the exact solution over each element $K \in \mathcal{T}_h$.

5.2 Hybrid Variable

Let us denote by $\Pi_h u$ the L^2-projection of u over Λ_h and introduce the following mesh-dependent norm

$$|\mu_h|^2_{-1/2,h} := \sum_{e \in \mathcal{E}_h} h_e \|\mu_h\|^2_{L^2(e)} \qquad \forall \mu_h \in \Lambda_h.$$

The next result demonstrates the superconvergence of the hybrid variable λ_h to the L^2-projection $\Pi_h u$ of u over Λ_h.

Theorem 3. *There exists a positive constant C such that*

$$|\Pi_h u - \lambda_h|_{-1/2,h} \leq C h^2 \left(\|u\|_{H^2(\Omega)} + \|f\|_{H^1(\Omega)}\right). \tag{13}$$

Proof. We closely follow the guidelines of the proof of Theorem 1.4 of [1]. For every $K \in \mathcal{T}_h$, we have

$$\begin{aligned}&(A(\boldsymbol{\sigma}_h - \boldsymbol{\sigma}), \boldsymbol{\tau}_h)_K - ((u_h - P_h u), \mathrm{div}\boldsymbol{\tau}_h)_K \\ &+((\lambda_h - \Pi_h u), \boldsymbol{\tau}_h \cdot \boldsymbol{n})_{\partial K} - \boxed{\left((A\boldsymbol{\sigma}_h, \boldsymbol{\tau}_h)_K - (A\boldsymbol{\sigma}_h, \boldsymbol{\tau}_h)_{K,h}\right)} = 0 \quad \forall \boldsymbol{\tau}_h \in \mathbb{RT}_0(K).\end{aligned}$$

The boxed term accounts for the quadrature error and is identically equal to zero in the analysis of [1]. Let us pick $\boldsymbol{\tau}_h \in \mathbb{RT}_0(K)$, as done in [1], in such a way that

$$\begin{cases} \boldsymbol{\tau}_h \cdot \boldsymbol{n}_e = \lambda_h - \Pi_h u & \text{on } e \in \partial K \\ \boldsymbol{\tau}_h \cdot \boldsymbol{n} = 0 & \text{on } \partial K \setminus e. \end{cases} \tag{14}$$

The above test function satisfies the following scaling properties

$$\|\boldsymbol{\tau}_h\|_{L^2(K)} \leq C h_K^{1/2} \|\lambda_h - \Pi_h u\|_{L^2(e)}, \ \ \|\mathrm{div}\boldsymbol{\tau}_h\|_{L^2(K)} \leq C h_K^{-1/2} \|\lambda_h - \Pi_h u\|_{L^2(e)}. \tag{15}$$

Using (14), (15) and (6), we obtain

$$\begin{aligned} \|\lambda_h - \Pi_h u\|_{L^2(e)} \leq C \big(& \|A\|_{L^\infty(K)} h_K^{1/2} \|\boldsymbol{\sigma} - \boldsymbol{\sigma}_h\|_{L^2(K)} + h_K^{-1/2} \|P_h u - u_h\|_{L^2(K)} \\ & + \boxed{\|A\|_{W^{1,\infty}(K)} h_K^{3/2} \|\boldsymbol{\sigma}_h\|_{L^2(K)}} \big), \end{aligned}$$

from which we get (13), by squaring both sides of the previous inequality and multiplying by the length h_e of edge e, then by using (11), (12) and the well-posedness of the DMH-FV problem (3) and, finally, by summing over all mesh elements.

Using (11), (12) and (13), and proceeding as in [1], Sect. 2, Theorem 2.2, we can prove the following result.

Theorem 4. *There exists a positive constant C such that*

$$\|u - u_h^*\|_{L^2(\Omega)} \leq C h^2 \left(\|u\|_{H^2(\Omega)} + \|f\|_{H^1(\Omega)} \right). \tag{16}$$

This latter result indicates that the piecewise linear (non-conforming) reconstruction of λ_h over $\mathcal{T}_h$ is optimally converging in the L^2 norm to the exact solution u as in the case of standard displacement–based formulations.

6 Numerical Results

In this section, we consider problem (1) in the case $a = e^{-\varphi}$, φ being a given piecewise linear function over $\mathcal{T}_h$ [6]. With this choice, system (1) represents the symmetrized form of the convection-diffusion model with convective term in gradient form that is widely used to describe transport phenomena in Electrochemistry and Semiconductor Device Modeling [3]. In order to carry out the numerical validation of the DMH-FV scheme, we set $\Omega \equiv (0,2) \times (0,1)$ and $\varphi(x,y) = -(2x+y)$, in such a way that the exact solution is $u = e^{-(x+3)}\, xy(x-2)(y-1)$. Figure 1 shows u_h and the non-conforming interpolant u_h^* of λ_h, computed on a triangulation with $h = 0.1237$. Figure 2 shows the corresponding error curves $\|u - u_h\|_{L^2(\Omega)}$, $\|P_h u - u_h\|_{L^2(\Omega)}$, $|\Pi_h u - \lambda_h|_{-1/2,h}$ and $\|u - u_h^*\|_{L^2(\Omega)}$. The obtained results are in complete agreement with the theoretical analysis of Sects. 4 and 5.

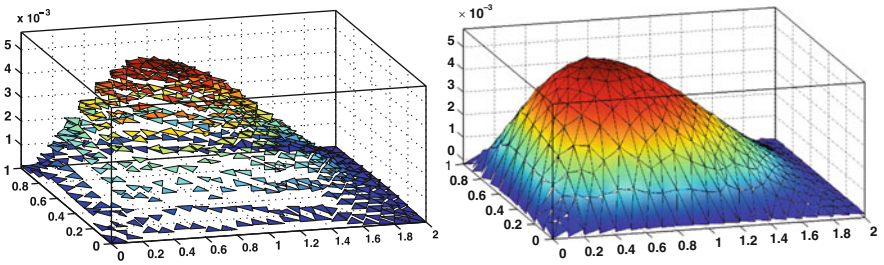

Fig. 1 *Left*: u_h; *right*: u_h^*

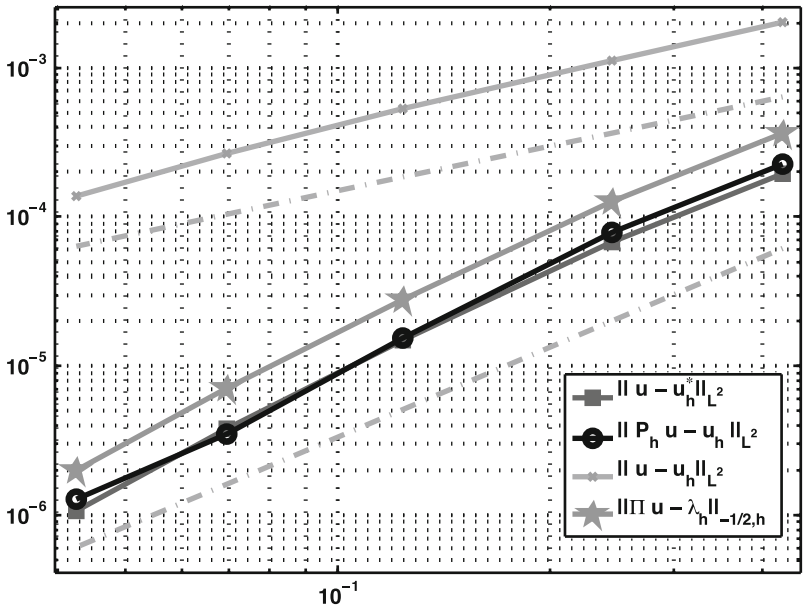

Fig. 2 Error curves as functions of the mesh size h

Acknowledgements The authors were supported by the GNCS Research Grant "Modelli Computazionali per Problemi Multifisica/Multiscala in Presenza di Bio-Interfacce" (2010).

References

1. D.N. Arnold and F. Brezzi. Mixed and Nonconforming Finite Element Methods: Implementation, Postprocessing and Error Estimates. *Math. Modeling and Numer. Anal.*, 19-1:7–32, 1985.
2. J. Baranger, J.F. Maitre, and F. Oudin. Connection between finite volume and mixed finite element methods. M^2AN, 30:445–465, 1996.

3. M. Brera, J.W. Jerome, Y. Mori, and R. Sacco. A conservative and monotone mixed-hybridized finite element approximation of transport problems in heteroge neous domains. *Computer Methods in Applied Mechanics and Engineering*, 199:2709–2720, 2010.
4. F. Brezzi and M. Fortin. *Mixed and Hybrid Finite Element Methods*. Springer Verlag, New York, 1991.
5. F. Brezzi, L.D. Marini, S. Micheletti, P. Pietra, R. Sacco, and S. Wang. Discretization of semiconductor device problems (i). In E.J.W. ter Maten P.G. Ciarlet, W.H.A. Schilders, editor, *Lecture Notes in Computational Science and Engineering*, volume XIII, pages 317–441. Elsevier North-Holland, Amsterdam, 2005.
6. F. Brezzi, L.D. Marini, and P. Pietra. Two-dimensional exponential fitting and applications to drift-diffusion models. *SIAM J. Numer. Anal.*, 26:1342–1355, 1989.
7. B. Delaunay. Sur la sphère vide. *Izv. Akad. Nauk. SSSR., Math. and Nat. Sci. Div.*, 6:793–800, 1934.
8. P.J. Frey and P.-L. George. *Mesh Generation. Application to Finite Elements (2nd Ed.)*. Wiley, London, 2008.
9. S. Micheletti, R. Sacco, and F. Saleri. On some mixed finite element methods with numerical integration. *SIAM J. Sci. Comput.*, 23-1:245–270, 2001.
10. A. Quarteroni and A. Valli. *Numerical Approximation of Partial Differential Equations*. Springer-Verlag, New York, Berlin, 1994.
11. P.A. Raviart and J.M. Thomas. A mixed finite element method for second order elliptic problems. In I. Galligani and E. Magenes, editors, *Mathematical Aspects of Finite Element Methods,I*. Springer-Verlag, Berlin, 1977.
12. H. G. Roos, M. Stynes, and L. Tobiska. *Numerical methods for singularly perturbed differential equations*. Springer-Verlag, Berlin Heidelberg, 1996.
13. R.S. Varga. *Matrix Iterative Analysis*. Englewood Cliffs, New Jersey, 1962.

On the Choice of Mesh for a Singularly Perturbed Problem with a Corner Singularity

Sebastian Franz, R. Bruce Kellogg, and Martin Stynes

Abstract A singularly perturbed elliptic problem is considered on the unit square. Its boundary data has a jump discontinuity at one corner of the square, so the solution of the problem exhibits a singularity there. To solve the problem numerically, the Galerkin finite element method is tested on various tensor-product meshes. It is demonstrated that the Shishkin mesh does not yield satisfactory results, but meshes with a sufficient degree of mesh grading will yield convergence in certain norms, uniformly in the singular perturbation parameter.

1 Introduction

Consider the singularly perturbed boundary value problem

$$-\varepsilon \Delta u - p u_x + q u = f \text{ in } Q := (0,1)^2, \tag{1a}$$

$$u(x,0) = g_s(x),\ u(x,1) = g_n(x) \text{ for } 0 < x < 1, \tag{1b}$$

$$u(0,y) = g_w(y),\ u(1,y) = g_e(y) \text{ for } 0 < y < 1. \tag{1c}$$

Here the coefficients p and q are constants with $p > 0$ and $q > 0$, while the parameter ε lies in $(0,1]$. The functions f, g_w, g_e, g_s, g_n are assumed to satisfy $f \in C^{2\ell,\alpha}(Q)$, $g_w, g_e, g_s, g_n \in C^{2\ell,\alpha}([0,1])$ for some non-negative integer ℓ and $\alpha \in (0,1)$.

S. Franz
Department of Mathematics and Statistics, University of Limerick, Limerick, Ireland
e-mail: sebastian.franz@ul.ie

R.B. Kellogg
Department of Mathematics, University of South Carolina, Columbia, SC 29208, USA
e-mail: rbmjk@windstream.net

M. Stynes (✉)
Department of Mathematics, National University of Ireland, Cork, Ireland
e-mail: m.stynes@ucc.ie

C. Clavero et al. (eds.), *BAIL 2010 – Boundary and Interior Layers, Computational and Asymptotic Methods*, Lecture Notes in Computational Science and Engineering 81,
DOI 10.1007/978-3-642-19665-2_13,

This problem was examined in [3, 4] while assuming an arbitrary but known degree of compatibility between the boundary data and the solution at the four corners of Q. Pointwise bounds on the solution u and its derivatives were derived in these papers. These bounds showed how the singularities induced by the degree of incompatibility of the data at the corners of Q interacted with the boundary layers in u that are caused by the convection-dominated nature of (1). These are characteristic layers along the sides $y = 0$ and $y = 1$ of Q and an exponential outflow layer along the side $x = 0$. It is noteworthy that the corner singularities at $(1, 0)$ and $(1, 1)$ induce large derivatives in the solution that have only a mild decay away from $x = 1$. In contrast, the corner singularities at $(0, 0)$ and $(0, 1)$ induce large derivatives in the solution that decay rapidly away from $x = 0$. These facts are shown in the derivative bounds of [3, 4]. (Note that in [3, 4] the convective direction is the reverse of that of the present paper.)

Bounds such as these are useful in the analysis of numerical methods for (1). In [2] they were used in the particular case where the boundary data is continuous at each corner of Q but no higher degree of compatibility was assumed; a Galerkin finite element method using bilinears on a tensor product Shishkin mesh was analysed and shown to converge, uniformly in the parameter ε, in the energy norm associated with this problem. Although the Shishkin mesh was designed only for the boundary layers described above, [2] shows that it is also able to handle the mild singularity associated with the corners of the domain (the solution of this problem lies in $H^2(\Omega)$).

A natural question now arises: if one reduces the compatibility still further by allowing the boundary data to have a jump discontinuity at one corner, will the Shishkin mesh still be adequate? That is, for the same Galerkin method, will one still obtain uniform convergence in some reasonable norm? In the present paper we shall investigate and answer this question.

2 The Test Problem and Its Numerical Computation

We construct a test problem of the form (1). The boundary data of this problem will have a discontinuity at the inflow corner $(1, 0)$ and be continuous at the other three corners.

For simplicity take $q \equiv 0$. To begin the construction, consider the half-plane problem

$$Lv := -\varepsilon \Delta v - p v_x = 0 \text{ for } x < 1, \qquad v(1, y) = g(y) \text{ for } y \in (-\infty, \infty).$$

Its solution v is given (see [3, Sect. 3.1]) by the formula

$$v(x, y) = \frac{1 - x}{2\pi\varepsilon} e^{p(1-x)/(2\varepsilon)} \int_{-\infty}^{\infty} g(t) \frac{1}{r} K_1(pr/(2\varepsilon))\, dt, \tag{2}$$

where $r = \sqrt{(1-x)^2 + (y-t)^2}$ and K_1 is a modified Bessel function of the second kind. Here the convective direction is into the half-plane and the function v has no boundary layer. Let us take the case: $p = 1$ and $g(y) = 1$ for $y > 0$, $g(y) = 0$ for $y < 0$. Then

$$v(x, y) = \frac{1-x}{2\pi\varepsilon}\, e^{(1-x)/(2\varepsilon)} \int_0^\infty \frac{1}{r} K_1(r/(2\varepsilon))\, dt. \tag{3}$$

This function has an interior layer along the line $y = 0$; see [3,4].

Now set $w(x, y) = v(x, y) - v(x, -y)$. Then $Lw = 0$ in the quarter-plane $x < 1$, $y > 0$ and $w(x, 0) = 0$ for $x < 1$, $w(1, y) = 1$ for $y > 0$. For the test problem of this paper we take $u = w\big|_Q$; see Fig. 1. It is easily seen that $u \in L_\infty(\Omega)$. This function has a characteristic boundary layer along the side $y = 0$ of Q but no other layers; the absence of an outflow layer at $x = 0$ is unimportant since here we are concerned only with the effect of the corner singularity at $(1, 0)$. This characteristic layer will require some form of mesh refinement along $y = 0$. Furthermore, the singularity at $(1, 0)$ may require mesh refinement along the side $x = 1$.

A weak formulation of (1) is $\varepsilon(\nabla u, \nabla w) - (u_x, w) = 0$ for all $w \in H_0^1(\Omega)$. To solve this numerically, a standard Galerkin finite element method will be used; see (4) below.

The mesh on the unit square is yet to be chosen. We confine our attention to tensor product meshes with possible refinement along the two sides $y = 0$ and $x = 1$.

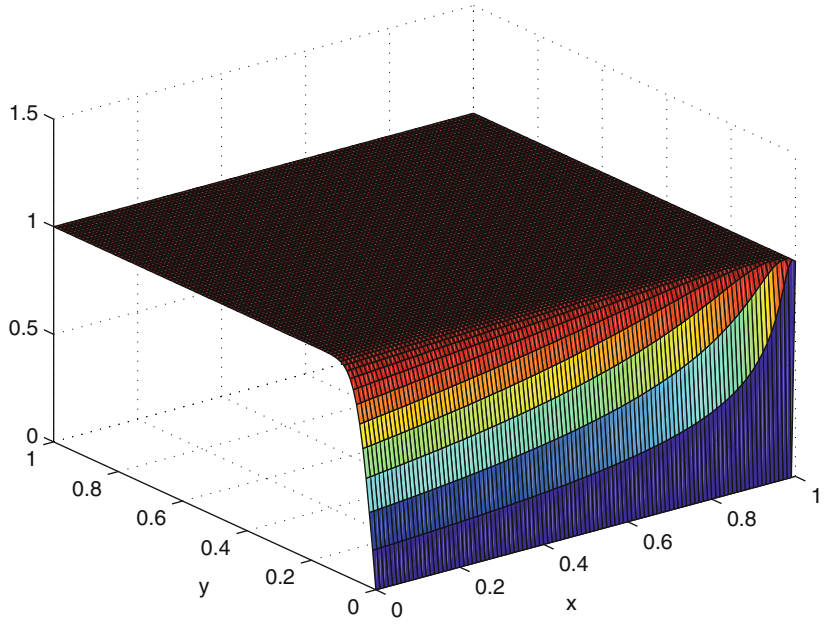

Fig. 1 Plot of test problem $u(x, y)$

A standard Shishkin mesh would be refined only along $y = 0$. We shall examine further geometric mesh refinement near $y = 0$ and $x = 1$, while maintaining the tensor product structure of the mesh. The precise definition of the mesh is given in (6).

On this mesh, our Galerkin method uses the space V^N of continuous, piecewise bilinears that vanish at boundary mesh points. The approximate solution u^N is defined to be the continuous piecewise bilinear function, with values at the boundary mesh points given by the values of u, and with values at the interior mesh points given by the solution to the linear system

$$\varepsilon(\nabla u^N, \nabla w) - (u_x^N, w) = 0 \quad \forall w \in V^N. \tag{4}$$

In (4), the parentheses are inner products in $L^2(Q)$. The value of u^N at the point $(1, 0)$ is, somewhat arbitrarily, taken to be 1.

2.1 Computational Aspects

Matlab 7.5.0 is used in our numerical experiments. The exact solution $u(x, y) = v(x, y) - v(x, -y)$ is obtained by setting $\xi = (1 - x)/(2\varepsilon)$, $\eta = y/(2\varepsilon)$ and $\tau = t/(2\varepsilon)$ to reformulate (3) as

$$\begin{aligned} v(x, y) = \hat{v}(\xi, \eta) &= \frac{\xi}{\pi} e^{\xi} \int_0^{\infty} \frac{1}{\sqrt{\xi^2 + (\eta - \tau)^2}} K_1\big(\sqrt{\xi^2 + (\eta - \tau)^2}\big)\, d\tau \\ &= I_1 + I_2, \end{aligned}$$

where

$$\begin{aligned} I_1 &= \frac{\xi}{\pi} e^{\xi} \int_{\eta}^{\infty} \frac{1}{\sqrt{\xi^2 + (\eta - \tau)^2}} K_1\big(\sqrt{\xi^2 + (\eta - \tau)^2}\big)\, d\tau \\ &= \frac{\xi}{\pi} e^{\xi} \int_0^{\infty} \frac{1}{\sqrt{\xi^2 + s^2}} K_1\big(\sqrt{\xi^2 + s^2}\big)\, ds \\ &= v(\xi, 0), \\ I_2 &= \frac{\xi}{\pi} e^{\xi} \int_0^{\eta} \frac{1}{\sqrt{\xi^2 + (\eta - \tau)^2}} K_1\big(\sqrt{\xi^2 + (\eta - \tau)^2}\big)\, d\tau \\ &= \frac{\xi}{\pi} e^{\xi} \int_0^{\eta} \frac{1}{\sqrt{\xi^2 + s^2}} K_1\big(\sqrt{\xi^2 + s^2}\big)\, ds. \end{aligned}$$

The changes of variable $s = \tau - \eta$ and $s = \eta - \tau$ were used in I_1 and I_2 respectively.

It follows that $v(x, -y) = \hat{v}(\xi, -\eta) = v(\xi, 0) - I_2$, on making the change of variable $s \mapsto -s$ in I_2. Thus, setting $\tilde{r}(s) = \sqrt{\xi^2 + s^2}$, we have

$$u(x,y) = v(x,y) - v(x,-y) = \frac{2\xi}{\pi} e^{\xi} \int_0^{\eta} \frac{1}{\tilde{r}(s)} K_1(\tilde{r}(s))\, ds$$
$$= \frac{2}{\pi} \int_0^{\eta} \exp\left(-\frac{s^2}{\xi + \tilde{r}(s)}\right) \frac{\xi}{\tilde{r}(s)} \left[e^{\tilde{r}(s)} K_1(\tilde{r}(s))\right] ds. \tag{5}$$

Note that the improper integral of (3) has now been replaced by an integral over a bounded interval; the above transformations have the effect of reducing roundoff error in the calculation. The term in square brackets is evaluated using the Matlab function `besselk(1,z,1)` with $z = \tilde{r}$. The integral is then computed using the built-in routine `quadgk`, an adaptive Gauss-Kronrod quadrature.

To evaluate energy norm errors, we shall need the first-order derivatives of u. For these we differentiate (5) directly, obtaining

$$u_y(x,y) = \frac{\xi}{\pi\varepsilon\tilde{r}(\eta)} e^{-\frac{\eta^2}{\xi+\tilde{r}(\eta)}} \left[e^{\tilde{r}(\eta)} K_1(\tilde{r}(\eta))\right],$$
$$u_x(x,y) =$$
$$-\frac{1}{\pi\varepsilon} \int_0^{\eta} e^{-\frac{s^2}{\xi+\tilde{r}(s)}} \left\{ \left[\frac{1+\xi}{\tilde{r}(s)} - \frac{2\xi^2}{\tilde{r}(s)^3}\right] \left[e^{\tilde{r}} K_1(\tilde{r}(s))\right] - \frac{\xi^2}{\tilde{r}(s)^2} \left[e^{\tilde{r}} K_0(\tilde{r}(s))\right] \right\} ds.$$

3 Numerical Results

Following the discussion in Sect. 2, we define the nodes of our tensor product $N \times N$ mesh as follows:

$$\begin{aligned} x_i &= 1 - [1 - (i/N)]^{1+\delta_x}, \quad i = 0, \ldots, N, \\ y_j &= \lambda_y (4j/N)^{1+\delta_y}, \quad j = 0, \ldots, N/4, \\ y_j &= \lambda_y + (1-\lambda_y)\frac{4j/N - 1}{3}, \quad j = N/4, \ldots, N, \end{aligned} \tag{6}$$

where we assumed that

$$\lambda_y := \min\{1/4, 2\sqrt{\varepsilon} \ln N\} \le \frac{1}{4}.$$

Here the positive integer N is the number of mesh intervals in each coordinate direction. The two parameters δ_x and δ_y are non-negative and user-chosen. For $\delta_x = 0$ we have an equidistant mesh in the x-direction while $\delta_x > 0$ gives a mesh that is graded approaching $x = 1$. The choice $\delta_y = 0$ produces a Shishkin mesh (i.e., piecewise equidistant) in the y-direction while $\delta_y > 0$ would provide additional grading in the layer region near $y = 0$. Away from the layer, i.e., for $y > \lambda_y$, we always have an equidistant mesh in the y-direction. See Fig. 2.

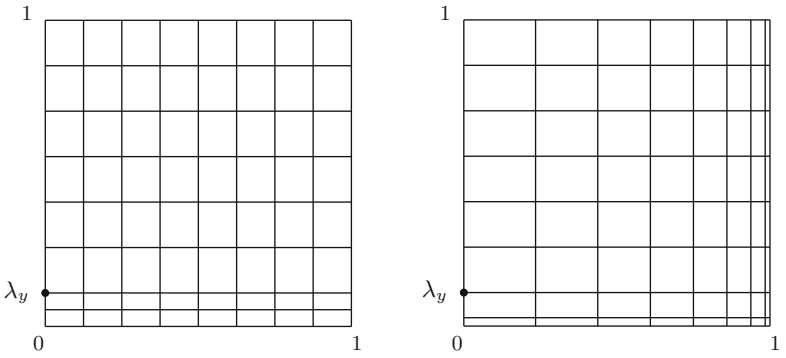

Fig. 2 8×8 meshes with (**a**) $\delta_x = \delta_y = 0$ (*Shishkin mesh*) (**b**) $\delta_x = \delta_y = 1$

We refer to the members of this family as *geometric meshes*. For other work on the use of mesh refinement in a problem with both boundary layers and corner singularities, we mention [1], which deals with a reaction-diffusion problem in an L-shaped domain, and with zero boundary conditions. The corner singularity is not as severe as in our problem, but the issue of approximating a function which has both types of singular behaviour is the same.

Our mesh in the y direction is an S-type mesh; these meshes were introduced (and analysed for problems without singularities) by Roos and Linß in [5].

When the Galerkin method (4) is applied on this mesh, the integrals are evaluated exactly. To measure the errors in the computed solution, we use the exact solution u as described in (5). The discontinuity in the boundary condition implies that $u \notin H^1(Q)$, the usual Sobolev space. Thus, setting $m(x, y) = \min\{\varepsilon, \sqrt{(x-1)^2 + y^2}\}$, we weaken the standard energy norm to

$$\|v\|_{1,m} = \left[\int_Q \left(m|\nabla v|^2 + v^2 \right) \right]^{1/2}. \tag{7}$$

In [3,4] it is shown that the solution u satisfies $|\nabla u(x, y)| \leq C\left[(1-x)^2 + y^2\right]^{-1/2}$. Therefore $\|u\|_{1,m} < \infty$.

When computing errors in the L_2 norm and the norm $\|\cdot\|_{1,m}$, we approximate the error integrals by Gaussian quadrature with 5×5 point evaluations in each mesh cell. Computations show that Gaussian quadrature with fewer points gives inaccurate results.

In Tables 1–4 we fix $\varepsilon = 10^{-6}$ (a small value that ensures the problem is singularly perturbed) and results are presented for various values of δ_x and δ_y. The rates of convergence are computed from the hypothesis $error = N^{-rate}$ in columns 3 and 5, while the rates of column 6 are computed assuming that $error = (N^{-1} \ln N)^{rate}$.

Table 1 is for the case $\delta_x = \delta_y = 0$, i.e., the standard Shishkin mesh. It is clear from the table that the L_2 convergence rate is less than 2, and rates for the energy norm convergence rates in column 5 and 6 are both less than 1.

Table 1 Geometric mesh with $\delta_x = \delta_y = 0$ (i.e., Shishkin mesh)

N	$\|u - u^N\|_{0,\Omega}$		$\|u - u^N\|_{1,m}$		
16	2.692e-02	2.11	3.161e-02	1.10	1.62
32	6.229e-03	1.96	1.475e-02	0.47	0.63
64	1.604e-03	1.73	1.068e-02	0.38	0.49
128	4.850e-04	1.38	8.204e-03	0.38	0.47
256	1.859e-04		6.298e-03		

Table 2 Geometric mesh with $\delta_x = 1$ and $\delta_y = \delta_x/2 = 1/2$

N	$\|u - u^N\|_{0,\Omega}$		$\|u - u^N\|_{1,m}$		
16	2.323e-02	2.59	2.639e-02	1.46	2.16
32	3.852e-03	2.57	9.570e-03	0.67	0.90
64	6.496e-04	2.43	6.032e-03	0.58	0.75
128	1.202e-04	2.06	4.022e-03	0.58	0.71
256	2.874e-05		2.697e-03		

Table 3 Geometric mesh with $\delta_x = 3/2$ and $\delta_y = 5/4$

N	$\|u - u^N\|_{0,\Omega}$		$\|u - u^N\|_{1,m}$		
16	2.592e-02	3.13	2.823e-02	1.92	2.84
32	2.963e-03	2.96	7.441e-03	0.84	1.14
64	3.808e-04	2.69	4.155e-03	0.78	1.00
128	5.889e-05	1.92	2.421e-03	0.81	1.01
256	1.559e-05		1.378e-03		

Table 4 Geometric mesh with $\delta_x = \delta_y = 2$

N	$\|u - u^N\|_{0,\Omega}$		$\|u - u^N\|_{1,m}$		
16	2.168e-02	3.53	2.463e-02	1.85	2.73
32	1.881e-03	3.02	6.813e-03	0.90	1.22
64	2.317e-04	1.95	3.648e-03	0.87	1.12
128	5.993e-05	1.88	1.995e-03	0.92	1.14
256	1.632e-05		1.055e-03		

An analysis that we shall publish elsewhere shows that for $\delta_x \geq 1$ and $\delta_y \geq \delta_x/2$, the L_2 error between u and its piecewise bilinear nodal interpolant is bounded by $CN^{-2}(\ln N)^{5/2}$, where the constant C is independent of ε and N. Thus we take $\delta_x = 1$ and $\delta_y = 1/2$ in Table 2, whose results are clearly superior to those of Table 1. In particular we now have $O(N^{-2})$ convergence in the L_2-norm; but the energy norm rates still fail to achieve first-order convergence.

Thus we try a further refinement of the mesh. Table 3 shows the results for $\delta_x = 3/2$ and $\delta_y = 5/4$. Here, in addition to $O(N^{-2})$ convergence in L_2, we have $O(N^{-1}\ln N)$ convergence in the energy norm.

Further increases of δ_x and δ_y give limited improvements of these results; see Table 4 for $\delta_x = \delta_y = 2$.

3.1 Outflow Corner Discontinuity

The situation is somewhat different if the boundary data discontinuity is moved from $(1, 0)$ to the outflow corner $(0, 0)$. One can again start from [3, Sect. 3.1] and,

Table 5 Outflow discontinuity, geometric mesh with $\delta_y = 0.5$

N	$\|u - u^N\|_{0,\Omega}$		$\|u - u^N\|_{1,m}$		
16	3.517e-03	1.81	1.401e-01	0.66	0.98
32	1.002e-03	1.91	8.861e-02	0.72	0.97
64	2.671e-04	1.97	5.391e-02	0.74	0.95
128	6.810e-05	2.04	3.227e-02	0.73	0.91
256	1.659e-05		1.944e-02		

similarly to Sect. 2, construct a function that we still call u which satisfies $Lu = 0$ on Q with a jump discontinuity in its boundary condition at the corner $(0, 0)$. This function has an outflow boundary layer along the side $x = 0$ and no other layer. Nevertheless we shall consider mesh refinement near $y = 0$ since the solutions of almost all boundary value problems associated with the operator L will have characteristic boundary layers here.

To solve the problem numerically we examine a mesh that is refined geometrically near the side $y = 0$ of Q exactly as in (6), and has a standard Shishkin mesh structure in the x variable: piecewise equidistant, and fine near $x = 0$ with mesh transition point $\lambda_x = \min\{1/2, 2\varepsilon \ln N\}$. In the case $\delta_y = 0$ one gets a Shishkin mesh that is fine near $x = 0$ and $y = 0$.

When measuring the error in our numerical solutions, the energy norm (7) is of course modified by redefining $m(x, y) = \min\{\varepsilon, \sqrt{x^2 + y^2}\}$. When our problem is solved numerically on the above Shishkin mesh, the results obtained are broadly similar to those of Table 1. Thus some mesh refinement is needed to obtain a more satisfactory rate of convergence in the energy norm.

Table 5 displays numerical results for the geometric mesh with $\delta_y = 0.5$; it shows that we have nearly $O(N^{-1} \ln N)$ convergence in the energy norm. This is in contrast to Tables 1–3 for the inflow corner discontinuity where much more mesh refinement was needed to attain this order of convergence.

Acknowledgements Research supported by Science Foundation Ireland under the Research Frontiers Programme 2008; Grant 08/RFP/MTH1536.

References

1. Vladimir B. Andreev and Natalia Kopteva. Pointwise approximation of corner singularities for a singularly perturbed reaction-diffusion equation in an L-shaped domain. *Math. Comp.*, 77(264):2125–2139, 2008.
2. Sebastian Franz, R. Bruce Kellogg, and Martin Stynes. Galerkin and streamline diffusion finite element methods on a Shishkin mesh for a convection-diffusion problem with corner singularities, accepted for publication in Math. Comp.
3. R. Bruce Kellogg and Martin Stynes. Corner singularities and boundary layers in a simple convection-diffusion problem. *J. Differential Equations*, 213(1):81–120, 2005.
4. R. Bruce Kellogg and Martin Stynes. Sharpened bounds for corner singularities and boundary layers in a simple convection-diffusion problem. *Appl. Math. Lett.*, 20(5):539–544, 2007.
5. H.-G. Roos and T. Linß. Sufficient conditions for uniform convergence on layer-adapted grids. *Computing*, 63(1):27–45, 1999.

Local Projection Stabilisation on Layer-Adapted Meshes for Convection-Diffusion Problems with Characteristic Layers (Part I and II)

Sebastian Franz and Gunar Matthies

Abstract For a singularly perturbed convection-diffusion problem with exponential and characteristic boundary layers on the unit square a discretisation based on layer-adapted meshes is considered. The standard Galerkin method and the local projection scheme are analysed for a general class of higher order finite elements based on local polynomial spaces lying between $\mathcal{P}_p$ and $\mathcal{Q}_p$. We will present two different interpolation operators for these spaces. The first one is based on values at vertices, weighted edge integrals and weighted cell integrals while the second one is based on point values only. The influence of the point distribution on the errors will be studied numerically.

We show convergence of order p in the ε-weighted energy norm for both the Galerkin method and the local projection scheme. Furthermore, the local projection methods provides a supercloseness result of order p in local projection norm.

1 Introduction

Let the singularly perturbed convection-diffusion problem be given by

$$-\varepsilon\Delta u - bu_x + cu = f \qquad \text{in } \Omega = (0,1)^2, \tag{1a}$$

$$u = 0 \qquad \text{on } \Gamma = \partial\Omega \tag{1b}$$

under the assumption that $b \in W^1_\infty(\Omega), c \in L_\infty(\Omega), b \geq \beta > 0$ with some constant β, and a small perturbation parameter $0 < \varepsilon \ll 1$.

S. Franz (✉)
Department of Mathematics and Statistics, University of Limerick, Limerick, Ireland
e-mail: sebastian.franz@ul.ie

G. Matthies
Universität Kassel, Fachbereich 10, Institut für Mathematik, Heinrich-Plett-Straße 40, 34132 Kassel, Germany
e-mail: matthies@mathematik.uni-kassel.de

C. Clavero et al. (eds.), *BAIL 2010 – Boundary and Interior Layers, Computational and Asymptotic Methods*, Lecture Notes in Computational Science and Engineering 81,
DOI 10.1007/978-3-642-19665-2_14,

This combination gives rise to an exponential layer of width $\mathcal{O}(\varepsilon)$ near the outflow boundary at $x = 0$ and to two parabolic layers of width $\mathcal{O}\left(\sqrt{\varepsilon}\right)$ near the characteristic boundaries at $y = 0$ and $y = 1$.

Problem (1) possesses a unique solution in $H_0^1(\Omega) \cap H^2(\Omega)$ if

$$c + b_x/2 \geq \gamma > 0 \tag{2}$$

holds. Assumption (2) can always be guaranteed by a simple transformation $\tilde{u}(x, y) = u(x, y)\mathrm{e}^{\varkappa x}$ with a suitably chosen constant $\varkappa$.

Due to the layers standard discretisations will not give accurate approximations on quasi-uniform meshes except the mesh width is of the same order as ε. Thus layer-adapted meshes based on *a priori* knowledge of the solution behaviour have been constructed, see [2, 18, 20]. We will use so called S-type meshes [19] combining the transition point of a standard Shishkin mesh and mesh generating functions inside the fine part.

Since the standard Galerkin methods lacks stability even on layer-adapted meshes, see [15, 21], a stabilisation term will be added to the standard discretisation. We will consider the one-level approach of the local projection stabilisation (LPSFEM), [3–5, 17]. However, we will not use enriched $\mathcal{Q}_r$-elements but consider a general class of higher order elements. To this end, let $p \geq 2$ be an arbitrary but fixed integer to indicate the polynomial degree of our ansatz functions.

This paper contains a condensed analysis of the LPSFEM applied to (1) on S-type meshes. For a full analysis see [11, 12].

Notation. In this paper, C denotes a generic constant which is always independent of the diffusion coefficient ε and the mesh parameter N. The usual Sobolev spaces $W_r^m(D)$ and $L_r(D)$ on any measurable two-dimensional subset $D \subset \Omega$ are used. We write $H^m(D)$ instead of $W_2^m(D)$ in the case $r = 2$. The $L_2(D)$-norm is denoted by $\|\cdot\|_{0,D}$ while the $(\cdot,\cdot)_D$ is the $L_2(D)$-inner product. The subscript D will always be dropped if $D = \Omega$.

By $\mathcal{P}_r(D)$ we denote the space of all polynomials with total degree less than or equal to r while $\mathcal{Q}_r(D)$ is the space of all polynomials with degree less than or equal to r in each variable separately.

2 Solution Decomposition and Layer-Adapted Meshes

We suppose there exists the following decomposition of the solution u of (1).

Assumption 1. The solution u of (1) can be decomposed as

$$u = v + w_1 + w_2 + w_{12}$$

where we have for all $x, y \in [0, 1]$ and $0 \leq i + j \leq p + 1$ the pointwise estimates

$$\left|\frac{\partial^{i+j} v}{\partial x^i \partial y^j}(x,y)\right| \le C, \quad \left|\frac{\partial^{i+j} w_1}{\partial x^i \partial y^j}(x,y)\right| \le C\varepsilon^{-i} \mathrm{e}^{-\beta x/\varepsilon},$$

$$\left|\frac{\partial^{i+j} w_2}{\partial x^i \partial y^j}(x,y)\right| \le C\varepsilon^{-j/2} \left(\mathrm{e}^{-y/\sqrt{\varepsilon}} + \mathrm{e}^{-(1-y)/\sqrt{\varepsilon}}\right),$$

$$\left|\frac{\partial^{i+j} w_{12}}{\partial x^i \partial y^j}(x,y)\right| \le C\varepsilon^{-(i+j/2)} \mathrm{e}^{-\beta x/\varepsilon} \left(\mathrm{e}^{-y/\sqrt{\varepsilon}} + \mathrm{e}^{-(1-y)/\sqrt{\varepsilon}}\right),$$

where w_1 covers the exponential boundary layer, w_2 the parabolic boundary layers, w_{12} the corner layers, and v is the regular part.

Remark 2. Kellogg and Stynes [14] proved the validity of Assumption 1 in the case of constant functions b, c provided f is smooth enough and fulfils certain compatibility conditions.

When discretising (1), we use in both x- and y-direction *S-type meshes* with N mesh intervals each. For this purpose let the mesh transition parameters be

$$\lambda_x := \frac{\sigma\varepsilon}{\beta} \ln N \le \frac{1}{2} \quad \text{and} \quad \lambda_y := \sigma\sqrt{\varepsilon} \ln N \le \frac{1}{4}$$

with some user-chosen positive parameter $\sigma \ge p+1$, where we assume for the mere sake of simplicity

$$\varepsilon \le \min\left\{\frac{\beta}{2\sigma}(\ln N)^{-1}, \frac{1}{16\sigma^2}(\ln N)^{-2}\right\}.$$

In the following, we assume that N is a multiple of 4. The domain Ω will be dissected by a tensor product mesh according to

$$x_i := \begin{cases} \frac{\sigma\varepsilon}{\beta}\phi\left(\frac{i}{N}\right), & i = 0, \ldots, N/2, \\ 1 - 2(1-\lambda_x)(1-\frac{i}{N}), & i = N/2, \ldots, N, \end{cases}$$

and

$$y_j := \begin{cases} \sigma\sqrt{\varepsilon}\phi\left(\frac{2j}{N}\right), & j = 0, \ldots, N/4, \\ (1-2\lambda_y)(\frac{2j}{N}-1) + \frac{1}{2}, & j = N/4, \ldots, 3N/4, \\ 1 - \sigma\sqrt{\varepsilon}\phi\left(2 - \frac{2j}{N}\right), & j = 3N/4, \ldots, N, \end{cases}$$

where ϕ is a monotonically increasing mesh-generating function satisfying $\phi(0) = 0$ and $\phi(1/2) = \ln N$. Given an arbitrary function ϕ fulfilling these conditions, an S-type mesh is defined. The final mesh is constructed by drawing lines parallel to the coordinate axes through these mesh points and is denoted by T^N. Figure 1 shows two examples of such meshes. The domain Ω is divided into the subdomains

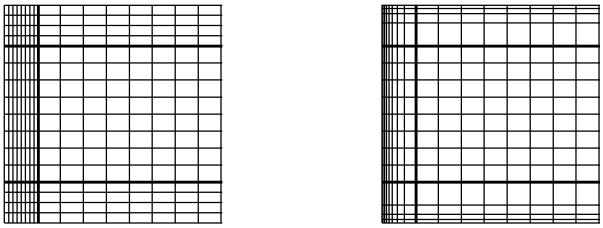

Fig. 1 Two S-type meshes: Shishkin mesh (*left*), Bakhvalov-Shishkin mesh (*right*)

with $\Omega_{12} := [0, \lambda_x] \times [\lambda_y, 1-\lambda_y]$ covering the exponential layer, $\Omega_{21} := [\lambda_x, 1] \times \big([0, \lambda_y] \cup [1-\lambda_y, 1]\big)$ the parabolic layers, $\Omega_{22} := [0, \lambda_x] \times \big([0, \lambda_y] \cup [1-\lambda_y, 1]\big)$ the corner layers, and $\Omega_{11} := [\lambda_x, 1] \times [\lambda_y, 1-\lambda_y]$ the remaining non-layer region.

Related to the mesh-generating function ϕ, we define by $\psi = \mathrm{e}^{-\phi}$ the mesh-characterising function ψ whose derivative yields information on the approximation quality of the mesh.

Two representatives of those meshes are the original Shishkin mesh [18] with $\phi(t) = 2t \ln N$ and $\max |\psi'| = 2 \ln N$, and the Bakhvalov-Shishkin mesh [16] with $\phi(t) = -\ln(1 - 2t(1 - N^{-1}))$ and $\max |\psi'| = 2$. Both meshes are shown in Fig. 1.

We assume for simplicity of the presentation that the maximal mesh sizes inside the layer regions

$$h := \max_{i=1,\dots,N/2} x_i - x_{i-1} \quad \text{and} \quad k := \max_{j=1,\dots,N/4} y_j - y_{j-1}$$

are both smaller than $CN^{-1} \max |\psi'|$.

3 General Finite Element Spaces and Interpolation

Let us come to the definition of the general local finite element space. It is given by

$$\mathcal{Q}_p^{\clubsuit}(\hat{\tau}) = \operatorname{span}\Big\{ \{1, \xi\} \times \{1, \eta, \dots, \eta^p\} \cup \{1, \xi, \dots, \xi^p\} \times \{1, \eta\} \cup \xi^2 \eta^2 \widetilde{\mathcal{Q}}(\hat{\tau}) \Big\}$$

with the space

$$\widetilde{Q}(\hat{\tau}) := \operatorname{span}\big\{ \xi^i \eta^j \ : \ i = 0, \dots, p-2, \ j = 0, \dots, k_i \big\}$$

satisfying $\mathcal{P}_{p-4}(\hat{\tau}) \subset \widetilde{\mathcal{Q}}(\hat{\tau}) \subset \mathcal{Q}_{p-2}(\hat{\tau})$ and $k_i \geq k_{i+1}$ for $i = 0, \dots, p-3$. Figure 2 shows a graphical representation of two example of $\mathcal{Q}_p^{\clubsuit}(\hat{\tau})$ in the case $p = 9$. A square at position (i, j) represents a basis function $\xi^i \eta^j$ of $\mathcal{Q}_p^{\clubsuit}(\hat{\tau})$. The

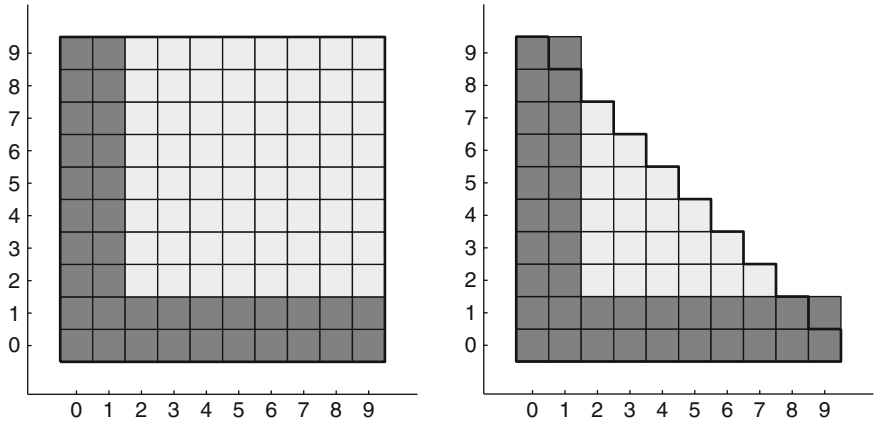

Fig. 2 Full space $\mathcal{Q}_p(\hat{\tau})$ (*left*), Serendipity space $\mathcal{Q}_p^{\oplus}(\hat{\tau})$ (*right*)

darker squares correspond to those functions present in all spaces we consider, while the lighter ones represent $\xi^2\eta^2\widetilde{\mathcal{Q}}(\hat{\tau})$. The left picture of Fig. 2 shows the standard $\mathcal{Q}_p$-space governed by taking $\widetilde{\mathcal{Q}}(\hat{\tau}) = \mathcal{Q}_{p-2}(\hat{\tau})$, while the right picture presents the serendipity space $\mathcal{Q}_p^{\oplus}$ defined by $\widetilde{\mathcal{Q}}(\hat{\tau}) = \mathcal{P}_{p-4}(\hat{\tau})$ for $p \geq 4$ and $\widetilde{\mathcal{Q}}(\hat{\tau}) = \emptyset$ for $p = 2, 3$.

We define our global finite element space as

$$V^N := \left\{ v \in H_0^1(\Omega) : v|_\tau \in \mathcal{Q}_p^{\clubsuit}(\tau) \ \forall \tau \in T^N \right\}$$

where $\mathcal{Q}_p^{\clubsuit}(\tau)$ is obtained from $\mathcal{Q}_p^{\clubsuit}(\hat{\tau})$ in the usual way by using the reference mapping $F_\tau : \hat{\tau} \to \tau$.

We now define two different interpolation operators. First, we consider an interpolation operator based on point evaluation at the vertices, line integrals along the edges and integrals over the cell interior.

Let $\hat{a}_i$ and $\hat{e}_i$, $i = 1, \ldots, 4$, denote the vertices and edges of the reference element $\hat{\tau}$, respectively. We define the vertex-edge-cell interpolation operator $\mathcal{I} : C(\hat{\tau}) \to \mathcal{Q}_p^{\clubsuit}(\hat{\tau})$ by

$$\mathcal{I}\hat{v}(\hat{a}_i) = \hat{v}(\hat{a}_i), \quad i = 1, \ldots, 4, \tag{3a}$$

$$\int_{\hat{e}_i} (\mathcal{I}\hat{v})\hat{q} = \int_{\hat{e}_i} \hat{v}\hat{q}, \quad i = 1, \ldots, 4, \quad \hat{q} \in \mathcal{P}_{p-2}(\hat{e}_i), \tag{3b}$$

$$\iint_{\hat{\tau}} (\mathcal{I}\hat{v})\hat{q} = \iint_{\hat{\tau}} \hat{v}\hat{q}, \qquad \hat{q} \in \widetilde{\mathcal{Q}}(\hat{\tau}). \tag{3c}$$

It can be proved that this interpolation operator is uniquely defined.

The interpolation operator $\mathcal{I}$ on the reference element $\hat{\tau}$ induces the global interpolation operator $I^N : C(\overline{\Omega}) \to V^N$ by

$$(I^N v)|_\tau := F_\tau \circ \mathcal{I} \circ F_\tau^{-1}(v|_\tau) \quad \forall \tau \in T^N,\ v \in C(\overline{\Omega}), \tag{4}$$

with the bijective reference mapping $F_\tau : \hat{\tau} \to \tau$.

Theorem 3. *For the finite element space V^N and the vertex-edge-cell interpolation operator I^N defined by (3) and (4), there holds the L_∞-stability*

$$\left\| I^N w \right\|_{L_\infty(\tau)} \leq C \|w\|_{L_\infty(\tau)} \quad \forall w \in C(\tau),\ \forall \tau \subset \overline{\Omega},$$

and the anisotropic error estimates

$$\begin{aligned}
\left\| w - I^N w \right\|_{L_q(\tau_{ij})} &\leq C \sum_{r=0}^{s} \left\| h_i^{s-r} k_j^r \frac{\partial^s w}{\partial x^{s-r} \partial y^r} \right\|_{L_q(\tau_{ij})}, \\
\left\| (w - I^N w)_x \right\|_{L_q(\tau_{ij})} &\leq C \sum_{r=0}^{t} \left\| h_i^{t-r} k_j^r \frac{\partial^{t+1} w}{\partial x^{t-r+1} \partial y^r} \right\|_{L_q(\tau_{ij})}, \\
\left\| (w - I^N w)_y \right\|_{L_q(\tau_{ij})} &\leq C \sum_{r=0}^{t} \left\| h_i^{t-r} k_j^r \frac{\partial^{t+1} w}{\partial x^{t-r} \partial y^{r+1}} \right\|_{L_q(\tau_{ij})}
\end{aligned}$$

for $\tau_{ij} \subset \overline{\Omega}$ and $q \in [1, \infty]$, $2 \leq s \leq p+1$, $1 \leq t \leq p$.

Using the technique given in [1] this theorem can be proved. Details can be found in [11].

The second interpolation operator we are interested in, is a point-value oriented interpolation operator. We consider two increasing sequences of $p+1$ points $-1 = \xi_0 < \xi_1 < \cdots < \xi_{p-1} < \xi_p = +1$ and $-1 = \eta_0 < \eta_1 < \cdots < \eta_{p-1} < \eta_p = +1$. The point-value oriented interpolation operator $\mathcal{J} : C(\hat{\tau}) \to \mathcal{Q}_p^{\clubsuit}(\hat{\tau})$ is defined by values on the edges including the vertices

$$(\mathcal{J}\hat{v})(\xi_i, \pm 1) := \hat{v}(\xi_i, \pm 1), \qquad i = 0, \ldots, p, \tag{5a}$$

$$(\mathcal{J}\hat{v})(\pm 1, \eta_j) := \hat{v}(\pm 1, \eta_j), \qquad j = 1, \ldots, p-1, \tag{5b}$$

and values in the interior

$$(\mathcal{J}\hat{v})(\xi_{i+1}, \eta_{j+1}) := \hat{v}(\xi_{i+1}, \eta_{j+1}), \qquad i = 0, \ldots, p-2,\ j = 0, \ldots, k_i. \tag{5c}$$

The interpolation operator $\mathcal{J}$ is uniquely determined, see [11] for details. Similarly as before we can define a global interpolation operator $J^N : C(\overline{\Omega}) \to V^N$ using the bijective reference mapping F_τ. It can be shown that all results from Theorem 3 are also valid for J^N. For details we refer again to [11].

4 Numerical Method and Convergence

We derive in this section bounds on the interpolation error and prove convergence of the Galerkin method and the LPSFEM. Although we will give in this section only results for the interpolation operator I^N, the same results hold true for the operator J^N. With the usual Galerkin bilinear form

$$a_{Gal}(u,v) := \varepsilon(\nabla u, \nabla v) + (cu - bu_x, v), \qquad u, v \in H_0^1(\Omega),$$

associated with problem (1), the standard Galerkin formulation of (1) is given by:

Find $\tilde{u}^N \in V^N$ such that

$$a_{Gal}(\tilde{u}^N, v^N) = (f, v^N) \qquad \forall v^N \in V^N. \tag{6}$$

Since the standard Galerkin discretisation lacks stability even on S-type meshes [15, 21], the local projection method is applied for stabilisation. Let π_τ denote the L_2-projection into the finite dimensional function space $D(\tau) := \mathcal{P}_{p-2}(\tau)$. The fluctuation operator $\kappa_\tau : L_2(\tau) \to L_2(\tau)$ is defined by $\kappa_\tau v := v - \pi_\tau v$.

In order to get additional control on the derivative in streamline direction, we define the stabilisation term

$$s(u,v) := \sum_{\tau \in T^N} \delta_\tau \big(\kappa_\tau(bu_x), \kappa_\tau(bv_x)\big)_\tau$$

with the cell-dependent parameters $\delta_\tau \geq 0$, $\tau \in T^N$, which will be constant inside each subdomain of Ω, i.e., $\delta_\tau = \delta_{ij}$ for $\tau \subset \Omega_{ij}$. It was stated in [10] for different stabilisation methods that stabilisation is best if only applied in $\Omega_{11} \cup \Omega_{21}$. Therefore, we set $\delta_{12} = \delta_{22} = 0$ in the following.

The stabilised discrete problem reads:

Find $u^N \in V^N$ such that

$$a_{LPS}(u^N, v^N) := a_{Gal}(u^N, v^N) + s(u^N, v^N) = (f, v^N) \qquad \forall v^N \in V^N. \tag{7}$$

The subsequent analysis uses the ε-weighted energy- and the LPS-norm

$$|||v|||_\varepsilon := \left(\varepsilon \|\nabla v\|_0^2 + \gamma \|v\|_0^2\right)^{1/2} \quad \text{and} \quad |||v|||_{LPS} := \left(|||v|||_\varepsilon^2 + s(v,v)\right)^{1/2}.$$

Theorem 4 (Interpolation error). *Let the solution u of (1) fulfil Assumption 1. Then, the interpolation operator I^N provides the following pointwise interpolation error bounds*

$$\left\| I^N u - u \right\|_{L_\infty(\Omega_{11})} \leq C N^{-(p+1)},$$
$$\left\| I^N u - u \right\|_{L_\infty(\Omega \setminus \Omega_{11})} \leq C \left(N^{-1} \max |\psi'| \right)^{p+1}.$$

Moreover, the L_2- and energy norm bounds

$$\left\| I^N u - u \right\|_0 \leq C \left(N^{-1} \max |\psi'| \right)^{p+1} \text{ and } \left| \left| \left| I^N u - u \right| \right| \right|_\varepsilon \leq C \left(N^{-1} \max |\psi'| \right)^p$$

hold true.

The proof of Theorem 4 uses the decomposition of Assumption 1 and Theorem 3 to bound the different parts of u in the several subdomains of Ω. Note the appearance of $\max |\psi'|$ in the estimates that refers to the quality of the underlying mesh.

Theorem 5 (Convergence Galerkin FEM and LPSFEM). *Let the solution u of (1) satisfy Assumption 1 and let $\tilde{u}^N$ denote the Galerkin solution of (6). We set*

$$C_\psi := 1 + N^{-1/2} \ln^{1/2} N \max |\psi'|. \tag{8}$$

Then, we have

$$\left| \left| \left| u - \tilde{u}^N \right| \right| \right|_\varepsilon \leq C C_\psi \left(N^{-1} \max |\psi'| \right)^p.$$

Let the LPSFEM solutions of (7) be denoted by u^N and let the stabilisation parameters be chosen according to

$$\delta_{11} \leq C N^{-2} \left(\max |\psi'| \right)^{2p}, \tag{9a}$$
$$\delta_{21} \leq C \varepsilon^{-1/2} \ln^{-1} N \left(N^{-1} \max |\psi'| \right)^2, \tag{9b}$$
$$\delta_{12} = \delta_{22} = 0. \tag{9c}$$

Then, we have

$$\left| \left| \left| u - u^N \right| \right| \right|_\varepsilon \leq C C_\psi \left(N^{-1} \max |\psi'| \right)^p \tag{10}$$

and

$$\left| \left| \left| I^N u - u^N \right| \right| \right|_{LPS} \leq C C_\psi \left(N^{-1} \max |\psi'| \right)^p. \tag{11}$$

Proof. The first result (10) follows from the triangle inequality, (4) and (11).

In order to prove (11), we use coercivity and the weak Galerkin orthogonality of the stabilised method and obtain

$$\left| \left| \left| I^N u - u^N \right| \right| \right|^2_{LPS} \leq a_{Gal} \left(I^N u - u, \chi \right) + s \left(I^N u, \chi \right).$$

Now the decomposition of Assumption 1 and anisotropic error estimates of I^N and κ_τ can be applied in the various subdomains of Ω.

For a complete proof see [12].

Note that in order to prove convergence of the LPSFEM no additional orthogonality of the interpolation operator is required and that the last estimate is a supercloseness result.

Remark 6. The factor C_ψ defined in (8) is bounded by a constant for Shishkin and the Bakhvalov-Shishkin meshes.

Remark 7. The choice (9) gives us the largest upper bounds for the whole class of S-type meshes such that convergence of order p holds. In particular, for the standard Shishkin mesh we obtain

$$\delta_{11} \le CN^{-2}\big(\ln N\big)^{2p}, \quad \delta_{21} \le C\varepsilon^{-1/2}N^{-2}\ln N, \quad \delta_{12} = \delta_{22} = 0 \tag{12}$$

while we get

$$\delta_{11} \le CN^{-2}, \quad \delta_{21} \le C\varepsilon^{-1/2}\ln^{-1} NN^{-2}, \quad \delta_{12} = \delta_{22} = 0. \tag{13}$$

for the Bakhvalov-Shishkin mesh.

5 Numerical Results

We consider the following singularly perturbed convection-diffusion problem for our numerical study:

$$-\varepsilon\Delta u - (2-x)u_x + \frac{3}{2}u = f \quad \text{in } \Omega \quad \text{and} \quad u = 0 \quad \text{on } \partial\Omega,$$

where the right-hand side f is chosen such that

$$u(x,y) = \left(\cos\frac{\pi x}{2} - \frac{\mathrm{e}^{-x/\varepsilon} - \mathrm{e}^{-1/\varepsilon}}{1-\mathrm{e}^{-1/\varepsilon}}\right)\frac{\left(1-\mathrm{e}^{-y/\sqrt{\varepsilon}}\right)\left(1-\mathrm{e}^{-(1-y)/\sqrt{\varepsilon}}\right)}{1-\mathrm{e}^{-1/\sqrt{\varepsilon}}}$$

is the solution. Note that Assumption 1 is satisfied.

The presented numerical results were obtained by the finite element package MooNMD [13]. All occurring systems of linear equations were solved directly by using package UMFPACK [6–9].

As parameters we use $\varepsilon = 10^{-12}$, $p = 5$, $\sigma = 6$. All numerical quadratures are carried out using a 8×8-Gaussian quadrature rule. For the LPSFEM we set the stabilisation parameters according to (12) for the Shishkin mesh and to (13) for the Bakhvalov-Shishkin mesh, both with $C = 0.001$.

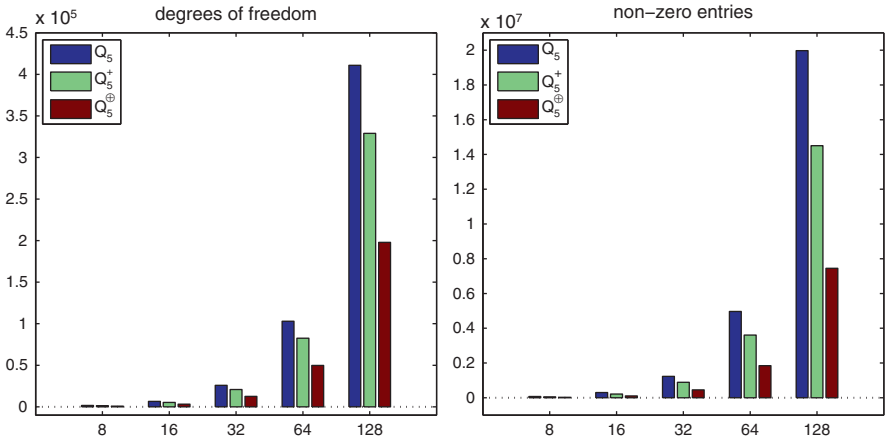

Fig. 3 Number of degrees of freedom (*left*), number of non-zero entries of stiffness matrix (*right*)

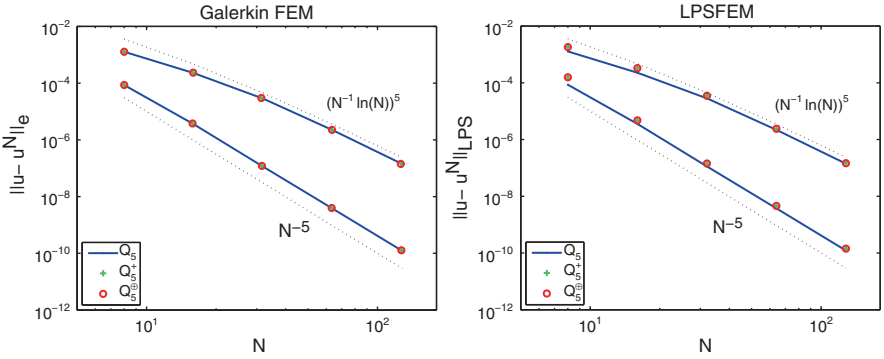

Fig. 4 Energy-norm errors for Galerkin FEM (*left*) and LPSFEM (*right*)

Figure 3 shows for three different choices of $\mathcal{Q}_p^{\clubsuit}$ the computational costs in terms of degrees of freedom and number of non-zero entries in the stiffness matrix. Clearly, the choice of the serendipity element $\mathcal{Q}_p^{\oplus}$ reduces the costs by a factor of about 2 compared to the full $\mathcal{Q}_p$-element while the standard enriched element $\mathcal{Q}_p^{+}$ [12], gained by taking $\widetilde{\mathcal{Q}}_p = \mathcal{Q}_{p-3} \oplus \operatorname{span}\{\xi^{p-2}, \eta^{p-2}\}$, lies in between.

Figure 4 shows the convergence of the two methods for the three different spaces on the Shishkin and the Bakhvalov-Shishkin mesh. The upper curves correspond to the Shishkin mesh and a convergence rate of $\mathcal{O}\left((N^{-1} \ln N)^5\right)$ is observable for the Galerkin FEM on the left and for the LPSFEM on the right. Note that the choice of the space has almost no effect on the quality of the computed solutions. However, the choice of the mesh has a much stronger effect – the lower curves correspond to the Bakhvalov-Shishkin mesh. We observe a convergence order of $\mathcal{O}\left(N^{-5}\right)$ and on the finest mesh three orders of magnitude difference.

Table 1 Galerkin discretisation with $Q_5^{\oplus}$, $N = 64$, and $\varepsilon = 10^{-12}$ for different point distribution types

	$\|u - u^N\|_\varepsilon$		$\|J^N u - u\|_\varepsilon$		$\|J^N u - u^N\|_\varepsilon$	
Type	S-mesh	B–S mesh	S-mesh	B–S mesh	S-mesh	B–S mesh
1	1.991-06	3.751-09	2.634-06	4.788-09	1.722-06	2.987-09
2	1.991-06	3.751-09	2.464-06	4.649-09	1.465-06	2.760-09
3	1.991-06	3.751-09	3.748-06	7.097-09	3.176-06	6.028-09

Table 2 Local projection stabilisation with $Q_5^{\oplus}$, $N = 64$, and $\varepsilon = 10^{-12}$ for different point distribution types

	$\|u - u^N\|_{LPS}$		$\|J^N u - u\|_{LPS}$		$\|J^N u - u^N\|_{LPS}$	
Type	S-mesh	B–S mesh	S-mesh	B–S mesh	S-mesh	B–S mesh
1	2.383-06	4.546-09	2.636-06	4.790-09	2.169-06	3.953-09
2	2.383-06	4.546-09	2.464-06	4.650-09	1.941-06	3.767-09
3	2.383-06	4.546-09	3.749-06	7.098-09	3.603-06	6.552-09

Finally, we want to study the influence of the distribution of the points which are used to define the interpolation operator $\mathcal{J}$. We have considered the case $\xi = \eta$ with three different choices:

type 1 equidistant point distribution $(-1, -0.6, -0.2, 0.2, 0.6, 1)$,

type 2 Gauss–Lobatto points $(-1, -0.765, -0.285, 0.285, 0.765, 1)$,

type 3 points condensed near 0 $(-1, -0.25, -0.083, 0.083, 0.25, 1)$.

Tables 1 and 2 show the errors for the methods based on the above given point distribution for a fixed mesh of $N = 64$. Clearly, the difference of the errors between those three different types is very small. Nevertheless, it can be observed that the Gauss-Lobatto points give the smallest interpolation- and closeness errors while type 3 generates the biggest errors. This is caused by the concentration of points near 0 which leads to a worse behaviour of the interpolation operator.

Since the finite element space V^N is not influenced by the choice of the interpolation points, the error $u - u^N$ is the same for all interpolation operators. This can be seen from the columns 2 and 3 in Tables 1 and 2.

Above consideration of the influence of point distributions on the behaviour of the interpolation operator J^N shows that it is sufficient to use an equidistant point distribution although the more sophisticated choice of Gauss–Lobatto points generates smaller interpolation errors.

Acknowledgements The author has been supported by Science Foundation Ireland under the Research Frontiers Programme 2008; Grant 08/RFP/MTH1536.

References

1. T. Apel. *Anisotropic finite elements: local estimates and applications*. Advances in Numerical Mathematics. B. G. Teubner, Stuttgart, 1999.
2. N. S. Bakhvalov. The optimization of methods of solving boundary value problems with a boundary layer. *U.S.S.R. Comput. Math. Math. Phys.*, 9(4):139–166, 1969.

3. R. Becker and M. Braack. A finite element pressure gradient stabilization for the Stokes equations based on local projections. *Calcolo*, 38(4):173–199, 2001.
4. R. Becker and M. Braack. A two-level stabilization scheme for the Navier-Stokes equations. In M. Feistauer, V. Dolejší, P. Knobloch, and K. Najzar, editors, *Numerical mathematics and advanced applications*, pages 123–130, Berlin, 2004. Springer-Verlag.
5. M. Braack and E. Burman. Local projection stabilization for the Oseen problem and its interpretation as a variational multiscale method. *SIAM J. Numer. Anal.*, 43(6):2544–2566, 2006.
6. T. A. Davis. Algorithm 832: UMFPACK V4.3—an unsymmetric-pattern multifrontal method. *ACM Trans. Math. Software*, 30(2):196–199, 2004.
7. T. A. Davis. A column pre-ordering strategy for the unsymmetric-pattern multifrontal method. *ACM Trans. Math. Software*, 30(2):167–195, 2004.
8. T. A. Davis and I. S. Duff. An unsymmetric-pattern multifrontal method for sparse LU factorization. *SIAM J. Matrix Anal. Appl.*, 18(1):140–158, 1997.
9. T. A. Davis and I. S. Duff. A combined unifrontal/multifrontal method for unsymmetric sparse matrices. *ACM Trans. Math. Software*, 25(1):1–20, 1999.
10. S. Franz. *Singularly perturbed problems with characteristic layers: Supercloseness and postprocessing*. PhD thesis, Department of Mathematics, TU Dresden, 2008.
11. S. Franz and G. Matthies. Convergence on Layer-Adapted Meshes and Anisotropic Interpolation Error Estimates of Non-Standard Higher Order Finite Elements. Mathematische Schriften Kassel 01/10, Universität Kassel, 2010. submitted for publication.
12. S. Franz and G. Matthies. Local projection stabilisation on S-type meshes for convection-diffusion problems with characteristic layers. *Computing*, 87(3–4):135–167, 2010.
13. V. John and G. Matthies. MooNMD - a program package based on mapped finite element methods. *Comput. Vis. Sci.*, 6(2–3):163–170, 2004.
14. R. B. Kellogg and M. Stynes. Sharpened and corrected version of: Corner singularities and boundary layers in a simple convection-diffusion problem. *J. Differential Equations*, 213(1):81–120, 2005.
15. T. Linß and M. Stynes. Numerical methods on Shishkin meshes for linear convection-diffusion problems. *Comput. Methods Appl. Mech. Eng.*, 190(28):3527–3542, 2001.
16. Linß, T. An upwind difference scheme on a novel Shishkin-type mesh for a linear convection-diffusion problem. *J. Comput. Appl. Math.*, 110(1):93–104, 1999.
17. G. Matthies, P. Skrzypacz, and L. Tobiska. A unified convergence analysis for local projection stabilisations applied to the Oseen problem. *M2AN Math. Model. Numer. Anal.*, 41(4):713–742, 2007.
18. J. J. H. Miller, E. O'Riordan, and G. I. Shishkin. *Fitted numerical methods for singular perturbation problems: Error estimates in the maximum norm for linear problems in one and two dimensions*. World Scientific Publishing Co. Inc., River Edge, NJ, 1996.
19. H.-G. Roos and T. Linß. Sufficient conditions for uniform convergence on layer-adapted grids. *Computing*, 63(1):27–45, 1999.
20. M. Stynes and E. O'Riordan. A uniformly convergent Galerkin method on a Shishkin mesh for a convection-diffusion problem. *J. Math. Anal. Appl.*, 214(1):36–54, 1997.
21. P. Sun, L. Chen, and J. Xu. Numerical studies of adaptive finite element methods for two dimensional convection-dominated problems. *J. Sci. Comput.*, 43:24–43, 2010.

A Singularly Perturbed Convection Diffusion Parabolic Problem with an Interior Layer

J.L. Gracia and E. O'Riordan

Abstract In this paper, we examine a singularly perturbed convection-diffusion problem where the coefficients are smooth, but the solution contains an interior layer, generated from the fact that the initial condition contains an internal layer.

1 Introduction

In [2], we examined the following singularly perturbed parabolic problem: Find $\hat{u}$ such that

$$\hat{\mathcal{L}}_\varepsilon \hat{u} := -\varepsilon \hat{u}_{ss} + \hat{a}(t)\hat{u}_s + \hat{u}_t = \hat{f}(s,t), \quad (s,t) \in Q := (0,1) \times (0,T], \quad \text{(1a)}$$

$$\hat{u}(s,0) = \hat{\phi}(s;\varepsilon), 0 \le s \le 1, \quad \text{(1b)}$$

$$\hat{u}(0,t) = \phi_L(t),\ \hat{u}(1,t) = \phi_R(t),\ 0 < t \le T, \quad \text{(1c)}$$

$$\hat{a}(t) > \alpha > 0, \quad \text{(1d)}$$

where the coefficient of the convection term only depends on the time variable, the initial condition $\hat{\phi}$ is smooth, but contains an interior layer in the vicinity of a point $s = p, 0 < p < 1$ and p is independent of ε. The function $\hat{\phi}$ is defined as the solution of a singularly perturbed problem of the form

$$-\varepsilon \hat{\phi}'' + \hat{b}(s)\hat{\phi} = \hat{f}_1(s), \quad |\hat{f}_1|_k \le C\varepsilon^{-k/2} e^{-\alpha \frac{|s-p|}{\sqrt{\varepsilon}}},$$

(see Sect. 4 for an example of such a function). The solution of problem (1) will exhibit an interior layer of width $\mathcal{O}(\sqrt{\varepsilon})$ (emanating from the initial condition),

J.L. Gracia (✉)
Department of Applied Mathematics, University of Zaragoza, Spain
e-mail: jlgracia@unizar.es

E. O'Riordan
School of Mathematical Sciences, Dublin City University, Ireland
e-mail: eugene.oriordan@dcu.ie

C. Clavero et al. (eds.), *BAIL 2010 – Boundary and Interior Layers, Computational and Asymptotic Methods*, Lecture Notes in Computational Science and Engineering 81,
DOI 10.1007/978-3-642-19665-2_15,

which travels along the characteristic curve associated with the reduced differential equation (formally set $\varepsilon = 0$ in (1a)) given by

$$\Gamma^* := \{(p(t),t) | p'(t) = \hat{a}(t),\ 0 < p(0) = p < 1\}.$$

In general a boundary layer of width $\mathcal{O}(\varepsilon)$ will also appear in the vicinity of the edge $x = 1$. We restrict the size of the final time T so that the interior layer does not interact with this boundary layer. Since $\hat{a} > 0$, the function $p(t)$ is monotonically increasing. Thus, we limit the final time T such that

$$\delta := (1 - p(T))(1 - p)^{-1} > 0. \tag{2}$$

Using the map [1] $X : (s,t) \to (x,t)$ given by

$$x(s,t) = \begin{cases} \dfrac{p}{p(t)} s, & s \le p(t), \\ 1 - \dfrac{1-p}{1-p(t)}(1-s), & s \ge p(t), \end{cases} \tag{3}$$

the differential equation (1a) transforms into

$$\begin{gathered} \mathcal{L}_\varepsilon u := \left(-\varepsilon u_{xx} + \kappa(x,t) u_x\right) + g(x,t) u_t = g(x,t) f(x,t),\ x \ne p, \\ u(x,0) = \phi(x;\varepsilon),\ 0 < x \le 1, u(0,t) = \phi_L(t),\ u(1,t) = \phi_R(t),\ 0 < t \le T, \\ \kappa(x,t) := \begin{cases} \dfrac{a(t)p(t)}{p}\left(\dfrac{p-x}{p}\right), & x < p, \\ \dfrac{a(t)(1-p(t))}{(1-p)}\dfrac{(x-p)}{(1-p)}, & x > p, \end{cases} \quad g(x,t) := \begin{cases} \left(\dfrac{p(t)}{p}\right)^2, & x < p, \\ \left(\dfrac{1-p(t)}{1-p}\right)^2, & x > p. \end{cases} \end{gathered} \tag{4}$$

Throughout this paper, we use the notation $\omega(x,t) := \hat{\omega}(s,t)$. In the transformed problem, the coefficient $\kappa(x,t)$ of the first derivative in space is positive, except along the internal line $x = p$ where it is zero.

The solution of problem (4) can be decomposed into the sum of a regular and singular (boundary and interior layers) components: $u = v + w + z$. The regular component is discontinuous along $(p(t),t)$ and the values on the edges $(p(t),t)$ and $(1,t)$ are defined such that no layers are present in the regular component. This regular component satisfies the bounds

$$\left\| \frac{\partial^{j+m} v}{\partial x^j \partial t^m} \right\| \le C(1 + \varepsilon^{2-(j+m)}),\ 0 \le j + 2m \le 4. \tag{5}$$

The continuous boundary layer function w is defined to be identically zero in $\Omega^- := (0,p)$ and in $\Omega^+ := (p,1)$ it satisfies the bounds

$$\left| \frac{\partial^{j+m} w}{\partial x^j \partial t^m}(x,t) \right| \le C \varepsilon^{1-m} \varepsilon^{-j} e^{-\frac{\alpha\delta(1-x)}{2\varepsilon}},\ 0 \le j \le 4,\ m = 1,2,\ (x,t) \in \Omega^+. \tag{6}$$

The discontinuous multi-valued interior layer function z satisfies the bounds

$$|z(x,t)| \le C e^{-\sqrt{\frac{\alpha}{\varepsilon}}(p-x)},\ (x,t) \in \Omega^-, \tag{7a}$$

$$|z(x,t)| \le C e^{-e^{-\frac{\|a\|t}{\delta(1-p)}}\sqrt{\frac{\alpha}{\varepsilon}}(x-p)},\ (x,t) \in \Omega^+, \tag{7b}$$

and for all $1 \le j + 2m \le 4$,

$$\left|\frac{\partial^{j+m} z}{\partial x^j \partial t^m}(x,t)\right| \le C\varepsilon^{-j/2} e^{-\sqrt{\frac{\alpha}{2\varepsilon}}(p-x)},\ (x,t) \in \Omega^-, \tag{7c}$$

$$\left|\frac{\partial^{j+m} z}{\partial x^j \partial t^m}(x,t)\right| \le C\varepsilon^{-j/2} e^{-e^{-\frac{\|a\|}{\delta(1-p)}T}\sqrt{\frac{\alpha}{2\varepsilon}}(x-p)}, (x,t)\in\Omega^+. \tag{7d}$$

We refer the reader to [2] for details on how these components are defined. Based on the bounds (7a,b) an appropriate piecewise-uniform mesh of Shishkin type can be defined (see Sect. 3) for problem (1). In addition, using the bounds (5), (6) and (7a,b), first order uniform convergence was established in [2] for a numerical method composed of a standard upwind finite difference operator and this piecewise uniform mesh.

This paper is a companion paper to [2]. Here we examine the effect of having the convective coefficient $\hat{a} = \hat{a}(s,t)$ depend on both time and space. We will see that the main changes are in the statement of the transformed problem and the establishment of the bounds (7c,d) on the derivatives of the interior layer component. Throughout the paper, c or C denotes a generic constant that is independent of the singular perturbation parameter ε and of all discretization parameters.

2 Continuous Problem

In passing, we note that when the convective term is independent of space, then the characteristic curve Γ^* is explicitly determined by

$$p(t) = p + \int_{s=0}^{t} \hat{a}(s)\, ds.$$

When the convective term depends on space then the path of Γ^* is implicitly defined by $p'(t) = \hat{a}(p(t),t)$. This is the first hint that allowing the convective coefficient to depend on space complicates the numerical analysis.

Note that the mapping (3), transforms the convection term $\hat{a}(s,t)$ into

$$\kappa(x,t) := \begin{cases} \dfrac{p(t)}{p}\Big(a(x,t) - \dfrac{x a(p,t)}{p}\Big), & x < p, \\ \dfrac{1-p(t)}{1-p}\Big(a(x,t) - \dfrac{(1-x)a(p,t)}{1-p}\Big), & x > p. \end{cases} \tag{8}$$

To immediately extend the analysis from [2] to the case of $\hat{a}(s,t)$, we require that $\kappa(x,t) > 0$, $(x,t) \in \Omega^- \cup \Omega^+$. Hence, in this paper we will assume that

$$\hat{a}(s,t) > \alpha > 0; \quad \frac{a(x,t)}{a(p,t)} > \begin{cases} \dfrac{x}{p}, & \text{in } \Omega^-, \\ \dfrac{1-x}{1-p}, & \text{in } \Omega^+. \end{cases} \tag{9}$$

It is convenient to impose a condition on the convective coefficient $\hat{a}(s,t)$ in the original (s,t)–variables. It is easy to show that $\hat{a}_{ss} < 0$, $(s,t) \in Q$ is a sufficient, but not a necessary, condition for (9) to be satisfied.

If the decomposition of the solution $u = v + w + z$ used in [2] is employed in the case of $\hat{a} = \hat{a}(x,t)$, then the bounds (5), (6) on the regular and boundary layer components can be easily established. In addition, one can also check that the bounds (7a,b) on the interior layer component still apply when $\hat{a}(s,t)$. However, the proof used in [2] to establish (7c,d) is not applicable in this paper. To be more precise, if we consider the homogeneous differential equation

$$\left(-\varepsilon z_{xx} + \kappa(x,t) z_x\right) + g(x,t) z_t = 0, \quad (x,t) \in \Omega^-.$$

When $\hat{a}(t)$ is independent of space, the stretched variable $\zeta = \dfrac{(p-x)\,p(t)}{p\sqrt{\varepsilon}}$, transforms this homogenous differential equation into the simple heat equation

$$-\tilde{z}_{\zeta\zeta} + \tilde{z}_t = 0,$$

where $\tilde{z}(\zeta,t) = z(x,t)$. From this heat equation, we can deduce bounds on the partial derivatives of the component z. However, when $\hat{a} = \hat{a}(s,t)$, this same change of variable does not cancel the convection term and therefore this particular argument does not allow us deduce the bounds (7c,d). In this paper, we simply assume that the bounds (7c,d) extend to the case where $\hat{a}$ can depend on both space and time.

3 Discrete Problem

Based on the bounds (7a,b), we propose the following mesh for both the cases $\hat{a} = \hat{a}(s,t)$ and $\hat{a} = \hat{a}(t)$: Let N and M be two positive integers. To approximate the solution we use a uniform mesh in time $\{t_j = j\Delta t, \mid \Delta t = T/M\}$ and a piecewise uniform mesh of Shishkin type in space $\{x_i\}_{i=1}^{N}$ (described below) in the transformed variables (x,t). The grid is given by $\overline{\Omega}^{N,M} = \{t_j\}_{j=0}^{M} \times \{x_i\}_{i=0}^{N}$. The Euler method is used to approximate the time variable and the upwind finite difference operator to approximate the space variable. The finite difference equation associated with each grid point is given by

$$(-\varepsilon\delta_x^2 U + \kappa D_x^- U + gD_t^- U)(x_i, t_j) = (g\, f)(x_i, t_j),\ x_i \neq p,\ t_j > 0, \quad (10a)$$

$$D_x^- U(p, t_j) = D_x^+ U(p, t_j), t_j > 0, \quad (10b)$$

$$-\varepsilon\delta_x^2 U(x_i, 0) + b(x_i)U(x_i, 0) = f_1(x_i),\ 0 < x_i < 1, \quad (10c)$$

$$U(0, t_j) = \phi_L(t_j), U(1, t_j) = \phi_R(t_j),\ t_j \geq 0, \quad (10d)$$

where b and f_1 are smooth functions (see Sect. 4 for an example). Here, $D_\star^+$, $D_\star^-$ denote the forward and backward finite difference to approximate the first order derivatives, and δ_x^2 the classical approximation of the second order derivative on a nonuniform mesh.

The space domain is discretized using a piecewise uniform Shishkin mesh which splits the space domain [0, 1] into four subintervals

$$[0, p - \tau_1] \cup [p - \tau_1, p + \tau_2] \cup [p + \tau_2, 1 - \sigma] \cup [1 - \sigma, 1], \quad (11)$$

where the transition parameters are defined by

$$\tau_1 := \min\{\frac{p}{2}, \sqrt{\frac{2\varepsilon}{\alpha}} \ln N\}, \quad \tau_2 := \min\{\frac{1-p}{2}, e^{\frac{\|a\|}{\delta(1-p)}T}\sqrt{\frac{2\varepsilon}{\alpha}} \ln N\}, \quad (12a)$$

$$\sigma := \min\{\frac{1-(p+\tau_2)}{2}, \frac{4\varepsilon}{\alpha\delta} \ln N\}. \quad (12b)$$

The grid points are uniformly distributed within each subinterval such that

$$x_0 = 0,\ x_{N/4} = p - \tau_1,\ x_{N/2} = p,\ x_{5N/8} = p + \tau_2,\ x_{7N/8} = 1 - \sigma,\ x_N = 1.$$

Analogously to the continuous problem, a decomposition of the solution of the discrete problem $U = V + W + Z$ was established in [2]. This decomposition, can be easily extended to the case $\hat{a} = \hat{a}(s, t)$, and these discrete counterparts satisfy the usual properties on the Shishskin mesh.

Define the global approximation

$$\bar{U}(x, t) := \sum_{i=0, j=1}^{N, M} U(x_i, t_j)\varphi_i(x)\psi_j(t)$$

where $\varphi_i(x)$ is the standard hat function centered at $x = x_i$ and $\psi_j(t) = M(t - t_{j-1}), t \in [t_{j-1}, t_j)$.

Theorem 1. *Assume (9) and that the bounds (7c,d) hold. For M sufficiently large so that*

$$M > (\ln N)\frac{(\|a\| + 1 - p)T}{(1-p)\delta^2},$$

is satisfied, then

$$\|\bar{U} - \hat{u}\|_{\bar{Q}} \leq CN^{-1}(\ln N)^2 + CM^{-1} \ln N,$$

where U is the discrete solution of (10) and $\hat{u}$ is the solution of the continuous problem (1), where $\hat{a}(s,t)$ is a function of both space and time.

Proof. Apply the arguments given in [2].

Remark 1. We note that a different choice of τ_2 can be used to define the mesh

$$\tau_2^*(t_j) = \min\{\frac{1-p}{2}, e^{\frac{\|a\|}{\delta(1-p)}t_j}\sqrt{\frac{2\varepsilon}{\alpha}}\ln N\}. \tag{13}$$

This mesh is time dependent and therefore interpolation is required to compute the solution with the two level numerical method (10) at each time level. The interpolation increases the computational cost of the method, but this new mesh places more mesh points within the interior layer at all time levels. In Sect. 4, we employ linear interpolation when implementing this choice of mesh.

4 Numerical Experiments

As the exact solutions of the problems of this section are unknown, we estimate the errors using the double mesh principle to compute the global differences:

$$d_\varepsilon^{N,M} := \left\| \bar{U}^{N,M} - \bar{U}^{2N,2M} \right\|_{\bar{\Omega}^{N,M}\cup\bar{\Omega}^{2N,2M}}, \quad d^{N,M} := \max_{S_\varepsilon} d_\varepsilon^{N,M}.$$

Here $\bar{U}$ denotes the linear interpolation of the numerical solution U and the singular perturbation parameter varies over the set $S_\varepsilon = \{2^0, 2^{-1}, \ldots, 2^{-30}\}$. From these values we calculate computed orders of convergence $q_\varepsilon^{N,M}$ and computed orders of uniform convergence $q^{N,M}$ using

$$q_\varepsilon^{N,M} := \log_2\left(d_\varepsilon^{N,M}/d_\varepsilon^{2N,2M}\right), \quad q^{N,M} := \log_2\left(d^{N,M}/d^{2N,2M}\right).$$

Example 1. The first test problem is given by

$$\begin{array}{l} -\varepsilon\hat{u}_{ss} + (1+s^2)\hat{u}_s + \hat{u}_t = 4s(1-s), \quad (s,t)\in(0,1)\times(0,0.15], \\ \hat{u}(s,0) = \hat{\phi}(s;\varepsilon), 0 < s \le 1,\ \hat{u}(0,t) = 0,\ \hat{u}(1,t) = 2,\ 0 < t \le 1, \end{array} \tag{14}$$

where the initial condition ϕ is the solution of the following problem

$$-\varepsilon\hat{\phi}'' + \hat{\phi} = 1 + \tanh(\frac{s-0.25}{2\sqrt{\varepsilon}}), \quad \hat{\phi}(0) = 0, \hat{\phi}(1) = 2. \tag{15}$$

Note that in this problem $\hat{a}_{ss} = 2 > 0$, but condition (9) still holds.

The mesh is defined by means of the transition points (12). In Table 1 we display the uniform differences and the corresponding orders of convergence, which exhibit

Table 1 Uniform differences and computed orders of uniform convergence $q^{N,M}$ for test problem (14)

	$N = 64$ $M = 64$	$N = 128$ $M = 128$	$N = 256$ $M = 256$	$N = 512$ $M = 512$	$N = 1,024$ $M = 1,024$
$d^{N,M}$	0.459E-01	0.228E-01	0.113E-01	0.531E-02	0.267E-02
$q^{N,M}_{uni}$	1.010	1.014	1.088	0.991	

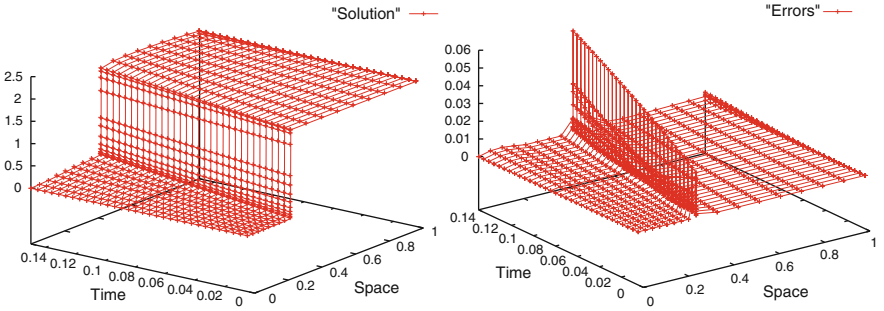

Fig. 1 Problem (14): Computed solution and two mesh differences for $\varepsilon = 10^{-8}$ and $N = M = 32$

first order convergence. In Fig. 1 the solution and the global differences are shown for $\varepsilon = 10^{-8}$ and $N = M = 32$.

Example 2. The second test problem is given by

$$\begin{aligned} &-\varepsilon \hat{u}_{ss} + (4 - s^2)\hat{u}_s + \hat{u}_t = 4s(1-s), \quad (s,t) \in (0,1) \times (0, 0.15], \\ &\hat{u}(s,0) = \hat{\phi}(s;\varepsilon), 0 < s \leq 1,\ \hat{u}(0,t) = 0,\ \hat{u}(1,t) = 2,\ 0 < t \leq 1, \end{aligned} \tag{16}$$

where the initial condition $\hat{\phi}$ is the solution of problem (15).

The mesh is defined by means of the transition points (12). In Table 2 we display the uniform differences and the corresponding orders of convergence, which again indicates first order convergence. In Fig. 2 the solution is shown for $\varepsilon = 10^{-8}$ and $N = M = 32$.

Test problem (16) is now approximated with the time dependent mesh (13). The results are given in Table 2. In Fig. 2 the computed solution is displayed for $\varepsilon = 10^{-8}$ and $N = M = 32$ and we observe that the grid inserts more mesh points into the interior layer than the time independent mesh (12). This is more clearly depicted in Fig. 3, where a zoom of the grid in space for both the dependent and independent grids is given in the transformed variables (x, t). Nevertheless, this new time-dependent mesh does not improve the order of uniform convergence provided by the time independent mesh and therefore we conclude that the independent grid has been computationally more efficient for this particular test example.

Acknowledgements This research was partially supported by the project MEC/FEDER MTM2007-63204 and the Diputación General de Aragón.

Table 2 Uniform differences and computed orders of uniform convergence for test problem (16) using time independent (*first row*) and dependent (*second row*) meshes

	N = 64 M = 64	N = 128 M = 128	N = 256 M = 256	N = 512 M = 512	N = 1024 M = 1024
$d^{N,M}$	0.474E+0	0.310E+0	0.135E+0	0.609E-1	0.336E-1
$q_{uni}^{N,M}$	0.615	1.199	1.148	0.860	
$d^{N,M}$	0.196E+00	0.120E+00	0.768E-01	0.455E-01	0.275E-01
$q_{uni}^{N,M}$	0.715	0.638	0.756	0.724	

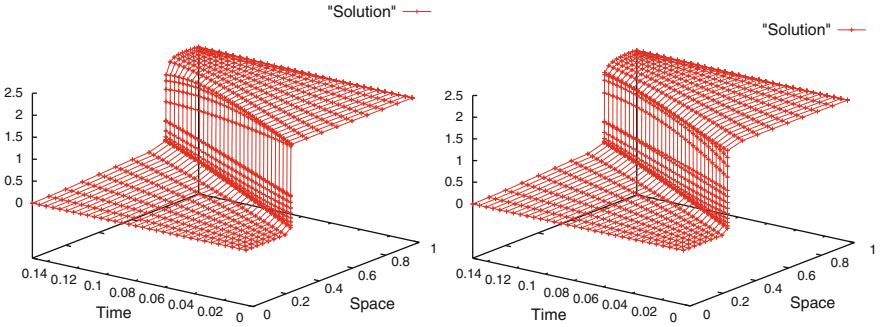

Fig. 2 Problem (16): Computed solution for $\varepsilon = 10^{-8}$ and $N = M = 32$ using a time independent (*left*) and dependent (*right*) meshes

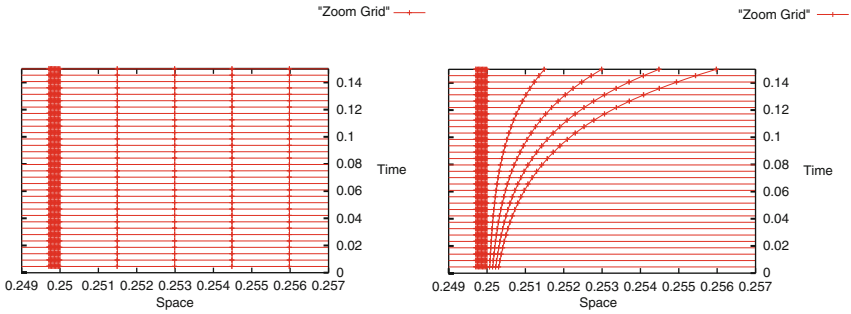

Fig. 3 Zoom of the time independent (*left*) and dependent (*right*) grids for test problem (16) for $\varepsilon = 10^{-8}$ and $N = M = 32$ in the transformed variables (x, t)

References

1. R.K. Dunne, E. O'Riordan and G.I. Shishkin, Singularly perturbed parabolic problems on non-rectangular domains, Proc. 2nd International Conference NAA'2000, Rousse, Bulgaria, (L. Vulkov, J. Wasniewski and P. Yalamov eds.) / Lecture Notes in Computer Science, Springer-Verlag, **1988**, 2001, 265–272.
2. J.L. Gracia, E. O'Riordan, A singularly perturbed time dependent convection diffusion problem with an interior layer. Preprint MS-10-02, Dublin City University, 2010, (abridged version submitted).

Mesh Adaptivity Using VMS Error Estimators: Application to the Transport Equation

G. Hauke, M.H. Doweidar, and S. Fuentes

Abstract Recently, it has been developed an explicit a-posteriori error estimator (Ainsworth and Oden, A posterior error estimation in finite element analysis, Wiley, 2000) especially suited for fluid dynamics problems solved with stabilized methods (Hauke et al., Variational multiscale a-posteriori error estimation for the multi-dimensional transport equation, Comput. Meth. Appl. Mech. Eng. 195, 1573–1593, 2006; Hauke et al., The multiscale approach to error estimation and adaptivity, Comput. Meth. Appl. Mech. Eng. **197**, 2701–2718, 2008; Hauke et al., Multiscale Methods in Computational Mechanics, vol. 55. Springer, 2010). The technology is based upon the theory that inspired stabilized methods, namely, the variational multiscale theory (Hughes, Comput. Meth. Appl. Mech. Eng. 127, 387–401, 1995; Hughes et al., Comput. Meth. Appl. Mech. Eng. 166, 3–24, 1998). The salient features of the formulation are that it can be readily implemented in existing codes, it is a very economical procedure and it yields very accurate local error estimates uniformly from the diffusive to the advective regime.

In this work, the variational multiscale error estimator is applied to develop adaptive strategies for the advection-diffusion-reaction equation. The performance of two local error norms and three strategies to adapt the mesh are investigated, with emphasis on flows with boundary and interior layers.

G. Hauke (✉) and S. Fuentes
LITEC (CSIC) – Universidad de Zaragoza, Area de Mecánica de Fluidos, C/María de Luna 3, 50018 Zaragoza, Spain
e-mail: ghauke@unizar.es

M.H. Doweidar
Area de Mecánica de Medios Continuos y Teoría de Estructuras, Departamento de Ingeniería Mecánica, Universidad de Zaragoza, C/María de Luna 7, 50018 Zaragoza, Spain
e-mail: mohamed@unizar.es

C. Clavero et al. (eds.), *BAIL 2010 – Boundary and Interior Layers, Computational and Asymptotic Methods*, Lecture Notes in Computational Science and Engineering 81,
DOI 10.1007/978-3-642-19665-2_16,

1 Preliminaries

1.1 Problem Setup

Strong Form

Consider a spatial domain Ω with boundary Γ, which is partitioned into two non-overlapping zones Γ_g and Γ_h. Let $\boldsymbol{x}$ and $\boldsymbol{y}$ be two points in $\overline{\Omega}$. The strong form of the boundary-value problem consists of finding $u : \Omega \to \mathbb{R}$ such that for the given essential boundary condition $\mathrm{g} : \Gamma_g \to \mathbb{R}$, the natural boundary condition $h : \Gamma_h \to \mathbb{R}$, and forcing function $f : \Omega \to \mathbb{R}$, the following equations are satisfied

$$\begin{cases} \mathcal{L}u = f \text{ in } \Omega \\ u = \mathrm{g} \text{ on } \Gamma_g \\ \mathcal{B}u = h \text{ on } \Gamma_h \end{cases} \tag{1}$$

where $\mathcal{L}$ is in principle a second-order differential operator and $\mathcal{B}$, an operator acting on the boundary that defines the natural boundary condition.

1.2 A Posteriori Error Estimators

Let us introduce a finite element mesh of elements Ω^e with boundary Γ^e. The finite element solution (given, in principle, by a stabilized method) is denoted as $\bar{u}$ and the error as u', such that $u = \bar{u} + u'$.

Three explicit a posteriori error estimators will be investigated, namely,

MS06L2 [4]

$$||u'(\boldsymbol{x})||_{\Omega^e} \approx \tau^e_{\text{flow}} \, ||\mathcal{L}\bar{u} - f||_{\Omega^e} \tag{2}$$

MS06P0 [4]

$$||u'(\boldsymbol{x})||_{\Omega^e} \approx \tau^e_{\text{flow}} \, \overline{(\mathcal{L}\bar{u} - f)} \sqrt{\text{meas}(\Omega^e)} \tag{3}$$

where the bar denotes the average value within the element.

MS08 [5]

$$\begin{aligned} ||u'(x)||_{L_r(\Omega^e)} \leq \; & \text{meas}(\Omega^e)^{1/r} \, \tau^e_{L_r} \\ & \times \left(||\mathcal{L}\bar{u} - f||_{L_\infty(\Omega^e)} + \tfrac{1}{2} \tfrac{\text{meas}(\Gamma^e)}{\text{meas}(\Omega^e)} ||[\![\mathcal{B}\bar{u}]\!]||_{L_\infty(\Gamma^e)} \right) \\ & \text{in } \Omega^e \end{aligned} \tag{4}$$

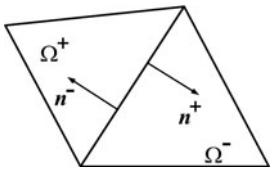

Fig. 1 Notation to define the jump across element interfaces

where typically, $r = 1$ or 2. Furthermore, $[\![\cdot]\!]$ denotes the jump operator of a function across a discontinuity. Following the notation of Fig. 1, where the respective outward unit normals to elements Ω^+ and Ω^- are $\boldsymbol{n}^+$ and $\boldsymbol{n}^-$, the jump of $\boldsymbol{v} \cdot \boldsymbol{n}$ is defined as [7]

$$[\![\boldsymbol{v} \cdot \boldsymbol{n}]\!] = \boldsymbol{n}^+ \cdot \boldsymbol{v}^+ + \boldsymbol{n}^- \cdot \boldsymbol{v}^- \tag{5}$$

The parameter τ^e_{flow} is the intrinsic *flow* time-scale, whereas $\tau^e_{L_r}$, the *error* time-scale. Their definitions can be found later, in the Numerical Test section.

Note that the first two methods give an estimate of the error in the L_2 norm, whereas the third method can give that estimate either in the L_2 or L_1 norms. Also, note that the first two methods lack the contribution of the jump term $[\![\mathcal{B}\bar{u}]\!]$ and, therefore, are only applicable to *advection-dominated* flows. The third formulation, MS08, is endowed with contributions stemming from element interior residuals and inter-element jumps and, therefore, can be applied to any regime from *advection-dominated* to *diffusion-dominated* flows.

2 Remeshing Strategies

It is assumed that the user provides the *target* error in the form of a constant local error norm $e^{L_r}_{\text{TOL}}$ in Ω^e or in the form of a constant pointwise error u_{TOL}. The error estimator provides an estimate of the error in the same local error norm $\eta^e_{L_r}$ (with $r = 1$ or 2). The remeshing strategy consists of an iterative process such that, given an initial mesh with mesh size distribution h_e and a stabilized finite element solution $\bar{u}$, from the estimated error and the user target error, the new mesh size distribution h'_e is calculated and a new mesh, generated. The process is repeated until convergence of the mesh. Three strategies have been investigated:

- To uniformly distribute the desired local error norm over the *old* mesh
- To uniformly distribute the desired local error norm over the *new* mesh
- To uniformly distribute the desired pointwise error

Convergence theory and suitable hypothesis yield the expressions of Table 1.

Table 1 Expressions to calculate the new mesh sizes h'_e from the old mesh sizes h_e, the estimated local error norm $\eta^e_{L_r}$ and the user tolerance $e^{L_r}_{\mathrm{TOL}}$ or u_{TOL}, for $r = 1$ or $r = 2$. β is the order of convergence of the finite element method

Method	User error	Error estimate in L_r norm
Local norm over *old* mesh	$e^{L_r}_{\mathrm{TOL}}$	$\frac{h'_e}{h_e} = \left(\frac{e^{L_r}_{\mathrm{TOL}}}{\eta^e_{L_r}}\right)^{\frac{1}{\beta}}$
Local norm over *new* mesh	$e^{L_r}_{\mathrm{TOL}}$	$\frac{h'_e}{h_e} = \left(\frac{e^{L_r}_{\mathrm{TOL}}}{\eta^e_{L_r}}\right)^{\frac{1}{\beta+2/r}}$
Pointwise error	u_{TOL}	$\frac{h'_e}{h_e} = \left(\frac{u^{L_1}_{\mathrm{TOL}}\,\mathrm{meas}(\Omega^e)^{1/r}}{\eta^e_{L_r}}\right)^{\frac{1}{\beta+2/r}}$

2.1 Numerical Test: L-Shaped Problem

The equation contemplated in this investigation is the transport equation, for which the differential and the natural boundary condition operators can be written as

$$\mathcal{L}u = \boldsymbol{a} \cdot \nabla u - \nabla \cdot (\kappa \nabla u) - su \tag{6}$$

$$\mathcal{B}u = \kappa \nabla u \cdot \boldsymbol{n} \tag{7}$$

with the velocity field $\boldsymbol{a} : \Omega \to \mathbb{R}$, the diffusion coefficient $\kappa : \Omega \to \mathbb{R}$, $\kappa \geq 0$, and the source parameter s, with $s > 0$ for production and $s < 0$ for dissipation.

For this partial differential equation, the *flow* time-scale τ_{flow} is defined according to [2] and the *error* time-scales are defined as follows,

$$\tau^e_{L_1} = \min\left(\frac{h_e}{2\,|a|}, \frac{h_e^2}{12\,\kappa}, \frac{1}{|s|}\right) \tag{8}$$

$$\tau^e_{L_2} = \min\left(\frac{h_e}{\sqrt{3}\,|a|}, \frac{h_e^2}{2\sqrt{30}\,\kappa}, \frac{1}{|s|}\right) \tag{9}$$

The numerical test, described in [9], considers the flow in a L-shaped domain and has zero essential boundary conditions along the boundary. The parameters of the problem are $\boldsymbol{a} = (1, 3)$, two values of $\kappa = 10^{-6}, 1$, $s = -1$ and the independent forcing function $f(\boldsymbol{x})$,

$$f(x, y) = 100r(r - 0.5)(r - 1/\sqrt{2}) \tag{10}$$

with $r^2 = (x - 0.5)^2 + (y - 0.5)^2$.

Figure 2 shows the exact solution for both viscosities. For $\kappa = 1$ the solution is fairly smooth, except at the corner, which is a singularity point. For $\kappa = 10^{-6}$, the solution displays sharp interior, boundary and outflow layers, a typical challenge of low viscosity flow solutions.

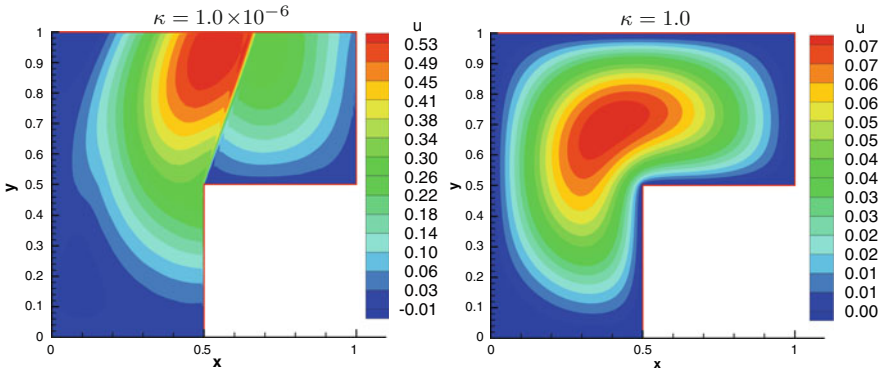

Fig. 2 Contour plots of the exact solutions

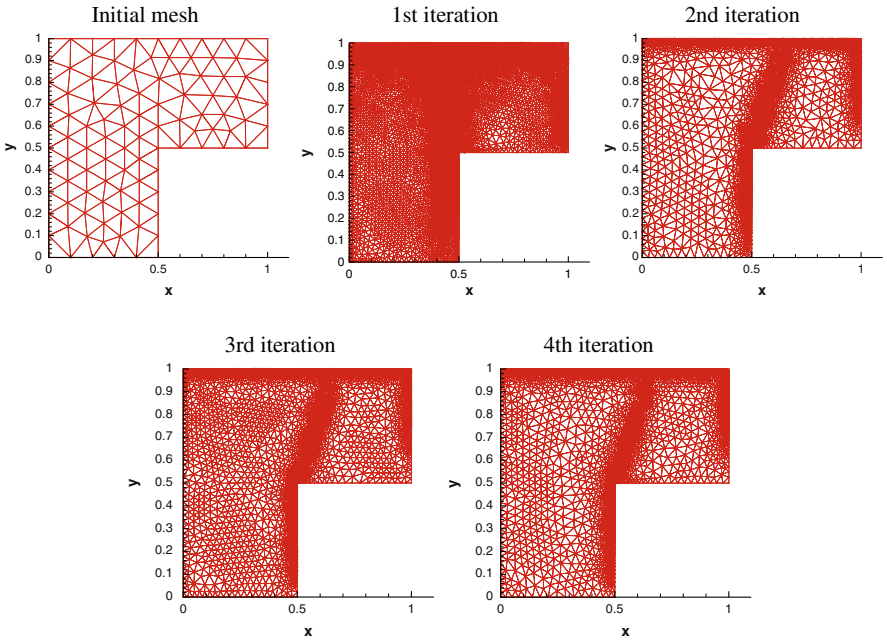

Fig. 3 Iterations of the remeshing process for $\kappa = 1.0 \times 10^{-6}$ and a user error tolerance of $e_{\text{TOL}}^{L_2} = 10^{-5}$

3 Results

Figure 3 displays the typical iterative process to adapt the mesh, including the initial mesh, which does not have any information about the flow features.

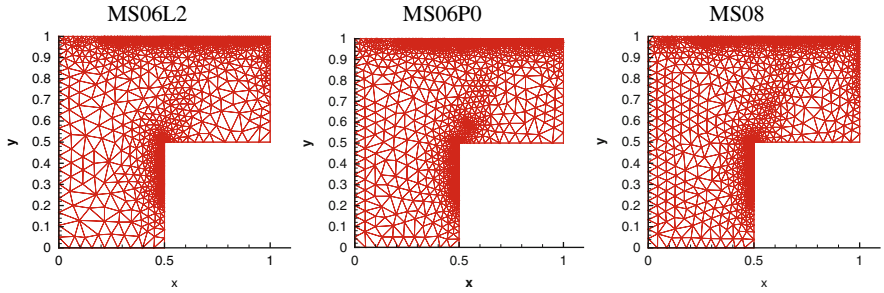

Fig. 4 Comparison of technologies for $\kappa = 1.0 \times 10^{-6}$ and a user error tolerance of $e_{\mathrm{TOL}}^{L_2} = 10^{-4}$. Uniform distribution of L_2 local error norm over the *old* mesh

Figure 4 compares the performance of the three technologies for the advection-dominated case. One can conclude that the three technologies generate very similar meshes, capturing the flow boundary and inner layers for the small error tolerance.

For the MS08 error estimator, Figs. 5, 6 compare for the L_1 and L_2 norms the three remeshing strategies for the advection-dominated and diffusion-dominated cases, respectively.

4 Conclusions

It has been shown that the three error estimators produce similar adapted meshes. For advection-dominated flows one can choose the more complex MS08 formulation or the simpler MS06.

The uniform distribution of the local error norm over the *old* mesh or the *new* mesh generates similar meshes, both for the L_1 and L_2 norms. In general, both norms give rise to good quality meshes. However, the uniform distribution of the local error norm over the *old* mesh in combination with the L_1 local norm produces oscillatory meshes and, therefore, it should be avoided as an adaptive strategy.

The uniform distribution of pointwise error produces sharper (finer) meshes around singularities than the even distribution of local error norms.

During the iteration process, the second mesh tends to be too fine. As a consequence, the error tolerance should be decreased slowly towards the user target error.

As a summary, it can be concluded that variational multiscale error estimators generate economic, good quality adapted meshes.

Acknowledgements Funding of the Ministry of Science and Innovation of Spain under contract MTM2009-13286 is gratefully acknowledged.

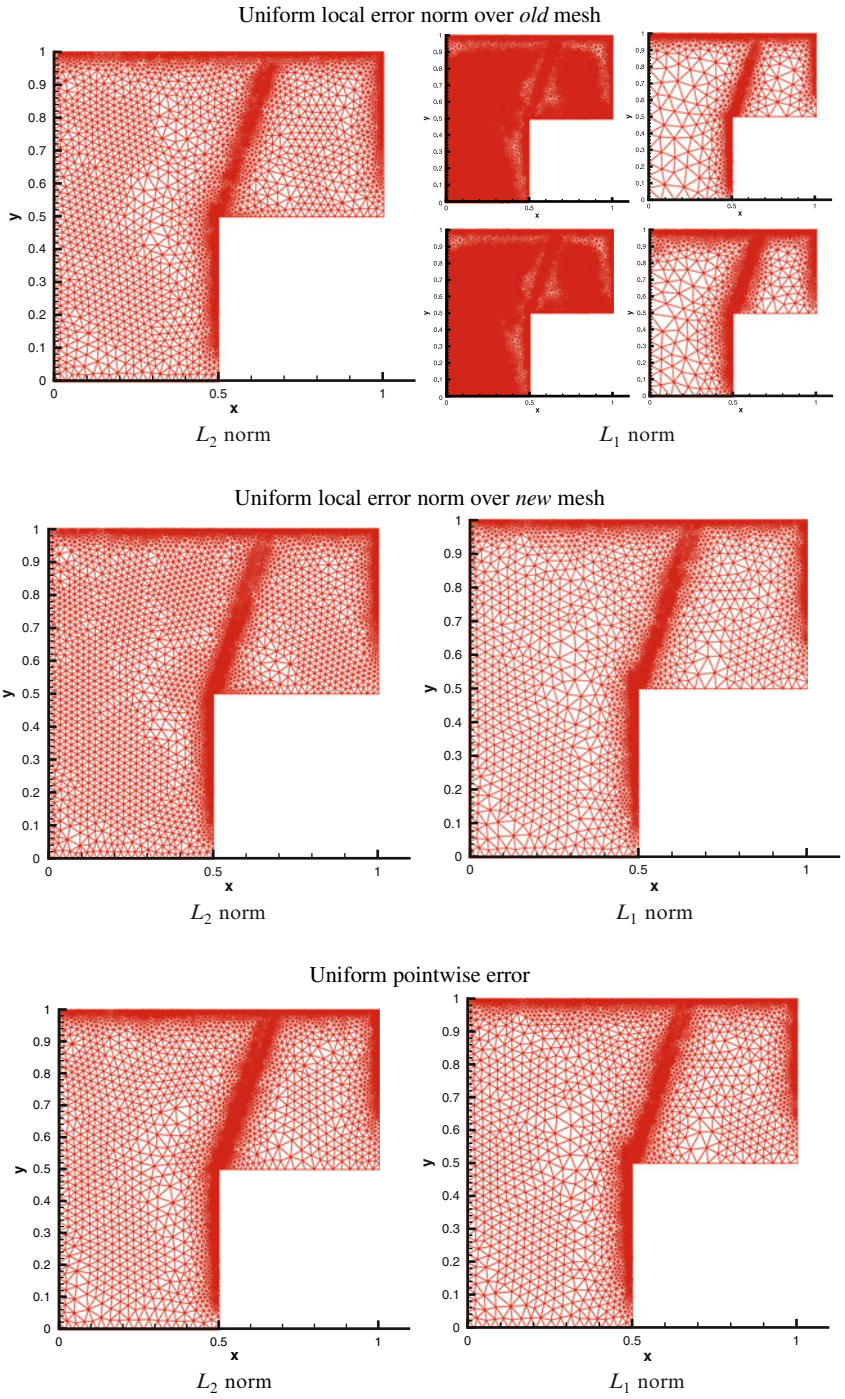

Fig. 5 Comparison of remeshing strategies. Fine meshes with $\kappa = 1.0 \times 10^{-6}$

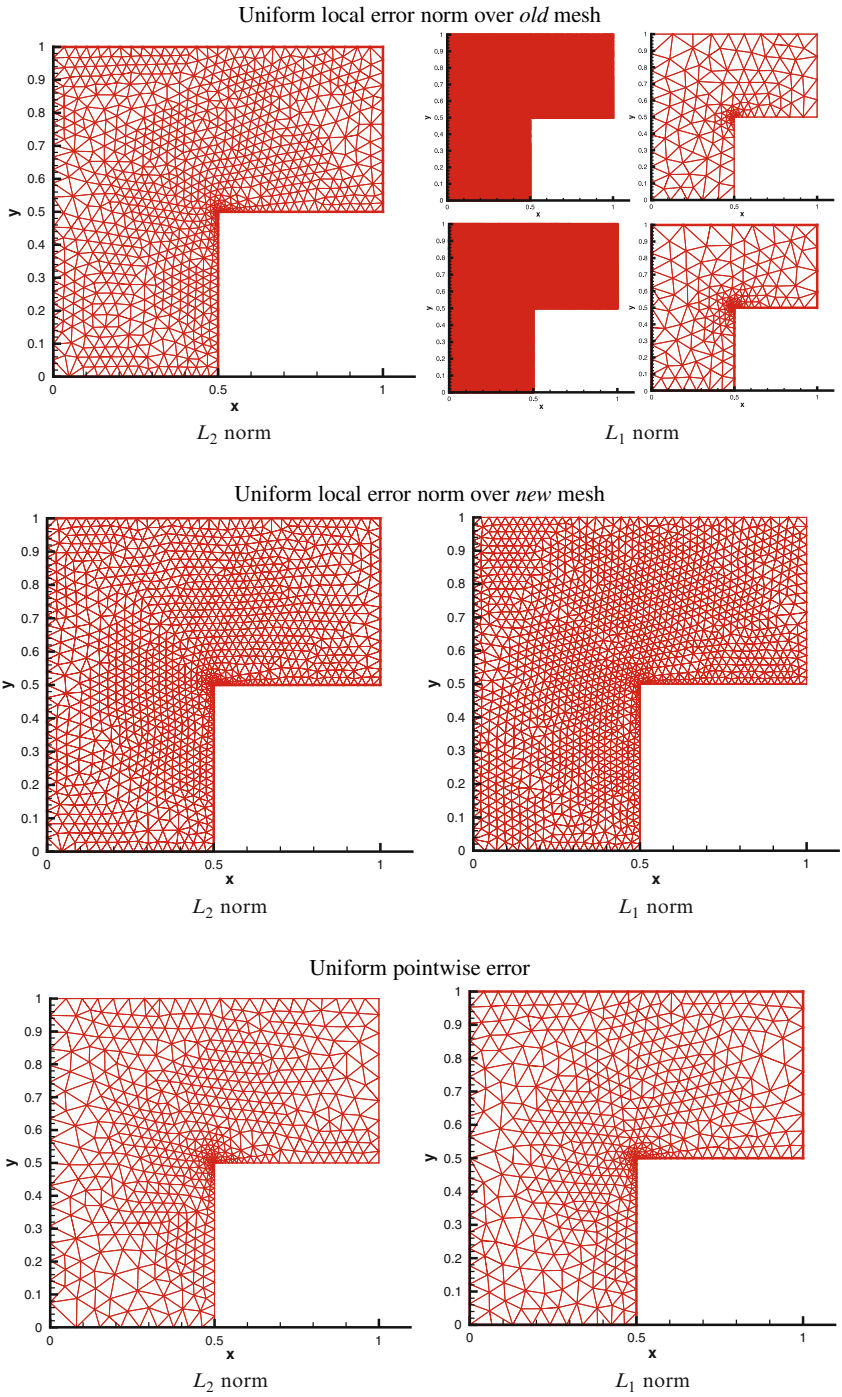

Fig. 6 Comparison of remeshing strategies. Fine meshes with $\kappa = 1.0$

References

1. Ainsworth, M., Oden, J.T.: A posterior error estimation in finite element analysis. John Wiley & Sons (2000)
2. Hauke, G.: A simple stabilized method for the advection-diffusion-reaction equation. Comput. Meth. Appl. Mech. Engrng. **191**, 2925–2947 (2002)
3. Hauke, G., Doweidar, M.H., Fuster, D.: A posteriori error estimation for computational fluid dynamics. The variational multiscale approach. In: E. Ramm, R. de Borst (eds.) Multiscale Methods in Computational Mechanics, *Lecture Notes in Applied and Computational Mechanics*, vol. 55. Springer (2010)
4. Hauke, G., Doweidar, M.H., Miana, M.: The multiscale approach to error estimation and adaptivity. Comput. Meth. Appl. Mech. Engrng. **195**, 1573–1593 (2006)
5. Hauke, G., Fuster, D., Doweidar, M.H.: Variational multiscale a-posteriori error estimation for the multi-dimensional transport equation. Comput. Meth. Appl. Mech. Engrg. **197**, 2701–2718 (2008)
6. Hughes, T.J.R.: Multiscale phenomena: Green's functions, the Dirichlet-to-Neumann formulation, subgrid scale models, bubbles and the origins of stabilized methods. Comput. Meth. Appl. Mech. Engrng. **127**, 387–401 (1995)
7. Hughes, T.J.R.: The finite element method:Linear static and dynamic finite element analysis. Dover Publications (2000)
8. Hughes, T.J.R., Feijoo, G.R., Mazzei, L., Quincy, J.B.: The variational multiscale method: A paradigm for computational mechanics. Comput. Meth. Appl. Mech. Engrng. **166**, 3–24 (1998)
9. John, V.: A numerical study of a posteriori error estimators for convection-diffusion equations. Comput. Methods Appl. Mech. Engrg. **190**, 757–781 (2000)

Numerical Simulation of Turbulent Incompressible and Compressible Flows Over Rough Walls

Petr Louda, Jaromír Příhoda, and Karel Kozel

1 Introduction

Wall roughness affects flow characteristics practically in all technical applications. In internal flows, the height of rough elements should be much smaller than the thickness of the shear layer (so called distributed roughness) and its influence on the flow cannot be directly simulated. Instead a model of rough wall is needed.

Wall roughness influences the flow structure only in the vicinity of the wall. The effect of wall roughness on the velocity profile can be expressed by the shift of the mean velocity profile in the logarithmic part of the wall region.

In this work, the SST k-ω model is used to compute two cases of incompressible flows over rough walls, and one case of compressible flow through a turbine cascade. Also Spalart-Allmaras model modified for rough walls [3] is tested on flat plate flow, but its results are not encouraging. Further, the same aproach as for the SST model is used for explicit algebraic Reynolds stress (EARSM) model by Wallin and Hellsten [5, 13]. This model uses k-ω system of equations very similar to SST one, and results show the effect of roughness can be incorporated with similar reliability as in the SST model. Results are compared with measurements and the effect of wall roughness shown by comparison with computation for smooth walls.

P. Louda (✉), and J. Příhoda
Institute of Thermomechanics v.v.i., Czech Academy of Sciences, Dolejškova 5, 182 00 Praha 8, Czech Republic,
e-mail: louda@it.cas.cz, prihoda@it.cas.cz

K. Kozel
Department of Technical Mathematis, Faculty of Mechanical Engineering, Czech Technical University in Prague, Karlovo nám. 13, 121 35 Praha 2, Czech Republic,
e-mail: karel.kozel@fs.cvut.cz

C. Clavero et al. (eds.), *BAIL 2010 – Boundary and Interior Layers, Computational and Asymptotic Methods*, Lecture Notes in Computational Science and Engineering 81,
DOI 10.1007/978-3-642-19665-2_17,

2 Mathematical and Numerical Model

The mathematical model of compressible turbulent flow is based on the Favre averaged Navier–Stokes equations in 2D case

$$\frac{\partial W}{\partial t} + \frac{\partial F_i}{\partial x_i} = \frac{\partial R_i}{\partial x_i},\ (i = 1,\ 2) \tag{1}$$

$$W = \begin{bmatrix} \rho \\ \rho u_1 \\ \rho u_2 \\ e \end{bmatrix},\ F_i = \begin{bmatrix} \rho u_i \\ u_i \rho u_1 + p\delta_{i1} \\ u_i \rho u_2 + p\delta_{i2} \\ u_i(e+p) \end{bmatrix},\ R_i = \begin{bmatrix} 0 \\ \sigma_{i1} - t_{i1} \\ \sigma_{i2} - t_{i2} \\ (\sigma_{ij} - t_{ij})u_j - q_i - q_i^t \end{bmatrix},$$

where ρ is mean density, u_i mean velocity vector, p mean static pressure, δ_{ij} is the Kronecker delta, σ_{ij} tensor of viscous stress, e mean total energy per unit volume and q_i heat flux vector. A state equation of perfect gas is assumed. The tensor t_{ij} is the Reynolds stress tensor and q_i^t turbulent heat flux. These terms are approximated by a turbulence model. For incompressible fluid flows, the corresponding system of simplified Navier–Stokes equations is used instead of the above system with $\rho = const$.

2.1 Turbulence Model

The eddy viscosity SST (Shear Stress Transport) model by Menter [4], defines the Reynolds stress tensor by eddy viscosity μ_t

$$t_{ij} = -\mu_t 2S_{ij} + \frac{2}{3}\rho k\delta_{ij},\ \mu_t = \frac{a_1 \rho k}{\max(a_1\omega, |\Omega| F_2)},\quad a_1 = 0.31 \tag{2}$$

where k is turbulent energy, ω specific dissipation rate and S_{ij} and Ω_{ij} are the strain rate tensor and the rotation tensor respectively. $|\Omega| = (\Omega_{ij}\Omega_{ij})^{1/2}$ is the absolute value of the rotation tensor. The function F_2 activates the Bradshaw hypothesis for the Reynolds shear stress $t_{12} = a_1 \rho k$, see [4].

The EARSM model by Wallin [13] can be expressed in terms of dimensionless anisotropy tensor a_{ij} as

$$\begin{aligned} t_{ij} &= a_{ij}\rho k + \frac{2}{3}\rho k\delta_{ij}, \\ a_{ij} &= \beta_1 \tau S_{ij} \\ &\quad + \beta_3 \tau^2 (\Omega_{ik}\Omega_{kj} - II_\Omega \delta_{ij}/3) + \beta_4 \tau^2 (S_{ik}\Omega_{kj} - \Omega_{ik}S_{kj}) \\ &\quad + \beta_6 \tau^3 (S_{ik}\Omega_{kl}\Omega_{lj} + \Omega_{ik}\Omega_{kl}S_{lj} - 2IV\delta_{ij}/3) \\ &\quad + \beta_9 \tau^4 (\Omega_{ik}S_{kl}\Omega_{lm}\Omega_{mj} - \Omega_{ik}\Omega_{kl}S_{lm}\Omega_{mj}), \end{aligned} \tag{3}$$

where τ is turbulent time scale and S_{ij}, Ω_{ij} are strain rate and rotation tensors, respectively. The invariants II_Ω, IV formed by S_{ij}, Ω_{ij} are given in Hellsten [5] as well as coefficients β. The original version of model by Wallin [13] has slightly different coefficients β. It should be noted, that only β_1, β_4 should be non-zero in a 2D mean flow. However, due to the necessary approximate explicit solution of the algebraic stress model, not all remaining coefficients are exactly zero in 2D. In this work the general 3D form of the model is used without regard to 2D geometrical configuration.

The turbulent heat flux is approximated by

$$q_i^t = q_i \frac{Pr}{\mu} \frac{\mu_t}{Pr_t}, \tag{4}$$

where the turbulent Prandtl number $Pr_t = 0.91$ and μ_t is defined using the linear part of the Reynolds stress tensor in the case of EARSM model.

Both turbulence models use the k-ω system of equations to estimate turbulent scales

$$\begin{aligned} \frac{D\rho k}{Dt} &= -t_{ij}\frac{\partial u_i}{\partial x_j} - \beta^* \rho k \omega + \frac{\partial}{\partial x_j}\left[(\mu + \sigma_k \mu_t)\frac{\partial k}{\partial x_j}\right], \\ \frac{D\rho \omega}{Dt} &= -\gamma \frac{\omega}{k} t_{ij}\frac{\partial u_i}{\partial x_j} - \beta \rho \omega^2 + \frac{\partial}{\partial x_j}\left[(\mu + \sigma_\omega \mu_t)\frac{\partial \omega}{\partial x_j}\right] + \rho \frac{\sigma_d}{\omega}\frac{\partial k}{\partial x_j}\frac{\partial \omega}{\partial x_j} \end{aligned} \tag{5}$$

where the derivative $D\cdot/Dt \equiv \partial\cdot/\partial t + \partial(u_j\cdot)/\partial x_j$. For the coefficients β^*, σ_k, γ, β, σ_ω, σ_d in the SST or EARSM model see [4] and [5] respectively.

2.2 Roughness Model

The effect of wall roughness on the velocity profile can be expressed by the shift of the mean velocity profile in the logarithmic part of the wall region Δu. According to Nikuradse [9] it is expressed using the equivalent sand grain roughness k_s

$$\frac{\Delta u}{u_\tau} = \frac{1}{\kappa} \ln \frac{u_\tau k_s}{\nu} - 3, \quad \kappa = 0.41 \tag{6}$$

where u_τ is the friction velocity. The velocity shift occurs also in a k-ω turbulence model if it is integrated up to the wall with wall value of ω which is not large enough. Wilcox [12] proposed value of ω on the rough wall in the form

$$\omega_w = \frac{u_\tau^2}{\nu} S_R, \quad S_R = \begin{cases} [50/\max(k_s^+, k_{\mathrm{smin}}^+)^2] & \text{for } k_s^+ < 25 \\ 100/k_s^+ & \text{for } k_s^+ \geq 25 \end{cases} \tag{7}$$

The smooth regime is reached for values $k_s^+ < 4$. Hellsten [5] observed that the wall shear stress is very sensitive to the value k_{smin}^+ which determines the smooth regime. To remove such dependence he proposed the following relation

$$k_{\text{smin}}^+ = \min[2.4(\Delta y_1^+)^{0.85}, 8] \tag{8}$$

where Δy_1^+ is the thickness of the grid cell next to the wall. The boundary condition given by (7) and (8) is used for the SST as well as the EARSM turbulence model.

The SST model is further modified according to Hellsten and Laine [6] by introduction of the function F_3 to prevent the activation of the SST limiter in the roughness layer

$$\mu_t = \frac{a_1 \rho k}{\max(a_1 \omega, |\Omega| F_2 F_3)}, \quad F_3 = 1 - \tanh\left(\frac{150\nu}{\omega y^2}\right)^4 \tag{9}$$

The function F_3 is equal zero near the wall and unity elsewhere.

3 Numerical Method

The system of governing equations is solved by the implicit upwind finite volume method. The cell centered finite volume method with quadrilateral finite volumes is applied for spatial discretization. The inviscid flux in the case of compressible flow is defined using the AUSM U-splitting [7]. A higher order of accuracy is achieved by the MUSCL interpolation in the directions of grid lines using the van Leer limiter. In the case of the steady incompressible flow an artificial compressibility method is used which consists of adding a pressure time derivative into the continuity equation

$$\frac{1}{a^2}\frac{\partial p}{\partial t} + \frac{\partial u_i}{\partial x_i} = 0, \tag{10}$$

where a is a positive constant parameter chosen for good convergence to a steady state. In this work a is approximately equal to the maximum velocity. The inviscid flux is discretized using the third order van Leer upwind interpolation in the direction of grid lines without limiter. The discretization of diffusive fluxes is central. The approximation of cell face derivatives needed in diffusive terms uses quadrilateral dual finite volumes constructed over each face of primary finite volume. The time integration uses the backward Euler implicit scheme. The non-linear discrete equations are linearized using the Newton method. The resulting block 5-diagonal system of algebraic equations is solved using block relaxation method with direct tri-diagonal solver for selected family of grid lines [2, 8].

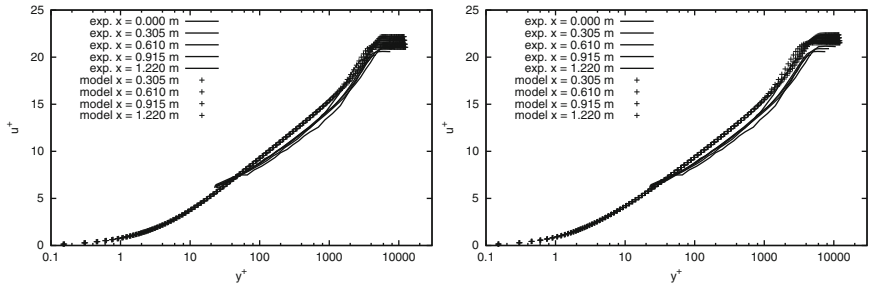

Fig. 1 Flat-plate flow, mean velocity profiles (*left*: SST model, *right*: EARSM model)

4 Computational Results

4.1 Flat Plate Flow

The roughness model was tested on the incompressible constant-pressure boundary layer. The measurement data are taken from Pimenta, Moffat and Kays [10]. The flat plate was covered by tightly packed spheres of 1.27 mm diameter, which corresponds to the equivalent sand roughness $k_s = 0.683$ mm. Numerical results are compared with experimental data for the free-stream velocity $U_e = 39.7$ m/s. Figure 1 shows mean velocity profiles in non-dimensional coordinates and Fig. 2 the distribution of the boundary layer thickness, here including also results of Spalart-Allmaras one-equation model. The computational results are in a good agreement with measurement, except for Spalart-Allmaras model which under-predicts wall shear stress.

4.2 Flow Over Ramp

Here an incompressible flow in a channel with ramp on the bottom wall according to measurements of Song and Eaton [11] is considered. The sketch of the channel with a smoothly contoured ramp formed by a circular arch with a radius of 127 mm is given in Fig. 3. The bottom wall was covered with 36-grit sandpaper from 1.3 m up-stream of the ramp to the ramp trailing edge. The wall roughness is characterized by the equivalent sand roughness $k_s = 2.4$ mm. Numerical simulation was carried out for the free stream velocity $U_e = 20$ m/s.

For smooth ramp, both SST and EARSM model give recirculation zone twice as long as measured (approx. 85 mm vs. 43 mm). In the case of rough ramp, the reattachment point is predicted nearly exactly. The separation point is not given exactly in the reference. Figure 4 shows profiles of mean velocity and shear Reynolds stress

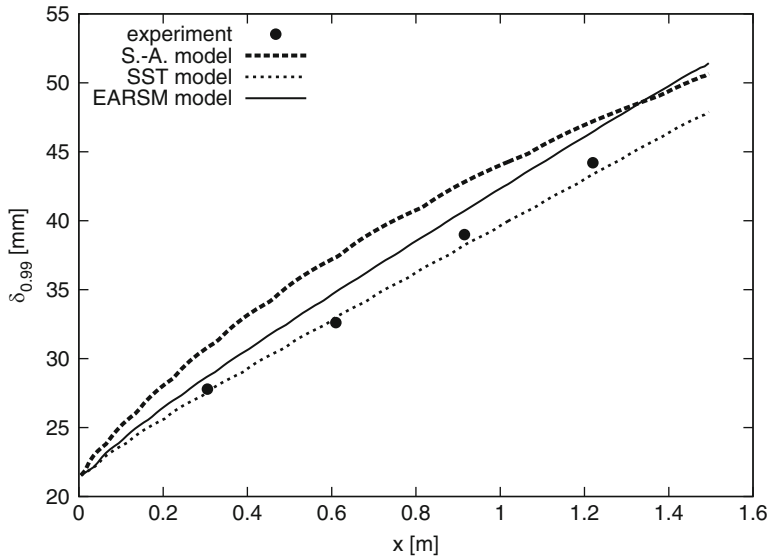

Fig. 2 Flat-plate flow, boundary layer thickness

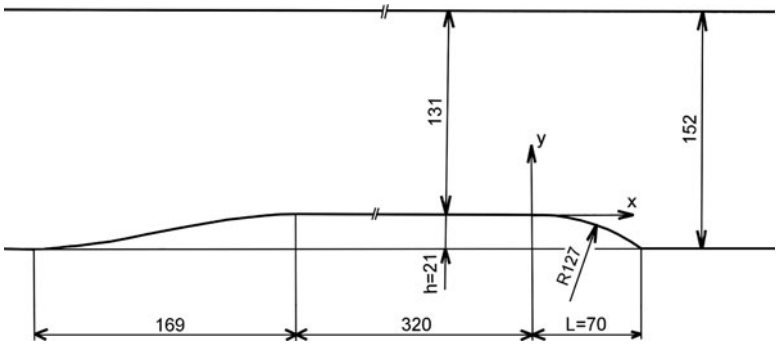

Fig. 3 Geometry of the circular ramp

compared to measurement [11]. The agreement with measurement is again better for the rough ramp than for smooth one (not shown).

4.3 Flow Through a Turbine Cascade

Finally, a subsonic flow through VS33 turbine blade cascade with the chord length $b = 75\,\text{mm}$ is considered. Two similar regimes are chosen which differ mainly by the roughness of the blade from measurements carried out by Ulrych et al. [1]. The value of $k_s = 0\,\text{mm}$ was considered for smooth blades, whereas for rough

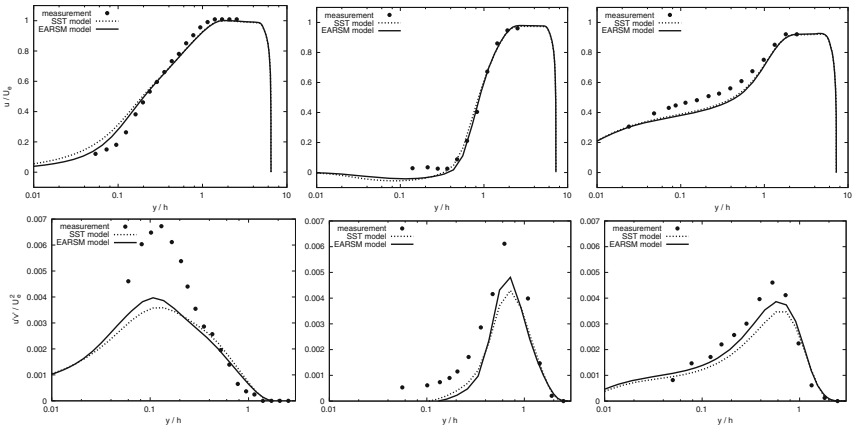

Fig. 4 Rough ramp: mean velocity and Reynolds shear stress in the middle of the ramp, at the end of the ramp, and 3 ramp lengths downstream (from left to right)

blades covered with carborundum particles with $Ra = 30\,\mu\text{m}$ the corresponding equivalent sand roughness $k_s = 0.174\,\text{mm}$ was used. The smooth regime is characterized by the isentropic outlet Mach number $M_{2is} = 0.88$, the Reynolds number $Re_{2is} = 8.4 \cdot 10^5$, and the angle of attack $\alpha_1 = 0°$ while the rough regime by values $M_{2is} = 0.90,\ Re_{2is} = 8.8 \cdot 10^5,\ \alpha_1 = 6°$. In both cases, the total temperature $T_0 = 293\ K$ and ratio of specific heats $\gamma = 1.4$ was considered.

The pressure and shear stress distribution on smooth and rough blades are shown in Fig. 5. There is no significant difference between SST and EARSM models. The roughness, as expected, influences mainly shear stress and not much the static pressure on the blade. The energy loss coefficient ξ was evaluated using the Laval numbers $\lambda_2,\ \lambda_{2is}$ according to relations

$$\xi = 100(1 - \lambda_2^2/\lambda_{iso2}^2),$$
$$\lambda_2^2 = \frac{\gamma+1}{2}\left[1 + \frac{\gamma-1}{2}M_{2is}^2\right]^{-1} M_{2is}^2, \quad \lambda_{iso2}^2 = \frac{\gamma+1}{\gamma-1}\left[1 - \left(\frac{p_2}{p_0}\right)^{\frac{\gamma-1}{\gamma}}\right] \tag{11}$$

where p_2 and p_0 are mean values of the static pressure behind the cascade and the total pressure obtained from mean mass and momentum fluxes. The overview of the loss coefficient is given in the Table 1. Although loss coefficients predicted by the both turbulence models differ, the wall roughness characterized by the parameter $Ra = 30\,\mu\text{m}$ causes always approximately equal increase in the loss coefficient by 62%–65%. The difference between measured and calculated losses for smooth blades could be caused by the fact that the prediction was carried out for turbulent flow only, without considering the laminar part. This difference is negligible for rough blades, as the laminar/turbulent transition occurs very early.

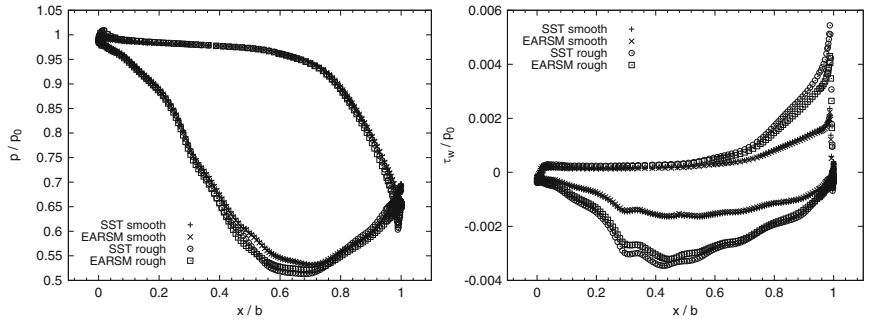

Fig. 5 Static pressure and friction on the blade

Table 1 Kinetic energy loss coefficient

	Measurement	SST model	EARSM model
Smooth blade	2.2%	4.3%	3.7%
Rough blade	6.6%	7.0%	6.1%
Increase by roughness	200%	62%	65%

5 Conclusions

The prescription of boundary conditions directly on the rough wall was tested in the framework of SST and EARSM turbulence models. Based on the considered cases, the roughness model developed for k-ω eddy viscosity model can be used in the EARSM model as well. This makes possible future 3D simulations with EARSM model and rough walls, where eddy viscosity models typically fail in capturing secondary flows. In the turbine cascade simulation the accounting for wall roughness causes same change in loss coefficient for both turbulence models, although this parameter is sensitive and different for both models. Nevertheless it can be assumed that the effect of wall roughness on the loss coefficient was adequately estimated.

Acknowledgements The research was partially supported by grant projects No. 103/09/0977 and P101/10/1230 of the Czech Science Foundation and by the Research Plans No. AV0Z20760514 and MSMT6840770010.

References

1. Ulrych, J., Benetka, J., Jelínek, T., Valenta, R., Tajč, L.: Experimental research of surface roughness impact on transonic flow in blade cascades, In: Proc. XVIII Symposium on Measuring Techniques in Turbomachinery, Thessaloniki, CD-ROM 7 p. (2006)
2. Louda P., Kozel K., Příhoda J.: Computation of turbulent compressible and incompressible flows. In: 8th International Symposium on Experimental and Computational Aerothermodynamics of Internal Flows, Lyon (2007)

3. Aupoix B., Spalart P.R.: Extension of the Spalart-Allmaras turbulence model to account for wall roughness, Int. J. Heat and Fluid Flow, **24**, 454–462 (2003)
4. Menter F. R.: Two-Equations Eddy-Viscosity Turbulence Models for Engineering Applications, AIAA J., Vol.32, **8**, 1598–1605 (1994)
5. Hellsten, A.: New advanced k-ω turbulence model for high-lift aerodynamics, AIAA J., **43**, 1857–1869 (2005)
6. Hellsten A., Laine S.: Extension of the k-ω SST turbulence model for flows over rough walls, AIAA Paper 97–3577 (1997)
7. Liou M.-S.: On a new class of flux splittings. Lecture Notes in Phys., **414**, 115–119 (1993)
8. Louda P., Kozel K., Příhoda J.: Numerical solution of 2D and 3D viscous incompressible steady and unsteady flows using artificial compressibility method. Int. J. for Numerical Methods in Fluids, **56**, 1399–1407 (2008)
9. Nikuradse J.: Strömungsgesetze in rauhen Rohren, VDI-Forschungsheft 361 (1933) (or NACA TM-1292, 1965)
10. Pimenta, M.M., Moffat, R.J., Kays, W.M.: The structure of a boundary layer on a rough wall with blowing and heat transfer, Jour. Heat Transfer, **101**, 193–198 (1979)
11. Song, S., Eaton, J.K.: The effects of wall roughness on the separated flow over a smoothly contoured ramp, Experiments in Fluids, **33**, 38–46 (2002)
12. Wilcox, D.: Reassessment of the scale-determining equation, AIAA J., **26**, 1299–1310 (1988)
13. Wallin, S.: Engineering turbulence modeling for CFD with a focus on explicit algebraic Reynolds stress models, PhD thesis, Royal Institute of Technology, Stockholm (2000)

A Projection-Based Variational Multiscale Method for the Incompressible Navier–Stokes/Fourier Model

Johannes Löwe, Gert Lube, and Lars Röhe

1 Introduction

In a bounded domain $\Omega \subset \mathbb{R}^d$, $d \in \{2, 3\}$, we consider the Navier–Stokes/Fourier equations as a model of non-isothermal, incompressible flows

$$\partial_t \mathbf{u} - \nabla \cdot (2\nu \mathbb{D}\mathbf{u}) + (\mathbf{u} \cdot \nabla)\mathbf{u} + \nabla p + \alpha \mathbf{g}\theta = \mathbf{f} \tag{1}$$

$$\nabla \cdot \mathbf{u} = 0 \quad \text{in } (0, T] \times \Omega \tag{2}$$

$$\partial_t \theta - \varkappa \Delta \theta + \mathbf{u} \cdot \nabla \theta = Q \tag{3}$$

$$\mathbf{u}|_{t=0} = \mathbf{u}_0, \quad \theta|_{t=0} = \theta_0 \quad \text{in } \{0\} \times \Omega \tag{4}$$

for velocity $\mathbf{u}$, pressure p, and temperature θ with appropriate boundary conditions. The deformation tensor is $\mathbb{D}\mathbf{u} = \frac{1}{2}(\nabla \mathbf{u} + (\nabla \mathbf{u})^t)$. Viscosity ν and diffusivity $\varkappa$, together with reference temperature $\theta_{\max} - \theta_{\min}$, characteristic length L, thermal expansion coefficient α and gravity vector $\mathbf{g}$ determine the relevant dimensionless Rayleigh number $Ra = \frac{\alpha |\mathbf{g}| L^3 (\theta_{\max} - \theta_{\min})}{\nu \varkappa}$.

In Sect. 2, we introduce a projection-based variational multiscale model. Section 3 is concerned with aspects of the numerical analysis of the semidiscrete model. Finally, in Sect. 4, the approach is applied to a benchmark problem of natural convection.

2 Variational Multiscale Model

Let $\mathcal{T}_h$ be an admissible triangulation of Ω s.t. $\overline{\Omega} = \cup_{K \in \mathcal{T}_h} \overline{K}$. For simplicity, we assume that Dirichlet boundary conditions for velocity and temperature are homogenized. Then, we seek conforming finite element (FE) approximations of

J. Löwe, G. Lube (✉), and L. Röhe
Institute for Numerical and Applied Mathematics, Georg-August University Göttingen, D-37083 Göttingen, Germany
e-mail: loewe/lube/roehe@math.uni-goettingen.de

C. Clavero et al. (eds.), *BAIL 2010 – Boundary and Interior Layers, Computational and Asymptotic Methods*, Lecture Notes in Computational Science and Engineering 81,
DOI 10.1007/978-3-642-19665-2_18,

velocity, pressure, and temperature in subspaces of

$$V = [H_0^1(\Omega)]^d, \quad Q = L_*^2(\Omega) = \{q \in L^2(\Omega) : \int_\Omega q \, dx = 0\}, \quad \Psi = H_0^1(\Omega).$$

Let us consider inf-sup stable velocity-pressure FE spaces $V_h \times Q_h \subset V \times Q$. The basic Galerkin FE method reads:
find $(\mathbf{u}_h, p_h, \theta_h)$: $[0,T] \to V_h \times Q_h \times \Psi_h$ s.t. for all $(\mathbf{v}_h, q_h, \psi_h) \in V_h \times Q_h \times \Psi_h$

$$\begin{aligned}(\partial_t \mathbf{u}_h, \mathbf{v}_h) + (2\nu \mathbb{D}\mathbf{u_h}, \mathbb{D}\mathbf{v_h}) + b_S(\mathbf{u}_h, \mathbf{u}_h, \mathbf{v}_h) + (\alpha \mathbf{g}\theta_h, \mathbf{v}_h) \\ -(p_h, \nabla \cdot \mathbf{v}_h) + (q_h, \nabla \cdot \mathbf{u}_h) = (\mathbf{f}, \mathbf{v}_h) \qquad (5)\\ (\partial_t \theta_h, \psi_h) + (\varkappa \nabla \theta_h, \nabla \psi_h) + c_S(\mathbf{u}_h, \theta_h, \psi_h) = (Q, \psi_h) \qquad (6)\end{aligned}$$

with the skew-symmetric form of the advective terms

$$\begin{aligned} b_S(\mathbf{u}, \mathbf{v}, \mathbf{w}) &:= [((\mathbf{u} \cdot \nabla)\mathbf{v}, \mathbf{w}) - ((\mathbf{u} \cdot \nabla)\mathbf{w}, \mathbf{v})]/2, \\ c_S(\mathbf{u}, \theta, \psi) &:= [((\mathbf{u} \cdot \nabla)\theta, \psi) - ((\mathbf{u} \cdot \nabla)\psi, \theta)]/2. \end{aligned}$$

The variational multiscale (VMS) approach, developed by Hughes [5], has been used as a tool for scale separation in turbulence since 2000; for a review see [3]. Consider a three-scale decomposition

$$V \ni \mathbf{v} = \underbrace{\overline{\mathbf{v}}_h + \tilde{\mathbf{v}}_h}_{=\mathbf{v}_h \in V_h} + \hat{\mathbf{v}}_h; \quad Q \ni q = \underbrace{\overline{q}_h + \tilde{q}_h}_{=q_h \in Q_h} + \hat{q}_h; \quad \Psi \ni \psi = \underbrace{\overline{\psi}_h + \tilde{\psi}_h}_{=\psi_h \in \Psi_h} + \hat{\psi}_h$$

with resolved scales $(\mathbf{v}_h, q_h, \psi_h) \in V_h \times Q_h \times \Psi_h \subset V \times Q \times \Psi$. Inspired by [8], for the model influence of $(\hat{\mathbf{v}}_h, \hat{q}_h, \hat{\psi}_h)$ on $(\tilde{\mathbf{v}}_h, \tilde{q}_h, \tilde{\psi}_h)$ define discontinuous FE spaces L_H, M_H for the deformation tensor and temperature gradient

$$\begin{aligned} &\{0\} \subseteq L_H \subseteq L := \left\{\mathbf{L} = (l_{ij}) \in [L^2(\Omega)]^{d\times d} \mid l_{ij} = l_{ji}, 1 \le i, j \le d\right\} \\ &\{0\} \subseteq M_H \subseteq M := [L^2(\Omega)]^d \end{aligned}$$

on $\mathcal{T}_H, H \ge h$ and the L^2-orthogonal projection operators $\Pi_H^u : L \to L_H$ and $\Pi_H^\theta : M \to M_H$ together with the fluctuation operators

$$\kappa_u(\mathbb{D}\mathbf{u}_h) := (Id - \Pi_H^u)(\mathbb{D}\mathbf{u}_h), \qquad \kappa_\theta(\nabla\theta_h) := (Id - \Pi_H^\theta)(\nabla\theta_h).$$

For the calibration of the subgrid models for velocity and temperature, we introduce cellwise constant terms $\nu_S(\mathbf{u}_h, \theta_h)$ and $\varkappa_S(\mathbf{u}_h, \theta_h)$ s.t.

$$\nu_S^K(\mathbf{u}_h, \theta_h) := \nu_S(\mathbf{u}_h, \theta_h)|_K, \qquad \varkappa_S^K(\mathbf{u}_h, \theta_h) := \varkappa_S(\mathbf{u}_h, \theta_h)|_K.$$

As model of the small unresolved pressure scales we add grad-div stabilization with cellwise constant $\gamma_K(\mathbf{u}_h, p_h) := \gamma(\mathbf{u}_h, p_h)|_K$ s.t.

$$(\gamma(\mathbf{u}_h, p_h)(\nabla \cdot \mathbf{u}_h), \nabla \cdot \mathbf{v}_h) := \sum_{K \in \mathcal{T}_h} \gamma_K(\mathbf{u}_h, p_h)(\nabla \cdot \mathbf{u}_h, \nabla \cdot \mathbf{v}_h)_K.$$

Summarizing, we obtain the following variational multiscale model:
find $(\mathbf{u}_h, p_h, \theta_h)$ s.t. for all $(\mathbf{v}_h, q_h, \psi_h) \in V_h \times Q_h \times \Psi_h$:

$$\begin{aligned}
&(\partial_t \mathbf{u}_h, \mathbf{v}_h) + 2\nu\,(\mathbb{D}\mathbf{u}_h, \mathbb{D}\mathbf{v}_h) + b_S(\mathbf{u}_h, \mathbf{u}_h, \mathbf{v}_h) + (\alpha \mathbf{g}\theta_h, \mathbf{v}_h) \\
&+ (\nu_S(\mathbf{u}_h, \theta_h)\kappa_u \mathbb{D}(\mathbf{u}_h), \kappa_u \mathbb{D}(\mathbf{v}_h)) + (\gamma(\mathbf{u}_h, p_h)\nabla \cdot \mathbf{u}_h, \nabla \cdot \mathbf{v}_h) \qquad (7)\\
&+ (\nabla \cdot \mathbf{u}_h, q_h) - (\nabla \cdot \mathbf{v}_h, p_h) = (\mathbf{f}, \mathbf{v}_h) \qquad (8)\\
&(\partial_t \theta_h, \psi_h) + (\varkappa \nabla \theta_h, \nabla \psi_h) + c_S(\mathbf{u}_h, \theta_h, \psi_h) \\
&+ (\varkappa_S(\mathbf{u}_h, \theta_h)\kappa_\theta(\nabla \theta_h), \kappa_\theta(\nabla \psi_h)) = (Q, \psi_h). \qquad (9)
\end{aligned}$$

3 A Priori Error Analysis of the Semidiscrete Model

Following [7], we obtain stability estimates for the VMS scheme (7)–(9).

Lemma 1. *Let* $\mathbf{f} \in L^1(0,T;L^2(\Omega))$, $Q \in L^1(0,T;L^2(\Omega))$ *and* $\mathbf{u}_0 \in [L^2(\Omega)]^d$, $\theta_0 \in L^2(\Omega)$. *Then we obtain for* $t \in (0,T]$ *control of kinetic and heat energy*

$$\begin{aligned}
\|\theta_h\|_{L^\infty(0,t;L^2(\Omega))} &\le K_1(Q, \theta_0) &&:= \|\theta_0\|_0 + \|Q\|_{L^1(0,t;L^2(\Omega))}\\
\|\mathbf{u}_h\|_{L^\infty(0,t;L^2(\Omega))} &\le K_2(\mathbf{f}, \mathbf{u}_0, Q, \theta_0) &&:= \|\mathbf{u}_0\|_0 + \|\mathbf{f}\|_{L^1(0,t;L^2(\Omega))} + C\alpha\|\mathbf{g}\|_0 K_1
\end{aligned}$$

and control of dissipation and subgrid terms

$$\begin{aligned}
\varkappa\|\nabla\theta_h\|^2_{L^2(0,t;L^2(\Omega))} + \int_0^t \sum_K \varkappa_S^K(\mathbf{u}_h, \theta_h)\|\kappa_\theta \nabla\theta_h\|^2_{0,K} dt &\le \frac{3}{2}K_1^2\\
\nu\|\mathbb{D}\mathbf{u}_h\|^2_{L^2(0,t;L^2(\Omega))} + \frac{1}{2}\int_0^t \sum_K \nu_S^K(\mathbf{u}_h, \theta_h)\|\kappa_u \mathbb{D}\mathbf{u}_h\|^2_{0,K} dt &\\
+ \frac{1}{2}\int_0^t \sum_K \gamma_K(\mathbf{u}_h, p_h)\|\nabla \cdot \mathbf{u}_h\|^2_{0,K} dt &\le 3K_2^2.
\end{aligned}$$

Now we introduce elementwise multiscale viscosities $\nu^K_{VMS}, \varkappa^K_{VMS}$ via

$$\sum_{K \in \mathcal{T}_h} \nu_S^K(\mathbf{u}_h, \theta_h)\,\|\kappa_u \mathbb{D}\mathbf{v}_h\|^2_{0,K} = \sum_{K \in \mathcal{T}_h} \underbrace{\nu_S^K(\mathbf{u}_h, \theta_h)\left(1 - \frac{\left\|\Pi_H^u \mathbb{D}\mathbf{v}_h\right\|^2_{0,K}}{\|\mathbb{D}\mathbf{v}_h\|^2_{0,K}}\right)}_{=:\nu^K_{\mathrm{VMS}}(\mathbf{v}_h) \ge 0} \|\mathbb{D}\mathbf{v}_h\|^2_{0,K},$$

$$\sum_{K\in\mathcal{T}_h} \varkappa_S^K(\mathbf{u}_h,\theta_h)\,\|\kappa_\theta\nabla\psi_h\|_{0,K}^2 = \sum_{K\in\mathcal{T}_h} \underbrace{\varkappa_S^K(\mathbf{u}_h,\theta_h)\left(1-\frac{\left\|\Pi_H^\theta\nabla\psi_h\right\|_{0,K}^2}{\|\nabla\psi_h\|_{0,K}^2}\right)}_{=:\varkappa_{\mathrm{VMS}}^K(\psi_h)\geq 0} \|\nabla\psi_h\|_{0,K}^2$$

where we applied the projector properties of the fluctuation operators.

In the following we will omit the dependency of the parameters on $\mathbf{u}_h, \theta_h$ for better readability. Using the modified elementwise viscosities

$$\nu_{\mathrm{mod}}^K(\mathbf{v}_h) := 2\nu + \nu_{\mathrm{VMS}}^K(\mathbf{v}_h), \quad \varkappa_{\mathrm{mod}}^K(\psi_h) := \varkappa + \varkappa_{\mathrm{VMS}}^K(\psi_h)$$

we define the following mesh-dependent expressions

$$|||\mathbf{u}(t)|||^2 := \|\mathbf{u}(t)\|_0^2 + \sum_{K\in\mathcal{T}_h}\int_0^t \left(\frac{\nu_{\mathrm{mod}}^K(\mathbf{u})}{2}\,\|\mathbb{D}\mathbf{u}\|_{0,K}^2 + \gamma_K(\mathbf{u}_h,p_h)\,\|\nabla\cdot\mathbf{u}\|_{0,K}^2\right) dt,$$

$$|[\theta(t)]|^2 := \|\theta(t)\|_0^2 + \sum_{K\in\mathcal{T}_h}\int_0^t \frac{1}{2}\varkappa_{\mathrm{mod}}^K(\theta)\,\|\nabla\theta\|_{0,K}^2\,dt.$$

The following semidiscrete a priori estimate is an extension of a previous result in [6] and [10] for the isothermal case. The proof takes advantage of the fact that, for inf-sup stable FE spaces for velocity/pressure, the space V_h^{div} of discretely divergence free functions is not empty. Thus one can separate estimates for velocity/temperature and pressure and apply an interpolation operator by Girault/Scott [2] in V_h^{div} on isotropic meshes.

Theorem 1. *For a sufficiently smooth solution* $(\mathbf{u},\theta)$ *of the Navier–Stokes/Fourier model with* $\nabla\mathbf{u} \in L^4(0,t;L^2\Omega))$, $\partial_t\mathbf{u} \in L^2(0,t;H^{-1}(\Omega))$ *and* $\nabla\theta \in L^4(0,t;L^2\Omega))$, $\partial_t\theta \in L^2(0,t;H^{-1}(\Omega))$, *it holds for the solution of (7)–(9) for all* $t\in(0,T)$*:*

$$\begin{aligned}|||(\mathbf{u}-\mathbf{u}_h)(t)|||^2 + |[(\theta-\theta_h)(t)]|^2 \\ \leq 2\inf_{\substack{\tilde{\mathbf{u}}_h\in L^2(0,t;V_h^{div})\\ \tilde{\theta}_h\in L^2(0,t;\Psi_h)}} |||(\mathbf{u}-\tilde{\mathbf{u}}_h)(t)|||^2 + |[(\theta-\tilde{\theta}_h)(t)]|^2\end{aligned}$$

$$+\inf_{\substack{\tilde{\mathbf{u}}_h\in L^4(0,t;V_h^{div})\\ \tilde{p}_h\in L^2(0,t;Q_h)\\ \tilde{\theta}_h\in L^2(0,t;\Psi_h)}} e^{\int_0^t g(s)ds}\left(\|(\mathbf{u}_h-\tilde{\mathbf{u}}_h)(0)\|_0^2 + \|(\theta_h-\tilde{\theta}_h)(0)\|_0^2 + \int_0^t g_2(s)ds\right)$$

with

$$g(t) := \frac{27C_{LT}^4}{2\nu_{\mathrm{mod}}^{\min}(\mathbf{e}_h^u)^3}\,\|\mathbb{D}\mathbf{u}\|_0^4 + \frac{8C_1^4}{\nu_{\mathrm{mod}}^{\min}(\mathbf{e}_h^u)\,\varkappa_{\mathrm{mod}}^{\min}(e_h^\theta)^2}\,\|\nabla\theta\|_0^4 + 2\alpha\,\|\mathbf{g}\|_\infty,$$

$$
\begin{aligned}
g_2(t) :=& 2 \sum_{K\in\mathcal{T}_h} \left[\min\left(\frac{9C_{Ko}^2}{\nu_{\mathrm{mod}}^{\min}(\mathbf{e}_h^u)}, \frac{1}{\gamma_K(\mathbf{u}_h)} \right) \left(\|p-\tilde{p}_h\|_{0,K}^2 + \gamma_K^2(\mathbf{u}_h)\, \|\nabla\cdot\epsilon^u\|_{0,K}^2 \right) \right. \\
&+ 6\Big(\nu + \nu_{\mathrm{VMS}}^K(\epsilon^u)\Big)\, \|\mathbb{D}\epsilon^u\|_{0,K}^2 + \Big(2\varkappa + 4\varkappa_{\mathrm{VMS}}^K(\epsilon^\theta)\Big) \left\|\nabla\epsilon^\theta\right\|_{0,K}^2 \\
&\left. + 6\nu_S^K(\mathbf{u}_h,\theta_h)\, \|\kappa_u \mathbb{D}\mathbf{u}\|_{0,K}^2 + 4\varkappa_S^K(\mathbf{u}_h,\theta_h)\, \|\kappa_\theta \nabla\theta\|_{0,K}^2 \right] \\
&+ \frac{6C_{Ko}^2}{\nu_{\mathrm{mod}}^{\min}(\mathbf{e}_h^u)}\, \|\partial_t\epsilon^u\|_{-1,\Omega}^2 + \frac{4}{\varkappa_{\mathrm{mod}}^{\min}(e_h^\theta)} \left\|\partial_t\epsilon^\theta\right\|_{-1,\Omega}^2 + \alpha|\mathbf{g}|_\infty \left\|\epsilon^\theta\right\|_0^2 \\
&+ \frac{6C_{LT}^2}{\nu_{\mathrm{mod}}^{\min}(\mathbf{e}_h^u)} \Big(C_F C_{Ko}\, \|\mathbb{D}\mathbf{u}\|_0^2 + \|\mathbf{u}_h\|_0\, \|\mathbb{D}\mathbf{u}_h\|_0 \Big)\, \|\mathbb{D}\epsilon^u\|_0^2 \\
&+ \frac{4C_1^2 C_{Ko}}{\varkappa_{\mathrm{mod}}^{\min}(e_h^\theta)} \left(C_F C_{Ko}\, \|\nabla\theta\|_0^2\, \|\mathbb{D}\epsilon^u\|_0^2 + \|\mathbf{u}_h\|_0\, \|\mathbb{D}\mathbf{u}_h\|_0 \left\|\nabla\epsilon^\theta\right\|_0^2 \right)
\end{aligned}
$$

where $\nu_{\mathrm{mod}}^{\min}(\mathbf{e}_h^u) := \min_{K\in\mathcal{T}_h} \nu_{\mathrm{mod}}^K(\mathbf{e}_h^u)$, $\varkappa_{\mathrm{mod}}^{\min}(e_h^\theta) := \min_{K\in\mathcal{T}_h} \varkappa_{\mathrm{mod}}^K(e_h^\theta)$ *and*

$$
\mathbf{u}_h - \mathbf{u} = (\mathbf{u}_h - \tilde{\mathbf{u}}_h) - (\mathbf{u} - \tilde{\mathbf{u}}_h) =: \mathbf{e}_h^u - \epsilon^u, \quad \theta_h - \theta = (\theta_h - \tilde{\theta}_h) - (\theta - \tilde{\theta}_h) =: e_h^\theta - \epsilon^\theta.
$$

C_F and C_{Ko} are the constants of the inequalities of Friedrichs and Korn. C_{LT} and C_1 are related to upper bounds of the advective terms.

Sketch of the proof: Please note that the regularity assumptions imply uniqueness of the continuous solution $(\mathbf{u}, p, \theta)$. Starting from the error equations for $\mathbf{e}_h^u$ and e_h^θ, careful estimates of the right hand side terms lead to

$$
\partial_t \left(\left\|\mathbf{e}_h^u\right\|_0^2 + \|e_h^\theta\|_0^2 \right) + g_1(t) \le g(t) \left(\left\|\mathbf{e}_h^u\right\|_0^2 + \|e_h^\theta\|_0^2 \right) + g_2(t)
$$

with $g(t)$ and $g_2(t)$ as stated in the Theorem and

$$
\begin{aligned}
g_1(t) :=& \frac{1}{4} \sum_{K\in\mathcal{T}_h} \nu_{\mathrm{mod}}^K(\mathbf{e}_h^u) \left\|\mathbb{D}\mathbf{e}_h^u\right\|_{0,K}^2 + \frac{1}{2} \sum_{K\in\mathcal{T}_h} \varkappa_{\mathrm{mod}}^K(e_h^\theta) \left\|\nabla e_h^\theta\right\|_{0,K}^2 \\
&+ \sum_{K\in\mathcal{T}_h} \gamma_K(\mathbf{u}_h, p_h)\, \|\nabla\cdot\mathbf{e}_h\|_{0,K}^2 .
\end{aligned}
$$

Gronwall's Lemma implies for all $t \in [0,T]$

$$
\left\|\mathbf{e}_h^u(t)\right\|_0^2 + \|e_h^\theta(t)\|_0^2 + \int_0^t g_1(s)ds \le e^{\int_0^t g(s)ds} \Big(\left\|\mathbf{e}_h^u(0)\right\|_0^2 + \|\mathbf{e}_h^\theta(0)\|_0^2 + \int_0^t g_2(s)ds \Big).
$$

Finally, the triangle inequality concludes the proof. For full details of the proof, we refer to [9]. □

Let us discuss the result for FE spaces $\mathbb{Q}_k/\mathbb{Q}_{k-1}/\mathbb{Q}_k$ or $\mathbb{P}_k/\mathbb{P}_{k-1}/\mathbb{P}_k$ for $(\mathbf{u}_h, p_h, \theta_h)$ on isotropic meshes. Moreover, we formally assume sufficiently smooth solutions $(\mathbf{u}, p, \theta)$ of the continuous model. In particular, it can be shown that the piecewise constants $\nu_{\text{mod}}^{\min}(\mathbf{e}_h^u)$, $\varkappa_{\text{mod}}^{\min}(e_h^\theta)$, and $\gamma_K(\mathbf{u}_h, p_h)$, occuring on the right hand side of the error estimate, remain bounded.

The third line of term $g_2(t)$ consists of model errors. Let us assume $\nu_S^K(\mathbf{u}_h, \theta_h), \varkappa_S^K(\mathbf{u}_h, \theta_h) = \mathcal{O}(h_K^2)$ for the subgrid functions. For the discontinuous spaces $L_H = [\mathbb{Q}_{k-2}^{disc}]^{d\times d}$, $M_H = [\mathbb{Q}_{k-2}^{disc}]^d$, or $\mathbb{Q}_{k-2}^{disc}$ replaced with $\mathbb{P}_{k-2}^{disc}$, the fluctuation operators provide an interpolation error of $\mathcal{O}(h_K^{2(k-1)})$. Thus the model error terms are of order $\mathbb{O}(h^{2k})$.

The remaining approximation terms in $g_2(t)$ are formally of order $\mathbb{O}(h^{2k})$, based on the V_h^{div}-interpolation operator on isotropic meshes, see [2]. Properly chosen subgrid parameters improve the estimate. see, e.g., the role of γ_K. Moreover, in term $g(t)$, viscosity ν is replaced with $\nu + \frac{1}{2}\min_K \nu_{VMS}^K(\mathbf{u}_h; \mathbf{u} - \tilde{\mathbf{u}}_h)$, which corresponds to an increased effective Reynolds number. A similar argument holds for $\varkappa$.

Let us finally consider the Gronwall factor $e^{\int_0^t g(s)ds}$. Following [4], this factor is unavoidable for unstable solutions of the Navier–Stokes problem. It can be avoided in case of (quasi-)exponentially stable solutions.

4 Application to Natural Convection Flow

For the spatial discretization we apply quadrilateral meshes with FE spaces $\mathbb{Q}_2/\mathbb{Q}_1/\mathbb{Q}_2$ for velocity/pressure/temperature within the FE package `deal.II`, see [1]. The arising semidiscrete problem of the form

$$\begin{pmatrix} M_u & 0 & 0 \\ 0 & M_\theta & 0 \\ 0 & 0 & 0 \end{pmatrix} \begin{pmatrix} \mathbf{u}_h'(t) \\ \boldsymbol{\theta}_h'(t) \\ \mathbf{p}_h'(t) \end{pmatrix} = \begin{pmatrix} \mathbf{f}_h(t) \\ \mathbf{q}_h(t) \\ 0 \end{pmatrix} - \begin{pmatrix} A_u(\mathbf{u}_h) & C & B \\ 0 & A_\theta(\mathbf{u}_h) & 0 \\ B^T & 0 & 0 \end{pmatrix} \begin{pmatrix} \mathbf{u}_h(t) \\ \boldsymbol{\theta}_h(t) \\ \mathbf{p}_h(t) \end{pmatrix}$$

is a DAE-system with differentiation index 2 and perturbation index 2. For the time discretization, we apply the BDF(2)-formula for velocity

$$\mathbf{u}_h'(t_{n+1}) \approx [3\mathbf{u}_h(t_{n+1}) - 4\mathbf{u}_h(t_n) + \mathbf{u}_h(t_{n-1})]/(2\tau_n)$$

and similarly for $\boldsymbol{\theta}_h'(t_{n+1})$. This results in favourable stability properties and does not lead to order reduction for the algebraic variable. A fixed-point iteration is performed for the arising non-linear implicit scheme.

In a next step, we have to introduce the non-isothermal viscosity model. We start from the residual stress tensor τ^R and residual temperature flux $\mathbf{h}$

$$\tau^R := \langle \mathbf{u} \otimes \mathbf{u} \rangle - \mathbf{u}_h \otimes \mathbf{u}_h \approx -2\nu_S \mathbb{D}\mathbf{u}_h, \qquad \mathbf{h} := \langle \mathbf{u}\theta \rangle - \mathbf{u}_h\theta_h \approx -\varkappa_S \nabla\theta_h$$

and apply the subgrid model of Smagorinsky-Edison [12]

$$\nu_S = (C_E \Delta)^2 \max\left(0\,, \|\mathbb{D}\mathbf{u}_h\|_F^2 + \frac{\beta}{Pr_S}\mathbf{g}\cdot\nabla\theta_h\right)^{1/2}, \qquad \varkappa_S = \nu_S/Pr_S$$

with $C_E = 0.21$ and $Pr_S = 0.4$. As filter width Δ we use an anisotropic scaling matrix that takes local mesh anisotropy and orientation into account. This approach gave better results than taking an isotropic filter width (e.g. length of shortest edge). The model reduces to the Smagorinsky model if $\mathbf{g}\cdot\nabla\theta_h = 0$. For wall bounded flows the turbulent viscosities may be multiplied by van Driest-type damping functions for reasonable near wall behavior. It is well known that the Smagorinsky model is over-diffusive. A reduction of model dissipation may then be established by an application of the fluctuation operators

$$\tau^R = -2\nu_S\kappa_u(\mathbb{D}\mathbf{u}_h), \qquad \mathbf{h} = -\varkappa_S\kappa_\theta(\nabla\theta_h).$$

In our implementation, we use an one-level approach with $H = h$ and the discontinuous spaces $L_h = [\mathbb{Q}_0^{disc}]^{d\times d}$ and $M_h = [\mathbb{Q}_0^{disc}]^d$.

Now we apply the method to natural convection in a differentially heated cavity $\Omega := (0,1)^d$. The numerical simulations in [12] in a three-dimensional cavity show that for appropriate boundary conditions in x_3-direction there appears a statistically two-dimensional flow. This motivates the present restriction to $d = 2$. Heating $\theta = \theta_{\max}$ and cooling $\theta = \theta_{\min}$ is performed at lateral boundaries, whereas the upper and lower boundaries are highly conducting. As suggested in [11] we use experimental data as boundary conditions on these walls. No-slip conditions $\boldsymbol{u} = \mathbf{0}$ for velocity are given at the whole boundary $\partial\Omega$. Computations were done on two meshes with 64 and 32 cells in each dimension. An anisotropic mesh refinement had been performed at all boundaries by transforming an equidistant reference mesh with $x = \hat{x} - \frac{19}{40\pi}\sin(2\pi\hat{x})$ and $y = \hat{y} - \frac{7}{16\pi}\sin(2\pi\hat{y})$. The maximum aspect-ratio of cells at the vertical walls was about 36:1.

Let us present some first results for time-averaged quantities of a low-turbulence flow at $Ra = 1.58 \times 10^9$. Here we used the projection-based VMS with Smagorinsky-Edison parametrization of the subgrid model without van Driest damping. On both meshes the results for velocity and temperature profiles, wall shear stress (see Figs. 1 and 2) and Nusselt number (not shown) are in good agreement to experimental data of [11]. Interestingly, we observed (for fixed parameters) no big difference of the solutions on the two grids with exception of wall-shear stress.

We used grad-div stabilization with constant $\gamma_K = 0.3$ to improve the mass conservation properties of the scheme. On the coarse grid with $n = 32$, we obtained $\|\nabla\cdot\mathbf{u}_h\|_0 = 0.0029$ for $\gamma = 0.3$ as opposed to $\|\nabla\cdot\mathbf{u}_h\|_0 = 0.0517$ for $\gamma = 0$, i.e., an improvement by a factor of 18.

One critical point of the simulation is the separation of the flow at the vertical walls and its reattachment at the horizontal walls. Experiments show small counter-rotating vortices in these corners, which we also found in our simulations on the fine mesh.

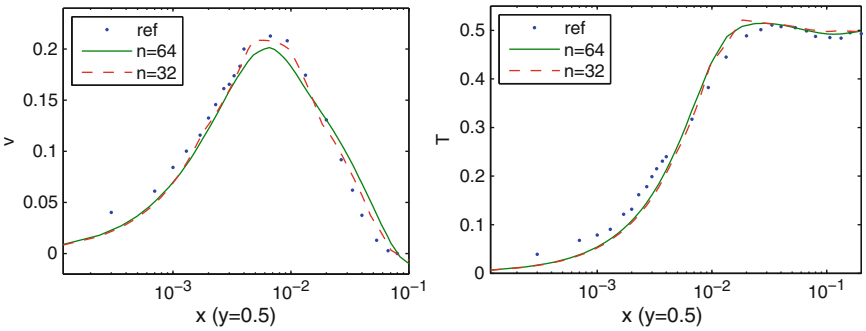

Fig. 1 Boundary layer profiles for horizontal velocity profile $v(x, 0.5)$ (*left*) and for horizontal temperature profile $T(x, 0.5)$ (*right*) and experimental data [11]

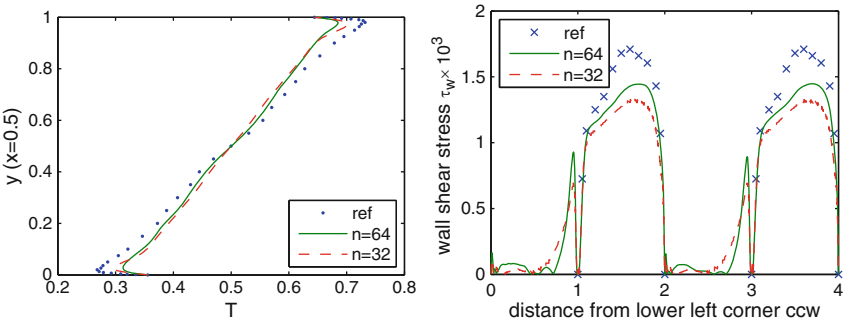

Fig. 2 Temperature profile on vertical centerline $T(0.5, y)$ (*left*) and wall shear stress (*right*) and experimental data of [11]

5 Summary and Outlook

In this paper, we applied a variational multiscale model to the time-dependent Navier–Stokes/Fourier model of incompressible and non-isothermal flows. For the case of piecewise nonlinear subgrid models for the unresolved velocity, temperature, and pressure fluctuations, an a priori analysis of the nonlinear semidiscrete problem was given. Finally, we applied the approach to the standard benchmark problem of natural convection problem in a differentially heated two-dimensional cavity.

Some open problems are the extension to Rayleigh-Benard convection and to mixed convection problems in indoor air-flow simulation. This will be considered in future research.

References

1. W. Bangerth, R. Hartmann, and G. Kanschat, `deal.II` *Differential Equations Analysis Library, Technical Reference*, 2007. `http://www.dealii.org`.
2. V. Girault and L. Scott, *A quasi-local interpolation operator preserving the discrete divergence*, Calcolo, 40 (2003), pp. 1–19.

3. V. GRAVEMEIER, *The variational multiscale method for laminar and turbulent flow*, Arch. Comput. Meth. Engrg., 13 (2006), pp. 249–324.
4. J.G. HEYWOOD AND R. RANNACHER, *Finite element approximation of the nonstationary Navier–Stokes problem, Part II: Stability of solutions and error estimates uniform in time*, SIAM J. Numer. Anal. 23 (1986) 4, 750–777.
5. T. HUGHES, *Multiscale phenomena: Green's functions, the Dirichlet-to-Neumann formulation, subgrid scale models, bubbles, and the origins of stabilized methods*, Comp. Meth. Appl. Mech. Engrg., 127 (1995), 387–401.
6. V. JOHN AND A. KINDL, *Finite element error analysis of a variational multiscale method for the Navier–Stokes equations*, Adv. Comp. Math., 28 (2008), 43–61.
7. O. LADYŽHENSKAYA, *New equations for the description of the viscous incompressible fluids and solvability in the large of the boundary value problems for them*, Proc. Steklov Inst. Math, 102 (1967), 95–118.
8. W. LAYTON, *A connection between subgrid scale eddy viscosity and mixed methods*, Appl. Math. Comput., 133 (2002), 147–157.
9. J. LÖWE AND G. LUBE, *A variational multiscale method for LES of the incompressible Navier–Stokes/Fourier Model and its application to natural convection flow*, NAM-Preprint, Univ. Göttingen 2010.
10. L. RÖHE AND G. LUBE, *Analysis of a variational multiscale method for Large-Eddy simulation and its application to homogeneous isotropic turbulence*. Comp. Meth. Appl. Mech. Engrg. 199 (2010) 37–40, 2331–2342.
11. Y.S. TIAN AND T.G. KARAYIANNIS, *Low turbulence natural convection in an air filled square cavity. Part I: the thermal and fluid flow fields*. Int. J. Heat Mass Transfer, 43 (2000), 849–866.
12. S.-H. PENG AND L. DAVIDSON, *Numerical investigation of turbulent buoyant cavity flow using Large-eddy simulation*. Int. Symp. Turbulence Heat Mass Transfer 3 (2000), 737–744.

Improved Mathematical and Numerical Modelling of Dispersion of a Solute from a Continuous Source

Niall Madden and Kajal Kumar Mondal

We present a refinement of a model due to Mondal and Mazumder [7] for dispersion of fine particles in an oscillatory turbulent flow. The model is based on the time-dependent advection-diffusion equation posed on a semi-infinite strip, whose solution represents the concentration of particles over time and down-stream distances.

The problem is solved by first mapping to a finite domain and then, using a monotone finite difference method on a tensor product, piecewise uniform mesh. The numerical results obtained for the related steady-state problem are compared with experimental data.

1 Introduction

This paper is concerned with a mathematical model for the dispersion of fine particles in an advection-dominated flow, and its numerical resolution. In presenting it, our goals are three-fold:

1. To present an improvement of the model in [7].
2. To outline how a layer adapted piecewise uniform ("Shishkin") mesh may be applied when solving this model, and further, to motivate the use of a parameter-robust method for this applied problem.
3. To obtain better agreement between the model's predictions and experimental data than that achieved in related studies.

N. Madden (✉)
National University of Ireland, Galway, Ireland, Supported by Science Foundation Ireland grant 08/RFP/CMS1205
e-mail: Niall.Madden@NUIGalway.ie

K.K. Mondal
Alipurduar College, Jalpaiguri, West Bengal, India, Supported by the Government of India, Department of Science & Technology, BOYSCAST Fellowship SR/BY/M-03/2008
e-mail: kkmondol@gmail.com

C. Clavero et al. (eds.), *BAIL 2010 – Boundary and Interior Layers, Computational and Asymptotic Methods*, Lecture Notes in Computational Science and Engineering 81,
DOI 10.1007/978-3-642-19665-2_19,

It is important to understand the basic mechanism of dispersion processes of passive contaminants in a stream or in the atmosphere from a continuous source; in particular it gives an insight to control the pollution level in the environment. It is shown in [7] how the spreading of injected particles is influenced by the combined action of oscillatory flow (with or without a non-zero mean), settling velocity, and vertically varying eddy diffusivity over the rough-surface for all time periods. The introduced particles are represented as a single point discontinuity at the in-flow boundary. In addition, a transformation is used to map the unbounded region to a bounded one. A finite difference method on a uniform grid is then used to solve the model numerically.

In Sect. 2 we present a mathematical model that is a modification of one described in [7]. The concentration of the particles introduced into the flow as a continuous source term and it is represented mathematically as a two-dimensional Dirac delta function, leading to an interior layer in the solution. Furthermore, we take the diffusivity term as being a combination of molecular diffusivity and turbulent eddy diffusivity (the earlier study neglected molecular diffusivity, leading to problems with the representation of the boundary conditions at the free surface).

In Sect. 3.1 we describe the transformation from the semi-infinite to a finite domain that has been used in related studies [4, 6, 7]. In Sect. 3.2 we give a simple example that demonstrates how the transformation effects the development of the interior layer, and so the choice of numerical procedure.

As stated, we wish to validate the model by comparison with a suitable set of experimental results. One such, widely cited study is [9]. However, those experiments are for a situation that is not as general as the model presented here allows; it corresponds to the steady case. Therefore, the numerical method described in Sect. 3.3 is only concerned with the solution of a two-dimensional (in space) advection-diffusion problem. We use a standard finite-difference discretization on a fitted piecewise uniform mesh of Shishkin type. The comparison between the experimental data and the numerical results are given in Sect. 4. We conclude with some observations, and an outline for future work.

2 The Model

Figure 1 gives a simple diagram of the coordinate system, representing a body of water in an infinitely long stream of finite depth. Expressed in dimensionless variables (see [7]), the rough stream bed is at $z = z_0 > 0$, and the free surface is at $z = 1$. The flow is assumed to be steady two dimensional flow, and is advection dominated, in the positive x-direction. The flow is turbulent, and the effects of this turbulence is represented in the model by an eddy diffusivity term that varies only with the vertical coordinate, z.

Particles are introduced into the stream at the point $x = 0, z = z_p$, their concentration represented in the source term as a distribution (Dirac delta). The equation is

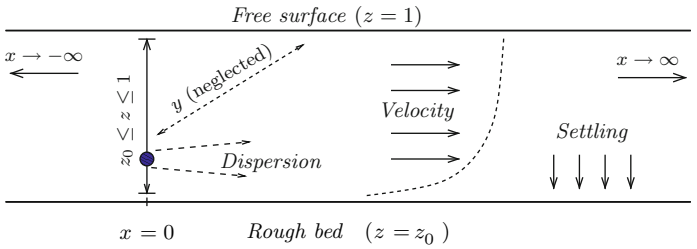

Fig. 1 Sketch of the coordinate system

$$\frac{\partial C}{\partial t} + u(z)\frac{\partial C}{\partial x} - \omega_s \frac{\partial C}{\partial z} = k_x(z)\frac{\partial^2 C}{\partial x^2} + \frac{\partial}{\partial z}\left(k_z(z)\frac{\partial C}{\partial z}\right) + f(x,z), \tag{1a}$$

on $(-\infty, \infty) \times (z_0, 1) \times (0, T]$, and subject to boundary and initial conditions

$$C(\pm\infty, z, t) = 0, \quad \left[k_z(z)\frac{\partial C}{\partial z} + \omega_s C\right]_{z=z_0,1} = 0, \qquad C(x,z,0) = 0, \tag{1b}$$

where z_0 is the boundary roughness height, ω_s is the settling velocity, and $f(x,z) = \delta(x)\delta(z - z_p)$, i.e., point source at $(x,z) = (0, z_p)$. Here the problem has been expressed in terms of dimensionless variables. That is, where D is the depth of the carrier fluid and where u_* is the friction velocity (taken as reference velocity), we take

$$x = \frac{x^*}{D}, \quad z = \frac{z^*}{D}, \quad t = \frac{t^* u_*}{D}, \quad u = \frac{u^*}{u_*}, \quad \omega_s = \frac{\omega_s^*}{u_*}.$$

We use the standard "log-law" as the steady velocity distribution $u(z)$ with an additional term, the wake function $W(z)$ which is required to incorporate the effects of wakes generated below the free surface. The combination of "log-law" and wake function is called the "log-wake law" and it is used for fully developed homogeneous turbulent flow. In our present study, we have not taken account the effect of inhomogeneous turbulent fluctuations, so the velocity distribution is

$$u(z) = \frac{1}{\kappa}\ln\left(\frac{z}{z_0}\right) + W(z),$$

where κ is the von-Kármán constant and z_0 is the equivalent bed roughness. The wake function $W(z)$ is taken as that of Coles [1]:

$$W(z) = \frac{2\Pi}{\kappa}\sin^2\left(\frac{\pi}{2}z\right),$$

where Π is the wake-strength parameter.

When the Reynolds decomposition is performed on the laminar advection-diffusion equation by decomposing the velocity ($u = \overline{u} + u'$) and concentration

($C = \overline{C} + C'$) into the sum of their mean and fluctuating parts, the term $\partial(\overline{u'C'})/\partial x_j$ represents the transport of concentration C due to turbulent fluctuations. Because the molecular diffusivity (k_{md}) is usually a very small quantity, $\overline{u'C'} \gg k_{\text{md}}\partial C/\partial x_j$, the effects for molecular diffusion is often negligible compared to the effects of turbulence, and so omitted from the model (e.g., as in [3, 12]). However, in this model the molecular diffusion *is* an important mechanism for mixing of the concentration to the flow at the smallest scales, and so we take the diffusivity profile as

$$k_x(z) = k_{\text{md}} + k_{\text{ed}}(z),$$

where $k_{\text{ed}}(z)$ is the eddy-diffusivity as proposed by Nezu and Rodi [8]:

$$k_{\text{ed}}(z) = \kappa(1-z)\left[\frac{1}{z} + \Pi\pi\sin(\pi z)\right]^{-1}.$$

Since our problem is posed in a fully developed homogeneous turbulent flow, we take $k_x(z) = k_z(z)$, and neglect the cross-stream diffusion terms.

Note that, since $k_{\text{ed}}(1) = 0$, if the settling velocity $\omega_s = 0$ and k_{md} neglected, then boundary condition at the free surface carries no physical significance, and the mathematical problem is ill-posed.

3 Numerical Solution of the Model

To compute an accurate numerical solution to model given above, several issues need to be addressed. Firstly, the problem is posed on a semi-infinite domain. Numerical solutions are only possible on finite domains, so the domain must either be truncated or transformed. Here we take the latter approach, discussed in Sect. 3.1, since it has proved successful in related studies. Then the layer(s) present in the solution must be resolved; a suitable method is described in Sect. 3.3.

3.1 Transformation of the Domain

In [7], a tanh-transformation from the domain $(x, z) \in (-\infty, \infty) \times [z_0, 1]$ to $(\zeta, z) \in (-1, 1) \times [z_0, 1]$ is made using

$$x = \frac{1}{2a}\log\left(\frac{1+\zeta}{1-\zeta}\right),$$

where a is a "stretching" factor, usually chosen based on computational experience. Following the transformation the model becomes

$$\frac{\partial C}{\partial t} + u(z)a(1-\zeta^2)\frac{\partial C}{\partial \zeta} - \omega_s \frac{\partial C}{\partial z} = a^2 k_\zeta(z)(1-\zeta^2)\left[(1-\zeta^2)\frac{\partial^2 C}{\partial \zeta^2} - 2\zeta\frac{\partial C}{\partial \zeta}\right] + \frac{\partial}{\partial z}\left(k_z(z)\frac{\partial C}{\partial z}\right) + \delta(\zeta)\delta(z-z_p), \tag{2a}$$

$$C(\pm 1, z, t) = 0, \quad \left[k_z(z)\frac{\partial C}{\partial z} + \omega_s C\right]_{z=z_0,1} = 0, \quad C(\zeta, z, 0) = 0. \tag{2b}$$

Remark 1. Although the full model as presented here is time-dependent, for the remainder of this paper we consider only the analogous steady problem. This is because we wish to compare our numerical results with experimental data. Since a reliable and well-tested set is available in the literature [9] for the steady case, we have opted to restrict our attention to that. We note that the issues concerning transformation from the semi-infinite domain to a finite one, and resolution of the interior layer, still feature.

3.2 A Simple Example

To consider how one might construct a suitable mesh for this problem, and to consider the effect of the transformation parameter, we present the following simple example: omit the $\partial C/\partial t$ term in (2a) above, and take $u \equiv 1$, $\omega_s = 0$, and constant viscosity $\varepsilon \approx k_\zeta(z_p) = k_z(z_p)$:

$$-\varepsilon a^2(1-\zeta^2)\left[(1-\zeta^2)\frac{\partial^2 C}{\partial \zeta^2} - 2\zeta\frac{\partial C}{\partial \zeta}\right] - \varepsilon\frac{\partial^2 C}{\partial z^2} + a(1-\zeta^2)\frac{\partial C}{\partial \zeta} = \delta(\zeta)\delta(z-z_p), \tag{3}$$

and the boundary conditions as in (2b) above.

In Fig. 2 we show the cross-section at $z = z_p$ of the computed solution, restricting to a small region around $\zeta = 0$ where the interior layer is most obvious. The given results are for $\varepsilon = 10^{-4}$, and cases $a = 10, 1$ and 0.1. As one would expect, taking relatively large values of a expands the layer in the computational domain, while for smaller values of a the layer is sharper.

In choosing a for a particular problem, we would like to take it as large as possible, so that the layer is easily resolved. However, taking a very large value of a will result in the region away from the layer being squeezed into the boundary. In practise, one usually is seeking values of the solution at certain points, so a should be small enough so that these are included in the computational domain. Thus we note that even when the problem data is fixed, one may be interested in solutions for different values of a. *Therefore, the use of a parameter uniform method is desirable.*

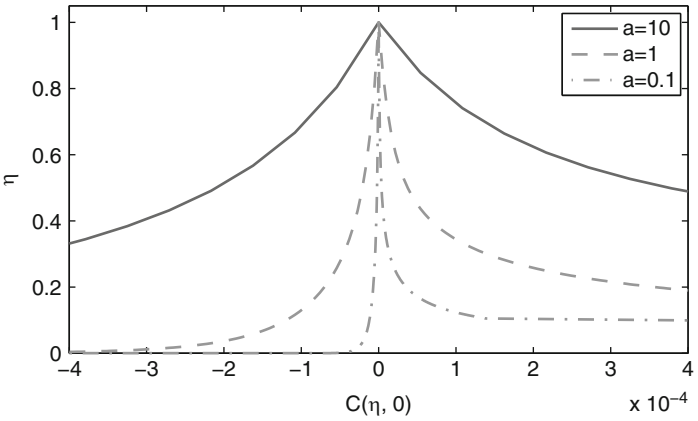

Fig. 2 Solution to (3) with $\varepsilon = 10^{-4}$ and $a = 10$, 1 and 0.1

3.3 The Numerical Method

To simplify notation, we restate the steady problem succinctly as

$$-\varepsilon_1(\zeta,z)\frac{\partial^2 C}{\partial\zeta^2} - \varepsilon_2(\zeta,z)\frac{\partial^2 C}{\partial z^2} + \beta_1(\zeta,z)\frac{\partial C}{\partial\zeta} + \beta_2(\zeta,z)\frac{\partial C}{\partial z} = \delta(\zeta)\delta(z-z_p). \quad (4)$$

Taking (for now) arbitrary meshes $\omega_\zeta : 0 = \zeta_0 < \zeta_1 < \cdots < \zeta_M = 1$, and $\omega_z : 0 = z_0 < z_1 < \cdots < z_N = 1$ in the ζ- and z-directions, one may form the tensor-product mesh $\omega := \omega_\zeta \times \omega_z$. We denote the mesh widths as $\Delta\zeta_i = \zeta_i - \zeta_{i-1}$ and $\Delta z_i = z_i - z_{i-1}$, and the approximation for $C(\zeta, z)$ at (ζ_i, z_j) as $C_{i,j}$. Derivatives with respect to ζ are discretized using standard second order finite difference:

$$D_\zeta^2 C_{i,j} := \frac{2}{\Delta\zeta_i + \Delta\zeta_{i+1}}\left(\frac{C_{i+1,j} - C_{i,j}}{\Delta\zeta_{i+1}} - \frac{C_{i,j} - C_{i-1,j}}{\Delta\zeta_i}\right),$$

and first-order upwinded finite difference:

$$D_\zeta^1 C_{i,j} := \left(\frac{C_{i,j} - C_{i-1,j}}{\Delta\zeta_i}\right).$$

The discretizations of the derivatives with respect to z are analogous, though with a suitable down-winding operator for $\partial C/\partial z$. The discrete problem is

$$\left(-\varepsilon_1(\zeta_i,z_j)D_\zeta^2 - \varepsilon_2(\zeta_i,z_j)D_z^2 + \beta_1(\zeta_i,z_j)D_\zeta^1 + \beta_2(\zeta_i,z_j)D_z^1\right)C_{i,j} = \delta(\zeta_i)\delta(z_j - z_p) \quad \text{for } i = 1,\ldots,M-1,\ j = 1,\ldots,N-1.$$

With a suitable implementation of the boundary conditions, this is easily solved.

We wish to construct a piecewise uniform Shishkin-type mesh that will resolve the interior layer; in particular we want the mesh to be refined around the injection point $(0, z_p)$. Define $\sigma_z = \varepsilon_2(0, z_p)/\beta_2(0, z_p)$, and set $\tau_z = \sigma_z \ln N$. If $\tau_z \geq 2(1-z_0)/N$, take ω_z to be the uniform mesh of N intervals on $[z_0, 1]$. Otherwise proceed as follows. Construct two meshes: ω_z^A is the uniform mesh with $N/2$ intervals on $[z_0, 1]$ and ω_z^B is the uniform mesh with $N/2$ intervals on $[z_p - \tau_z/2, z_p + \tau_z/2]$. Then take ω_z to be the union of $\omega_z^A \backslash [z_p - \tau_z/2, z_p + \tau_z/2]$ and ω_z^B. The mesh ω_ξ is constructed in an analogous fashion.

Remark 2. This construction varies slightly from the usual Shishkin mesh, which selects appropriate transition points at which to switch between a course and fine piecewise uniform mesh. In this case, since the injection point may be close to one of the boundaries, the construction given here is easier to implement, and ensures uniform mesh widths in the regions away from the injection point.

4 Numerical Results

We compare our numerical results for the steady problem (i.e., (2a–2b) but with the time derivative omitted) with experimental results of [9]. A heat source was treated as the passive tracers and the wind flow maintained in such a way that the flow yielded an approximate logarithmic velocity profile $u^* = u_* \log(z^*/z_0^*)/\kappa$ with roughness height $z_0^* = 0.12$ mm and $\kappa = 0.38$. We take the molecular viscosity to be $k_{\text{md}} = 10^{-6}$. The wake-strength parameter is taken as $\Pi = 0.09$, see [11]. The heat source was situated at 60 mm above the zero plane of the surface and the depth of the carrier fluid was $D = 540$ mm, giving the non-dimensional height of the source as $z_p = 60/540$.

The vertical and downstream distances were normalized by the heat source height z_p and the concentration C has been normalized as $C^n = C$ by a temperature scale of the form: $\Theta^* = F/\big(z_p u(z_p)\big)$, where F is the constant flux of contaminant through a plane normal to the flow.

Measurements of the concentration are available from [9] at four down-stream locations: $x = 0.2778, 0.8333, 1.6667$, and 3.3333. These are shown, left to right, as circles in Fig. 3 below. The closest down-stream station is our main interest of location where the interior layer is much more stronger than the other three locations. That diagram also shows the model's predictions at each of these four down-stream locations. For the first location, we took $a = 0.02$ (chosen by inspection to resolve the portion of the later of interest). When the problem is reformulated as in (4) this leads to values of $\varepsilon_1(0, z_p)$ and $\varepsilon_2(0, z_p)$ required to form the mesh described in Sect. 3.3 as 0.0062 and 0.0390, respectively. Clearly excellent agreement can be observed between the data concentration measurements and the predictions when the fitted mesh described above is employed. We also give the predictions obtained using a uniform mesh. As was observed in [7], that approach overestimates the width of the layer, and underestimate the strength of the concentration.

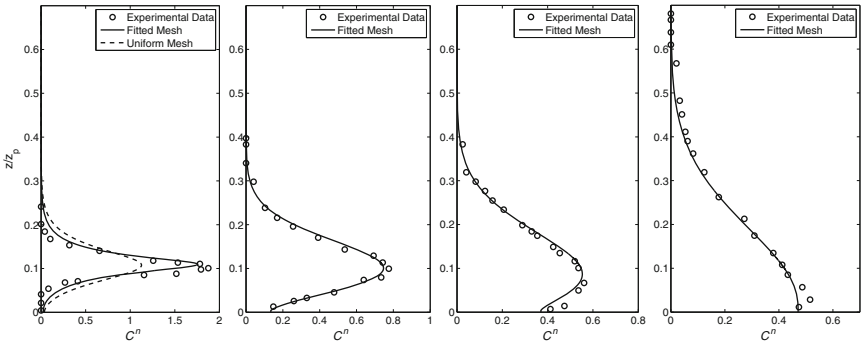

Fig. 3 Comparisons at the four down-stream locations

For the remaining three down-stream distances we took $a = 0.4$ and give the results just for a fitted mesh; the results for a uniform mesh are very similar. Again excellent agreement is found between measurements and numerical results, though at these distances the layer is not as strong.

5 Conclusions and Observations

We have provided an improved model for dispersion of settling particles in an advection-driven flow, shown how to employ a piecewise uniform Shishkin-type mesh, and found excellent agreement between the experimental measurements and the numerical results.

The use of Shishkin meshes for singularly perturbed problems has been widely studied; see e.g., [2,5,10]. The majority of studies are concerned with obtaining uniform convergence results for model problems; this study adds to the smaller number dealing with models that can be validated against experimental data. Much further work is required, however, to provide a mathematical justification for the approach for this specific problem.

References

1. D. Coles. The law of wake in the turbulent boundary layer. *J. Fluid Mech.*, 1(2):191–226, 1956.
2. N. Kopteva and E. O'Riordan. Shishkin meshes in the numerical solution of singularly perturbed differential equations. *Int. J. Numer. Anal. Model.*, 7(3):393–415, 2010.
3. B.S. Mazumder and D.C. Dalal. Contaminant dispersion from an elevated time-dependent source. *J. Comput. Appl. Math.*, 126(1-2):185–205, 2000.
4. B.S. Mazumder and S. Bandyopadhyay. On solute dispersion from an elevated line source in an open-channel flow. *J. Eng. Math.*, 40:197–209, 2001.
5. J.J.H. Miller, E. O'Riordan, and G.I. Shishkin. *Fitted numerical methods for singular perturbation problems*. World Scientific, 1996.

6. K.K. Mondal and B.S. Mazumder. On dispersion of settling particles from an elevated source in an open-channel flow. *J. Comput. Appl. Math.*, 193(1):22 – 37, 2006.
7. K.K. Mondal and B.S. Mazumder. Dispersion of fine settling particles from an elevated source in an oscillatory turbulent flow. *European J. Mech. - B/Fluids*, 27(6):707–725, 2008.
8. I. Nezu and W. Rodi. Open-channel flow measurements with a laser doppler anemometer. *J. Hydrol. Eng.*, 112(5):335–355, 1986.
9. M.R. Raupach and B.J. Legg. Turbulent dispersion from an elevated line source: measurements of wind-concentration moments and budgets. *J. Fluid Mech.*, 136:111–137, 1983.
10. H.-G. Roos, M. Stynes, and L. Tobiska. *Robust Numerical Methods for Singularly Perturbed Differential Equations*, Springer-Verlag, 2008.
11. T. Song, W.H. Graf and U. Lemmin, Uniform flow in open channel with movable bed. *J. Hydraul. Res.*, 32(6):861–876, 1994.
12. P.J. Sullivan and H. Yip. Near-field contaminant dispersion from an elevated line-source. *(ZAMP)*, 38:409–423, 1987.

Numerical Method for a Nonlinear Singularly Perturbed Interior Layer Problem

E. O'Riordan and J. Quinn

Abstract Nonlinear singularly perturbed interior layer problems are examined. Numerical results are presented for a numerical method consisting of a monotone scheme on a Shishkin mesh refined around the approximate location of the interior layer.

1 Introduction

In this paper, we examine nonlinear singularly perturbed problems of the form

$$(\varepsilon u'' - uu' - bu)(x) = 0, \quad b(x) \geqslant 0, \quad x \in (0,1), \quad u(0) > 0 > u(1). \tag{1}$$

We show that solutions to (1) can exhibit an interior layer centered around a unique point $p_\varepsilon \in (0,1)$. However, the exact location of this point p_ε is not explicitly determined. We construct a numerical method based on the approximate location of this point given in [4].

In [7], the time dependent problem corresponding to (1) is examined. A numerical scheme is constructed that uses a classical approach when $\varepsilon \geqslant CN^{-2/5}$ and a sophisticated shock-capturing algorithm when $\varepsilon \leqslant CN^{-2/5}$. A parameter-uniform error bound of the form

$$\|u - U^N\| \leqslant CN^{-1/5}$$

is established. Note that $\|\cdot\|$ is the standard pointwise maximum norm, N is the number of mesh steps and throughout the paper, C denotes a constant independent of ε and N. The algorithm given in [7] is intricate, mainly due to the fact that the location of the internal layer needs to be accurately determined at all time levels. Below

E. O'Riordan (✉) and J. Quinn
School of Mathematical Sciences, Dublin City University, Dublin, Ireland
e-mail: eugene.oriordan@dcu.ie, jason.quinn25@mail.dcu.ie

C. Clavero et al. (eds.), *BAIL 2010 – Boundary and Interior Layers, Computational and Asymptotic Methods*, Lecture Notes in Computational Science and Engineering 81,
DOI 10.1007/978-3-642-19665-2_20,

we confine our discussion to the steady-state problem (1). However, the numerical algorithm in Sect. 4 has some common attributes with the algorithm given in [7].

We present numerical results for a monotone scheme on a piecewise-uniform Shishkin mesh which suggest that this method is essentially first order convergent when applied to (1). However we do not provide any numerical analysis for this scheme in this paper. Note that throughout the paper, the notation $f^{(k)}$ denotes the k-th derivative of f.

2 Continuous Problem

Consider the following problem class: Find $y_\varepsilon \in C^2(0,1)$ such that

$$\begin{aligned} (\varepsilon y_\varepsilon'' - y_\varepsilon y_\varepsilon' - b y_\varepsilon)(x) = 0, \quad x \in \Omega := (0,1), \\ y_\varepsilon(0) = A > 0, \quad y_\varepsilon(1) = B < 0, \qquad (P_\varepsilon) \\ b \in C^2[(0,1)], \quad b(x) \geqslant 0, \quad x \in \bar{\Omega}. \end{aligned}$$

The left and right reduced solutions, r_L and r_R respectively, satisfy

$$-r_{L/R}(r_{L/R}' + b)(x) = 0, \quad r_L(0) = A, \quad r_R(1) = B. \tag{2}$$

These equations are easily solved. We are interested in the occurrence of an interior layer and for convenience we assume that

$$r_L(x) = A - \int_0^x b(t)\,dt > 0 \text{ and } r_R(x) = B + \int_x^1 b(t)\,dt < 0, \forall x \in \Omega. \tag{3}$$

From the analysis in [4], the necessary conditions for the occurrence of an interior layer in the solution to (P_ε) are: if

$$r_L(x) > 0, \quad \text{for} \quad x \in [0, x_L], \quad 0 < x_L \leq 1; \tag{4a}$$

$$r_R(x) < 0, \quad \text{for} \quad x \in [x_R, 1], \quad 0 \leq x_R < 1; \tag{4b}$$

$$x_R < x_L; \text{ and } J(x) := \int_{r_R(x)}^{r_L(x)} s\,ds \text{ has a zero at } x^* \in [x_R, x_L]; \tag{4c}$$

then an ε-width interior layer occurs around the point x^*. In our case, from (3), we have $x_L \equiv 1$ and $x_R \equiv 0$. Solving for x^* from (4) we have that

$$\int_0^{x^*} b(t)\,dt = \frac{1}{2}(A + B + \int_0^1 b(t)\,dt). \tag{5}$$

Lemma 1. *The problem (P_ε) has a unique solution $y_\varepsilon \in C^2(\Omega)$, satisfying $B \leqslant y_\varepsilon(x) \leqslant A$, $x \in \bar{\Omega}$.*

Proof. Use constant upper and lower solutions (see [6]) to establish the existence of y_ε and to bound y_ε. Suppose y_1 and y_2 are two solutions of (P_ε) and define $\omega := y_1 - y_2$. Then ω satisfies

$$\varepsilon\omega'' - y_1\omega' - (y_2' + b)\omega = 0, \quad x \in \Omega, \quad \omega(0) = 0, \quad \omega(1) = 0. \tag{6}$$

Uniqueness follows by noting that 0 is both a lower and upper solution of (6). □

By using a proof by contradiction argument with (P_ε), one can show that y_ε cannot have a positive internal minimum or a negative internal maximum. Hence $y_\varepsilon' < 0$ on Ω. Thus there exists a unique point $p_\varepsilon \in (0, 1)$ such that

$$y_\varepsilon(p_\varepsilon) = 0. \tag{7}$$

We split the problem (P_ε) into left and right problems defined either side of p_ε. The left problem is defined to be: Find y_L such that

$$(\varepsilon y_L'' - y_L y_L' - b y_L)(x) = 0,\ x \in (0, p_\varepsilon), \quad y_L(0) = A, \quad y_L(p_\varepsilon) = 0, \quad (P_L)$$

and the right problem is given by: Find y_R such that

$$(\varepsilon y_R'' - y_R y_R' - b y_R)(x) = 0,\ x \in (p_\varepsilon, 1), \quad y_R(p_\varepsilon) = 0, \quad y_R(1) = B. \quad (P_R)$$

Using upper and lower solutions for (P_L) we have

$$0 \leqslant y_L(x) \leqslant A, \quad x \in [0, p_\varepsilon]. \tag{8}$$

For the problem (P_L), existence and uniqueness of a solution holds as with (P_ε). Hence $y_\varepsilon(x) \equiv y_L(x), 0 \leq x \leq p_\varepsilon$. We decompose the solution y_L as $y_L = v_L + w_L$. The regular component v_L is defined as the solution of

$$(\varepsilon v_L'' - v_L v_L' - b v_L)(x) = 0,\ x \in (0, p_\varepsilon),\ v_L(0) = A, v_L(p_\varepsilon) = (r_L + \varepsilon v_1)(p_\varepsilon), \tag{9}$$

where $v_L = v_0 + \varepsilon v_1 + \varepsilon^2 v_2$; $v_0 \equiv r_L$ and v_1,v_2 satisfy the nonlinear problems

$$v_0 v_1' + (v_0' + b)v_1 = v_0'', \qquad v_1(0) = 0, \tag{10a}$$

$$\varepsilon v_2'' - v_L v_2' - (v_0' + \varepsilon v_1' + b)v_2 = v_1 v_1' - v_1'', \quad v_2(0) = v_2(p_\varepsilon) = 0. \tag{10b}$$

The layer component w_L is defined as the solution of the nonlinear problem

$$(\varepsilon w_L' - \frac{1}{2}(y_L + v_L)w_L)'(x) - b w_L(x) = 0,\ x \in (0, p_\varepsilon), \tag{11a}$$

$$w_L(0) = 0, \quad w_L(p_\varepsilon) = -v_L(p_\varepsilon). \tag{11b}$$

Bounds on both components v_L and w_L and their derivatives are given in the following lemma.

Lemma 2. *Assuming (3), for $k = 0, 1, 2, 3$, the solutions v_L and w_L of (9) and (11) respectively, uniquely exist and satisfy the bounds*

$$-v_L(p_\varepsilon)e^{-\frac{r_L(p_\varepsilon)}{2\mu}(p_\varepsilon - x)/\varepsilon} \leqslant w_L(x) \leqslant -v_L(p_\varepsilon)e^{-\mu A(p_\varepsilon - x)/\varepsilon}, \ \mu > 1,$$
$$\|v_L^{(k)}\| \leqslant C(1 + \varepsilon^{2-k}), \quad |w_L^{(k)}(x)| \leqslant C\varepsilon^{-k}e^{-\frac{C}{\varepsilon}(p_\varepsilon - x)}, \quad x \in [0, p_\varepsilon].$$

Proof. The existence and uniqueness of v_L and its bounds are obtained in the same manner as in [6] including the bound

$$v_L(x) \geqslant r_L(p_\varepsilon) - C\varepsilon \geqslant s r_L(p_\varepsilon) > 0, \quad 0 < s < 1, \quad x \in [0, p_\varepsilon]. \tag{12}$$

We bound the layer component as follows. Clearly 0 is an upper solution for (11). Consider the terminal value problem (t.v.p)

$$\varepsilon \underline{w}' - \frac{1}{2}(y_L + v_L)\underline{w} = 0, \quad x \in [0, p_\varepsilon), \quad \underline{w}(p_\varepsilon) = w_L(p_\varepsilon). \tag{13}$$

Using (8) and (12) we have $y_L + v_L \geqslant s r_L(p_\varepsilon)$. Thus using lower and upper solutions (for t.v.p.'s [5]), it can be shown that $w_L(p_\varepsilon)e^{-\frac{1}{2\varepsilon}s r_L(p_\varepsilon)(p_\varepsilon - x)} \leqslant \underline{w}(x) \leqslant 0$. This, in turn, can be used to show that $\underline{w}$ is a lower solution for (11). Bound the derivatives of w_L as in [6, Lemma 3.4]. We finish by bounding the layer component away from zero. The equation in (11) can also be written as

$$(\varepsilon w_L'' - y_L w_L' - (v_L' + b)w_L)(x) = 0. \tag{14}$$

Using (8) we have $y_L \leqslant A$ and from (10) we have $v_L' + b = O(\varepsilon)$. Thus for sufficiently small ε we can show, using upper and lower solutions, that

$$|w_L(x)| \geqslant |w_L(p_\varepsilon)|e^{-\mu A(p_\varepsilon - x)/\varepsilon}, \quad \mu > 1, \quad x \in [0, p_\varepsilon].$$

□

Analysis of (P_R) is analogous to that of (P_L) with an equivalent decomposition $y_R = v_R + w_R$ and the following Lemma is established in the same manner.

Lemma 3. *Assuming (3), for $k = 0, 1, 2, 3$, if $y_R = v_R + w_R$ is the decomposition of y_R into a regular and layer component then v_R and w_R uniquely exist and satisfy the bounds*

$$|v_R(p_\varepsilon)|e^{-\mu|B|(x - p_\varepsilon)/\varepsilon} \leqslant w_R(x) \leqslant |v_R(p_\varepsilon)|e^{-\frac{|r_R(p_\varepsilon)|}{2\mu}(x - p_\varepsilon)/\varepsilon}, \quad \mu > 1,$$
$$\|v_R^{(k)}\| \leqslant C(1 + \varepsilon^{2-k}), \quad |w_R^{(k)}(x)| \leqslant C\varepsilon^{-k}e^{-\frac{C}{\varepsilon}(x - p_\varepsilon)}, \quad x \in [p_\varepsilon, 1].$$

Note that the location of the point p_ε has not been determined.

2.1 Alternative Problem

We now consider an alternative problem to simulate an interior layer at a known point q, close to p_ε: Find z_ε such that

$$z_\varepsilon(x) := \{z_L(x),\ x \le q; \qquad z_R(x),\ x > q\},$$

where z_L and z_R satisfy

$$(\varepsilon z_L'' - z_L z_L' - b z_L)(x) = 0,\ x \in (0,q),\ z_L(0) = A,\ z_L(q) = 0, \qquad (Q_L)$$
$$(\varepsilon z_R'' - z_R z_R' - b z_R)(x) = 0,\ x \in (q,1),\ z_R(q) = 0,\ z_R(1) = B. \qquad (Q_R)$$

The problems (Q_L) and (Q_R) are analogues of (P_L) and (P_R). We decompose z_L into a regular component g_L and a layer component s_L and similarly $z_R = g_R + s_R$. Bounds on these components and their derivatives are given in the following lemma.

Lemma 4. *Assuming (3) and (4), for $k = 0,1,2,3$, if $z_L = g_L + s_L$ and $z_R = g_R + s_R$ are the decompositions into a regular and layer component of z_L and z_R respectively then*

$$g_L(x) = r_L(x) + O(\varepsilon) \quad x \in [0,q] \quad \text{and} \quad g_R(x) = r_R(x) + O(\varepsilon) \quad x \in [q,1],$$
$$-g_L(q)e^{-\frac{r_L(q)}{2\mu}(q-x)/\varepsilon} \le s_L(x) \le -g_L(q)e^{-\mu A(q-x)/\varepsilon}, \qquad \mu > 1, \quad x \in [0,q],$$
$$|g_R(q)|e^{-\mu|B|(x-q)/\varepsilon} \le s_R(x) \le |g_R(q)|e^{-\frac{|r_R(q)|}{2\mu}(x-q)/\varepsilon}, \quad \mu > 1, \quad x \in [q,1],$$
$$\|g_L^{(k)}\| \le C(1+\varepsilon^{2-k}) \quad \text{and} \quad |s_L^{(k)}(x)| \le C\varepsilon^{-k}e^{-\frac{C}{\varepsilon}(q-x)}, \quad x \in [0,q],$$
$$\|g_R^{(k)}\| \le C(1+\varepsilon^{2-k}) \quad \text{and} \quad |s_R^{(k)}(x)| \le C\varepsilon^{-k}e^{-\frac{C}{\varepsilon}(x-q)}, \quad x \in [q,1].$$

Proof. Analogous to the proof of Lemma 2. □

Remark 1. The assumption in (4) is not used in the proof of Lemma 4. However, in Sect. 4, we explain the motivation for choosing $q = x^*$ as defined in (4) and thus we require the existence of $x^* \in (0,1)$.

We now present a bound on $\|y_\varepsilon - z_\varepsilon\|$ under the assumption that

$$|p_\varepsilon - q| \le C\varepsilon. \tag{15}$$

Lemma 5. *Assuming (15), if y_ε is the solution of (P_ε) and z_ε is the solution of (Q_L),(Q_R) then*

$$\|y_\varepsilon - z_\varepsilon\| \le \frac{C}{\varepsilon}|p_\varepsilon - q| \quad \text{on } \bar{\Omega}.$$

Proof. Without loss of generality, assume that $p_\varepsilon < q$. We will examine the difference $d_\varepsilon := y_\varepsilon - z_\varepsilon$ over the intervals $[0, p_\varepsilon]$, $[p_\varepsilon, q]$ and $[q, 1]$ separately. On each interval, using (P_ε) and (Q_L),(Q_R), d_ε satisfies

$$(\varepsilon d_\varepsilon' - \frac{1}{2}(y_\varepsilon + z_\varepsilon)d_\varepsilon)'(x) - b d_\varepsilon(x) = 0. \tag{16}$$

Considering d_ε over $[0, p_\varepsilon]$ we have $d_\varepsilon(0) = 0$. Using Lemma 4, (15) and the inequality $1 - e^{-t} \leqslant t$, $0 < t < 1$ we have

$$\begin{aligned} |d_\varepsilon(p_\varepsilon)| =& |-z_L(p_\varepsilon)| \leqslant |-g_L(p_\varepsilon) + g_L(q)e^{-\mu A(q-p_\varepsilon)/\varepsilon}| \\ &\leqslant \|g_L'\||p_\varepsilon - q| + g_L(q)|1 - e^{-\mu A(q-p_\varepsilon)/\varepsilon}| \leqslant \frac{C}{\varepsilon}|p_\varepsilon - q|. \end{aligned}$$

It follows using constant upper and lower solutions that $|d_\varepsilon(x)| \leqslant C/\varepsilon|p_\varepsilon - q|$ for $x \in (0, p_\varepsilon)$. Bound $d_\varepsilon(q)$ in the same fashion to complete the proof. □

3 The Discrete Problem

To numerically approximate the solution of (P_ε) we consider the following discretisation of (Q_L), (Q_R): Find Z_ε such that

$$Z_\varepsilon(x_i) = \{Z_L(x_i), x_i \leq q; \qquad Z_R(x_i), x_i > q\},$$

where Z_L and Z_R satisfy

$$(D^+(\varepsilon D^- Z_L - \frac{1}{2}Z_L^2) - bZ_L)(x_i) = 0, x_i \in I^-, Z_L(0) = A, Z_L(q) = 0, \quad (Q_L^N)$$

$$(D^-(\varepsilon D^+ Z_R - \frac{1}{2}Z_R^2) - bZ_R)(x_i) = 0, x_i \in I^+, Z_R(q) = 0, Z_R(1) = B, \quad (Q_R^N)$$

on a piecewise-uniform mesh Ω_ε^N. Note that D^+, D^- denote the standard forward and backward finite difference operators. Motivated by Lemma 4, the mesh Ω_ε^N is defined as

$$x_i \in \Omega_\varepsilon^N : x_i = \begin{cases} \frac{4(q-\sigma_0)}{N} i, & 0 \leqslant i \leqslant \frac{N}{4}, \\ q - \sigma_0 + \frac{4\sigma_0}{N}(i - \frac{N}{4}), & \frac{N}{4} < i \leqslant \frac{N}{2}, \\ q + \frac{4\sigma_1}{N}(i - \frac{N}{2}), & \frac{N}{2} < i \leqslant \frac{3N}{4}, \\ q + \sigma_1 + \frac{4(1-q-\sigma_1)}{N}(i - \frac{3N}{4}), & \frac{3N}{4} < i \leqslant N, \end{cases} \tag{17a}$$

$$\sigma_j := \min\{\tfrac{q+(1-2q)j}{2}, \tfrac{\mu}{\gamma_j}\varepsilon \ln N\}, \ \gamma_0 = r_L(q), \ \gamma_1 = |r_R(q)|, \ \mu > 2, \tag{17b}$$

$$I^- = \{x_i : x_i \in \Omega_\varepsilon^N, i < N/2\} \quad \text{and} \quad I^+ = \{x_i : x_i \in \Omega_\varepsilon^N, i > N/2\}. \tag{17c}$$

In [6], numerical analysis was presented for a nonlinear singularly perturbed problem with a boundary turning point. Using the same techniques of analysis, one can establish the following lemma.

Lemma 6. *Assuming (3), if z_ε is the solution of (Q_L), (Q_R) and Z_ε is the solution of (Q_L^N), (Q_R^N) then*

$$|(Z_\varepsilon - z_\varepsilon)(x_i)| \leqslant CN^{-1}\ln N, \quad x_i \in \Omega_\varepsilon^N.$$

Finally, combining Lemmas 5 and 6 we have that

Lemma 7. *Assuming (3), if y_ε is the solution of (P_ε) and Z_ε is the solution of (Q_L^N), (Q_R^N) then*

$$|(y_\varepsilon - Z_\varepsilon)(x_i)| \leqslant \frac{C}{\varepsilon}|p_\varepsilon - q| + CN^{-1}\ln N, \quad x_i \in \Omega_\varepsilon^N. \tag{18}$$

Observe that if the point q was within $O(\varepsilon)$ of the point p_ε, then Lemma 7 would not suffice to guarantee convergence.

4 Numerical Results

The numerical algorithm described in Sect. 3 solves two boundary turning point problems joined together at q. The algorithm involves a non-linear monotone finite difference operator and a Shishkin mesh centered about an unspecified point q. In this final section, we present an algorithm which linearizes this discrete problem using a continuation method (see [3] for details) and takes $q := x^*$, where x^* is given in (5). At each new time level in the continuation method, we do not determine where the interpolant of the discrete approximation is zero. We employ a scheme, motivated by [1], which preserves the monotonicity of the finite difference operator. Find $Y_{i,j} := Y_\varepsilon(x_i, t_j)$ such that

$$\begin{aligned}
&\varepsilon D_x^- D_x^+ Y_{i,j} - \frac{1}{2}Y_{i,j}^- D_x^- Y_{i,j} - bY_{i,j} = D_t^- Y_{i,j}, \quad \text{if} \quad Y_{i,j-1} \geqslant 0\\
&\varepsilon D_x^+ D_x^- Y_{i,j} - \frac{1}{2}Y_{i,j}^+ D_x^+ Y_{i,j} - bY_{i,j} = D_t^- Y_{i,j}, \quad \text{if} \quad Y_{i,j-1} < 0\\
&\qquad Y_{i,j}^- := (Y_{i,j-1} + Y_{i-1,j-1}),\ Y_{i,j}^+ := (Y_{i+1,j-1} + Y_{i,j-1}), \qquad (A_\varepsilon^N)\\
&\qquad\qquad x_i \in \Omega_\varepsilon^N, \quad Y_\varepsilon(0,t_j) = A, \quad Y_\varepsilon(1,t_j) = B,\\
&Y_\varepsilon(x_i,0) = \left\{ r_L(x_i);\ \text{if } x_i < x^*; \quad 0,\ \text{if } x_i = x^*; \quad r_R(x_i),\ \text{if } x_i > x^* \right\},
\end{aligned}$$

where r_L and r_R are the reduced solutions (2) and Ω_ε^N is the mesh described in (17) with $q = x^*$ given in (5). Note that Ω_ε^N remains fixed with $q := x^*$ at all time levels. We continue to iterate in j until $\max_{x_i \in \Omega_\varepsilon^N} \left| Y_{i,j} - Y_{i,j-1} \right| \leqslant 10^{-6}$.

Table 1 Computed double mesh rates for algorithm (A_ε^N) applied to problem (P_ε), with $b(x) \equiv 0.5$, $A = 1$ and $B = -1.1$

	p_ε^N				
ε	**N = 32**	**N = 64**	**N = 128**	**N = 256**	**N = 512**
$\mathbf{2^0}$	1.14	1.07	1.03	1.03	0.98
$\mathbf{2^{-1}}$	1.17	1.17	0.89	1.04	0.97
$\mathbf{2^{-2}}$	−0.1	1.82	0.84	0.88	1.02
$\mathbf{2^{-3}}$	1.66	2.45	0.02	1.45	0.71
$\mathbf{2^{-4}}$	1.65	1.68	0.90	1.48	0.89
$\mathbf{2^{-5}}$	0.90	1.29	1.54	1.07	1.40
$\mathbf{2^{-6}}$	0.62	0.71	0.92	1.12	1.19
$\mathbf{2^{-7}}$	0.61	0.74	0.84	0.98	1.09
$\mathbf{2^{-8}}$	0.60	0.72	0.81	0.89	1.05
$\mathbf{2^{-9}}$	0.60	0.71	0.79	0.85	0.99
$\mathbf{2^{-10}}$	0.59	0.71	0.78	0.83	0.94
$\mathbf{2^{-11}}$	0.59	0.71	0.78	0.82	0.92
$\mathbf{2^{-12}}$	0.59	0.71	0.78	0.82	0.91
$\mathbf{2^{-13}}$	0.59	0.71	0.77	0.82	0.90
.	.	.	.	.	.
.	.	.	.	.	.
$\mathbf{2^{-20}}$	0.59	0.71	0.77	0.82	0.90
$\mathbf{p^N}$	0.90	0.75	0.82	0.82	0.90

Example. Consider (P_ε) with $b(x) \equiv 0.5$, $A = 1$ and $B = -1.1$. The mesh defined in (17) is used with $q = x^* = 0.4$ [solved from (5)] and we choose $\mu = 2.1$ in (17b). Table 1 displays the computed rates of convergence p_ε^N and the uniform rates of convergence p^N, using the double mesh principle [2]. The computed uniform rates p^N are tending to first order for this example.

Remark 2. For any given value of ε, using asymptotic arguments Howes [4, Theorem 5.5] indicates that the point x^* is within an $O(\varepsilon)$ neighbourhood of the unknown shock location p_ε. That is, p_ε is located within the fine mesh centered about x^*. In the above numerical algorithm, the center of the shock layer is initially located at x^*, but shifts position at each new time level. In the numerical experiments, we have observed that when the continuation method stops iterating, the shock layer is still located within the fine mesh region. If it is positioned at the mesh point (in the fine mesh) closest to the point p_ε, then by Lemma 7 we have generated a first order approximation to the exact solution of (P_ε). Hence, this paper can only be viewed as containing an interim result. Until one has information about the terminal shock location, one cannot conclude that the algorithm (A_ε^N) is a first order numerical method for the problem (P_ε).

Remark 3. Based on Lemma 7, we deduce that when b is not constant then x^* should be calculated exactly from (5) or at least approximated to within $O(\varepsilon)$ of its exact value.

Acknowledgements This research was supported by the Irish Research Council for Science, Engineering and Technology.

References

1. L. Abrahamsson, S. Osher, Monotone Difference Schemes for Singular Perturbation Problems, *SIAM J. Numer. Anal.*, 19, (5), 1982, 979–992.
2. P.A. Farrell, A.F. Hegarty, J.J.H. Miller, E. O'Riordan and G.I. Shishkin, *Robust Computational Techniques for Boundary Layers*, Chapman and Hall/CRC, Boca Raton, FL. (2000).
3. P.A. Farrell, E. O'Riordan and G.I. Shishkin, A class of singularly perturbed semilinear differential equations with interior layers, *Mathematics of Computation*, 74, (252), 2005, 1759–1776.
4. F.A. Howes Boundary-interior layer interactions in nonlinear singular perturbation theory, *Memoirs of the American Mathematical Society*, 15, (203), 1978.
5. G.S. Ladde, V. Lakshmikantham and A.S. Vatsala *Monotone Iterative Techniques for Nonlinear Differential Equations*. Pitman Publishing, London, (1985).
6. E. O'Riordan and J. Quinn Parameter-uniform numerical methods for some linear and non-linear singularly perturbed convection diffusion boundary turning point problems, *Dublin City University, Preprint MS-10-02* (2010) (to appear in BIT).
7. G.I. Shishkin, Difference approximation of the dirichlet problem for a singularly perturbed quasilinear parabolic equation in the presence of a transition layer, *Russian Acad. Sci. Dokl. Math.*, 48, (2), 1994, 346–352.

Large-Eddy Simulation of Wall-Bounded Turbulent Flows: Layer-Adapted Meshes vs. Weak Dirichlet Boundary Conditions

Lars Röhe and Gert Lube

1 Introduction

In a bounded domain $\Omega \subseteq \mathbb{R}^3$, we consider the incompressible Navier–Stokes model to determine velocity $\mathbf{u}$ and pressure p s.t.

$$\partial_t \mathbf{u} - \nabla \cdot (2\nu \mathbb{D}\mathbf{u}) + (\mathbf{u} \cdot \nabla)\mathbf{u} + \nabla p = \mathbf{f} \qquad \text{in } (0,T] \times \Omega \tag{1}$$

$$\nabla \cdot \mathbf{u} = 0 \qquad \text{in } [0,T] \times \Omega \tag{2}$$

$$\mathbf{u}|_{t=0} = \mathbf{u}^0 \qquad \text{in } \Omega \tag{3}$$

together with appropriate boundary conditions on the boundary $\partial\Omega$. The deformation tensor is denoted by $\mathbb{D}\mathbf{u} = \frac{1}{2}(\nabla\mathbf{u} + (\nabla\mathbf{u})^t)$. The Reynolds number $Re = \frac{\mathbf{U}L}{\nu}$ relies on viscosity ν, a reference length L, and velocity $\mathbf{U}$.

In Sect. 2, we introduce a variational multiscale (VMS) finite element model. Aspects of the numerical analysis of the semi-discrete model are addressed in Sect. 3. Section 4 is concerned with the application of the approach to a benchmark problem of wall-bounded flows in a channel. In particular, we discuss the problem whether a layer-adapted mesh in the boundary layer regions or a weak implementation of boundary conditions for the velocity at the wall is appropriate.

2 Variational Multiscale Approach

For simplicity, we consider no-slip boundary conditions and thus, for a weak formulation, the spaces

$$V = [H_0^1(\Omega)]^3, \qquad Q = L^2_*(\Omega) := \{q \in L^2(\Omega) : \int_\Omega q \, dx = 0\}.$$

G. Lube (✉) and L. Röhe
Institute for Numerical and Applied Mathematics, Georg-August University Göttingen, D-37083 Göttingen, Germany
e-mail: lube@math.uni-goettingen.de, roehe@math.uni-goettingen.de

C. Clavero et al. (eds.), *BAIL 2010 – Boundary and Interior Layers, Computational and Asymptotic Methods*, Lecture Notes in Computational Science and Engineering 81,
DOI 10.1007/978-3-642-19665-2_21,

By $\|\cdot\|_{0,G}$ we denote the standard L^2-norm on a measurable domain $G \subseteq \Omega$. Moreover, let $\|\cdot\|_0 = \|\cdot\|_{0,\Omega}$.

Let $\mathcal{T}_h$ be an admissible (possibly anisotropic) mesh s.t. $\overline{\Omega} = \cup_{K\in\mathcal{T}_h}\overline{K}$. We consider finite element (FE) spaces $V_h \times Q_h \subset V \times Q$ for velocity/pressure subject to the discrete inf-sup stability condition

$$\exists \beta \neq \beta(h) \;\; s.t. \;\; \inf_{q_h\in Q_h}\sup_{\mathbf{v}_h\in V_h}\frac{(q_h, \nabla\cdot\mathbf{v_h})}{\|q_h\|_0\|\nabla\mathbf{v}_h\|_0} \geq \beta > 0.$$

The basic Galerkin FE method reads:
find $(\mathbf{u}_h, p_h)$: $[0,T] \to V_h \times Q_h$ s.t. $\forall(\mathbf{v}_h, q_h) \in V_h \times Q_h$

$$\begin{aligned}(\partial_t\mathbf{u}_h, \mathbf{v}_h) + (2\nu\mathbb{D}\mathbf{u}_h, \mathbb{D}\mathbf{v}_h) + b_S(\mathbf{u}_h, \mathbf{u}_h, \mathbf{v}_h) - (p_h, \nabla\cdot\mathbf{v}_h) &= (\mathbf{f}, \mathbf{v}_h)\\ (q_h, \nabla\cdot\mathbf{u}_h) &= 0\end{aligned}$$

with the skew-symmetric advective term

$$b_S(\mathbf{u}, \mathbf{v}, \mathbf{w}) := [((\mathbf{u}\cdot\nabla)\mathbf{v}, \mathbf{w}) - ((\mathbf{u}\cdot\nabla)\mathbf{w}, \mathbf{v})]/2.$$

We consider the following three-scale decomposition

$$V \ni \mathbf{v} = \underbrace{\overline{\mathbf{v}}_h + \tilde{\mathbf{v}}_h}_{=\mathbf{v}_h\in V_h} + \hat{\mathbf{v}}_h; \qquad Q \ni q = \underbrace{\overline{q}_h + \tilde{q}_h}_{=q_h\in Q_h} + \hat{q}_h$$

with resolved scales $(\mathbf{v}_h, q_h) \in V_h \times Q_h \subset V \times Q$. The influence of the small unresolved scales $(\hat{\mathbf{v}}_h, \hat{q}_h)$ on $(\tilde{\mathbf{v}}_h, \tilde{q}_h)$ will be modelled following the variational multiscale approach, see [5]. Define the FE space L_H for the deformation tensor on $\mathcal{T}_H$, $H \geq h$

$$\{0\} \subseteq L_H \subseteq L := \left\{\mathbf{L} = (l_{ij}) \mid l_{ij} = l_{ji} \in L^2(\Omega)\ \forall i, j \in \{1,2,3\}\right\}$$

and the L^2-orthogonal projection operator $\Pi_H : L \to L_H$. The model of the small unresolved velocity scales is defined by means of the fluctuation operator

$$\kappa(\mathbb{D}\mathbf{v}_h) := (Id - \Pi_H)(\mathbb{D}\mathbf{v}_h).$$

For the calibration of the subgrid model for velocity, we introduce cellwise constant terms $\nu_T(\mathbf{u}_h)$ s.t. $\nu_T^K(\mathbf{u}_h) := \nu_T(\mathbf{u}_h)|_K$.

As a model of the small unresolved pressure scales, we add the so-called grad-div stabilization [11] with cellwise constant $\gamma_K(\mathbf{u}_h) := \gamma(\mathbf{u}_h)|_K$ s.t.

$$(\gamma(\mathbf{u}_h)(\nabla\cdot\mathbf{u}_h), \nabla\cdot\mathbf{v}_h) := \sum_{K\in\mathcal{T}_h}\gamma_K(\mathbf{u}_h)(\nabla\cdot\mathbf{u}_h, \nabla\cdot\mathbf{v}_h)_K.$$

Finally, the VMS model reads as follows: find $(\mathbf{u}_h, p_h)$ s.t.

$$\begin{aligned}(\partial_t \mathbf{u}_h, \mathbf{v}_h) + 2\nu\,(\mathbb{D}\mathbf{u}_h, \mathbb{D}\mathbf{v}_h) + b_S(\mathbf{u}_h, \mathbf{u}_h, \mathbf{v}_h) \\ + (\nu_T(\mathbf{u}_h)\kappa(\mathbb{D}\mathbf{u}_h), \kappa(\mathbb{D}\mathbf{v}_h)) + (\gamma_T(\mathbf{u}_h)\nabla\cdot\mathbf{u}_h, \nabla\cdot\mathbf{v}_h) \\ + (\nabla\cdot\mathbf{u}_h, q_h) - (\nabla\cdot\mathbf{v}_h, p_h) = \quad (\mathbf{f}, \mathbf{v}_h)\end{aligned} \tag{4}$$

for all $(\mathbf{v}_h, q_h) \in V_h \times Q_h$.

3 Aspects of the Numerical Analysis

The following sketch of the semi-discrete analysis is an extension of a result in [7]. It takes advantage of the fact that, for inf-sup stable FE spaces for velocity/pressure, the space V_h^{div} of discretely divergence free functions is not empty. In particular, we can separate estimates for velocity and pressure. Moreover, an additional pressure stabilization is not required.

Following the approach in [9], we obtain the following stability estimates which are valid on arbitrary admissible grids.

Lemma 1. *Let* $\mathbf{f} \in L^1(0,T;L^2(\Omega)), \mathbf{u}_0 \in [L^2(\Omega)]^3$. *Then, for all* $t \in (0,T]$, *there is control of kinetic energy*

$$\|\mathbf{u}_h\|_{L^\infty(0,t;L^2(\Omega))} \leq K(\mathbf{f}, \mathbf{u}_0) \equiv \|\mathbf{u}_0\|_0 + \|\mathbf{f}\|_{L^1(0,t;L^2(\Omega))}$$

and of the dissipation and subgrid terms

$$\begin{aligned}\nu\|\mathbb{D}\mathbf{u}_h\|^2_{L^2(0,t;L^2(\Omega))} + \frac{1}{2}\int_0^t \sum_K \nu_T^K(\mathbf{u}_h)\|\kappa(\mathbb{D}\mathbf{u}_h)\|^2_{0,K}dt \\ + \frac{1}{2}\int_0^t \sum_K \gamma_K(\mathbf{u}_h)\|\nabla\cdot\mathbf{u}_h\|^2_{0,K}dt \leq 3K^2(\mathbf{f}, \mathbf{u}_0).\end{aligned}$$

We introduce elementwise multiscale viscosities $\nu^K_{\mathrm{VMS}}(\mathbf{u}_h, \mathbf{v}_h)$ via

$$\sum_{K\in\mathcal{T}_h} \nu_T^K(\mathbf{u}_h)\,\|\kappa(\mathbb{D}\mathbf{v}_h)\|^2_{0,K} = \sum_{K\in\mathcal{T}_h} \underbrace{\nu_T^K(\mathbf{u}_h)\left(1 - \frac{\|\Pi_H\mathbb{D}\mathbf{v}_h\|^2_{0,K}}{\|\mathbb{D}\mathbf{v}_h\|^2_{0,K}}\right)}_{=:\nu^K_{\mathrm{VMS}}(\mathbf{u}_h,\mathbf{v}_h)\geq 0} \|\mathbb{D}\mathbf{v}_h\|^2_{0,K}$$

where we take advantage of the projector properties of the fluctuation operator κ. Then we define the following mesh-dependent expression for the analysis

$$|||\mathbf{u}(t)|||^2 := \|\mathbf{u}(t)\|_0^2 + \sum_{K\in\mathcal{T}_h}\int_0^t \left(\frac{\nu^K_{mod}(\mathbf{u},\mathbf{u}_h)}{2}\,\|\mathbb{D}(\mathbf{u})\|^2_{0,K} + \gamma_K(\mathbf{u}_h)\,\|\nabla\cdot\mathbf{u}\|^2_{0,K}\right)dt$$

with modified elementwise viscosities:

$$\nu_{\text{mod}}^K(\mathbf{u}_h, \mathbf{v}_h) := 2\nu + \nu_{\text{VMS}}^K(\mathbf{u}_h, \mathbf{v}_h).$$

Then we obtain the following a priori estimate for the semi-discrete scheme.

Theorem 1. *For a sufficiently smooth solution* $\mathbf{u}$ *of the Navier–Stokes model (1)–(3) it holds for the solution of the VMS model (4) for all* $t \in (0, T)$*:*

$$|||(\mathbf{u} - \mathbf{u}_h)(t)|||^2 \leq 2 \inf_{\tilde{\mathbf{u}}_h \in L^2(0,t;V_h^{div})} |||(\mathbf{u} - \tilde{\mathbf{u}}_h)(t)|||^2$$

$$+ e^{\int_0^t \frac{27C_{LT}^4}{2\nu_{mod}^{min}(\mathbf{u}_h, \mathbf{e}_h^u)^3} \|\mathbb{D}\mathbf{u}(s)\|_0^4 ds} \inf_{\substack{\tilde{\mathbf{u}}_h \in L^4(0,t;V_h^{div}) \\ \tilde{p}_h \in L^2(0,t;Q_h)}} \left(\|(\mathbf{u}_h - \tilde{\mathbf{u}}_h)(0)\|_0^2 + \int_0^t A(s) ds \right)$$

with

$$\begin{aligned} A(t) :=& 2 \sum_{K \in \mathcal{T}_h} \Big[6\nu_T^K(\mathbf{u}_h) \, \|\kappa \mathbb{D}\mathbf{u}\|_{0,K}^2 + 6\Big(\nu + \nu_{VMS}^K(\mathbf{u}_h, \epsilon^u)\Big) \, \|\mathbb{D}\epsilon^u\|_{0,K}^2 \\ &+ \min\left(\frac{9C_{Ko}^2}{\nu_{mod}^{min}(\mathbf{u}_h, \mathbf{e}_h^u)}, \frac{1}{\gamma_K(\mathbf{u}_h)} \right) \Big(\|p - \tilde{p}_h\|_{0,K}^2 + \gamma_K^2(\mathbf{u}_h) \, \|\nabla \cdot \epsilon^u\|_{0,K}^2 \Big) \Big] \\ &+ \frac{6C_{LT}^2}{\nu_{mod}^{min}(\mathbf{u}_h, \mathbf{e}_h^u)} \Big(C_F C_{Ko} \, \|\mathbb{D}\mathbf{u}\|_0^2 + \|\mathbf{u}_h\|_0 \, \|\mathbb{D}\mathbf{u}_h\|_0 \Big) \, \|\mathbb{D}\epsilon^u\|_0^2 \\ &+ \frac{6C_{Ko}^2}{\nu_{mod}^{min}(\mathbf{u}_h, \mathbf{e}_h^u)} \, \|\partial_t \epsilon^u\|_{-1,\Omega}^2 \,, \end{aligned}$$

where $\nu_{mod}^{min}(\mathbf{u}_h, \mathbf{e}_h^u) := \min_K \nu_{mod}^K(\mathbf{u}_h(t), \mathbf{v}_h(t))$ *and*

$$\mathbf{u}_h - \mathbf{u} = (\mathbf{u}_h - \tilde{\mathbf{u}}_h) - (\mathbf{u} - \tilde{\mathbf{u}}_h) =: \mathbf{e}_h^u - \epsilon^u.$$

C_F *and* C_{Ko} *are the constants of the inequalities of Friedrichs and Korn.* C_{LT} *is related to an upper bound of the advective term.*

Remark 1. The first r.h.s. term in the first line of term $A(t)$ is related to the VMS-model error. For the remaining approximation terms in A, we can apply the interpolation operator by Girault/Scott [6] in V_h^{div} on isotropic meshes and a standard interpolation operator for the pressure. Then these terms are formally of order $\mathbb{O}(h^{2k})$ for FE spaces $\mathbb{Q}_k/\mathbb{Q}_{k-1}$ or $\mathbb{P}_k/\mathbb{P}_{k-1}$ for velocity/pressure, the choice $L_H = [Q_{k-2}^{disc}]^{3\times 3}$, and $\nu_T^K \in [0, Ch_K^2]$.

Sketch of the proof: From the weak form of (1)–(3) and (4), we obtain the error equation

$$\frac{1}{2}\partial_t \left\|\mathbf{e}_h^u\right\|_0^2 + \sum_{K\in\mathcal{T}_h} \nu_{\text{mod}}^K(\mathbf{u}_h, \mathbf{e}_h^u) \left\|\mathbb{D}\mathbf{e}_h^u\right\|_{L^2(K)}^2 + \sum_{K\in\mathcal{T}_h} \gamma_K(\mathbf{u}_h) \left\|\nabla\cdot\mathbf{e}_h^u\right\|_{L^2(K)}^2$$
$$= \left(\partial_t\epsilon^u, \mathbf{e}_h^u\right) + (2\nu\mathbb{D}\epsilon, \mathbb{D}\mathbf{e}_h^u) + b_S(\mathbf{u}, \mathbf{u}, \mathbf{e}_h^u) - b_S(\mathbf{u}_h, \mathbf{u}_h, \mathbf{e}_h^u) - (p - \lambda_h, \nabla\cdot\mathbf{e}_h^u)$$
$$+ \sum_{K\in\mathcal{T}_h} \Big[\gamma_K(\mathbf{u}_h)\left(\nabla\cdot\epsilon^u, \nabla\cdot\mathbf{e}_h^u\right)_K + \nu_T^K(\mathbf{u}_h)\left(\kappa\mathbb{D}\epsilon^u, \kappa\mathbb{D}\mathbf{e}_h^u\right)_K$$
$$-\nu_T^K(\mathbf{u}_h)\left(\kappa\mathbb{D}\mathbf{u}, \kappa\mathbb{D}\mathbf{e}_h^u\right)_K\Big], \quad \forall\lambda_h \in Q_h.$$

Careful estimates of the right hand side terms lead to

$$\partial_t \left\|\mathbf{e}_h^u(t)\right\|_0^2 + d(t) \le g(t) \left\|\mathbf{e}_h^u(t)\right\|_0^2 + A(t)$$

with

$$g(t) := \frac{27C_{LT}^4}{2\nu_{\text{mod}}^{\min}(\mathbf{u}_h, \mathbf{e}_h^u)^3} \|\mathbb{D}\mathbf{u}(t)\|_0^4,$$
$$d(t) := \frac{1}{4}\sum_{K\in\mathcal{T}_h} \nu_{\text{mod}}^K(\mathbf{u}_h, \mathbf{e}_h^u) \left\|\mathbb{D}\mathbf{e}_h^u(t)\right\|_{0,K}^2 + \sum_{K\in\mathcal{T}_h} \gamma_K(\mathbf{u}_h) \|\nabla\cdot\mathbf{e}_h(t)\|_{0,K}^2,$$

and $A(t)$ as given in the Theorem. Gronwall's Lemma implies for all $t \in [0, T]$

$$\left\|\mathbf{e}_h^u(t)\right\|_0^2 + \int_0^t d(s)ds \le e^{\int_0^t g(s)ds}\big(\left\|\mathbf{e}_h^u(0)\right\|_0^2 \|_0^2 + \int_0^t A(s)ds\big).$$

Finally, the triangle inequality concludes the proof. For full details of the proof, we refer to [12]. □

In the remaining part of the paper, we will discuss how the given approach can be adapted to the case of turbulent channel flows.

4 Application to Turbulent Channel Flow

For the spatial discretization, we apply hexahedral meshes with FE spaces $\mathbb{Q}_2/\mathbb{Q}_1$ for velocity/pressure within the FE package `deal.II`, see [2]. The arising semi-discrete problem of the form

$$\begin{pmatrix} M_u & 0 \\ 0 & 0 \end{pmatrix}\begin{pmatrix} \mathbf{u}_h'(t) \\ \mathbf{p}_h'(t) \end{pmatrix} = \begin{pmatrix} \mathbf{f}_h(t) \\ 0 \end{pmatrix} - \begin{pmatrix} A_u(\mathbf{u}_h) & B \\ B^T & 0 \end{pmatrix}\begin{pmatrix} \mathbf{u}_h(t) \\ \mathbf{p}_h(t) \end{pmatrix}$$

is a DAE-system with differentiation index 2 and perturbation index 2. For the time discretization, we apply the BDF(2)-formula

$$\mathbf{u}_h'(t_{n+1}) \approx \frac{1}{2\delta t}[3\mathbf{u}_h(t_{n+1}) - 4\mathbf{u}_h(t_n) + \mathbf{u}_h(t_{n-1})]$$

which provides favourable stability properties and does not lead to order reduction for the pressure. A fixed-point iteration is applied for the resulting non-linear implicit scheme.

The calibration of the viscosity model is motivated by the Boussinesq approximation of the residual stress tensor via

$$\tau^R := \langle \mathbf{u} \otimes \mathbf{u} \rangle - \mathbf{u}_h \otimes \mathbf{u}_h \approx -2\nu_T \mathbb{D}\mathbf{u}_h$$

together with the classical Smagorinsky model and van-Driest damping

$$\nu_T(\mathbb{D}\mathbf{u}_h)|_K = \left[C_S \Delta_K (1 - \exp(-\frac{u_\tau \mathrm{dist}(S_K, \partial\Omega)}{26\nu}) \right]^2 \|\mathbb{D}\mathbf{u}_h(S_K)\|_F .$$

Here, S_K denotes the center of gravity of element K and u_τ denotes the wall friction velocity, see below. In the experiments below, we apply a one-level approach with $H = h$ and $L_h = \{0\}$. On each element $K \in \mathcal{T}_h$, the filter width is given by $\Delta_K = \mathrm{meas}(K)/(2(k-1))$ with element order k of V_h. The Smagorinsky constant $C_S^2 = 0.0942$ is taken from Lilly's argument for isotropic homogeneous turbulence, see [12].

A reduction of model dissipation can be established by application of the fluctuation operator

$$\tau^R \approx -2\nu_T(\mathbb{D}\mathbf{u}_h)\kappa(\mathbb{D}\mathbf{u}_h).$$

with the fluctuation operator $\kappa := Id - \Pi_h$, the L^2-orthogonal projection $\Pi_h : L \to L_h$, and $L_h = {\mathbb{Q}_0}^{d\times d}$.

4.1 Turbulent Channel Flow at Moderate Reynolds Number Re_τ

We start with channel flow at a moderate Reynolds number $Re_\tau = 180$ (corresponding to $Re = 5{,}644$ in channel center) for which an anisotropic grid resolution of the boundary layer regions is feasible. The Reynolds number $Re_\tau = Hu_\tau/\nu$ is defined via the half width H of the channel and wall-friction velocity u_τ satisfying Spalding's form of the law of the wall

$$y^+ = f(u^+) := u^+ + e^{-5.5\chi}\Big(e^{\chi u^+} - 1 - \chi u^+ - \frac{1}{2}(\chi u^+)^2 - \frac{1}{6}(\chi u^+)^3\Big)$$

with $y^+ := \frac{y u_\tau}{\nu}$, $u^+ := \frac{\|\mathbf{u}_h\|}{u_\tau}$, and $\chi = 0.4$.

A careful description of the set-up of the problem (but with different scaling) is given in [8]. We performed simulations with N^3 grid points, with equidistant distribution of elements in x_1, x_3-directions and anisotropic distribution in x_2-direction according to

$$x_2 = y = \tanh(2(2i/(N) - 1))/\tanh(2), \qquad \text{for } i = 0, ..., N.$$

Statistical averaging $\langle\cdot\rangle$ is performed over all homogeneous directions x_1, x_3, t. As an example of first-order statistics, we present in Fig. 1 the mean streamwise velocity $U = \langle \mathbf{u_h} \rangle \mathbf{e}_1$ and its normalized variant U^+. Compared to direct numerical simulation (DNS) results of [10], we obtain very good agreement in the viscous sub-layer whereas slight deviations can be found in the log-layer and in the center of the channel. As examples of second-order statistics, the normalized fluctuations $\langle u_1', u_2' \rangle^+$ and $\langle u_1', u_1' \rangle^+$ are shown in Fig. 2. The agreement with the DNS data is very good in the vicinity of the wall and (for such relatively coarse grid) reasonable in the core of the channel.

Numerical experiments in [1] with lowest-order Taylor-Hood elements on anisotropic grids show a potential influence of a large aspect ratio $a_\Omega := \max_K h_K/\rho_K$ where h_K and ρ_K denote the diameter of K resp. the diameter of the largest ball in K. Here we obtained for $N = 32$ grid points in x_2-direction a value of $a_\Omega \approx 20$. A modification of the V_h^{div}-interpolation results of [6] to Cartesian tensor-product meshes provides the (non-optimal?) result

$$\|\mathbf{u} - \tilde{\mathbf{u}}_h\|_{0,K} + \rho_K |\mathbf{u} - \tilde{\mathbf{u}}_h|_{1,K} \lesssim a(\omega_K) \sum_{|\alpha|=l} h_K^\alpha \|D^\alpha \mathbf{u}\|_{0,\omega(K)}, \quad \forall u \in H^l(\omega(K))$$

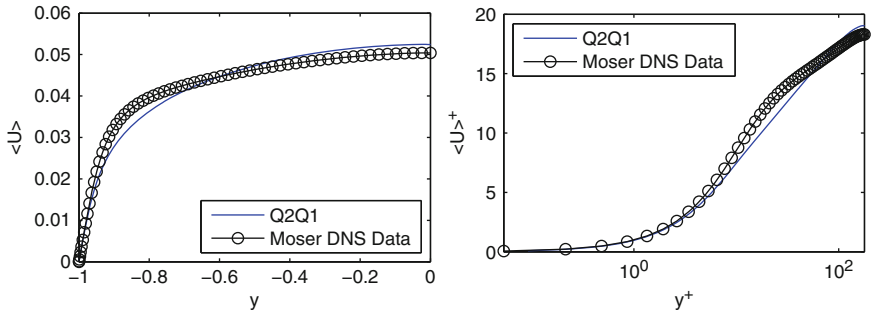

Fig. 1 Channel flow at $Re_\tau = 180$ with 32^3 grid points: mean streamwise velocity $U = \langle \mathbf{u_h} \rangle \boldsymbol{e}_1$ (*left*) and its normalized variant $U^+ = U/u_\tau$ (*right*)

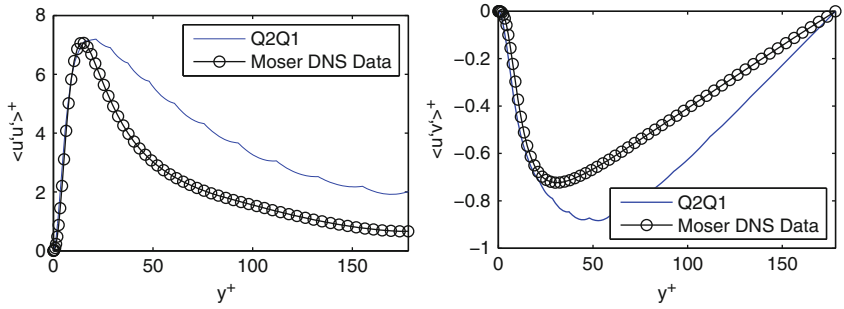

Fig. 2 Channel flow at $Re_\tau = 180$ with 32^3 grid points: normalized fluctuations $\langle u_1, u_1' \rangle$ (*left*) and $\langle u_1', u_2' \rangle$ (*right*)

where $a(\omega_K)$ denotes the aspect ratio of the patch $\omega_K \supset K$. This limits the applicability of layer-adapted meshes with Taylor-Hood elements to moderate values of Re_τ.

4.2 Turbulent Channel Flow at Higher Reynolds Numbers

A proper anisotropic resolution of near-wall region in LES for higher Re_τ is not feasible. Near-wall modelling with adaption of wall-functions on isotropic grid may be considered as a remedy. Here we follow the approach in [3, 4] with weak implementation of wall boundary conditions on isotropic grids.

The simplest variant [3] is a weak nonsymmetric or symmetric penalty-type implementation of Dirichlet condition $\mathbf{u}_h = \mathbf{0}$ at the wall Γ_W and is performed by adding the following terms

$$-\sum \left((2\nu \mathbb{D}\mathbf{u}_h \cdot \mathbf{n}, \mathbf{v}_h)_{\partial K \cap \Gamma_W} \pm (\mathbf{u}_h, 2\nu \mathbb{D}\mathbf{v}_h \cdot \mathbf{n})_{\partial K \cap \Gamma_W} + (\mathbf{u}_h, \tau_B \mathbf{v}_h)_{\partial K \cap \Gamma_W} \right).$$

Here the Dirichlet penalty factor is taken as $\tau_B := \frac{u_\tau^2}{\|\mathbf{u}_h\|}$ with tangential velocity $\mathbf{u}_h$ and wall-friction velocity u_τ. A similar approach is realized on inflow and outflow parts of the channel.

In particular, for the non-symmetric case, symmetric testing $\mathbf{v}_h = \mathbf{u}_h$ gives immediately control of $\sum_K \tau_B \|\mathbf{u}_h\|^2_{0,\partial K \cap \Gamma_W}$. A modification of the numerical analysis in Sect. 3 is possible, but will not considered.

A refined variant of a weak implementation of Dirichlet conditions, including advective and pressure parts of the traction operator, is given in [4]. Convincing numerical results for channel flows on (rather fine) isotropic grids are reported in [3, 4] for Reynolds numbers $Re_\tau \in \{395, 950, 2003\}$.

5 Summary: Outlook

We applied a variational multiscale model to the time-dependent Navier–Stokes model. For wall-bounded flows in a channel, we discussed two variants: anisotropic mesh resolution in boundary layers for moderate Re_τ and isotropic meshes with near-wall modelling via weak Dirichlet conditions for higher Re_τ. The a priori analysis of the arising nonlinear semi-discrete problem given in [12] can be adapted to both situations.

We believe that the current approach in airbus industry, e.g. at DLR (German Aerospace Center), with delayed detached eddy simulation (DDES) with LES away from layers and RANS in layer regions can be cast into the framework of the proposed projection-based VMS method. In particular, an application of the approach to problems with separation is in order.

References

1. T. APEL, H.M. RANDRIANARIVONY, *Stability of discretizations of the Stokes problem on anisotropic meshes*, Math. Comput. Simulation, 61 (2003), 437–447.
2. W. BANGERTH, R. HARTMANN, G. KANSCHAT, `deal.II` — *a general purpose object oriented finite element library*, ACM Trans. Math. Software, 33 (2007), article 24.
3. Y. BAZILEVS, C. MICHLER, V.M. CALO, T.J.R. HUGHES, *Weak Dirichlet boundary conditions for wall-bounded turbulent flows*, Comp. Meth. Appl. Mech. Engrg., 196 (2007), 4853–4862.
4. Y. Bazilevs, C. Michler, V.M. Calo, T.J.R. Hughes: Isogeometric variational multiscale modeling of wall-bounded turbulent flows with weakly-enforced boundary conditions on unstretched meshes. Comput. Meths. Appl. Mech. Engrg. 199 (2010), 780–790.
5. L.C. BERSELLI, T. ILIESCU, W.J. LAYTON, *Mathematics of Large Eddy Simulation of Turbulent Flows*, Springer, Berlin, Heidelberg, 2006.
6. V. GIRAULT, L. SCOTT, *A quasi-local interpolation operator preserving the discrete divergence*, Calcolo, 40 (2003), 1–19.
7. V. JOHN, S. KAYA, *Finite element error analysis of a variational multiscale method for the Navier-Stokes equations*, Adv. Comp. Math., 28 (2008), 43–61.
8. V. JOHN, M. ROLAND, *Simulations of the turbulent channel flow at* $Re_\tau = 180$ *with projection-based finite element variational multiscale methods*, Int. J. Numer. Meth. Fluids 55 (2007), 407–429.
9. O. LADYŽHENSKAYA, *New equations for the description of motion of viscous incompressible fluids and solvability in the large of boundary value problems for them*, Proc. Steklov Inst. Math, 102 (1967), 95–118.
10. D.R. MOSER, J. KIM, N.N. MANSOUR, *Direct numerical simulation of turbulent channel flow up to* $Re_\tau = 590$, Physics of Fluids 11 (1999), 943–945.
11. M. OLSHANSKII, G. LUBE, T. HEISTER, J. LÖWE, *Grad-div stabilization and subgrid pressure models for the incompressible Navier-Stokes equations*, Comp. Meth. Appl. Mech. Engrg., 198 (2009), 3975–3988.
12. L. RÖHE, G. LUBE, *Analysis of a variational multiscale method for Large-Eddy simulation and its application to homogeneous isotropic turbulence*, Comp. Meth. Appl. Mech. Engrg. 199 (2010) 37-40, 2331–2342.

Improved Scheme on Adapted Locally-Uniform Meshes for a Singularly Perturbed Parabolic Convection-Diffusion Problem

G.I. Shishkin

Abstract For a Dirichlet problem for a singularly perturbed parabolic convection-diffusion equation with small parameter ε multiplying the highest-order derivative, a finite difference scheme with improved accuracy is constructed that converges *almost ε-uniformly with order of the convergence rate close to 2* for fixed values of ε. When constructing the scheme, *monotone* classical approximations of the differential equation on a priori adapted locally-uniform meshes are used. To improve accuracy of the scheme, *the Richardson technique on embedded grids* is applied.

1 Problem Formulation: Aim of Research

In the domain $\overline{G}$, where

$$G = D \times (0, T], \quad \overline{G} = G \bigcup S, \quad D = (0,\, d), \tag{1}$$

we consider the initial-boundary value problem for the singularly perturbed parabolic convection-diffusion equation

$$L\,u(x,t) = f(x,t), \;\; (x,t) \in G, \quad u(x,t) = \varphi(x,t), \;\; (x,t) \in S. \tag{2}$$

Here

$$L_2 \equiv \varepsilon\, a(x,t)\, \frac{\partial^2}{\partial x^2} + b(x,t)\, \frac{\partial}{\partial x} - c(x,t) - p(x,t)\, \frac{\partial}{\partial t}, \quad (x,t) \in G,$$

the functions $a(x,t)$, $b(x,t)$, $c(x,t)$, $p(x,t)$, $f(x,t)$ and $\varphi(x,t)$ are assumed to be sufficiently smooth on $\overline{G}$ and S, respectively, moreover, $a(x,t),\ b(x,t),\ p(x,t) > 0$ and $c(x,t) \geq 0$; the parameter ε takes arbitrary values in the interval $(0, 1]$.

G.I. Shishkin
Institute of Mathematics and Mechanics, Russian Academy of Sciences, Moscow, Russia
e-mail: shishkin@imm.uran.ru

C. Clavero et al. (eds.), *BAIL 2010 – Boundary and Interior Layers, Computational and Asymptotic Methods*, Lecture Notes in Computational Science and Engineering 81,
DOI 10.1007/978-3-642-19665-2_22,

We assume that the data of the problem (2), (1) on the set of corner points $S^c = S_0 \bigcap \overline{S}^L$ satisfy compatibility conditions that guarantee the required smoothness of the solution on $\overline{G}$ (see, e.g., [1]). Here $S = S_0 \bigcup S^L$, S_0 and S^L are the lower and lateral parts of the boundary; $S_0 = \overline{S}_0$; $S^L = S^l \bigcup S^r$, where S^l and S^r are the left and right parts of the lateral boundary.

For small values of the parameter ε, a regular boundary layer appears in a neighbourhood of the set $S^l = \{(x,t) : x = 0,\ 0 < t \le T\}$.

Now we give some *definitions* [10]. Let $z(x,t)$, $(x,t) \in \overline{G}_h$, be a solution of a difference scheme and let the function $z(x,t)$ satisfy the estimate

$$|u(x,t) - z(x,t)| \le M \lambda \left(\varepsilon^{-\nu} N^{-1}, N_0^{-1}\right), \quad (x,t) \in \overline{G}_h, \tag{3}$$

where $\lambda(\xi_1, \xi_2) \to 0$ for $\xi_1, \xi_2 \to 0$ uniformly with respect to the parameter ε; $\nu \ge 0$. By definition, the solution of this scheme converges on the set $\overline{G}_h$ *uniformly with respect to the parameter* ε (or, briefly, ε-*uniformly*) if $\nu = 0$ in the estimate (3). Otherwise, we say that the scheme does not converge ε-uniformly on $\overline{G}_h$. But if the scheme converges for $N^{-1} = o(\varepsilon^{\nu})$, moreover, the constant M in the estimate (3), in general, depends on ν, however in general, there is no convergence for $N^{-1} = O(\varepsilon^{\nu})$, we say that the scheme converges with *defect* ν. In that case when the value ν can be chosen arbitrarily small, and also the solution of the difference scheme *controlled by the value* ν satisfies estimate (3), we say that the scheme converges on $\overline{G}_h$ *almost* ε-*uniformly with defect* ν (or, briefly, *almost* ε-*uniformly*).

For problem (2), (1), the defect of the classical scheme (7) on the uniform grid (6) equals 1. Difference schemes in [5–9] on adapted locally-uniform meshes (uniform on these subsets where the more precise solution is computed) converge almost ε-uniformly, but with order of the convergence rate not higher than one for fixed values of the parameter ε.

Our *aim* for the boundary value problem (2), (1) is to construct an almost ε-uniformly convergent scheme on a priori adapted locally-uniform meshes with order of the convergence rate for fixed values of the parameter ε close to two.

2 A Priori Estimates for the Solution of Problem (2), (1)

Here we give a priori estimates for solutions and derivatives of the boundary value problem (2), (1); the derivation of these estimates is similar to that in [2,4,10]. Write the solution of the problem as the sum of the functions

$$u(x,t) = U(x,t) + V(x,t), \quad (x,t) \in \overline{G}, \tag{4}$$

where $U(x,t)$ and $V(x,t)$ are the regular and singular parts of the solution. For

$$a,\ b,\ c,\ p,\ f \in C^{l,l}(\overline{G}), \quad \varphi \in C^{l,l}(\overline{G}), \quad l = 3n + 1,$$

where $n > 0$ is integer [n characterizes the number of terms in asymptotic expansions of the components $U(x,t)$ and $V(x,t)$], and for appropriate compatibility conditions in corner points (see, e.g., [10]) we obtain the estimate

$$\left|\frac{\partial^{k+k_0}}{\partial x^k\,\partial t^{k_0}}\,U(x,t)\right| \le M\,, \quad \left|\frac{\partial^{k+k_0}}{\partial x^k\,\partial t^{k_0}}\,V(x,t)\right| \le M\,\varepsilon^{-k}\,\exp(-m\,\varepsilon^{-1}\,x), \qquad (5)$$

$$(x,t) \in \overline{G}, \quad k + 2k_0 \le K^*,$$

where $K^* = n + 1$ and $m \in (0, m_0)$ with $m_0 = \min_{\overline{G}}[a^{-1}(x,t)\,b(x,t)]$.

3 Richardson Method for a Classical Scheme

We construct a difference scheme based on a classical approximation of problem (2), (1). On the set $\overline{G}$ we introduce the uniform grid

$$\overline{G}_h = \overline{G}_h^{\,u} = \overline{\omega}^u \times \overline{\omega}_0^u, \qquad (6)$$

where $\overline{\omega}^u$ and $\overline{\omega}_0^u$ are uniform meshes with the step-sizes $h = d\,N^{-1}$ on the interval $[0,d]$ and $h_t = T\,N_0^{-1}$ on $[0,T]$, where $N+1$ and N_0+1 are the numbers of points in the meshes $\overline{\omega}$ and $\overline{\omega}_0$, respectively. We approximate problem (2), (1) by the finite difference scheme [3]

$$\Lambda\,z(x,t) = f(x,t),\ \ (x,t) \in G_h, \quad z(x,t) = \varphi(x,t),\ \ (x,t) \in S_h \qquad (7)$$

Here $\Lambda \equiv \varepsilon\,a(x,t)\,\delta_{x\overline{x}} + b(x,t)\,\delta_x - c(x,t) - p(x,t)\,\delta_{\overline{t}}, (x,t) \in G_h$, $G_h = G \cap \overline{G}_h$, $S_h = S \cap \overline{G}$, $\delta_{x\overline{x}}\,z(x,t)$ is the central difference derivative on the uniform mesh, and $\delta_x\,z(x,t)$ and $\delta_{\overline{x}}\,z(x,t)$, $\delta_{\overline{t}}\,z(x,t)$ are the first-order (forward and backward) difference derivatives. Taking into account the estimate (5) with $K = 4$, we obtain the following estimate for the solution of the scheme (7), (6):

$$|u(x,t) - z(x,t)| \le M\left[\left(\varepsilon + N^{-1}\right)^{-1}\,N^{-1} + N_0^{-1}\right], \quad (x,t) \in \overline{G}_h. \qquad (8)$$

Now we describe the Richardson method used to improve accuracy of discrete solutions for the standard basic scheme. On the set $\overline{G}$ we construct grids

$$\overline{G}_h^{\,i} = \overline{G}_h^{\,u\,i} = \overline{\omega}^{\,i} \times \overline{\omega}_0^i,\ \ i = 1,2, \qquad (9a)$$

where $\overline{\omega}^{\,i} = \overline{\omega}^{\,u\,i}$, $\overline{\omega}_0^i = \overline{\omega}_0^{u\,i}$ are uniform meshes in x and t. Here $\overline{G}_h^{\,2} = \overline{G}_{h(6)}$ is the *basic grid*, and $\overline{G}_h^{\,1}$ is the *"coarsed" grid*. The step-sizes h^1 and h_0^1 in the meshes $\overline{\omega}^{\,1}$ on the interval $[0,d]$ and $\overline{\omega}_0^1$ on the interval $[0,T]$ are k^* times more than the step-sizes h^2 and h_0^2 in the meshes $\overline{\omega}^{\,2}$ and $\overline{\omega}_0^2$. The numbers of points in

the meshes $\overline{\omega}^2$ and $\overline{\omega}_0^2$ are $N^{(2)}+1$ and $N_0^{(2)}+1$, respectively, and the numbers of points in the meshes $\overline{\omega}^1$ and $\overline{\omega}_0^1$ are $N^{(1)}+1$ and $N_0^{(1)}+1$, respectively:

$$N^{(2)} = N,\ N_0^{(2)} = N_0;\quad N^{(1)} = (k^*)^{-1}\,N,\ N_0^{(1)} = (k^*)^{-1}\,N_0. \tag{9b}$$

Define

$$\overline{G}_h^0 = \overline{G}_h^1 \cap \overline{G}_h^2. \tag{9c}$$

Let $z^i(x,t)$, $(x,t) \in \overline{G}_h^i$, $i = 1,\ 2$ be solutions of the difference schemes

$$\begin{aligned} \Lambda_{(7)} z^i(x,t) &= f(x,t), \quad (x,t) \in G_h^i, \\ z^i(x,t) &= \varphi(x,t), \quad (x,t) \in S_h^i,\ \ i = 1,2. \end{aligned} \tag{10a}$$

Set

$$\begin{aligned} z^0(x,t) &= \gamma\, z^1(x,t) + (1-\gamma)\, z^2(x,t), \quad (x,t) \in \overline{G}_h^0, \\ \gamma &= \gamma(k^*) = -(k^*-1)^{-1}. \end{aligned} \tag{10b}$$

The function $z^0_{(10)}(x,t)$, $(x,t) \in \overline{G}_h^0$, is the solution of the difference *scheme of the Richardson method* (10), (9). Thus, setting *basic grid* $\overline{G}^1_{h\,(9a)}$, we define the solution of the problem (10), (9):

$$z^0(x,t) = z^0(x,t;\,\overline{G}_h^1),\ \ (x,t) \in \overline{G}_h^0;\quad \overline{G}_h^0 = \overline{G}_h^0(\overline{G}_h^1). \tag{10c}$$

In the case of the estimate (5) with $K = 6$, we obtain the estimate

$$|u(x,t) - z^0(x,t)| \le M\,\left[N^{-2}\,(\varepsilon + N^{-1})^{-2} + N_0^{-2}\right],\ \ (x,t) \in \overline{G}_h^0. \tag{11}$$

4 Scheme on Local-Uniform Grids

We give an algorithm, based on the algorithm in [8], of constructing a local-uniform (adapted in the boundary layer) grid and a discrete solution on it.

On the set $\overline{G}$ we introduce the *basic grid* $\overline{G}_{1h}$ that we use for constructing a standard scheme of the Richardson method on the first iteration:

$$\overline{G}_{1h} \equiv \overline{G}_{h(6)}. \tag{12a}$$

The grid $\overline{G}_{1h\,(12a)}$ *defines the solution of the Richardson method scheme* $z_1^0(x,t)$ on the grid $\overline{G}_{1h}^0$ *on the first iteration*

$$z_1^0(x,t) = z^0_{1\,(10c)}(x,t;\,\overline{G}_{1h}),\quad (x,t) \in \overline{G}_{1h}^0;\quad \overline{G}_{1h}^0 = \overline{G}^0_{1h\,(10c)}(\overline{G}_{1h}),$$

where $\overline{G}^{\,0}_{1h} = \overline{\omega}^{\,0}_1 \times \overline{\omega}^{\,0}_0$. This solution is constructed on the base of the components $z^i_1(x,t)$, $(x,t) \in \overline{G}^{\,i}_{1h}$, $i = 1,2$, considered on the grids:

$$\overline{G}^{\,2}_{1h}, \quad \overline{G}^{\,1}_{1h} \tag{12b}$$

where $\overline{G}^{\,2}_{1h} = \overline{G}_{1h(12a)}$ is the basic grid and $\overline{G}^{\,1}_{1h}$ is the coarsed grid. For the set $\overline{G}$, the functions $z_1(x,t)$, $z^i_1(x,t)$ and the grids $\overline{G}_{1h}$, $\overline{G}^{\,i}_{1h}$ we shall use also the notations $\overline{G}_{(1)}$, $z_{(1)}(x,t)$, $z^i_{(1)}(x,t)$ and $\overline{G}_{(1)h}$, $\overline{G}^{\,i}_{(1)h}$, respectively; $i = 0,1,2$.

Let the value $d_1 \in \overline{\omega}^{\,0}_1$ be found in some a way (see, e.g., (17) in Sect. 5) such that for $x \geq d_1$ the discrete solution $z^0_1(x,t)$, $(x,t) \in \overline{G}^{\,0}_{1h}$, is a good approximation the solution of the problem (2), (1), moreover,

$$|u(x,t) - z^0_1(x,t)| \leq M\,\delta, \quad (x,t) \in \overline{G}^{\,0}_{1h}, \quad x \geq d_1, \quad d_1 \in [0,d), \tag{13a}$$

where $\delta > 0$ is an arbitrary sufficiently small number specifying the required accuracy of the discrete solution, and M is a constant independent of δ.

For $x < d_1 > 0$, we shall make more precise the solution of the discrete problem, i.e., we shall construct a *scheme of the Richardson method on the second iteration*. We define the subdomain $\overline{G}_{(2)}$, on which we shall refine the grids $\overline{G}^{\,i}_{1h}$ in order to do the discrete solution more precise:

$$\overline{G}_{(2)} = G_{(2)} \bigcup S_{(2)}, \;\; G_{(2)} = G_{(2)}(d_1), \;\; G_{(2)} = D_{(2)} \times (0,T], \;\; D_{(2)} = (0,d_1).$$

On the subdomain $\overline{G}_{(2)}$ we introduce the basic grid

$$\overline{G}_{(2)h} = \overline{\omega}_{(2)} \times \overline{\omega}_0,$$

where $\overline{\omega}_{(2)}$ is an uniform mesh on $\overline{D}_{(2)}$ with the step-size $h_{(2)}$ and the number of nodes $N+1$; construct the coarsed grid $\overline{G}^{\,1}_{(2)h}$. On the set $\overline{G}^{\,i}_{(2)h}$, $i = 1,2$, we find the solution $z^i_{(2)}(x,t)$ of the discrete problem

$$\Lambda_{(7)}\, z^i_{(2)}(x,t) = f(x,t), \qquad (x,t) \in G^i_{(2)h},$$

$$z^i_{(2)}(x,t) = \begin{cases} z^i_1(x,t), & (x,t) \in S^i_{(2)h} \setminus S, \\ \varphi(x,t), & (x,t) \in S^i_{(2)h} \bigcap S, \end{cases} \quad i = 1,2,$$

where $G^i_{(2)h} = G_{(2)} \bigcap \overline{G}^{\,i}_{(2)h}$, $S^i_{(2)h} = S_{(2)} \bigcap \overline{G}^{\,i}_{(2)h}$. We define the discrete sets $\overline{G}^{\,i}_{2h}$, $i = 1,2$, on $\overline{G}$ and the functions $z^i_2(x,t)$, $(x,t) \in \overline{G}^{\,i}_{2h}$, i.e., components of the Richardson scheme, by the relations

$$\overline{G}^{\,i}_{2h} = \overline{G}^{\,i}_{(2)h} \cup \left\{ \overline{G}^{\,i}_{1h} \setminus \overline{G}_{(2)} \right\}, \quad z^i_2(x,t) = \begin{cases} z^i_{(2)}(x,t), & (x,t) \in \overline{G}^{\,i}_{(2)h}, \\ z^i_1(x,t), & (x,t) \in \overline{G}^{\,i}_{1h} \setminus \overline{G}_{(2)}, \end{cases}$$

where $i = 1, 2$. Further, taking account of the grids $\overline{G}^{\,i}_{2h}$, $i = 1, 2$, and the components $z^i_2(x,t)$, we construct the grid $\overline{G}^{\,0}_{2h}$ and the function $z^0_2(x,t)$ on this set, i.e., *the solution of the Richardson method on the second iteration*. If turns out that $d_2 > 0$, then we continue the computations.

For $k = K$ and $d_{K-1} > 0$, where K is a given fixed number (the number of iterations for improving the grid solution), $K \geq 1$, we set

$$\overline{G}^{\,0}_h = \overline{G}^{\,K\,0}_h \equiv \overline{G}^{\,0}_{Kh}, \quad z^0(x,t) = z^{K\,0}(x,t) \equiv z^0_K(x,t). \tag{12e}$$

The grid $\overline{G}^{\,0}_h$ and the function $z^0(x,t)$ in (12e) are constructed using the grid sets $\overline{G}^{\,i}_{(k)h}$ and the functions $z^i_{(k)}(x,t)$, $(x,t) \in \overline{G}^{\,i}_{(k)h}$, $k = 1, \ldots, K$, $i = 1, 2$.

We call the function $z^0_{(6)}(x,t)$, $(x,t) \in \overline{G}^{\,0}_{h(12)}$, *the solution of scheme* (7), (12), which is *the scheme of the Richardson method on locally-uniform meshes*.

5 Difference Scheme on Adapted Meshes

We consider a difference scheme on a priori adapted meshes constructed using a majorant to the singular component of the discrete solution. We denote by $z_v(x,t)$, $(x,t) \in \overline{G}_h$ the solution of the difference problem

$$\Lambda_{(7)}\, z(x,t) = L_{(2)}\, v(x,t), \quad (x,t) \in G_h, \quad z(x,t) = v(x,t), \quad (x,t) \in S_h,$$

where $v \in C^{2,1}(G) \bigcap C(\overline{G})$. Write the solution of problem (7), (6) as the sum

$$z(x,t) = z_U(x,t) + z_V(x,t), \quad (x,t) \in \overline{G}_h, \tag{14}$$

where $z_U(x,t)$ and $z_V(x,t)$ are grid functions approximating the components $U(x,t)$ and $V(x,t)$ in the representation (3); $z_V(x,t)$ is the function of the grid boundary layer. The function

$$W(x) = W(x;\, \varepsilon, h) = (1 + m^0 \varepsilon^{-1} h)^{-n}, \quad x = x^n \in \overline{D}^{\,\infty}_h, \quad x^n = nh, \tag{15}$$

where $\overline{D}^{\,\infty}_h$ is an uniform grid on the semiaxis $\overline{D}^{\,\infty} = [0, \infty)$ with step-size h, is a majorant (up to a constant-multiplier) for the singular component $z_V(x,t)$ in representation (14) for the solution of the difference scheme (7) on the grid (6), where $h_{(6)} = h_{(15)}$ and $m^0 = \min\limits_{\overline{G}} [a^{-1}(x,t) b(x,t)]$. We say that the value

$$\eta = \eta(\delta;\, \varepsilon, h), \tag{16a}$$

is the *width of the grid boundary layer*, if η is the minimum of the value η_0 satisfying the estimate

$$W(x;\,\varepsilon,h)\le\delta,\quad x\in\overline{D}_h^{\infty},\quad x\ge\eta_0. \tag{16b}$$

On the uniform grid $\overline{D}_{h(15)}^{\infty}$ with step-size h we associate the value $\{a;\,h\}^e$ to the value $a\ge 0$; the value $\{a;\,h\}^e$ is defined by the relation

$$\{a;\,h\}^e=\begin{cases} a & for\ \ h\left[h^{-1}a\right]^e=a,\\ h\left\{h\left[h^{-1}a\right]^e+1\right\} & for\ \ h\left[h^{-1}a\right]^e<a,\end{cases}$$

where $[\,a\,]^e$ is the integer part of the number a. Write the value η in the form

$$\eta=\eta(\delta;\,\varepsilon,h)=\{a;\,h\}^e,\ \ where\ \ a=h\,\ln\delta^{-1}\ln^{-1}(1+m^0\varepsilon^{-1}h). \tag{16c}$$

For $(x,t)\in\overline{G}_{h(6)}^{u}$ with $x\ge\eta(\delta;\,\varepsilon,h)$, we have $|z_V(x,t)|\le M\delta$ ([10], Chap. 11, [8]).

Define the values d_k in the algorithm in Sect. 4 by the relations

$$d_k=d_k(\delta;\,\varepsilon,h^1_{(k)}),\quad k=1,\dots,K; \tag{17a}$$

$$d_1=\min\left[\eta(\delta;\,\varepsilon,h^1_{(1)}),\,d\right],\quad k=1,$$

$$d_k=\left\{\begin{matrix}\min\left[\eta(\delta;\,\varepsilon,h^1_{(k)}),\,d_{k-1}\right] & for\ \eta(\delta;\,\varepsilon,h^1_{(k)})<m\,d_{k-1}\\ d_{k-1} & for\ \eta(\delta;\,\varepsilon,h^1_{(k)})\ge m\,d_{k-1}\end{matrix}\right\},\ k=2,\dots,K,$$

m is a sufficiently small constant; $h^1_{(k)}=k^*\,d_{k-1}\,N^{-1}$ for $k\ge 1$, $d_0=d$. Set

$$\delta=\delta(N)\to 0\ \ for\ \ N\to\infty. \tag{17b}$$

The difference scheme (7), (12), (17) defined by the values N,N_0,ε,K (where $N,N_0\to\infty$, $\varepsilon\in(0,1]$, $K\ge 1$) is the *the scheme of the Richardson method on locally-uniform a priori adapted meshes*.

For the solution of the scheme (7), (12), (17) in the case of estimates (5) for $K^*=6$ the following estimate holds:

$$|u(x,t)-z^0_K(x,t)|\le \tag{18}$$

$$\begin{cases}M\left[\delta(N)+N^{-2}\ln^2N+N_0^{-2}\right],\quad x\ge d_K, & (x,t)\in\overline{G}_h,\\ M\left[(\varepsilon+d_{K-1}\,N^{-1})^{-2}\,d^2_{K-1}\,N^{-2}+\delta(N)+N^{-2}\ln^2N+N_0^{-2}\right], & (x,t)\in\overline{G}^0_h.\end{cases}$$

Thus, the difference scheme (7), (12), (17) for given number of iterations K converges ε-uniformly outside the d_K-neighbourhood of the boundary S_1^L with the first

order of accuracy $\delta = \delta(N)$, close to the second order in N and with the second order in N_0, and it also converges on the whole set $\overline{G}_h$ under the condition

$$\varepsilon^{-1} = o\big((d_{K-1})^{-1} N\big). \tag{19}$$

For the solution of the Richardson method scheme (7), (12), (17) with $\delta = N^{-2}$, the following estimate holds:

$$|u(x,t) - z^0_K(x,t)| \le \tag{20a}$$

$$\le \begin{cases} M\left[N^{-2}\ln^2 N + N_0^{-2}\right], & x \ge d_{K-1}, \\ M\left[(\varepsilon^{-1} N^{-K}\ln^2 N)^2 + N^{-2}\ln^4 N + N_0^{-2}\right], & x < d_{K-1}; \quad (x,t) \in \overline{G}^0_{Kh}. \end{cases}$$

The value d_K satisfies the estimate

$$d_K \le d_{K-1} \le M\, N^{-K+1}\, \ln^2 N,\ \varepsilon \in (0,1]. \tag{20b}$$

Thus, for $N, N_0 \to \infty$, outside the d_{K-1}-neighbourhood of the boundary S^l, K-th iteration of the Richardson method scheme (7), (12), (17) converges with an accuracy order close to 2; in the d_{K-1}-neighbourhood, the scheme converges on $\overline{G}^0_{K\,h}$ under the condition $N^{-K}\ln^2 N \ll \varepsilon$; for large values of K the scheme converges almost ε-uniformly with the defect ν satisfying the estimate

$$\nu < \nu(K) \equiv 1/(K-m). \tag{21}$$

Theorem 5.1 *Let the estimate* (5) *for* $K = 6$ *be satisfied. Then the solution* $z^0_K(x,t)$, $(x,t) \in \overline{G}_{K\,h(12)}$ *of the Richardson method scheme (7), (12), (17) converges under the condition* $N^{-K}\ln^2 N \ll \varepsilon$. *The function* $z^0_K(x,t)$ *and the defect* ν *of the almost* ε*-uniform convergence satisfy the estimates (20) and (21), respectively.*

The Richardson technique allows us to construct *almost* ε*-uniformly convergent schemes on locally-uniform meshes*, and with the *high convergence rate for fixed values of the parameter* ε. Principles of proof to Theorem 5.1 are similar to those given in [8, 10]. The full presentation of results of the present paper is given in the paper submitted for another publication.

Acknowledgements This research was supported by the Russian Foundation for Basic Research under grant No.10-01-00726.

References

1. Ladyzhenskaya, O.A., Solonnikov, V.A., Uraltseva, N.N.: Linear and Quasilinear Equations of Parabolic Type. Nauka, Moscow (1967). (in Russian); Translations of Mathematical Monographs, **23**, American Mathematical Society, Providence, R.I. (1967).
2. Miller, J.J.H., O'Riordan, E., Shishkin, G.I.: Fitted Numerical Methods for Singular Perturbation Problems. World Scientific, Singapore (1996).

3. Samarskii, A.A.: Theory of Difference Schemes. Nauka, Moscow (1989) (in Russian).
4. Shishkin, G.I.: Grid Approximations of Singularly Perturbed Elliptic and Parabolic Equations. Ural Branch of RAS, Ekaterinburg (1992) (in Russian).
5. Shishkin, G.I.: A posteriori adapted (to the solution gradient) grids in the approximation of singularly perturbed convection-diffusion equations. Vychisl. Tekhnol., **6**, 72–87 (2001) (in Russian).
6. Shishkin, G.I.: Approximation of singularly perturbed reaction-diffusion equations on adaptive grids. Mat. Model., **13**, 103–118 (2001).
7. Shishkin, G.I.: The use of solutions on embedded grids in the approximation of a singularly perturbed parabolic convection-diffusion equation on adaptive grids. Comp. Math. Math. Phys., **46**, 1539–1559 (2006).
8. Shishkin, G.I.: A finite difference scheme on a priori adapted meshes for a singularly perturbed parabolic convection-diffusion equation. Numer. Math. Theor. Meth. Appl., **1**, 214–234 (2008).
9. Shishkin, G.I., Shishkina, L.P., Hemker, P.W.: A class of singularly perturbed convection-diffusion problems with a moving interior layer, *A Posteriori* Adaptive Mesh Technique. Comp. Methods in Appl. Math., **4**, 105–127 (2004).
10. Shishkin, G.I., Shishkina, L.P.: Difference Methods for Singular Perturbation Problems. Series: Monographs & Surveys in Pure & Applied Math. Chapman and Hall/CRC (2009).

Flux Difference Schemes for Parabolic Reaction-Diffusion Equations with Discontinuous Data

L.P. Shishkina and G.I. Shishkin

Abstract For an initial-boundary value problem for a singularly perturbed parabolic reaction-diffusion equation on a composed domain, a conservative flux difference scheme on flux piecewise-uniform grids is constructed whose solution and also normalized diffusion flux converge (in the maximum norm) independent of the perturbation parameter ε at the rate $\mathcal{O}\big(N^{-2}\ln^2 N + N_0^{-1}\big)$.

1 Problem Formulation: Aim of Research

On the composed domain

$$\overline{G} = \overline{G}_1 \bigcup \overline{G}_2 \tag{1}$$

with the interface boundary $S^{int} = \overline{G}_1 \bigcap \overline{G}_2$ between the subdomains $\overline{G}_1$ and $\overline{G}_2$, we consider the initial-boundary value problem for the singularly perturbed parabolic reaction-diffusion equation[1]

$$L_{(2)}\, u(x,t) = f(x,t), \quad (x,t) \in G_i, \quad i = 1,2, \tag{2a}$$

$$l_0\, u(x,t) = l_1\, u(x,t) = 0,\ (x,t) \in S^{int}, \quad u(x,t) = \varphi(x,t),\ (x,t) \in S. \tag{2b}$$

Here $\overline{G} = G \bigcup S$, $G = D \times (0,T]$, $\overline{G}_i = G_i \bigcup S_i$ $G_i = D_i \times (0,T]$, $\overline{D} = [d_{*1}, d_1^*]$, $\overline{D}_1 = [d_{*1}, 0]$, $\overline{D}_2 = [0, d_1^*]$, $d_1^* \geq d > 0$, $-d_{*1} \geq d > 0$,

[1]Notation $L_{(j)}$ ($m_{(j)}$, $M_{(j)}$, $G_{h(j)}$) means that these operators (constants, grids) are introduced in formula (j).

L.P. Shishkina (✉) and G.I. Shishkin
Institute of Mathematics and Mechanics, Russian Academy of Sciences, Ekaterinburg, Russia
e-mail: Lida@convex.ru

C. Clavero et al. (eds.), *BAIL 2010 – Boundary and Interior Layers, Computational and Asymptotic Methods*, Lecture Notes in Computational Science and Engineering 81,
DOI 10.1007/978-3-642-19665-2_23, © Springer-Verlag Berlin Heidelberg 2011

$$L_{(2)} \equiv \varepsilon^2 \frac{\partial}{\partial x}\left(a(x,t)\frac{\partial}{\partial x}\right) - c(x,t) - p(x,t)\frac{\partial}{\partial t},$$
$$l_0\, u(x,t) \equiv u(x+0,t) - u(x-0,t),$$
$$l_1\, u(x,t) \equiv a(x+0,t)\frac{\partial}{\partial x}u(x+0,t) - a(x-0,t)\frac{\partial}{\partial x}u(x-0,t).$$

The coefficients $a(x,t)$, $c(x,t)$, $p(x,t)$ and the right-hand side $f(x,t)$ are assumed to be sufficiently smooth on the sets $\overline{G}_i$, $i = 1,2$, moreover, $a(x,t)$, $p(x,t) > 0$, $c(x,t) \geq 0$. The boundary function $\varphi(x,t)$ is sufficiently smooth on the sets S_0 and $\overline{S}^L$ and is continuous on S, where S_0 and S^L are lower and lateral parts of the boundary S, moreover, $S_0 = \overline{S}_0$. The parameter ε takes arbitrary values in $(0,1]$. The derivative multiplied by ε^2 in the differential equation is written in divergent form. For $\varepsilon \to 0$, the boundary and interior parabolic layers appear in neighbourhoods of the sets $\overline{S}^L$ and S^{int}.

In [3,4] it is shown that even for regular problems with discontinuous data solutions of difference schemes, which are not conservative, do not converge to solutions of boundary value problems in the maximum norm.

Our *aim* for the boundary value problem (2), (1) is to construct an ε-uniformly convergent conservative difference *scheme on a flux grid* that approximates both the solution and a *diffusion flux*.

2 A Priori Estimates for Solutions and Derivatives

Here we give a priori estimates for solutions and derivatives of the problem (2), (1) that are established with using the technique from [1,2,5,6].

Using a comparison Theorem [5], we obtain the estimate

$$|u(x,t)| \leq M\left[\max_{\overline{G}}|f(x,t)| + \max_{S}|\varphi(x,t)|\right], \quad (x,t) \in \overline{G}. \tag{3}$$

Assume that the data of the problem (2), (1) satisfy the condition

$$a \in C^{l_\alpha+1,(l_\alpha+1)/2}(\overline{G}_i),\ c,\ p,\ f \in C^{l_\alpha,l_\alpha/2}(\overline{G}_i),\ \varphi \in C^{l_\alpha}(S_0)\bigcap C^{l_\alpha/2}(\overline{S}^L), \tag{4a}$$

where $l_\alpha = l + \alpha$, $l \geq 0$, $\alpha > 0$, $i = 1,2$. Moreover, on the set of *corner points* $S^c = \overline{S}^L \bigcap S_0$ of the set $\overline{G}$, and also on the set of *interior corner points* $S^d = \overline{S}^{int} \bigcap S_0$ of the sets $\overline{G}_1$ and $\overline{G}_2$, additional conditions are satisfied that guarantee smoothness of the problem solution on the sets $\overline{G}_1$ and $\overline{G}_2$.

Definition. Set $\varphi_0(x) = \varphi(x,t)$, $(x,t) \in S_0$. Let the function $\varphi(x,t)$, $(x,t) \in S$, satisfy the condition $\varphi(\cdot,0) \in C^{l_\alpha}(\overline{D})$ ($\varphi_0 \in C^{l_\alpha}(\overline{D})$), moreover, for the function $\varphi(x,t)$ considered on $\overline{S}^L$, the derivatives $(\partial^{k_0}/\partial t^{k_0})\,\varphi(x,t)$ for $(x,t) \in S^c$, $k_0 \leq l/2$ are defined. Using the function $\varphi_0(x)$ prescribed on the set S_0 and the

equation (2a), we find the derivative in t of the function $u(x,t)$ on S_{0i} which are lower boundaries of the sets $\overline{G}_i$, $i = 1,2$. We denote this derivative by $(\partial/\partial t)\,\varphi_{0,t=0}(x)$. Further, using equations obtained by differentiation in x and t of the equation (2a), we find derivatives in t up to order $k_0 \le [l/2]_i$, where $[a]_i$ is the integer part of the number $a \ge 0$; we denote these derivatives by $(\partial^{k_0}/\partial t^{k_0})\,\varphi_{0,t=0}(x)$, $x \in \overline{D}_i$, $i = 1,2$. We say that the data of the boundary value problem *on the set* $S^{cd} = S^c \bigcup S^d$ satisfy a *compatibility condition* that ensures continuity of the derivatives in t of the function $u(x,t)$ on S^{cd} up to order K_0, or, briefly, the data of the problem satisfy on S^{cd} a *compatibility condition of the derivatives in t up to order* K_0 [1,2], if the following condition holds:

$$(\partial^{k_0}/\partial t^{k_0})\,\varphi(x,t) = (\partial^{k_0}/\partial t^{k_0})\,\varphi_{0,t=0}(x), \qquad (x,t) \in S^c,$$
$$(\partial^{k_0}/\partial t^{k_0})\,\varphi_{0,t=0}(x-0) = (\partial^{k_0}/\partial t^{k_0})\,\varphi_{0,t=0}(x+0), \ (x,t) \in S^d,$$

where $0 \le k_0 \le K_0$. For the stated conditions, $K_0 \le [l/2]_i$. □

Compatibility conditions of the problem data on the set S^{cd} that guarantee continuity of the derivatives in x and t: $(\partial^{k+k_0}/\partial x^k\,\partial t^{k_0})\,u(x,t)$ up to order $k + 2k_0 \le K$, $K = 2/$, K_0, on the sets $\overline{G}_i$, $i = 1,2$, are necessary and sufficient.

Suppose that on the set S^{cd} compatibility conditions of the derivatives in t up to order $K_0 = l/2$ (assume that the value l is even) are satisfied that guarantee the smoothness

$$u \in C^{l+\alpha,(l+\alpha)/2}\big(\overline{G}_i\big), \quad i = 1,2. \tag{4b}$$

Write the solution of the problem (2), (1) in each subdomain as the sum of the functions

$$u(x,t) = U(x,t) + V(x,t), \quad (x,t) \in \overline{G}_i, \quad i = 1,2, \tag{5}$$

where $U(x,t)$ and $V(x,t)$ are the regular and singular parts of the solution. The function $U(x,t)$, $(x,t) \in \overline{G}_i$, is the restriction to $\overline{G}$ of the function $U^e(x,t)$, $(x,t) \in \overline{G}_i^e$. The function $U^e(x,t)$ is the solution of the problem

$$L^e_{(2)i}\,U^e(x,t) = f^e(x,t), \ (x,t) \in G_i^e, \quad U^e(x,t) = \varphi^e(x,t), \ (x,t) \in S_i^e.$$

Here $S_i^e = S(G_i^e)$; the domain G_i^e is an extension of G_i beyond the boundary S_i^L, the set $\overline{G}_i^e$ includes $\overline{G}_i$ together with its m-neighborhood; the coefficients of the operator $L^e_{(2)i}$ and the right-hand side $f^e(x,t)$ are smooth extensions of those in (2), (1) from the set G_i to $\overline{G}_i^e$; $\varphi^e(x,t)$ is a smooth function, moreover, $\varphi^e(x,t) = \varphi(x,t)$, $(x,t) \in S_{0i}$. The function $V(x,t)$ is the solution of the problem

$$L\,V(x,t) = 0, \ (x,t) \in G_i, \quad V(x,t) = \begin{cases} \varphi(x,t) - U(x,t), & (x,t) \in S_i \bigcap S, \\ u(x,t) - U(x,t), & (x,t) \in S_i \setminus S. \end{cases}$$

The functions $U(x,t)$ and $V(x,t)$ are not continuous on S^{int}.

For the components $U_0^e(x,t)$ and $v_U^e(x,t)$ in the representation

$$U^e(x,t) = U_0^e(x,t) + v_U^e(x,t), \quad (x,t) \in \overline{G}^e, \tag{6}$$

where $v_U^e(x,t)$ is the remainder term, $U_0^e(x,t)$ and $v_U^e(x,t)$ are solutions of the problems

$$L^e U_0^e(x,t) \equiv \left\{ -c^e(x,t) - p^e(x,t)\,\frac{\partial}{\partial t} \right\} U_0^e(x,t) = f^e(x,t), (x,t) \in \overline{G}^e \setminus S_{i0}^e,$$

$$U_0^e(x,t) = \varphi^e(x,t), (x,t) \in S_{i0}^e;$$

$$L_{(2)i}^e v_U^e(x,t) = -\varepsilon^2 \frac{\partial}{\partial x}\left(a^e(x,t)\,\frac{\partial}{\partial x}\right) U_0^e(x,t), \ (x,t) \in G_i^e,$$

$$v_U^e(x,t) = \varphi^e(x,t) - U_0^e(x,t), \qquad (x,t) \in S_i^e, \ i = 1,2,$$

we obtain the estimates

$$\left| \frac{\partial^{k+k_0}}{\partial x^k \partial t^{k_0}} U_0^e(x,t) \right| \le M, \quad \left| \frac{\partial^{k+k_0}}{\partial x^k \partial t^{k_0}} v_U^e(x,t) \right| \le M\,\varepsilon^{2-k}, \quad (x,t) \in \overline{G}_i^e,$$

where $i = 1,2$, $k + 2k_0 \le K$, $K = l$. Thus, we have

$$\left| \frac{\partial^{k+k_0}}{\partial x^k \partial t^{k_0}} U(x,t) \right| \le M\,[1 + \varepsilon^{2-k}], \quad (x,t) \in \overline{G}_i, \ k + 2k_0 \le K, \ i = 1,2, \tag{7}$$

where $K = l$. For the function $V(x,t)$ with regard to estimates (3), (7), we obtain the estimate

$$|V(x,t)| \le M\,\exp\bigl(-m\,\varepsilon^{-1}\,r(x,\Gamma_i)\bigr), \quad (x,t) \in \overline{G}_i, \ i = 1,2, \tag{8}$$

where $r(x,\Gamma_i)$ is a distance from the point x, $x \in \overline{D}_i$, to the boundary $\overline{G}_i$ of the set $\overline{D}_i$, m is an arbitrary constant.

Find estimates of derivatives for the function $V(x,t)$, assuming

$$a(x,t) = a(x), \quad c(x,t) = c(x), \quad p(x,t) = p(x), \quad (x,t) \in \overline{G}_i, \ i = 1,2. \tag{9}$$

By applying the operators $\partial^{k_0}/\partial t^{k_0}$, $1 \le k_0 \le K_t$, $K_t = l/2$, to the problem (2), we find that $(\partial^{k_0}/\partial t^{k_0})\,u \in C^{\alpha}(\overline{G}_i)$, $i = 1,2$. For the derivative $(\partial^{k_0}/\partial t^{k_0})\,u(x,t)$, $(x,t) \in \overline{G}$, we obtain the estimate

$$\left| (\partial^{k_0}/\partial t^{k_0})\,u(x,t) \right| \le M, \quad (x,t) \in \overline{G}_i, \ 0 \le k_0 \le K_t, \ i = 1,2, \tag{10}$$

Further, considering the function $u(x,t)$ in each subdomain $\overline{G}_i$ as the solution of the initial-boundary value problem with boundary conditions satisfying the condition (10), and with regard to the estimate (7), we find

$$\left| \frac{\partial^{k+k_0}}{\partial x^k \, \partial t^{k_0}} V(x,t) \right| \le M \, \exp\bigl(- m \, \varepsilon^{-1} \, r(x, \Gamma_i) \bigr), \quad (x,t) \in \overline{G}_i, \;\; i = 1,2, \quad (11)$$

where $k + 2k_0 \le K$, $K \le l$, $m = m_{(8)}$.

Theorem 2.1 *Let the data of the initial-boundary value problem (2), (1) satisfy the conditions (4), (9) for* $l \;\ge\; 2$. *Then for the components of the solution in the representation (5), the estimates (7), (11) are satisfied.*

Remark 1 The statement of Theorem 2.1 preserves in the case when only the coefficients $a(x,t)$, $c(x,t)$ are independent of t, or the coefficient $c(x,t)$ equals zero and also when the condition (9) holds only in the m-neighbourhood of the set S^{int}. □

3 Conservative Difference Scheme on Flux Grids

For the initial-boundary value problem (2), (1), we propose a difference scheme on flux grids considered for regular problems in [3].

On the set $\overline{G}$ we introduce the rectangular grid

$$\overline{G}_h = \overline{D}_h \times \overline{\omega}_0 = \overline{\omega} \times \overline{\omega}_0, \quad (12a)$$

where $\overline{\omega}$ and $\overline{\omega}_0$ are meshes on the intervals $\overline{D}$ and $[0,T]$, respectively, in general, nonuniform; the point $x = 0$ belongs to the mesh $\overline{\omega}$. We denote by $N+1$ and N_0+1 the numbers of nodes in the meshes $\overline{\omega}$ and $\overline{\omega}_0$. Let

$$x^0, \, x^1, \, \ldots, \, x^i, \, \ldots, \, x^N, \quad (12b)$$

be nodes in the mesh $\overline{\omega}$, where $x^0 = d_{*1}$, $x^N = d_1^*$. Set $h^i = x^{i+1} - x^i$, x^i, $x^{i+1} \in \overline{\omega}$, $h = \max_i h^i$, $h_t^j = t^{j+1} - t^j$, t^j, $t^{j+1} \in \overline{\omega}_0$, $h_t = \max_j h_t^j$; assume to be satisfied the conditions $h \le M \, N^{-1}$ and $h_t \le M \, N_0^{-1}$.

To construct a difference scheme, we apply the integro-interpolational method [3].

For the problem (2), (1) we have the difference scheme

$$\Lambda_{(13)} \, z(x,t) = f_h(x,t), \;\; (x,t) \in G_h, \quad z(x,t) = \varphi(x,t), \;\; (x,t) \in S_h. \quad (13)$$

Here $G_h = G \cap \overline{G}_h$, $S_h = S \cap \overline{G}_h$,

$$\Lambda_{(13)}\, z(x,t) \equiv \varepsilon^2\, \delta_{\widehat{x}} \left(a_{i-1/2}(x,t)\, \delta_{\overline{x}}\, z(x,t)\right) - c_h(x,t)\, z(x,t) - p_h(x,t)\, \delta_{\overline{t}}\, z(x,t),$$

$\delta_{\widehat{x}} \left(a_{i-1/2}(x,t)\, \delta_{\overline{x}}\, z(x,t)\right)$, $\delta_{\overline{t}}\, z(x,t)$ are difference derivatives (see [3]):

$$\delta_{\widehat{x}} \left(a_{i-1/2}(x,t)\, \delta_{\overline{x}}\, z(x,t)\right) = \frac{1}{\hbar} \left\{a_{i+1/2}(x,t)\, \delta_x\, z(x,t) - a_{i-1/2}(x,t)\, \delta_{\overline{x}}\, z(x,t)\right\},$$

$$\delta_x\, z(x,t) = \frac{1}{h^i}\left(z(x^{i+1},t) - z(x,t)\right), \quad \delta_{\overline{x}}\, z(x,t) = \frac{1}{h^{i-1}}\left(z(x,t) - z(x^{i-1},t)\right),$$

$$a_{i-1/2}(x,t) = a\left(2^{-1}\,(x^{i-1} + x^i), t\right), \quad a_{i+1/2}(x,t) = a\left(2^{-1}\,(x^i + x^{i+1}), t\right),$$

$$\delta_{\overline{t}} z(x,t) = \left(h^{j-1}\right)^{-1}\left(z(x,t) - z(x,t^{j-1})\right),\ (x,t) = (x^i, t^j), \hbar = 2^{-1}(h^i + h^{i-1}),$$

the functions $c_h(x,t)$, $p_h(x,t)$, $f_h(x,t)$, $(x,t) \in G_h$ are defined by the relation

$$v_h(x,t) = \begin{cases} v(x,t), & x \neq 0, \\ (h^i + h^{i-1})^{-1}\, \left\{h^i\, v_{i+1/2}(x,t) + h^{i-1}\, v_{i-1/2}(x,t)\right\}, & x = x^i = 0, \end{cases}$$

where $v(x,t)$ is one of the functions $c(x,t)$, $p(x,t)$, $f(x,t)$. In a similar way it is possible to write out a scheme when $\{x\} \cap \overline{\omega} = \emptyset$.

The difference operator $\Lambda_{(13)}$ is ε-uniformly monotone.

On $\overline{G}$ we construct the grid on which the scheme converges ε-uniformly:

$$\overline{G}_h = \overline{G}_h^s = \overline{\omega}^s \times \overline{\omega}_0, \tag{14a}$$

where $\overline{\omega}_0 = \overline{\omega}_0^u$ is an uniform mesh, $\overline{\omega}^s = \overline{\omega}^s(\sigma)$ is the piecewise-uniform mesh on $[d_{*1}, d_1^*]$ condensed in neighbourhoods of the interval and of the point $x = 0$. The step-sizes in the meshes $\overline{\omega}^s$ are constant on the intervals

$$[d_{*1}, d_{*1} + \sigma], \quad [-\sigma, \sigma], \quad [d_1^* - \sigma, d_1^*], \quad \textit{and} \quad [d_{*1} + \sigma, -\sigma], \quad [\sigma, d_1^* - \sigma], \tag{14b}$$

and they equal, respectively, to $h^{(1)} = 8\,\sigma\, N^{-1}$ and $h^{(2)} = 2\,[d - 4\,\sigma]\, N^{-1}$, where $d = d_1^* - d_{*1}$. The value σ is defined by the relation

$$\sigma = \sigma(\varepsilon, N) = \min\left[4^{-1}\,|d_{*1}|,\ 4^{-1}\,d_1^*,\ M\,\varepsilon\,\ln N\right], \quad M = 2\,m_{(8)}^{-1}.$$

For the solution of the scheme (13), (14) we obtain the ε-uniform estimate

$$|u(x,t) - z(x,t)| \leq M\left[N^{-2}\,\ln^2 N + N_0^{-1}\right], \quad (x,t) \in \overline{G}_h. \tag{15}$$

In the scheme (13), (12), the function $w_{h\,i+1/2}(x,t) = -\varepsilon^2\, a_{i+1/2}(x,t)\, \delta_x\, z(x,t)$, $(x,t) \in \overline{G}_h$, $x \neq d_*$, corresponds to the function $w_{i+1/2}(x,t) = -\varepsilon^2\, a_{i+1/2}(x,t)\, (\partial/\partial\, x)\, u(x,t)$, i.e., the diffusion flux for the diffusion coefficient $\varepsilon^2\, a_{i+1/2}(x,t)$ in "middle points" of the grid $\overline{G}_{h\,(12)}$.

On the set $\overline{G}$ we introduce the basic ("main") grid $\overline{G}_h^b$

$$\overline{G}_h^b = \overline{G}_{h(12)}; \quad \overline{G}_h^b = \overline{\omega}^b \times \overline{\omega}_{0(12)}, \quad \overline{\omega}^b = \overline{\omega}_{(12)} \tag{16a}$$

and "auxiliary" grid G_h^a

$$G_h^a = \omega^a \times \overline{\omega}_{0(12)}. \tag{16b}$$

Here ω^a is the mesh with "half-integer" nodes $x_{\frac{1}{2}}, x_{1+\frac{1}{2}}, \ldots, x_{i+\frac{1}{2}}, \ldots, x_{N-\frac{1}{2}}$, where $x_{i+\frac{1}{2}} = x_{i+\frac{1}{2}}(x^i, x^{i+1}) = 2^{-1}(x^i + x^{i+1})$, $x^i,\ x^{i+1} \in \overline{\omega}^b$.

For the problem (2), (1) we have the difference scheme on the grid $\overline{G}_{h(16)}$

$$\Lambda z(x,t) = f_h(x,t), \quad (x,t) \in G_h^b, \ \ z(x,t) = \varphi(x,t), \quad (x,t) \in S_h^b. \tag{17}$$

$$\Lambda z(x,t) \equiv \varepsilon^2 \delta_{\widehat{x}}\big(a(x^{(-1)},t)\,\delta_{\overline{x}} z(x,t)\big) - c_h(x,t)\,z(x,t) - p_h(x,t)\,\delta_{\overline{t}} z(x,t).$$

Here and further $(x,t) \in G_h^b$, $(x^{(-1)},t)$, $(x^{(1)},t) \in G_h^a$, where $x^{(1)} = x^{(1)}(x)$, $x^{(-1)} = x^{(-1)}(x)$, $x^{(1)}(x) \equiv x_{i+\frac{1}{2}}$ for $x = x^i$, $x^{(-1)}(x) \equiv x_{i-\frac{1}{2}}$ for $x = x^i$, $x^i \in \overline{\omega}^b$, $x_{i+\frac{1}{2}},\ x_{i-\frac{1}{2}} \in \omega^a$.

In the scheme (17), (16), the function $w_h(x^{(1)},t) = -\varepsilon^2\, a(x^{(1)},t)\,\delta_x z(x,t)$, i.e., *grid diffusion flux*, is defined on the *flux grid* $G^a_{h(16b)}$. We call the set of the grids $\overline{G}_h^b$ and $\overline{G}_h^a$ also the *flux* grids. We call the difference scheme (17), (16) the *scheme on the flux grid* (16).

The scheme (17), (16) allows us to compute the flux $w_h(x^{(1)},t)$, $(x^{(1)},t) \in G_h^a$. This scheme is conservative under the condition

$$p(x,t) = p(x), \quad (x,t) \in \overline{G}_i, \quad i = 1,2. \tag{18}$$

The difference schemes (17), (16) and (13), (12) are equivalent.

Theorem 3.1 *Let for the components of the solution to initial-boundary value problem (2), (1), the estimates (7), (11) be satisfied for* $K = 4$. *Then the solution of the difference scheme* (13), *(14)* (*scheme* (17), *(16), (14)*) *converges to the solution of the initial-boundary value problem* ε*-uniformly. The discrete solutions satisfy the estimate (15).*

4 Flux Difference Scheme on Flux Grids

Here we perform the problem (2), (1) and the difference scheme (17), (16) to a "canonic form" containing the flux in explicit form.

Write the problem (2), (1) in the form

$$L^1(u(x,t), w(x,t)) \equiv w(x,t) + \varepsilon^2\, a(x,t)\,\frac{\partial}{\partial x}\,u(x,t) = 0, \tag{19}$$

$$L^2(u(x,t),w(x,t)) \equiv \frac{\partial}{\partial x}\, w(x,t) + c(x,t)\, u(x,t) + p(x,t)\frac{\partial}{\partial t}\, u(x,t) = -f(x,t),$$

$$(x,t) \in G_i, \quad i = 1,2,$$

$$l^1(u(x,t),w(x,t)) \equiv u(x+0,t) - u(x-0,t) = 0,$$

$$l^2(u(x,t),w(x,t)) \equiv w(x+0,t) - w(x-0,t) = 0, \quad (x,t) \in S^{int},$$

$$u(x,t) = \varphi(x,t), \quad (x,t) \in S.$$

Here the function $w(x,t)$, $(x,t) \in \overline{G}_i$, $i = 1,2$, is the diffusion flux; the perturbation parameter ε^2 characterizes the diffusion coefficient $\varepsilon^2\, a(x,t)$.

For the problem (19), (1) we have the difference scheme on the grid (16)

$$\Lambda^1\big(z(x,t),\ w_h(x,t)\big) \equiv w_h(x^{(1)},t) + \varepsilon^2\, a(x^{(1)},t)\, \delta_x\, z(x,t) = 0, \tag{20}$$

$$\Lambda^2\big(z(x,t),\ w_h(x,t)\big) \equiv \delta_{x^{(1)}}\, w_h(x^{(-1)},t) + c_h(x,t)\, z(x,t) + p_h(x,t)\, \delta_{\bar{t}}\, z(x,t)$$

$$= -f_h(x,t), \ \ (x,t) \in G_h, \quad (x^{(1)},t),\ (x^{(-1)},t) \in G_h^a,$$

$$z(x,t) = \varphi(x,t), \quad (x,t) \in S_h, \quad x^{(1)} = x^{(1)}_{(17)}(x), \ \ x^{(-1)} = x^{(-1)}_{(17)}(x).$$

The set of discrete equations (20), (16) connecting the function $z(x,t)$, $(x,t) \in \overline{G}_h$, and the discrete diffusion flux $w_h(x^{(1)},t)$, $(x^{(1)},t) \in G_h^a$, is the canonic *flux difference scheme* on flux grids; the function $z(x,t)$ is the *solution* of this scheme, the function $w_h(x^{(1)},t)$ is the grid *flux* corresponding to this solution.

Under the condition (18), the scheme (20), (16) is *conservative*.

Note that the function $\varepsilon^{-1}\, w(x^{(1)},t)$ is ε-uniformly bounded; we call it the *normalized diffusion flux*.

For the solution of the difference scheme (20), (16), (14), the estimate (15) holds. Under the condition (9), the normalized diffusion flux $\varepsilon^{-1}\, w_h(x,t)$ satisfies the estimate

$$\varepsilon^{-1} \left| w(x^{(1)},t) - w_h(x^{(1)},t) \right| \le M \left[N^{-2} \ln^2 N + N_0^{-1} \right], \ \ (x^{(1)},t) \in G_h^a. \tag{21}$$

Theorem 4.1 *Let the data of the initial-boundary value problem (2), (1) satisfy the condition (9), and let the components of the solution to this problem in the representation (5) satisfy the estimates (7), (11) for $K = 6$. Then the solution of the difference scheme (20), (16), (14) converges to the solution of the initial-boundary value problem (19), (1) ε-uniformly. The discrete solutions satisfy and the normalized diffusion flux satisfy the estimates (15) and (21), respectively.*

Remark 2 Let $\overline{z}(x,t)$, $(x,t) \in \overline{G}$ be the linear interpolant constructed on elementary rectangular elements in the partition of the set $\overline{G}$ using the values $z(x,t)$, $(x,t) \in \overline{G}_h$, in the vertices of the elementary rectangles. Let $\overline{w}_h(x,t)$, $(x,t) \in \overline{G}_i$, $i = 1,2$, be the linear interpolant constructed on elementary rectangular elements in the partition of the set $\overline{G}_i$ using the values $w_h(x,t)$, $(x,t) \in G_h^a$ in the vertices of the

elementary rectangles from $\overline{G}_i$; we extend these linear interpolants on elementary rectangular elements to the sets $\overline{G}_i, i = 1, 2$, with preserving linearity in x. The functions $\overline{z}(x,t)$ and $\overline{w}_h(x,t), (x,t) \in \overline{G}$, satisfy the estimates (15) and (21) from Theorem 4.1, where $z(x,t)$ and $w_h(x,t)$ are, respectively, $\overline{z}(x,t)$ and $\overline{w}_h(x,t)$, and $\overline{G}_h$ and G_h^a is $\overline{G}$. □

The full presentation of results of the present paper is given in the paper submitted for publication in a mathematical journal.

Acknowledgements This research was supported by the Russian Foundation for Basic Research under grant No.10-01-00726.

References

1. Friedman, A.: Partial Differential Equations of Parabolic Type, Prentice-Hall, Inc., Englewood Cliffs, N.J. (1964).
2. Ladyzhenskaya, O.A., Solonnikov, V.A., Uraltseva, N.N.: Linear and Quasilinear Equations of Parabolic Type. Nauka, Moscow (1967). (in Russian); Translations of Mathematical Monographs, **23**, American Mathematical Society, Providence, R.I. (1967).
3. Samarskii, A.A.: Theory of Difference Schemes. Nauka, Moscow (1989) (in Russian).
4. Samarskii, A.A.: Introduction to the Theory of Difference Schemes. Nauka, Moscow (1971) (in Russian).
5. Shishkin, G.I.: Grid Approximations of Singularly Perturbed Elliptic and Parabolic Equations. Ural Branch of RAS, Ekaterinburg (1992) (in Russian).
6. *Shishkin, G.I., Shishkina, L.P.*: Difference Methods for Singular Perturbation Problems. Series: Monographs & Surveys in Pure & Applied Math. Chapman and Hall/CRC (2009).

Numerical Approximation of Flow Induced Vibration of Vocal Folds

P. Sváček and J. Horáček

1 Introduction

In this paper the numerical study of a simplified model of airflow through glottal region of the human vocal tract is addressed and the self-oscillating vocal fold is modelled. The main attention is paid to comparison of approximation of a coupled fluid–structure interaction problems to results of aeroelastic model published in [5]. In order do compare these approaches a simplified geometrical domain is considered. In [5] the aeroelastic problem was modelled as 1d flow, which allows to determine flutter boundary (i.e. flow velocity for which the instability occurs followed by the vocal folds self-oscillations creating the human voice source). Here, a more general model is developed, the airflow through two-dimensional channel interacts with vibrations of channel walls induced by aerodynamical forces. The mathematical model is described by the airflow governed by the incompressible Navier–Stokes equations (as flow velocities in the glottal region are typically lower than $100\,\mathrm{m\,s^{-1}}$). The structure vibrations are described with the aid of two-degrees of freedom model and governed by linearized system of ordinary differential equations. The problem is numerically approximated by finite element method stabilized by Galerkin-Least Squares(GLS) method, cf. [4] modified for the application on moving domains (cf. [8]).

P. Sváček (✉)
Department of Technical Mathematics, Faculty of Mechanical Engineering,
CTU in Prague, Karlovo nam. 13, Praha 2, Czech Republic
e-mail: Petr.Svacek@fs.cvut.cz

J. Horáček
Institute of Thermomechanics, Academy of Sciences of the Czech Republic, Dolejškova 5,
Praha 8, Czech Republic
e-mail: jaromirh@it.cas.cz

C. Clavero et al. (eds.), *BAIL 2010 – Boundary and Interior Layers, Computational and Asymptotic Methods*, Lecture Notes in Computational Science and Engineering 81,
DOI 10.1007/978-3-642-19665-2_24,

2 Mathematical Model

The mathematical model consists of domain description (geometry), fluid flow model, structure motion model and interface, boundary and initial conditions. A simplified geometry of the channel is chosen in order to obtain results similar to the results of the simplified mathematical model (1d) from [5].

2.1 Geometry

The geometry of vocal folds depends on the tension in the vocal folds and varies with the fundamental vibration frequency, loudness and mode of phonation. For the purposes of numerical analysis in this paper the geometry of the vocal folds is chosen either as $a_f(x) = 0.77120\,x$ [m] (linear shape, approximation of the vocal fold for *female*) or $a_i(x) = -159.861(x-5.812\times10^{-3})^2+5.4\times10^{-3}$ [m] (parabolic shape, approximation of the vocal fold for *male*), see Fig. 1. Here, $x \in \langle 0, L\rangle$ [m]. The density, thickness and length of the vocal fold are $\rho_h = 1,020\ \mathrm{kg\,m^{-3}}$, $h =$ 18 mm and $L = 6.8$ mm, respectively. The channel height (at time $t = 0$) is chosen as $H_0 = \max_{x\in\langle 0,L\rangle} a(x) + g_0$, where g_0 is the initial gap.

2.2 Flow Model

To describe the flow model on moving domains the Arbitrary Lagrangian–Eulerian (ALE) method is used. ALE method is based on an ALE mapping $\mathcal{A}_t(\xi)$ of a reference point ξ from the reference (two dimensional) domain $\xi \in \Omega_0$ onto the

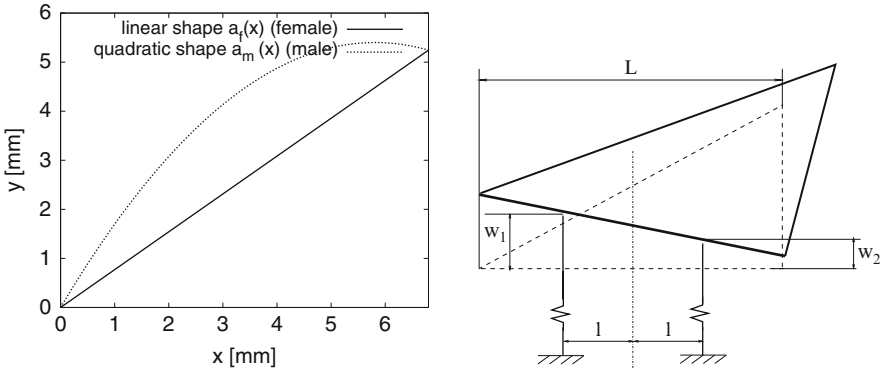

Fig. 1 The considered geometry of vocal folds (*left*) and example of the vocal fold in displaced position (*right*)

computational domain Ω_t at time instant t. The fluid flow is governed by the incompressible Navier–Stokes equations written in ALE form

$$\frac{D^{\mathcal{A}}\mathbf{v}}{Dt} + ((\mathbf{v} - \mathbf{w}_D)\cdot\nabla)\mathbf{v} - \nu\triangle\mathbf{v} + \nabla p = 0, \qquad \nabla\cdot\mathbf{v} = 0, \qquad \text{in } \Omega_t, \quad (1)$$

where $\mathbf{v} = \mathbf{v}(x,t)$ is the flow velocity vector ($\mathbf{v} = (v_1, v_2)$), $p = p(x,t)$ is the kinematic pressure (i.e. pressure divided by the constant fluid density ρ_∞), ν is the kinematic viscosity, $D^{\mathcal{A}}/Dt$ is the ALE derivative (i.e. time derivative with respect to the fixed point in the reference domain Ω_0), and $\mathbf{w}_D$ is the domain velocity.

The boundary of the computational domain $\partial\Omega_t$ consists of mutually disjoint parts Γ_D (wall), Γ_I (inlet), Γ_O (outlet), Γ_S (axis of symmetry) and the moving part Γ_{Wt} (oscillating wall). The following boundary conditions are prescribed

$$\begin{array}{cccc} \text{a)} & \mathbf{v}(x,t) = \mathbf{0} & x \in \Gamma_D, & \text{b)} \quad \mathbf{v}(x,t) = \mathbf{w}_D(x,t) \quad x \in \Gamma_{Wt}, \\ \text{c)} & \mathbf{v}(x,t) = (V_0, 0) & x \in \Gamma_I, & \text{d)} \quad v_2(x,t) = 0, \quad \frac{\partial v_1}{\partial y}(x,t) = 0 \quad x \in \Gamma_S \end{array}$$
$$\text{e)} - \quad (p - p_{ref})\mathbf{n} + \tfrac{1}{2}(\mathbf{v}\cdot\mathbf{n})^{-}\mathbf{v} + \nu\frac{\partial\mathbf{v}}{\partial\mathbf{n}} = 0, \quad \text{on } \Gamma_O, \quad (2)$$

where $\mathbf{n}$ denotes the unit outward normal vector, p_{ref} denotes a reference pressure value, V_0 is the inlet flow velocity magnitude. Further, α^- denotes the negative part of α. Finally, we prescribe the initial condition $\mathbf{v}(x,0) = \mathbf{v}^0(x)$ for $x \in \Omega_0$. The initial configuration Ω_0 is shown in Fig. 2 for linear shape of the vocal fold.

2.3 Structure Model

The geometry of the channel and of the vibrating glottal region is chosen similarly as in [6] (see Fig. 2), where vibrations are part of the solution. The vibrating part (vocal folds) of the channel walls is governed by an aeroelastic two degrees of freedom model, i.e. the motion of Γ_{Wt} is governed by the displacements $w_1(t)$ and $w_2(t)$ (upward positive) of the two masses m_1 and m_2, respectively (see Fig. 3). The displacements $w_1(t)$ and $w_2(t)$ are then described by the following equations (see [6] for details)

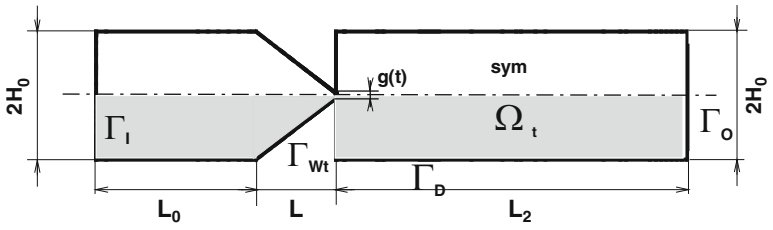

Fig. 2 The symmetric domain occupied by fluid and the computational domain Ω_t with boundary parts (*lower part, shaded*)

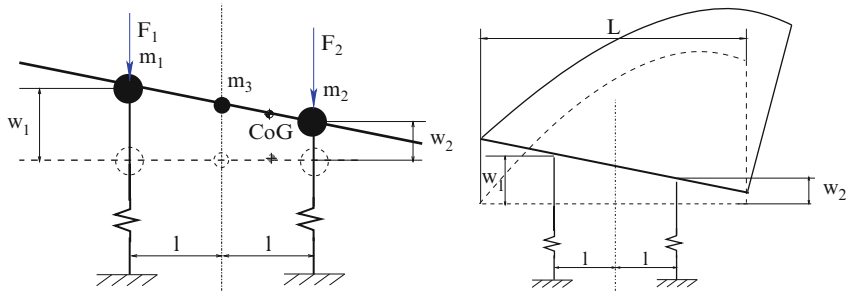

Fig. 3 Aeroelastic two degrees of freedom model (with masses m_1, m_2, m_3) in displaced position (displacements w_1 and w_2) and aerodynamic forces F_1 and F_2 (*left*) and deformation of the vocal fold shaped element (*right*)

$$\begin{pmatrix} m_1 + \frac{m_3}{4} & \frac{m_3}{4} \\ \frac{m_3}{4} & m_2 + \frac{m_3}{4} \end{pmatrix} \begin{pmatrix} \ddot{w_1} \\ \ddot{w_2} \end{pmatrix} + \mathbb{B} \begin{pmatrix} \dot{w_1} \\ \dot{w_2} \end{pmatrix} + \begin{pmatrix} c_1 & 0 \\ 0 & c_2 \end{pmatrix} \begin{pmatrix} w_1 \\ w_2 \end{pmatrix} = \begin{pmatrix} -F_1 \\ -F_2 \end{pmatrix}, \quad (3)$$

where m_1, m_2, m_3 are masses, c_1, c_2 are spring constants, and $\mathbb{B}$ is the matrix of the proportional structural damping. Here, F_1, F_2 are the aerodynamical forces (downward positive). The fluid flow model (1) is coupled with the structure motion model (3) by interface conditions. The proportional damping matrix is chosen

$$\mathbb{B} = \varepsilon_1 \mathbb{M} + \varepsilon_2 \mathbb{K}.$$

2.4 Coupling Conditions

The flow and structure models are coupled by **(A)** the deformation of the vocal fold, **(B)** kinematic boundary condition for flow velocity, **(C)** aerodynamical forces. The deformation of the domain Ω_t depends on the displacements $w_1(t)$, $w_2(t)$ of structure model (3) . The kinematic boundary condition for flow velocity is given by (2b) and depends on structural velocity. The aerodynamic forces F_1 F_2 in (3) depends on flow velocity $\mathbf{v}$ and pressure p resulting from (1). Particularly, any point $\xi = (\xi_1, \xi_2) \in \Gamma_{W0}$ of the vibrating lower part of the vocal folds is transformed on $\mathcal{A}_t(\xi) = (X, \xi_2) \in \Gamma_{Wt}$, where

$$X = \frac{1}{2l} \left[(\xi_1 - L_1 - l) w_1(t) + (\xi_1 - L_1 + l) w_2(t) \right],$$

where $L_1 = L/2$. The grid velocity is then computed by $\mathbf{w}_D(x,t) = \frac{d\mathcal{A}_t(\xi)}{dt}$ where $x = \mathcal{A}_t(\xi)$. The aerodynamical forces (the viscous terms are neglected) are evaluated by

$$F_1(t) = \frac{h}{2l} \int_0^L (l - x + L_1) p(x,t)\, dx, \quad F_2(t) = \frac{h}{2l} \int_0^L (l + x - L_1) p(x,t)\, dx.$$

3 Numerical Approximation

FEM is well known as a general discretization method for partial differential equations. Nevertheless, the straightforward application of FEM procedures often fails in the case of incompressible Navier–Stokes equations. The reason is that momentum equations are of advection–diffusion type with dominating advection and the Galerkin FEM leads to unphysical solutions if the grid is not fine enough in regions of strong gradients (e.g. in boundary layer). In order to obtain physically admissible correct solutions it is necessary to apply suitable mesh refinement (e.g. anisotropically refined mesh, cf. [3]) combined with a stabilization technique, cf. [1, 4, 7]. In this work, the FEM is stabilized with the aid of Galerkin-Least Squares (GLS) method, cf. [4]) modified for the application on moving domains (cf. [8]).

The detailed description of the numerical approximation of flow model can be found, e.g. in [8]. The flow problem (1) is discretized in time by backward difference formula of second order (BDF2), formulated weakly and spatially discretized by the finite element method based on anisotropically refined triangulation and Taylor Hood finite elements for velocity/pressure approximation. Furthermore, the time and space discretized linearized problem of the arising large system of linear equations needs to be solved in a fast and efficient manner. Here, the solution is performed by the application of direct solver as UMFPACK (cf. [2]), where different stabilization procedures can be easily applied even when the anisotropically refined grids are employed.

The motion equations are discretized with the aid of the 4th order Runge-Kutta method and the coupled fluid–structure model is solved with the aid of partitioned strongly coupled scheme. This means that per every time step the fluid flow and the structure motion are approximated repeatedly in order to converge to a solution which satisfy all interface conditions.

4 Numerical Results

4.1 Input Data for Aeroelastic Model

For the computations the fluid density $\rho = 1.2\,\mathrm{kg\,m^{-3}}$, and fluid kinematic viscosity $\nu = 1.58 \times 10^{-5}\,\mathrm{m^2\,s^{-1}}$ were chosen. The length l i.e. the distance of the masses from the center was $l = L/2$, the lengths of sub- and supra-glottal regions were $L_0 = 1.5L$ and $L_2 = 5L$, respectively. The height of the channel was $2H_0$, where $H_0 = g_0 + \max_{x\in\langle 0,L\rangle} a(x)$, where $2g_0$ is the initial gap $g(0) = 2g_0$. The initial gap g_0 for Model F and Model M was chosen 0.25 mm and 0.2 mm, respectively.

Using the given shape and dimension of the vocal fold and using the structural density ρ_h the total mass m, the moment of inertia I and the excentricity e is computed. The system is then replaced by the equivalent three mass system where

$m_{1,2} = \frac{1}{2l^2}(I + m\,e^2 \pm m\,e\,l)$ and $m = m_1 + m_2 + m_3$. The structural parameters were chosen according [5], see Table 1.

4.2 Aeroelastic Response

The solution of the aeroelastic system was performed for two cases represented by Table 1. The solution of the flow model (1), structure model (3) and interface conditions was numerically approximated in a simplified geometry shown in Fig. 2. The aeroelastic response is shown in Fig. 4 for *Model F* and in Fig. 5 for *Model M* in time domain in terms of displacements $w_1(t)$ and $w_2(t)$. The vibrations of the

Table 1 Structural parameters considered for the aeroelastic system in numerical examples; f_1, f_2 are the corresponding natural frequencies of the structure in vacuo

	Model F	Model M
Shape	$a_f(x)$	$a_m(x)$
m (kg)	3.274×10^{-4}	4.812×10^{-4}
I (kg m^{-2})	1.341×10^{-9}	2.351×10^{-9}
e (m)	1.133×10^{-3}	0.771×10^{-3}
c_1 (N m^{-1})	44.8	56
c_2 (N m^{-1})	84.6	174.3
f_1 (Hz)	100	100
f_2 (Hz)	160	160

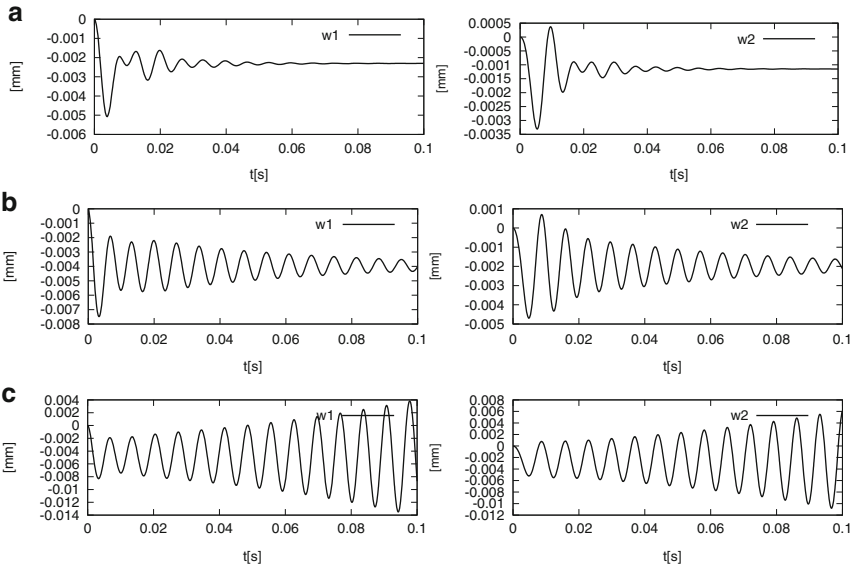

Fig. 4 The aeroelastic response of the system $w_1(t)$,$w_2(t)$ for the inlet velocity (**a**) $V_0 = 0.2\,\mathrm{m\,s^{-1}}$, (**b**) $V_0 = 0.3\,\mathrm{m\,s^{-1}}$ and (**c**) $V_0 = 0.34\,\mathrm{m\,s^{-1}}$

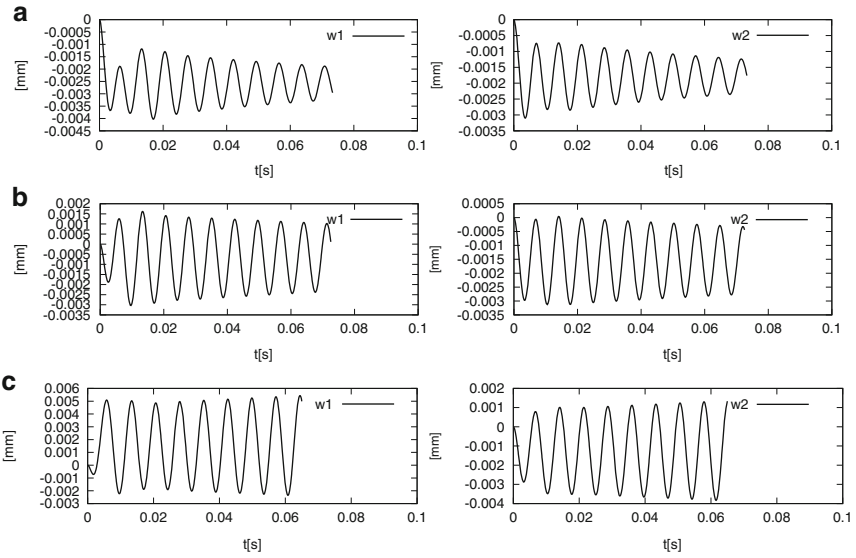

Fig. 5 The aeroelastic response of the system $w_1(t)$,$w_2(t)$ for the inlet velocity (**a**) $V_0 = 0.575\,\mathrm{m\,s^{-1}}$, (**b**) $V_0 = 0.6\,\mathrm{m\,s^{-1}}$ and (**c**) $V_0 = 0.625\,\mathrm{m\,s^{-1}}$

structure die in time after a time period due to both structural and strong aerodynamic damping for lower flow velocities. With increasing flow velocity the flutter type of instability can be observed, which is in good agreement with results presented in [5]. The physical meaning of the instability is so-called phonation onset which is an important voice production characteristic in humans.

5 Conclusion

In this paper the numerical method for an analysis of a simplified model of airflow through of glottal region was described and an attention was paid to comparison of approximation of a coupled fluid–structure interaction problems to results of aeroelastic model published in [5]. The flutter type of instability was observed for inlet velocities which agrees with results [5]. The numerical results are in general in good agreement with the physiological data known for human voice source. The developed numerical method improves the previous approximate solution for finding the phonation onset parameters given by the aeroelastic instability of the vocal folds.

Acknowledgements This research was supported under the Project OC 09019 “Modelling of voice production based on biomechanics” within the program COST of the Ministry of Education of the Czech Republic, under grant No. 201/08/0012 of the Grant Agency of the Czech Republic and the Research Plan MSM 6840770003 of the Ministry of Education of the Czech Republic.

References

1. R. Codina. Stabilization of incompressibility and convection through orthogonal sub-scales in finite element methods. *Computational Method in Applied Mechanical Engineering*, 190:1579–1599, 2000.
2. T. A. Davis and I. S. Duff. A combined unifrontal/multifrontal method for unsymmetric sparse matrices. *ACM Transactions on Mathematical Software*, 25:1–19, 1999.
3. V. Dolejší. Anisotropic mesh adaptation technique for viscous flow simulation. *East-West Journal of Numerical Mathematics*, 9:1–24, 2001.
4. T. Gelhard, G. Lube, M. A. Olshanskii, and J.-H. Starcke. Stabilized finite element schemes with LBB-stable elements for incompressible flows. *Journal of Computational and Applied Mathematics*, 177:243–267, 2005.
5. J. Horáček and J. G. Švec. Instability boundaries of a vocal fold modelled as a flexibly rigid body vibrating in a channel conveying fluid. *AMD, American Society of Mechanical Engineers, Applied Mechanics Division*, 253(2):1043–1054, 2002.
6. J. Horáček, P. Šidlof, and J.G. Švec. Numerical simulation of self-oscillations of human vocal folds with Hertz model of impact forces. *Journal of Fluids and Structures*, 20(6):853–869, 2005.
7. P. Sváček and M. Feistauer. Application of a Stabilized FEM to Problems of Aeroelasticity. In *Numerical Mathematics and Advanced Application*, pages 796–805, Berlin, 2004. Springer.
8. P. Sváček, M. Feistauer, and J. Horáček. Numerical simulation of flow induced airfoil vibrations with large amplitudes. *Journal of Fluids and Structure*, 23(3):391–411, 2007.

Fundamental Properties of the Solution of a Singularly Perturbed Degenerate Parabolic Problem

Martin Viscor and Martin Stynes

Abstract A singularly perturbed degenerate parabolic problem is considered. The behaviour of its solution u depends on three parameters that are determined by the data of the problem. Theoretical bounds on u are stated in terms of these parameters and extensive numerical experiments verify the sharpness of these bounds.

1 Introduction

Consider the singularly perturbed initial-boundary value problem

$$Lu(x,t) := \varepsilon u_{xx}(x,t) - x^{\alpha} u_t(x,t) = f(x,t,\varepsilon) \text{ for } (x,t) \in \Omega, \tag{1a}$$

subject to the Dirichlet initial and boundary conditions

$$u(0,t) = \varphi_L(t,\varepsilon) \quad \text{for } 0 < t \le T, \tag{1b}$$

$$u(x,0) = \varphi_0(x,\varepsilon) \quad \text{for } 0 \le x \le 1, \tag{1c}$$

$$u(1,t) = \varphi_R(t,\varepsilon) \quad \text{for } 0 < t \le T, \tag{1d}$$

where $\Omega := (0,1)\times(0,T]$ for some fixed $T > 0$, the small parameter $\varepsilon \in (0,1]$ and $\alpha > 0$ is a positive constant. The functions f and φ are smooth; precise hypotheses will be given in Sect. 2.

The vanishing of the coefficient x^{α} of u_t at the boundary $x = 0$ of $\bar{\Omega}$ means that the parabolic differential operator L of (1a) is degenerate and consequently the standard theory of parabolic partial differential equations is inapplicable – even for fixed $\varepsilon > 0$. The analysis of (1) is hampered by this factor and also by the singularly perturbed nature of (1a), which is caused by the small parameter ε. The solution u

M. Stynes (✉) and M. Viscor
Department of Mathematics, University College Cork, Cork, Ireland
e-mail: m.stynes@ucc.ie, m.viscor@ucc.ie

C. Clavero et al. (eds.), *BAIL 2010 – Boundary and Interior Layers, Computational and Asymptotic Methods*, Lecture Notes in Computational Science and Engineering 81,
DOI 10.1007/978-3-642-19665-2_25,

has boundary layers, as is usual in singularly perturbed problems, but the complexity of the layer along $x = 0$ is increased by the degeneracy of the problem; see Sect. 5 for more information.

Problems like (1) arise when one models the transfer of heat over a rectangle in a medium that moves with velocity x^α along the x-axis and conducts heat only across the flow; see [5] and also [4].

Notation. We use $\|\cdot\|$ to denote the maximum norm on $C(\bar{\Omega})$. The quantity C denotes a generic constant that is independent of ε, x and t.

2 Existence and Regularity of u

The standard classical theory of parabolic partial differential equations cannot be applied to (1) because the coefficient x^α of u_t is not bounded from below by any positive constant in Ω and also fails to lie in the functional spaces used in [2, 3]. Hence an alternative proof of the existence and regularity of u is needed.

Lemma 1. *Consider the problem* (1)*. Assume that* $\alpha < 4$*,*

$$f, f_t \in C(\bar{\Omega}),$$
$$\varphi_0(x) \in C^2[0,1] \text{ and } \varphi_0 \text{ is of bounded variation on } [0,1],$$
$$\varphi_L, \varphi_R \in C^2(0,T],$$

for each fixed $t \in [0,T]$*, the function* $f(\cdot,t)$ *is of bounded variation on* $[0,1]$*,*

for i=0,1,2, $\lim_{t\to 0^+} \frac{\partial^i}{\partial t^i}\varphi_L(t)$ *and* $\lim_{t\to 0^+} \frac{\partial^i}{\partial t^i}\varphi_R(t)$ *exist and are finite,*

$$\lim_{t\to 0^+} \psi_L(t) = \psi_0(0), \quad \lim_{t\to 0^+} \psi_R(t) = \psi_0(1).$$

Then the problem (1) *has a unique solution in* $C(\bar{\Omega}) \cap C^{2,1}(\bar{\Omega} \setminus \{(0,0),(1,0)\})$.

Proof. The proof is an extension of an argument from [1]. It is based on an explicit construction of the solution in the form of an infinite series containing Bessel functions. For full details see [6].

Remark 1. Consider a function $g \in C(0,1)$. To show that its Bessel series converges uniformly to g on $(0,1)$, one needs the integral $\int_0^1 x^{-1/2} g(x)dx$ to be convergent. For our problem this condition becomes $|\int_0^1 x^{-\alpha/4} f(x,t)dx| \le C$ for $0 \le t \le T$; this is why the condition $\alpha < 4$ is needed in Lemma 1. Nevertheless our numerical experience is the same for $\alpha \ge 4$ as for $\alpha < 4$.

3 Main Properties of u

Unlike the singularly perturbed parabolic operator $v \mapsto \varepsilon v_{xx} - v_t$, in general $\|u\|$ [where u is the solution of (1)] is not bounded uniformly with respect to the parameter ε. The bound on $\|u\|$ depends on the structure of $f(x,t,\varepsilon)$ and on the boundary data. Set

$$\nu = \frac{1}{2+\alpha}.$$

Definition 1. Let $\beta \geq 0$ be the largest constant such that for all $\varepsilon \in (0,1]$

$$\begin{aligned}
&|f(x,t,\varepsilon)| \leq M \max\{\varepsilon^{\beta\nu}, x^{\beta}\}, \quad (x,t) \in \bar{\Omega}\\
&|\varphi_L(t,\varepsilon)| \leq M\varepsilon^{(\beta-\alpha)\nu}, \quad 0 < t \leq 1\\
&|\varphi_R(t,\varepsilon)| \leq M, \quad 0 < t \leq 1,\\
&|\varphi_0(x,\varepsilon)| \leq \begin{cases} M\varepsilon^{(\beta-\alpha)\nu} & \text{for } 0 \leq x \leq \varepsilon^{\nu},\\ Mx^{\beta-\alpha} & \text{for } \varepsilon^{\nu} \leq x \leq 1 \end{cases}
\end{aligned}$$

hold true with some constant M that is independent of ε, x, β and α.

Remark 2. The constant β is well defined except when $f(x,t)$ and the boundary data are all identically zero – in this case $\beta = \infty$ and $u \equiv 0$. We exclude this trivial case from our analysis.

The following result reveals the significance of β.

Theorem 1. *Let u be the solution of* (1)*. Then*

$$|u(x,t)| \leq \begin{cases} C\varepsilon^{(\beta-\alpha)\nu} & \textit{for } 0 \leq x \leq \varepsilon^{\nu},\\ Cx^{\beta-\alpha} & \textit{for } \varepsilon^{\nu} \leq x \leq 1. \end{cases}$$

Proof. These bounds can be shown by barrier function arguments, but these are more complicated than for non-degenerate problems: a quadratic function of the form $C\varepsilon^{(\beta-\alpha)\nu}[\varepsilon^{-2\nu}a_1x^2 + \varepsilon^{-\nu}a_2x + a_3]$ on $[0,\varepsilon^{\nu}] \times [0,T]$ is combined with an algebraic function $Cx^{\beta-\alpha}$ on $[\varepsilon^{\nu},1] \times [0,T]$. See [6] for details.

Numerical evidence suggests that the bounds of Theorem 1 are sharp – see Sect. 4. Note that for $\beta < \alpha$ the solution $u(x,t)$ becomes large for x close to 0 as $\varepsilon \to 0$. On the other hand for $\beta > \alpha$ the solution $u(x,t)$ remains small for x close to 0 as $\varepsilon \to 0$. When $\alpha = \beta$ the solution u remains of moderate size for all values of ε.

Considering the bounds of Theorem 1, define the continuous function

$$\eta(x) = \begin{cases} \varepsilon^{(\alpha-\beta)\nu} & \text{for } 0 \leq x \leq \varepsilon^{\nu},\\ x^{\alpha-\beta} & \text{for } \varepsilon^{\nu} \leq x \leq 1, \end{cases}$$

and the weighted norm

$$\|u\|_\eta = \max_{(x,t)\in\bar{\Omega}} |\eta(x)u(x,t)|.$$

Then Theorem 1 implies that $\|u\|_\eta \le C$. Thus $\|u\|_\eta$ is bounded uniformly in ε for all permissible values of α and β, unlike $\|u\|$.

4 Experimental Verification of Dependence of u on $\alpha, \beta, \varepsilon$

We provide numerical results for problem (1) with

$$f(x,t) = (x^\beta + \varepsilon^{\beta\nu})(e^t - 1)\left[1 - x/4 + \sin(2\pi x)/2 + xt + t^2\right] \qquad (2)$$

and homogeneous initial-boundary data

$$\varphi_0(x) = 0 \text{ for } 0 \le x \le 1, \qquad \varphi_L(t) = \varphi_R(t) = 0 \text{ for } 0 < t \le 1.$$

Various values of α and β will be used in our experiments to test the sharpness of Theorem 1. Our solutions u are computed using the numerical method of [6] on a mesh that is fine enough to ensure the accuracy of our numerical results (this is guaranteed by the theory of [6], which will be published elsewhere; a special case has appeared already in [7]).

4.1 Case $\beta = \alpha$

In this case, $\|u\|$ is uniformly bounded with respect to ε (see Theorem 1) as can be seen from Fig. 1 and Table 1.

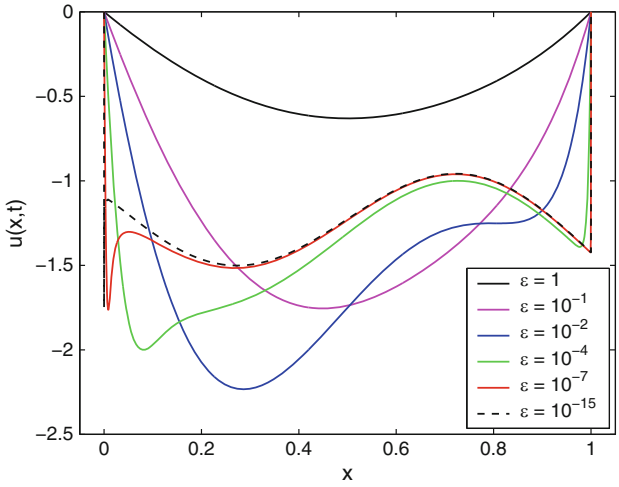

Fig. 1 Solution of (1) and (2) at $t = 1$, $\alpha = \beta = 1.25$

Table 1 Values of $\|u\|$, $\beta = \alpha$

$\varepsilon\backslash\alpha$	0.25	1.25	2.25	3.25	4.25	5.25	6.25	7.25	8.25
10^{0}	0.734	0.630	0.581	0.555	0.540	0.530	0.524	0.519	0.516
10^{-1}	2.157	1.755	1.513	1.340	1.208	1.104	1.023	0.956	0.903
10^{-2}	2.645	2.233	1.984	1.802	1.678	1.594	1.535	1.488	1.447
10^{-3}	2.478	2.213	2.141	2.023	1.888	1.764	1.662	1.583	1.525
10^{-4}	2.260	1.999	2.035	2.041	1.998	1.920	1.829	1.739	1.658
10^{-5}	2.087	1.860	1.882	1.933	1.960	1.952	1.914	1.856	1.789
10^{-10}	2.008	1.746	1.648	1.606	1.600	1.615	1.643	1.677	1.710
10^{-15}	2.010	1.749	1.642	1.577	1.536	1.512	1.501	1.502	1.511
10^{-20}	2.010	1.750	1.644	1.578	1.536	1.501	1.501	1.501	1.501

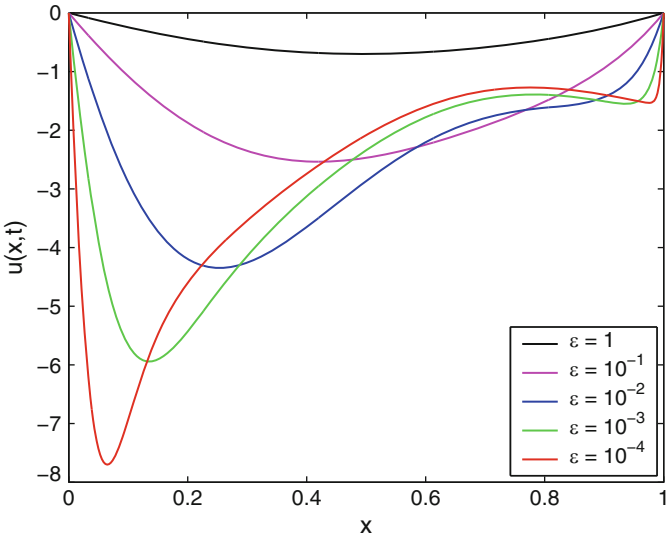

Fig. 2 Solution of (1) and (2) at $t = 1$, $\alpha = 1.25$, $\beta = 0.75$

Remark 3. Shishkin [5] considered the case $f(x,t,\varepsilon) = x^{\alpha} f_1(x,t) + \varepsilon^{\nu} f_2(x,t)$, where f_1 and f_2 are well behaved. This is a subcase of our case $\beta = \alpha$. In [7] we improved some of his results for this problem.

4.2 Case $\beta < \alpha$

Now Theorem 1 states that $\|u\|$ is bounded by negative powers of ε as $\varepsilon \to 0$. This can be seen in Fig. 2 and Table 2. Furthermore, Fig. 3 and Table 3 show that, as expected, $\|u\|_{\eta}$ remains bounded uniformly with respect to ε. From Table 3 one also

Table 2 Values of $\|u\|$, $\beta = 0.75$

$\varepsilon\backslash\alpha$	1.25	2.25	3.25	4.25	5.25	6.25	7.25	8.25
10^{0}	0.6999	0.7345	0.7533	0.7642	0.7708	0.7751	0.7779	0.7798
10^{-3}	5.94e00	2.24e01	5.08e01	8.71e01	1.27e02	1.68e02	2.07e02	2.44e02
10^{-6}	1.43e01	2.15e02	1.18e03	3.77e03	8.74e03	1.64e04	2.68e04	3.95e04
10^{-9}	4.04e01	2.33e03	2.92e04	1.64e05	5.72e05	1.48e06	3.12e06	5.69e06
10^{-12}	1.17e02	2.65e04	7.68e05	7.57e06	3.97e07	1.40e08	3.74e08	8.29e08
10^{-15}	3.39e02	3.04e05	2.06e07	3.59e08	2.84e09	1.36e10	4.64e10	1.25e11
10^{-18}	9.81e02	3.48e06	5.52e08	1.72e10	2.06e11	1.35e12	5.86e12	1.92e13
10^{-21}	2.84e03	3.99e07	1.48e10	8.22e11	1.50e13	1.34e14	7.48e14	2.97e15

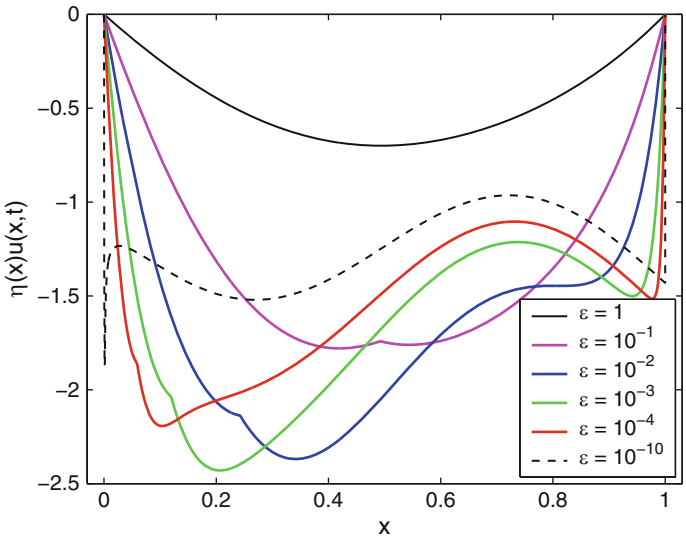

Fig. 3 Solution of (1) and (2) multiplied by $\eta(x)$ at $t = 1$, $\alpha = 1.25$, $\beta = 0.75$.

observes that the value of $\|u\|_\eta$ increases approximately linearly as α increases; our theory does not include this.

4.3 Case $\beta > \alpha$

In this case, $\|u\|$ is uniformly bounded in ε by Theorem 1. Moreover, the theorem implies that u is small close to $x = 0$ when ε is small. This can be clearly seen from Fig. 4. Figure 5 shows that $\|u\|_\eta$ remains uniformly bounded with respect to ε. Table 4 demonstrates that the value of $\|u\|_\eta$ now depends on α and β more strongly than in the case $\beta < \alpha$.

Table 3 Values of $\|u\|_\eta$, $\beta = 0.75$

$\varepsilon\backslash\alpha$	1.25	2.25	3.25	4.25	5.25	6.25	7.25	8.25
10^{0}	0.699	0.734	0.753	0.764	0.770	0.775	0.777	0.779
10^{-3}	2.430	2.660	2.778	2.861	2.950	3.063	3.203	3.370
10^{-6}	1.933	2.225	2.601	2.997	3.372	3.708	4.005	4.263
10^{-9}	1.873	2.042	2.286	2.588	2.933	3.305	3.690	4.073
10^{-12}	1.873	2.016	2.208	2.437	2.704	3.004	3.331	3.683
10^{-15}	1.875	2.016	2.193	2.396	2.622	2.871	3.145	3.442
10^{-18}	1.876	2.018	2.193	2.387	2.596	2.820	3.062	3.320
10^{-21}	1.876	2.019	2.195	2.387	2.590	2.803	3.027	3.264

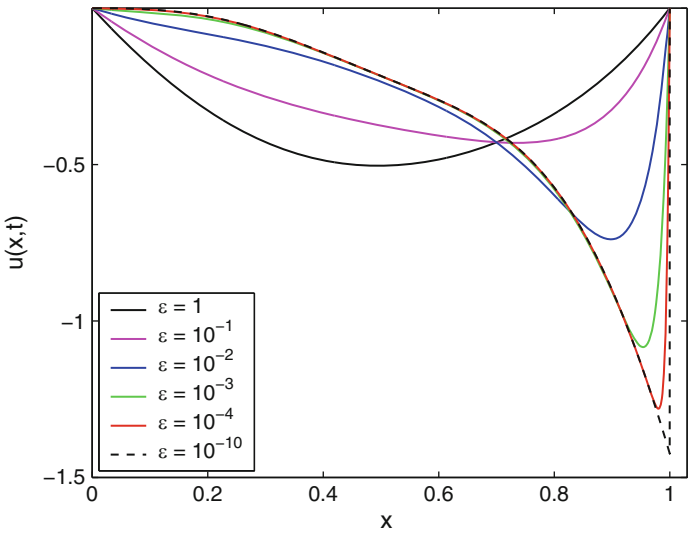

Fig. 4 Solution of (1) and (2) at $t = 1$, $\alpha = 1.25$, $\beta = 3.75$

5 Layers

The layer at $x = 0$ depends strongly on the value of α but the layer at $x = 1$ is much more independent of this parameter. This can be clearly seen from Fig. 6. The width of the $x = 0$ layer is shown in [6] to be $O(\varepsilon^{1/(2+\alpha)})$ while the width of the $x = 1$ layer, where x^α is well behaved, is $O(\varepsilon^{1/2})$ as in non-degenerate problems; these assertions are illustrated in Fig. 7.

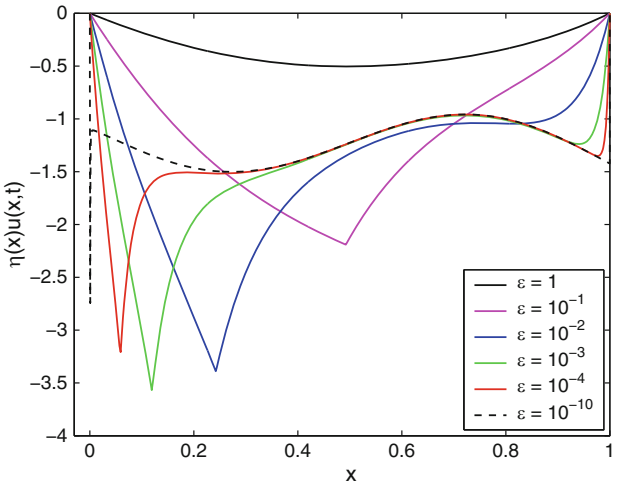

Fig. 5 Solution of (1) and (2) multiplied by $\eta(x)$ at $t = 1$, $\alpha = 1.25$, $\beta = 3.75$

Table 4 Values of $\|u\|_\eta$, $\alpha = 1.25$

$\varepsilon \backslash \beta$	2.25	3.25	4.25	5.25	6.25	7.25	8.25	9.25	10.25
10^{0}	0.554	0.515	0.494	0.481	0.473	0.468	0.464	0.461	0.459
10^{-2}	2.452	2.973	3.964	5.881	9.738	17.86	35.81	77.31	177.7
10^{-4}	2.195	2.762	3.896	6.220	11.20	22.41	48.85	114.0	281.4
10^{-6}	1.985	2.472	3.440	5.410	9.604	18.98	40.94	94.80	236.5
10^{-8}	1.940	2.408	3.335	5.216	9.209	18.11	38.89	89.70	219.2
10^{-10}	1.934	2.399	3.360	5.188	9.149	17.97	38.56	88.87	217.0
10^{-12}	1.936	2.400	3.361	5.190	9.152	17.97	38.57	88.88	217.0
10^{-14}	1.937	2.402	3.364	5.195	9.162	17.99	38.62	88.99	217.3

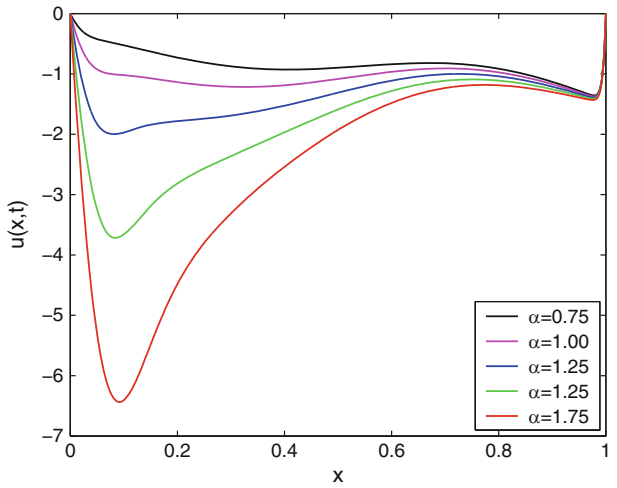

Fig. 6 Solution of (1) and (2) at $t = 1$, $\beta = 1.25$, $\varepsilon = 10^{-4}$

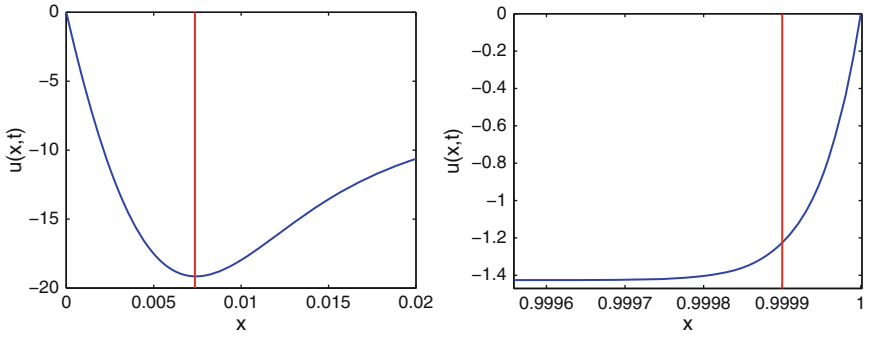

Fig. 7 Detail of solution of (1) and (2) at $t = 1$ with $\alpha = 1.75$, $\beta = 1.25$, $\varepsilon = 10^{-8}$, so $\varepsilon^{1/(2+\alpha)} \doteq 0.0074$ and $\varepsilon^{1/2} = 0.0001$; *vertical lines* indicate these layer widths

Acknowledgements This research was supported by the Mathematics Applications Consortium for Science and Industry in Ireland (MACSI) under the Science Foundation Ireland (SFI) Mathematics Initiative.

References

1. C. Y. Chan and W. Y. Chan. Existence of classical solutions for degenerate semilinear parabolic problems. *Appl. Math. Comput.*, 101(2-3):125–149, 1999.
2. A. Friedman. *Partial differential equations of parabolic type*. Prentice-Hall Inc., Englewood Cliffs, N.J., 1964.
3. O. A. Ladyženskaja, V. A. Solonnikov, and N. N. Uralceva. *Linear and quasilinear equations of parabolic type*. Translated from the Russian by S. Smith. Translations of Mathematical Monographs, Vol. 23. American Mathematical Society, Providence, R.I., 1967.
4. H. Ockendon. Channel flow with temperature-dependent viscosity and internal viscous dissipation. *J. Fluid Mech.*, 93:737–746, 1979.
5. G. I. Shishkin. Difference approximation of singularly perturbed parabolic equations that are degenerate on the boundary. *Comput. Math. Math. Phys.*, 31(10):53–63, 1991.
6. M. Viscor. *Numerical modelling of industrial processes exhibiting layer phenomena*. PhD thesis, University College Cork, 2010.
7. M. Viscor and M. Stynes. A robust finite difference method for a singularly perturbed degenerate parabolic problem. I. *Int. J. Numer. Anal. Model.*, 7(3):549–566, 2010.

High Reynolds Channel Flows: Variable Curvature

M. Zagzoule, P. Cathalifaud, J. Cousteix, and J. Mauss

Abstract Two-dimensional laminar flow, at high Reynolds number Re, of an incompressible Newtonian fluid in a curved channel connected to two fitting tangent straight channels at its upstream and downstream extremities is considered. The Successive Complementary Expansion Method (SCEM) is adopted. This method leads to an asymptotic reduced model called Global Interactive Boundary Layer (GIBL) which gives a uniformly valid approximate solution of the flow field in the whole domain. To explore the effect of the variable curvature on the flow field, the bend has an elliptical median line. The validity of the proposed GIBL model is confronted to the numerical solution of complete Navier–Stokes equations. This comparison includes the wall shear stress which is a very sensitive measure of the flow field. The GIBL results match very well the complete Navier–stokes results for curvatures K_{max} up to 0.4, curvature variations $|K'_{max}|$ up to 0.7 and eccentricities e up to $\simeq 0.943$ in the whole geometrical domain. The upstream and downstream effects as well as the impact of the curvature discontinuities and the behaviour in the entire bend are well captured by the GIBL model.

1 Mathematical Formulation

1.1 Geometrical Configuration

As a typical illustration we consider a 2D bend connected to two fitting tangent straight channels at its upstream and downstream extremities (see Fig. 1). The bend starts at $x = 0$, the median line is denoted $H(x, y) = 0$. Generalized coordinates

M. Zagzoule (✉), P. Cathalifaud, and J. Mauss
Université de Toulouse, INPT, UPS, CNRS, IMFT, 31400 Toulouse, France
e-mail: zagzoule@imft.fr, catalifo@imft.fr, mauss@cict.fr

J. Cousteix
DMAE, ONERA, ISAE, Toulouse, France
e-mail: Jean.Cousteix@onecert.fr

C. Clavero et al. (eds.), *BAIL 2010 – Boundary and Interior Layers, Computational and Asymptotic Methods*, Lecture Notes in Computational Science and Engineering 81,
DOI 10.1007/978-3-642-19665-2_26,

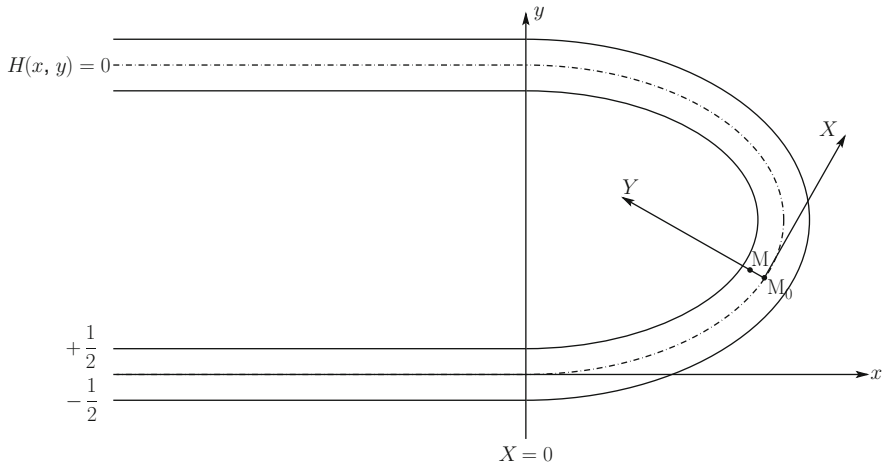

Fig. 1 Geometrical configuration and coordinate system

(X, Y) are used and are defined such that: X and Y are distances along and perpendicular to $H = 0$ with the wall boundaries located at $Y = \pm 1/2$. In the straight parts this coordinate system reduces to the Cartesian one (x, y). The velocity components U and V are respectively parallel and perpendicular to $H = 0$, thus

$$\mathbf{V} = U\boldsymbol{\tau} + V\mathbf{n}\,, \quad \text{where} \quad \boldsymbol{\tau} = \mathbf{X} \text{ and } \mathbf{n} = \mathbf{Y}\,.$$

$\boldsymbol{\tau}$ and $\mathbf{n}$ are unit vectors respectively tangent and normal to the median line. $K(X)$ is the algebraic curvature of the median line. Since $(\boldsymbol{\tau}, \mathbf{n})$ is direct, hence $K < 0$ in the case of Fig. 1.

1.2 Navier–Stokes Equations in Generalized Coordinates

In the previously defined generalized coordinate system the continuity equation and the Cauchy equations are

$$\frac{\partial U}{\partial X} + \frac{\partial}{\partial Y}\left[(1 + KY)V\right] = 0$$

$$\frac{1}{1 + KY}U\frac{\partial U}{\partial X} + V\frac{\partial U}{\partial Y} + K\frac{UV}{1 + KY}$$

$$= -\frac{1}{1 + KY}\frac{\partial P}{\partial X} + \frac{1}{1 + KY}\left[\frac{\partial \sigma_{XX}}{\partial X} + \frac{\partial}{\partial Y}(1 + KY)\sigma_{XY} + K\sigma_{XY}\right]$$

$$\frac{1}{1+KY}U\frac{\partial V}{\partial X}+V\frac{\partial V}{\partial Y}-\frac{K}{1+KY}U^2$$
$$=-\frac{\partial P}{\partial Y}+\frac{1}{1+KY}\left[\frac{\partial \sigma_{XY}}{\partial X}+\frac{\partial}{\partial Y}(1+KY)\sigma_{XY}-K\sigma_{XX}\right]$$

where, for a newtonian fluid

$$\sigma_{XX}=\frac{2}{(1+KY)R_e}\left(\frac{\partial U}{\partial X}+KV\right)$$
$$\sigma_{XY}=\frac{1}{(1+KY)R_e}\left(\frac{\partial V}{\partial X}+(1+KY)\frac{\partial U}{\partial Y}-KU\right)$$
$$\sigma_{YY}=\frac{2}{R_e}\frac{\partial V}{\partial Y}$$

The Reynolds number R_e is given by $R_e=\frac{\rho U^* H^*}{\mu^*}$, where U^* and H^* are characteristic velocity and length, ρ the density and μ^* the viscosity.

These equations must be solved with boundary conditions,

$$U=V=0 \quad \text{for} \quad Y=\pm 1/2$$

1.3 The O(δ) Navier–Stokes Equations

The variable curvature $K=\delta k(X)$ and its variation in X are now considered small, δ being a small positive parameter. Since we are considering a high Reynolds number basic flow dominated by its longitudinal component, all the terms are small except U, $\frac{\partial U}{\partial Y}$ and $\frac{\partial^2 U}{\partial Y^2}$ which are of order 1. Then, to order δ included, continuity equation and Navier–Stokes equations can be written in the stationary case,

$$\frac{\partial U}{\partial X}+\frac{\partial V}{\partial Y}=0 \qquad (1)$$

$$U\frac{\partial U}{\partial X}+V\frac{\partial U}{\partial Y}+\frac{\partial P}{\partial X}-\frac{1}{R_e}\left(\frac{\partial^2 U}{\partial X^2}+\frac{\partial}{\partial Y}\left[(1+KY)\frac{\partial U}{\partial Y}\right]\right)=0 \qquad (2)$$

$$U\frac{\partial V}{\partial X}+V\frac{\partial V}{\partial Y}-KU^2+\frac{\partial P}{\partial Y}-\frac{1}{R_e}\left(\frac{\partial^2 V}{\partial X^2}+\frac{\partial^2 V}{\partial Y^2}\right)=0 \qquad (3)$$

Note that in this O(δ) approximation the curvature is appearing only twice : in the viscous term of the longitudinal momentum equation as a "variable viscosity" and in the KU^2 centrifugal/inertial part of the transversal momentum equation. The streamline curvature creates a radial pressure gradient which is very important for upstream influence. To simplify the notation the unknowns are still denoted (U, V, P), even if now it is a *uniformly valid approximation*.

1.4 The GIBL Model for a Curved Channel

1.4.1 A: Velocity Field

We seek a solution in the form: $U = u_0 + \delta u$, $V = \delta v$, where $u_0(Y) = \frac{1}{4} - Y^2$ is the basic unperturbed Poiseuille flow.

According to the Successive Complementary Expansion Method (SCEM), developed by [3], the core approximation,

$$U = u_0(Y) + \delta u_1(X, Y, \delta) + \dots , \tag{4}$$

$$V = \delta v_1(X, Y, \delta) + \dots , \tag{5}$$

can be complemented to build a Uniformly Valid Approximation (UVA) [4] :

$$U = u_0(Y) + \delta \left(u_1(X, Y, \delta) + U_{BL}^{+}(X, \eta^{+}, \delta) + U_{BL}^{-}(X, \eta^{-}, \delta)\right) \tag{6}$$

$$V = \delta \left(v_1(X, Y, \delta) + \varepsilon[V_{BL}^{+}(X, \eta^{+}, \delta) + V_{BL}^{-}(X, \eta^{-}, \delta)]\right) \tag{7}$$

the dependence on the Reynolds number being implicit; the terms U_{BL} and V_{BL}, being of order 1, are correcting terms respectively to u_1 and v_1 in the upper and lower boundary layers such that, $\lim_{\eta \to \infty} U_{BL} = 0$, and $\lim_{\eta \to \infty} V_{BL} = 0$. The boundary layer variables $\eta^{\pm}$ are given by, $\eta^{+} = \frac{\frac{1}{2} - Y}{\varepsilon}$ and $\eta^{-} = \frac{\frac{1}{2} + Y}{\varepsilon}$. The form of V is imposed by the continuity equation. In the longitudinal equation, in order to have the same order for the inertial and viscous terms and since $u_0 = \mathrm{O}(\varepsilon)$ in the boundary layer, we take $\varepsilon = \mathrm{O}_S\left(R_e^{-\frac{1}{3}}\right)$. The first significant perturbation is obtained when, in the boundary layer, ε and δ are of the same order, i.e. $\delta = \mathrm{O}\left(R_e^{-\frac{1}{3}}\right)$, which allows U to be negative. A characteristic number that links the Reynolds number R_e and the curvature δ is thus defined by $\mu = \delta R_e^{\frac{1}{3}}$. The parameter μ can be seen as the ratio between the curvature δ and the boundary layer thickness ε. The challenging case is therefore μ being $\mathrm{O}(1)$, which is our assumption.

1.4.2 B: Pressure Field

In the core flow $P = p_0(X) + \delta p_1(X, Y, \delta) + \dots$. Then a UVA for the pressure is as follows:

$$P = p_0(X) + \delta \left[p_1(X, Y, \delta) + \Delta(\varepsilon)(P_{BL}^{+}(X, \eta^{+}, \delta) + P_{BL}^{-}(X, \eta^{-}, \delta))\right]$$

where the P_{BL} terms satisfy $\lim_{\eta\to\infty} P_{BL} = 0$ and $\Delta(\varepsilon)$ is a gauge function not yet determined. A careful analysis of the various orders of magnitude [8], in the core flow, and especially in the boundary layer, shows that $\Delta = \mathrm{O}(\varepsilon^3)$. Now, from (3), it can be seen that in the whole field, boundary layer and core, we have the key result,

$$\frac{\partial P}{\partial X} = \frac{\mathrm{d}p_0}{\mathrm{d}X} + \delta\left(\frac{\partial p_1}{\partial X} + \mathrm{O}(\varepsilon^3)\right) \tag{8}$$

Thus at the considered order, in (2), $\dfrac{\partial P}{\partial X}$ can be replaced by $\dfrac{\partial P_1}{\partial X}$, given by:

$$\frac{\partial P_1}{\partial X} = \frac{\mathrm{d}p_0}{\mathrm{d}X} + \delta\frac{\partial p_1}{\partial X}\ . \tag{9}$$

The long scale approximation [6, 7] yields a simplified model for the pressure gradient [8] :

$$\frac{\partial P_1}{\partial X} = \frac{\mathrm{d}p_0}{\mathrm{d}X} + \delta\left(A''' + k'\right)\int_{\eta_c}^{\eta} u_0^2(\eta')\,\mathrm{d}\eta' \quad + \delta B'(X) \tag{10}$$

where A is the so called displacement function, ($u_1 = A(X)u_0'$, $v_1 = -u_0 A'(X)$).

1.4.3 C: GIBL

Finally the global interactive boundary layer model (GIBL) for the straight and variable curved channel parts consists of the generalized boundary layer equations:

$$\frac{\partial U}{\partial X} + \frac{\partial V}{\partial Y} = 0 \tag{11}$$

$$U\frac{\partial U}{\partial X} + V\frac{\partial U}{\partial Y} = -\frac{\partial P_1}{\partial X} + \frac{1}{R_e}\frac{\partial}{\partial Y}\left[(1+KY)\frac{\partial U}{\partial Y}\right] \tag{12}$$

$$\text{where}\quad \frac{\partial P_1}{\partial X} = \frac{\mathrm{d}p_0}{\mathrm{d}X} + \delta\left(A''' + k'\right)\int_{\eta_c}^{\eta} u_0^2(\eta')\,\mathrm{d}\eta' \quad + \delta B'(X)$$

with $U = V = 0$ for $Y = \pm 1/2$. This model is uniformly valid in the whole flow field, involving U and V instead of their boundary layers values U_{BL} and V_{BL}. Consequently we have in the core flow $V = V_1$ where, in the case of the long scale approximation, $V1 = -\delta u_0 A'(X)$.

Thus using this last relation as a coupling condition imposed at the median line the numerical resolution of the GIBL model is done through an iterative procedure in which the calculation domain is swept from upstream to downstream.The sweeping is repeated until convergence is achieved on A and B and finally on the shear stress. See [1, 8] for more details.

2 Results and Discussion

Figures 2–4 present several cases where the wall shear stress ($C_f = \mp \frac{2}{R_e} \left.\frac{\partial U}{\partial Y}\right|_{Y=\pm\frac{1}{2}}$) as obtained by the GIBL model is compared to the numerical solution of the complete Navier–Stokes equations for $R_e = 1{,}000$. At the inlet of the upstream straight tangent channel a parabolic profile was given while at the outlet of the downstream channel a constant zero pressure was prescribed. The GIBL results match very well the complete Navier–stokes results for K_{max} up to 0.4 and the eccentricity e up to $\simeq 0.943$ in the whole geometrical domain. The upstream and downstream effects as well as the impact of the curvature discontinuities at the junctions are well captured, and the behaviour in the entire bend is quantitatively well reproduced by the GIBL model .

The behaviour of the wall shear stress in the upstream tangent channel is similar to the case of a distal constant curvature bend [8]: some distance ahead from the junction with the bend the normalised shear stress increases at the internal wall and decreases at the external wall relatively to the upstream Poiseuille flow. The length

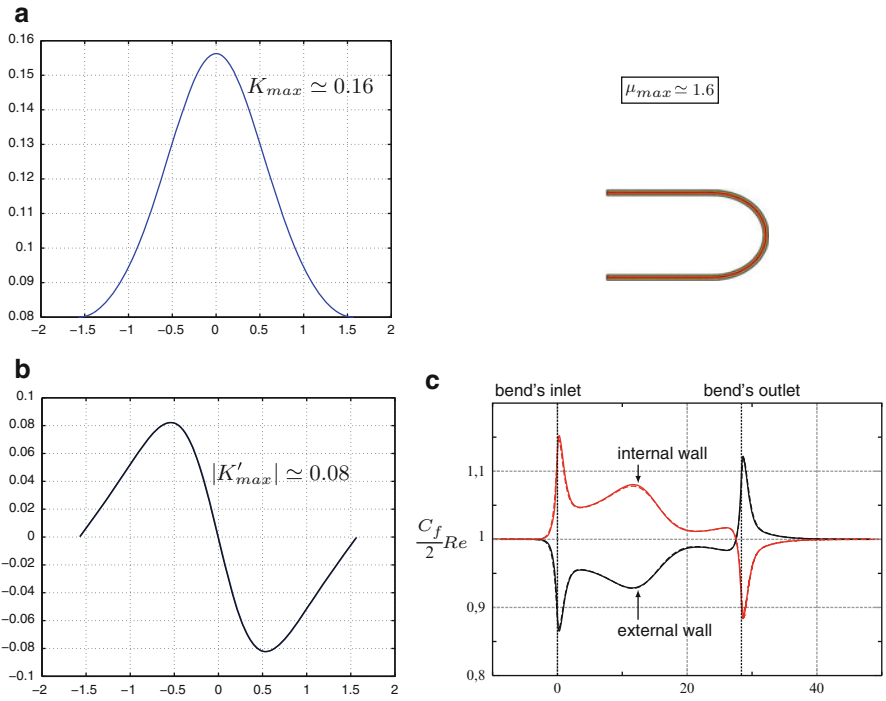

Fig. 2 Elliptical bend $[-\pi/2, \pi/2]$; $R_e = 1{,}000$, major semi-axis $a = 10$, minor semi-axis $b = 8$, eccentricity $e = 0.6$; (**a**) Median line curvature K evolution; (**b**) dK/dX evolution; (**c**) Wall shear stress; *straight lines*: NS results; *dashed lines*: GIBL results

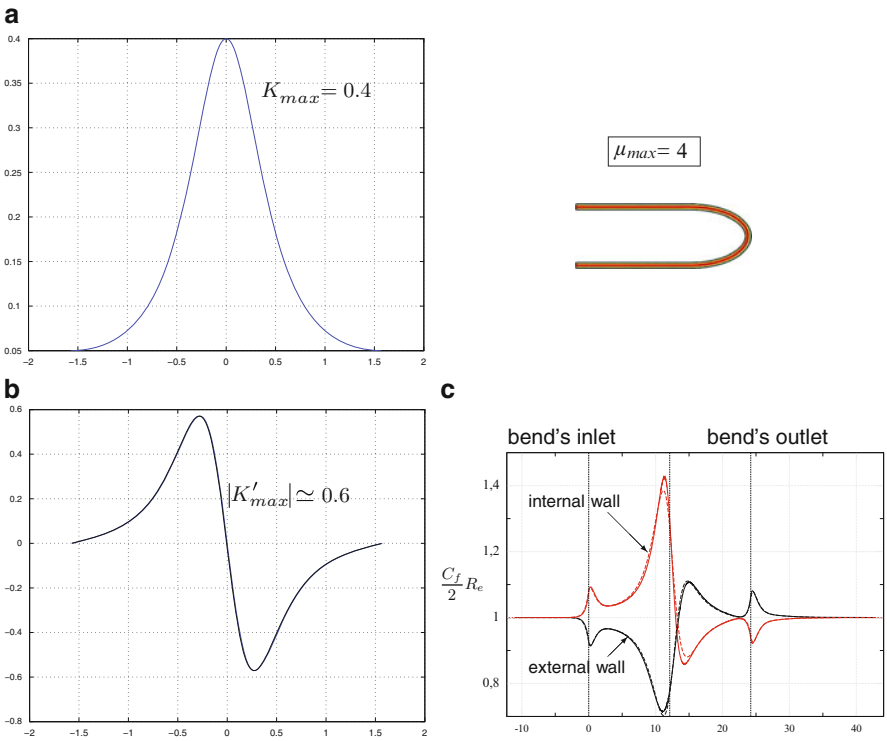

Fig. 3 Elliptical bend $[-\pi/2, \pi/2]$; $R_e = 1{,}000$, major semi-axis $a = 10$, minor semi-axis $b = 5$, eccentricity $e \simeq 0.866$; (**a**) Median line curvature K evolution; (**b**) dK/dX evolution; (**c**) Wall shear stress; *straight lines*: NS results; *dashed lines*: GIBL results

of this upstream influence to an incoming Poiseuille flow was shown asymptotically by Smith[5] to be, for high Reynolds, of the order of $R_e^{\frac{1}{7}}$ whatever the nature of the distal perturbation is. In a companion paper [2] this result is confirmed numerically and by a modal analysis.

In the tree cases tested the median line curvature $K(X)$ increases up to the middle of the bend where $K_{max}$is reached and then decreases, while the maximum of its variation K'_{max} is reached just before the middle of the bend. Both $K(X)$ and $K'(X)$ combined to the fluid inertia modulate the shape and the peaks of the internal and external wall shear stresses. The wall shear stress peaks are attained just before the middle of the bend.

Figure 2 shows the case of a channel having an elliptical median line that deviates little from a circle, with its major semi-axis $a = 10$ and its minor semi-axis $b = 8$, hence an eccentricity $e = 0.6$. For a circular bend of radius equal to 10, thus having a constant curvature $\delta = 0.1$, an established flow occurs in the bend at the same Reynolds number, that is a constant value of the shear stress is attained and maintained in a large part of the bend away from the discontinuities [8]. On the

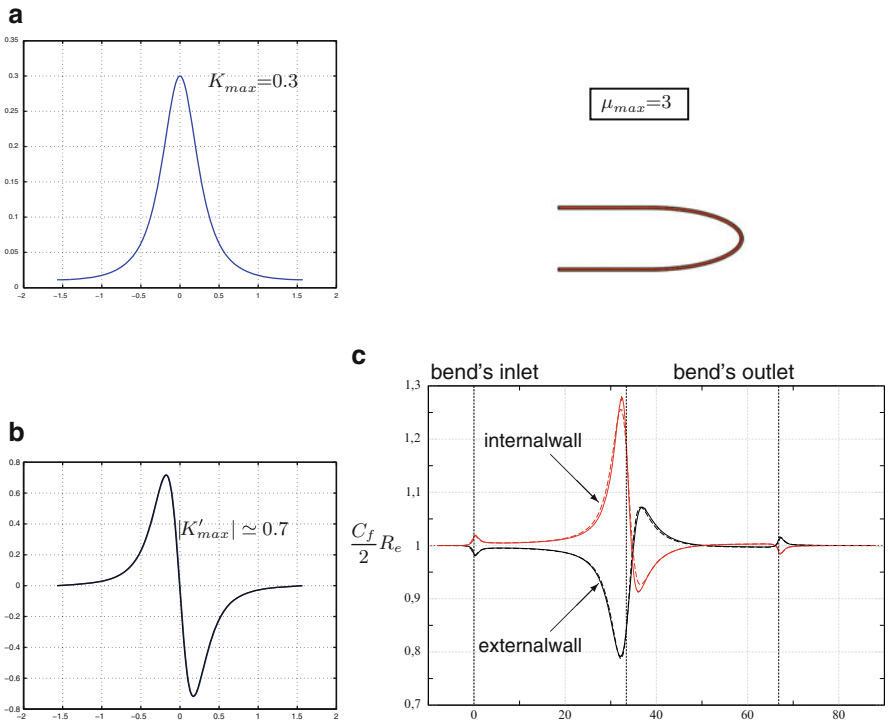

Fig. 4 Elliptical bend $[-\pi/2, \pi/2]$; $R_e = 1{,}000$, major semi-axis $a = 30$, minor semi-axis $b = 10$, eccentricity $e \simeq 0.943$; (**a**) Median line curvature K evolution; (**b**) dK/dX evolution; (**c**) Wall shear stress; *straight lines*: NS results; *dashed lines*: GIBL results

contrary it is seen here that a small deviation from a circular median line, i.e. a small variable curvature with $K_{max} \simeq 0.16$ and $|K'_{max}| \simeq 0.08$, has a clear influence in the spatial evolution of the wall shear stress. No constant wall shear stress is to be expected when the curvature varies as can be clearly deduced from the pressure gradient expression of (10) which is a function of the curvature variation $K'(X)$, not to mention the viscous term since $K = \delta k'(X)$ in the longitudinal momentum equation (12). In the case of Fig. 2, the wall shear stress peaks just before the middle of the bend are less than those induced by the discontinuities at the upstream and downstream junctions with the straight tangent channels.

In Fig. 3 the ellipticity of the median line is increased with $K_{max} = 0.4$, $|K'_{max}| \simeq 0.6$ and $e \simeq 0.866$. Here the peaks of the shear stress inside the bend are larger than those which occur at the discontinuities. The key parameter μ is now equal to 4 leading to slight differences in the wall shear stress peaks inside the bend between the GIBL model and the complete Navier–Stokes equations results.

To isolate more the variable curvature effects from those induced by the discontinuities of the junctions in one hand and to test the GIBL model validity with a stronger eccentricity on the other hand we run the case of Fig. 3 where $e \simeq 0.943$

with $K_{max} \simeq 0.3$ and $|K'_{max}| \simeq 0.7$. Here the junction discontinuities are smaller than the previous cases and $\mu = 3$.

The GIBL accuracy is mainly dependent on the key parameter $\mu = \delta R_e^{\frac{1}{3}}$ since this asymptotic model has been built under the assumption that μ is O(*1*) . Not presented in the present work, quite good agreement is achieved even when $\mu \simeq 11$, i.e. when $K_{max} \simeq 1.1$ and $K'_{max} \simeq 3$, which is out of the formal range of validity of the GIBL model.

References

1. P. Cathalifaud, J. Mauss, and J. Cousteix. Nonlinear aspects of high reynolds number channel flow. *Eur. J. of Mech. B/Fluids*, 29 (4):295–304, 2010.
2. P. Cathalifaud, M. Zagzoule, J. Cousteix, and J. Mauss. High reynolds channel flows: Upstream interaction of various wall deformations. *Lecture Notes in Computational Science and Engineering*, 2011.
3. J. Cousteix and J. Mauss. *Asymptotic analysis and boundary layers*, volume XVIII, Scientific Computation. Springer, Berlin, Heidelberg, 2007.
4. J. Cousteix and J. Mauss. Interactive boundary layer models for channel flow. *Eur. J. of Mech. B/Fluids*, 28:72–87, 2009.
5. F. T. Smith. Upstream interactions in channel flows. *Journal of Fluid Mechanics*, 79:631–655, 1977.
6. F. T. Smith. On the high reynolds number theory of laminar flows. *IMA J. Appl. Math.*, 28 (3):207–281, 1982.
7. K. Stewartson and P. G. Williams. Self induced separation. *Proc. Roy. Soc. London*, A312:181–206, 1969.
8. M. Zagzoule, P. Cathalifaud, J. Cousteix, and J. Mauss. Uniformly valid asymptotic flow analysis in curved channels. *submitted to Physics of fluids*, 2010.

Editorial Policy

1. Volumes in the following three categories will be published in LNCSE:

i) Research monographs
ii) Tutorials
iii) Conference proceedings

Those considering a book which might be suitable for the series are strongly advised to contact the publisher or the series editors at an early stage.

2. Categories i) and ii). Tutorials are lecture notes typically arising via summer schools or similar events, which are used to teach graduate students. These categories will be emphasized by Lecture Notes in Computational Science and Engineering. **Submissions by interdisciplinary teams of authors are encouraged.** The goal is to report new developments – quickly, informally, and in a way that will make them accessible to non-specialists. In the evaluation of submissions timeliness of the work is an important criterion. Texts should be well-rounded, well-written and reasonably self-contained. In most cases the work will contain results of others as well as those of the author(s). In each case the author(s) should provide sufficient motivation, examples, and applications. In this respect, Ph.D. theses will usually be deemed unsuitable for the Lecture Notes series. Proposals for volumes in these categories should be submitted either to one of the series editors or to Springer-Verlag, Heidelberg, and will be refereed. A provisional judgement on the acceptability of a project can be based on partial information about the work: a detailed outline describing the contents of each chapter, the estimated length, a bibliography, and one or two sample chapters – or a first draft. A final decision whether to accept will rest on an evaluation of the completed work which should include

– at least 100 pages of text;
– a table of contents;
– an informative introduction perhaps with some historical remarks which should be accessible to readers unfamiliar with the topic treated;
– a subject index.

3. Category iii). Conference proceedings will be considered for publication provided that they are both of exceptional interest and devoted to a single topic. One (or more) expert participants will act as the scientific editor(s) of the volume. They select the papers which are suitable for inclusion and have them individually refereed as for a journal. Papers not closely related to the central topic are to be excluded. Organizers should contact the Editor for CSE at Springer at the planning stage, see *Addresses* below.

In exceptional cases some other multi-author-volumes may be considered in this category.

4. Only works in English will be considered. For evaluation purposes, manuscripts may be submitted in print or electronic form, in the latter case, preferably as pdf- or zipped ps-files. Authors are requested to use the LaTeX style files available from Springer at http://www. springer.com/authors/book+authors?SGWID=0-154102-12-417900-0.

For categories ii) and iii) we strongly recommend that all contributions in a volume be written in the same LaTeX version, preferably LaTeX2e. Electronic material can be included if appropriate. Please contact the publisher.

Careful preparation of the manuscripts will help keep production time short besides ensuring satisfactory appearance of the finished book in print and online.

5. The following terms and conditions hold. Categories i), ii) and iii):

Authors receive 50 free copies of their book. No royalty is paid.
Volume editors receive a total of 50 free copies of their volume to be shared with authors, but no royalties.

Authors and volume editors are entitled to a discount of 33.3 % on the price of Springer books purchased for their personal use, if ordering directly from Springer.

6. Commitment to publish is made by letter of intent rather than by signing a formal contract. Springer-Verlag secures the copyright for each volume.

Addresses:

Timothy J. Barth
NASA Ames Research Center
NAS Division
Moffett Field, CA 94035, USA
barth@nas.nasa.gov

Michael Griebel
Institut für Numerische Simulation
der Universität Bonn
Wegelerstr. 6
53115 Bonn, Germany
griebel@ins.uni-bonn.de

David E. Keyes
Mathematical and Computer Sciences
and Engineering
King Abdullah University of Science
and Technology
P.O. Box 55455
Jeddah 21534, Saudi Arabia
david.keyes@kaust.edu.sa

and

Department of Applied Physics
and Applied Mathematics
Columbia University
500 W. 120 th Street
New York, NY 10027, USA
kd2112@columbia.edu

Risto M. Nieminen
Department of Applied Physics
Aalto University School of Science
and Technology
00076 Aalto, Finland
risto.nieminen@tkk.fi

Dirk Roose
Department of Computer Science
Katholieke Universiteit Leuven
Celestijnenlaan 200A
3001 Leuven-Heverlee, Belgium
dirk.roose@cs.kuleuven.be

Tamar Schlick
Department of Chemistry
and Courant Institute
of Mathematical Sciences
New York University
251 Mercer Street
New York, NY 10012, USA
schlick@nyu.edu

Editor for Computational Science
and Engineering at Springer:
Martin Peters
Springer-Verlag
Mathematics Editorial IV
Tiergartenstrasse 17
69121 Heidelberg, Germany
martin.peters@springer.com

Lecture Notes in Computational Science and Engineering

1. D. Funaro, *Spectral Elements for Transport-Dominated Equations.*
2. H.P. Langtangen, *Computational Partial Differential Equations.* Numerical Methods and Diffpack Programming.
3. W. Hackbusch, G. Wittum (eds.), *Multigrid Methods V.*
4. P. Deuflhard, J. Hermans, B. Leimkuhler, A.E. Mark, S. Reich, R.D. Skeel (eds.), *Computational Molecular Dynamics: Challenges, Methods, Ideas.*
5. D. Kröner, M. Ohlberger, C. Rohde (eds.), *An Introduction to Recent Developments in Theory and Numerics for Conservation Laws.*
6. S. Turek, *Efficient Solvers for Incompressible Flow Problems.* An Algorithmic and Computational Approach.
7. R. von Schwerin, ***M**ulti **B**ody **S**ystem **SIM**ulation.* Numerical Methods, Algorithms, and Software.
8. H.-J. Bungartz, F. Durst, C. Zenger (eds.), *High Performance Scientific and Engineering Computing.*
9. T.J. Barth, H. Deconinck (eds.), *High-Order Methods for Computational Physics.*
10. H.P. Langtangen, A.M. Bruaset, E. Quak (eds.), *Advances in Software Tools for Scientific Computing.*
11. B. Cockburn, G.E. Karniadakis, C.-W. Shu (eds.), *Discontinuous Galerkin Methods.* Theory, Computation and Applications.
12. U. van Rienen, *Numerical Methods in Computational Electrodynamics.* Linear Systems in Practical Applications.
13. B. Engquist, L. Johnsson, M. Hammill, F. Short (eds.), *Simulation and Visualization on the Grid.*
14. E. Dick, K. Riemslagh, J. Vierendeels (eds.), *Multigrid Methods VI.*
15. A. Frommer, T. Lippert, B. Medeke, K. Schilling (eds.), *Numerical Challenges in Lattice Quantum Chromodynamics.*
16. J. Lang, *Adaptive Multilevel Solution of Nonlinear Parabolic PDE Systems.* Theory, Algorithm, and Applications.
17. B.I. Wohlmuth, *Discretization Methods and Iterative Solvers Based on Domain Decomposition.*
18. U. van Rienen, M. Günther, D. Hecht (eds.), *Scientific Computing in Electrical Engineering.*
19. I. Babuška, P.G. Ciarlet, T. Miyoshi (eds.), *Mathematical Modeling and Numerical Simulation in Continuum Mechanics.*
20. T.J. Barth, T. Chan, R. Haimes (eds.), *Multiscale and Multiresolution Methods.* Theory and Applications.
21. M. Breuer, F. Durst, C. Zenger (eds.), *High Performance Scientific and Engineering Computing.*
22. K. Urban, *Wavelets in Numerical Simulation.* Problem Adapted Construction and Applications.

23. L.F. Pavarino, A. Toselli (eds.), *Recent Developments in Domain Decomposition Methods.*

24. T. Schlick, H.H. Gan (eds.), *Computational Methods for Macromolecules: Challenges and Applications.*

25. T.J. Barth, H. Deconinck (eds.), *Error Estimation and Adaptive Discretization Methods in Computational Fluid Dynamics*.

26. M. Griebel, M.A. Schweitzer (eds.), *Meshfree Methods for Partial Differential Equations*.

27. S. Müller, *Adaptive Multiscale Schemes for Conservation Laws*.

28. C. Carstensen, S. Funken, W. Hackbusch, R.H.W. Hoppe, P. Monk (eds.), *Computational Electromagnetics*.

29. M.A. Schweitzer, *A Parallel Multilevel Partition of Unity Method for Elliptic Partial Differential Equations*.

30. T. Biegler, O. Ghattas, M. Heinkenschloss, B. van Bloemen Waanders (eds.), *Large-Scale PDE-Constrained Optimization*.

31. M. Ainsworth, P. Davies, D. Duncan, P. Martin, B. Rynne (eds.), *Topics in Computational Wave Propagation*. Direct and Inverse Problems.

32. H. Emmerich, B. Nestler, M. Schreckenberg (eds.), *Interface and Transport Dynamics.* Computational Modelling.

33. H.P. Langtangen, A. Tveito (eds.), *Advanced Topics in Computational Partial Differential Equations.* Numerical Methods and Diffpack Programming.

34. V. John, *Large Eddy Simulation of Turbulent Incompressible Flows.* Analytical and Numerical Results for a Class of LES Models.

35. E. Bänsch (ed.), *Challenges in Scientific Computing - CISC 2002.*

36. B.N. Khoromskij, G. Wittum, *Numerical Solution of Elliptic Differential Equations by Reduction to the Interface.*

37. A. Iske, *Multiresolution Methods in Scattered Data Modelling.*

38. S.-I. Niculescu, K. Gu (eds.), *Advances in Time-Delay Systems.*

39. S. Attinger, P. Koumoutsakos (eds.), *Multiscale Modelling and Simulation.*

40. R. Kornhuber, R. Hoppe, J. Périaux, O. Pironneau, O. Wildlund, J. Xu (eds.), *Domain Decomposition Methods in Science and Engineering.*

41. T. Plewa, T. Linde, V.G. Weirs (eds.), *Adaptive Mesh Refinement – Theory and Applications.*

42. A. Schmidt, K.G. Siebert, *Design of Adaptive Finite Element Software.* The Finite Element Toolbox ALBERTA.

43. M. Griebel, M.A. Schweitzer (eds.), *Meshfree Methods for Partial Differential Equations II.*

44. B. Engquist, P. Lötstedt, O. Runborg (eds.), *Multiscale Methods in Science and Engineering.*

45. P. Benner, V. Mehrmann, D.C. Sorensen (eds.), *Dimension Reduction of Large-Scale Systems.*

46. D. Kressner, *Numerical Methods for General and Structured Eigenvalue Problems.*

47. A. Boriçi, A. Frommer, B. Joó, A. Kennedy, B. Pendleton (eds.), *QCD and Numerical Analysis III*.

48. F. Graziani (ed.), *Computational Methods in Transport.*

49. B. Leimkuhler, C. Chipot, R. Elber, A. Laaksonen, A. Mark, T. Schlick, C. Schütte, R. Skeel (eds.), *New Algorithms for Macromolecular Simulation.*

50. M. Bücker, G. Corliss, P. Hovland, U. Naumann, B. Norris (eds.), *Automatic Differentiation: Applications, Theory, and Implementations.*

51. A.M. Bruaset, A. Tveito (eds.), *Numerical Solution of Partial Differential Equations on Parallel Computers.*

52. K.H. Hoffmann, A. Meyer (eds.), *Parallel Algorithms and Cluster Computing.*

53. H.-J. Bungartz, M. Schäfer (eds.), *Fluid-Structure Interaction.*

54. J. Behrens, *Adaptive Atmospheric Modeling.*

55. O. Widlund, D. Keyes (eds.), *Domain Decomposition Methods in Science and Engineering XVI.*

56. S. Kassinos, C. Langer, G. Iaccarino, P. Moin (eds.), *Complex Effects in Large Eddy Simulations.*

57. M. Griebel, M.A Schweitzer (eds.), *Meshfree Methods for Partial Differential Equations III.*

58. A.N. Gorban, B. Kégl, D.C. Wunsch, A. Zinovyev (eds.), *Principal Manifolds for Data Visualization and Dimension Reduction.*

59. H. Ammari (ed.), *Modeling and Computations in Electromagnetics: A Volume Dedicated to Jean-Claude Nédélec.*

60. U. Langer, M. Discacciati, D. Keyes, O. Widlund, W. Zulehner (eds.), *Domain Decomposition Methods in Science and Engineering XVII.*

61. T. Mathew, *Domain Decomposition Methods for the Numerical Solution of Partial Differential Equations.*

62. F. Graziani (ed.), *Computational Methods in Transport: Verification and Validation.*

63. M. Bebendorf, *Hierarchical Matrices.* A Means to Efficiently Solve Elliptic Boundary Value Problems.

64. C.H. Bischof, H.M. Bücker, P. Hovland, U. Naumann, J. Utke (eds.), *Advances in Automatic Differentiation.*

65. M. Griebel, M.A. Schweitzer (eds.), *Meshfree Methods for Partial Differential Equations IV*.

66. B. Engquist, P. Lötstedt, O. Runborg (eds.), *Multiscale Modeling and Simulation in Science.*

67. I.H. Tuncer, Ü. Gülcat, D.R. Emerson, K. Matsuno (eds.), *Parallel Computational Fluid Dynamics 2007.*

68. S. Yip, T. Diaz de la Rubia (eds.), *Scientific Modeling and Simulations*.

69. A. Hegarty, N. Kopteva, E. O'Riordan, M. Stynes (eds.), *BAIL* 2008 – *Boundary and Interior Layers.*

70. M. Bercovier, M.J. Gander, R. Kornhuber, O. Widlund (eds.), *Domain Decomposition Methods in Science and Engineering XVIII.*

71. B. Koren, C. Vuik (eds.), *Advanced Computational Methods in Science and Engineering.*

72. M. Peters (ed.), *Computational Fluid Dynamics for Sport Simulation.*

73. H.-J. Bungartz, M. Mehl, M. Schäfer (eds.), *Fluid Structure Interaction II - Modelling, Simulation, Optimization.*

74. D. Tromeur-Dervout, G. Brenner, D.R. Emerson, J. Erhel (eds.), *Parallel Computational Fluid Dynamics 2008.*

75. A.N. Gorban, D. Roose (eds.), *Coping with Complexity: Model Reduction and Data Analysis.*

76. J.S. Hesthaven, E.M. Rønquist (eds.), *Spectral and High Order Methods for Partial Differential Equations.*

77. M. Holtz, *Sparse Grid Quadrature in High Dimensions with Applications in Finance and Insurance.*

78. Y. Huang, R. Kornhuber, O.Widlund, J. Xu (eds.), *Domain Decomposition Methods in Science and Engineering XIX.*

79. M. Griebel, M.A. Schweitzer (eds.), *Meshfree Methods for Partial Differential Equations V.*

80. P.H. Lauritzen, C. Jablonowski, M.A. Taylor, R.D. Nair (eds.), *Numerical Techniques for Global Atmospheric Models.*

81. C. Clavero, J.L. Gracia, F.J. Lisbona (eds.), *BAIL 2010 - Boundary and Interior Layers, Computational and Asymptotic Methods.*

For further information on these books please have a look at our mathematics catalogue at the following URL: www.springer.com/series/3527

Monographs in Computational Science and Engineering

1. J. Sundnes, G.T. Lines, X. Cai, B.F. Nielsen, K.-A. Mardal, A. Tveito, *Computing the Electrical Activity in the Heart.*

For further information on this book, please have a look at our mathematics catalogue at the following URL: www.springer.com/series/7417

Texts in Computational Science and Engineering

1. H. P. Langtangen, *Computational Partial Differential Equations.* Numerical Methods and Diffpack Programming. 2nd Edition
2. A. Quarteroni, F. Saleri, P. Gervasio, *Scientific Computing with MATLAB and Octave.* 3rd Edition
3. H. P. Langtangen, *Python Scripting for Computational Science.* 3rd Edition
4. H. Gardner, G. Manduchi, *Design Patterns for e-Science*.
5. M. Griebel, S. Knapek, G. Zumbusch, *Numerical Simulation in Molecular Dynamics*.
6. H. P. Langtangen, *A Primer on Scientific Programming with Python.* 2nd Edition
7. A. Tveito, H. P. Langtangen, B. F. Nielsen, X. Cai, *Elements of Scientific Computing.*

For further information on these books please have a look at our mathematics catalogue at the following URL: www.springer.com/series/5151